Reconstruction of the Arctic Ocean environment during the Eocene *Azolla* interval using geochemical proxies and climate modeling

Eveline N. Speelman

GEOLOGICA ULTRAIECTINA

Mededelingen van de Faculteit Geowetenschappen - Universiteit Utrecht

No. 331

Promotor:
Prof. dr. ir. J.S. Sinninghe Damsté, NIOZ and Utrecht University

Co-promotor:
Dr. G.J. Reichart, Utrecht University

Members of the dissertation committee:
Prof. dr. ir. H.A. Dijkstra, Utrecht University (The Netherlands)
Prof. dr. H. Brinkhuis, Utrecht University (The Netherlands)
Prof. M. Pagani, Yale University (USA)
Prof. dr. J.J. Middelburg, Utrecht University (The Netherlands)

Contact:
Eveline Neletta Speelman
e.speelman@geo.uu.nl
enspeelman@yahoo.com

The research presented in this thesis was funded by the Darwin Center for Biogeosciences and Utrecht University.
Additional financial support was provided by Statoil.

ISBN/AEN: 978-90-5744-192-9
LPP Contribution Series 31
Printed by Wöhrman Print Service, Zutphen

Contents

Chapter 1

Introduction

1.1 Reconstructing past climates

Earth's climate has varied greatly over geologic time, also in response to fluctuating atmospheric CO_2 concentrations. At present, climate change results in a global increase in temperature and precipitation, concurrent with rising atmospheric CO_2 concentration (IPCC, 2007). Prolonged periods of global warm climates, with higher temperatures especially at high latitudes, have been recognized in the geologic record (e.g. Zachos et al., 2001). The Eocene for instance, appears to have been substantially warmer than today and was characterized by high (>1000 ppm) pCO_2 levels (Pearson and Palmer, 2000). Such intervals offer a window to future analogues of enhanced greenhouse conditions. These can provide important clues to understanding processes involved in environmental change, enabling anticipation of future climate changes and associated consequences in response to anthropogenic greenhouse gas emissions.

Information on environmental change stored in the geological record is retrieved using so-called proxy relationships, which relate measurable biological, physical or chemical variables in the fossil record to environmental parameters. Besides numerous other proxy signal carriers, like ice cores, corals, speleothems, microfossils (e.g. foraminifera and pollen), and inorganic matter (e.g. clay minerals), molecular fossils (i.e. lipid biomarkers) can be used for paleoclimate reconstructions in a wide range of environmental settings (e.g. Peters et al., 2005). Lipid biomarkers found in extracts of lake and marine sediments are quite resistant to postdepositional degradation and are structurally similar to, or are diagenetic alteration products of, specific natural products (compounds produced by living organisms). Typically, when found in sediments, the presence of certain biomarkers provides informa-

tion on environmental conditions prevailing during the lifetime of their source organisms. Moreover, the hydrogen isotopic composition of biomarkers (e.g. plant wax *n*-alkanes) contains information on past precipitation and humidity conditions (e.g. Sauer et al., 2001). Similarly, their carbon isotopic composition can provide information on (past) carbon cycling and may be indicative of atmospheric pCO_2 levels (Hayes, 1993).

In addition to the reconstruction of past climate as such, proxies are used to validate and calibrate global climate model simulations, in this way enhancing our understanding of the complex atmosphere-ocean-biosphere interactions during times of climate change. Likewise, these models can be used to extrapolate proxy-based climate reconstructions quantitatively and link different proxies mechanistically. Ultimately, this will improve model performance, thereby increasing accuracy and precision of predictions of future climate change. The study presented here focuses on constraining paleo-environmental conditions through a combination of biomarker analyses and climate modeling, during a specific interval in the Eocene.

1.2 Sediments from the Eocene Arctic

In 2004 sediment cores were taken at the Lomonosov Ridge during Integrated Ocean Drilling Program (IODP) Expedition 302, otherwise known as the Arctic coring expedition (ACEX). This ridge is a fragment of continental crust that rifted from the Eurasian continental margin during the Late Palaeocene (~57 Ma ago) (Glebovsky et al., 2006) and is currently located in the central Arctic Ocean. The age model for the ACEX core was established using biostratigraphical and cosmogenic isotope data (Backman et al., 2008). In addition, dinocyst events encountered in the ACEX record could be calibrated against ODP Leg 151 Site 913B, located in the adjacent Norwegian-Greenland Sea, for which a good magnetostratigraphy is available (Eldrett et al., 2004). Hence, the ACEX sediment cores provided the first geologic record from the Central Arctic, shedding more light on past changes in high latitude climate.

The Arctic was not always ice-covered: for example, in one of the cores exceptionally high concentrations of intact micro- and megaspores of the aquatic floating fern *Azolla* have been found, indicating that this freshwater fern grew and reproduced *in situ* in the Arctic Ocean (Moran et al., 2006; Brinkhuis et al., 2006). At site 913B the top of the so-called *Azolla* interval is dated at 48.1 Ma (magnetic polarity chronozone C21r), while the onset of the *Azolla* phase is dated at approximately 49.3 Ma, giving a total duration of 1.2 Ma for the entire *Azolla* interval based on the timescale of Gradstein et al. (2004). However, due to incomplete recovery of the ACEX core for the Eocene (Lutetian-Ypresian), the onset of the *Azolla* interval is

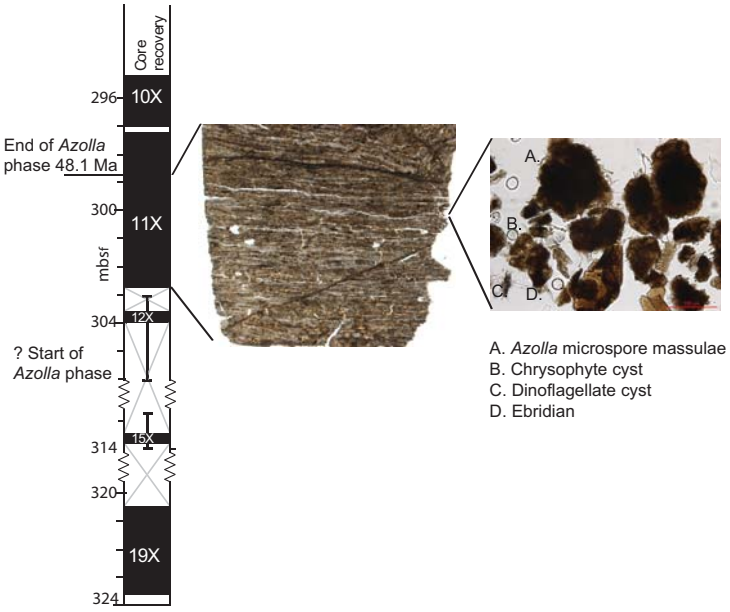

Figure 1.1: ACEX core recovery. Close-up of laminated sediment (courtesy of M. Collinson) and image of fossil content, showing *Azolla* microspore massulae, Chrysophyte cysts, Dinoflagellates and Ebridians.

missing (Fig. 1.1), and sediments used for analyses described in this thesis have an approximate timespan of ~160.000 yrs.

1.3 What is *Azolla*?

Azolla Lamarck, belonging to the order of the Salviniales Britt, is a genus of aquatic floating ferns (Fig. 1.2) with seven extant species, distributed throughout tropical and temperate regions (Saunders and Fowler, 1993). Extant *Azolla* grows well in water with maximum salinity levels of 2.5 ‰, but perishes when salinity is higher than 3.5 ‰ (van Kempen et al., under review). This freshwater fern ranks amongst the fastest growing plants on Earth, with doubling rates of < 2 days and is capable of fixing large amounts of carbon (Wagner, 1997). Dinitrogen fixing bacterial symbionts are known to inhabit a special cavity within the dorsal leaf lobe of *Azolla* (Peters and Meeks, 1989). These cyanobacteria, e.g. *Anabaena azollae*, fix atmospheric nitrogen and subsequently release it to *Azolla*, satisfying both its own requirement for combined nitrogen and that of its host. In exchange, the fern provides the endosymbiont with a protected environment and supplies it with a carbon source in the form of sucrose (Peters and Meeks, 1989). Through this symbiosis the aquatic fern *Azolla* is not limited by fixed nitrogen availability (Braun-Howland and Nierzwicki-Baer, 1990) and thence *Azolla* growth depends primarily on phos-

Figure 1.2: Photographs of extant *Azolla filiculoides* (courtesy M. van Kempen).

phorus availability. Under favourable conditions extant *Azolla* may outcompete other macrophytes, bloom fast, and form thick floating mats.

In the geological record *Azolla* is present throughout the Cenozoic (Collinson et al., 2002 and references therein). Previously, also mass abundances of *Azolla* remains have been recognized all around the Eocene Arctic and adjacent Nordic Seas (e.g., Manum et al., 1989; Eldrett et al., 2004) (Fig. 1.3). However, concentrations of *Azolla* megaspores, with or without attached microspore massulae and clusters of dispersed microspore massulae, recovered at the Lomonosov Ridge site are several orders of magnitude higher (Brinkhuis et al., 2006) and are comparable to those documented in Palaeogene microlaminated freshwater pond facies (Collinson, 2002). The well-calibrated Eocene *Azolla* event is also used as a stratigraphic marker horizon (Brinkhuis et al., 2006; Bujak, Brinkhuis, unpublished exploration data).

1.4 Arctic Eocene environmental conditions

As illustrated in Figure 1.3, the Arctic Ocean was almost completely enclosed in the Early/Middle Eocene (Scotese, 1988), with the still shallow Fram Strait (Jakobsson et al., 2007) and epicontinental West Siberian Sea Strait/Turgai Strait (Akhmetiev, 2009) forming the only, probably even intermittent, connections between the Arctic Basin and the open oceans.

Vertebrate fauna recovered from Ellesmere Island in the 1970s provided some of the first evidence that temperatures in the early Eocene Arctic were substantially

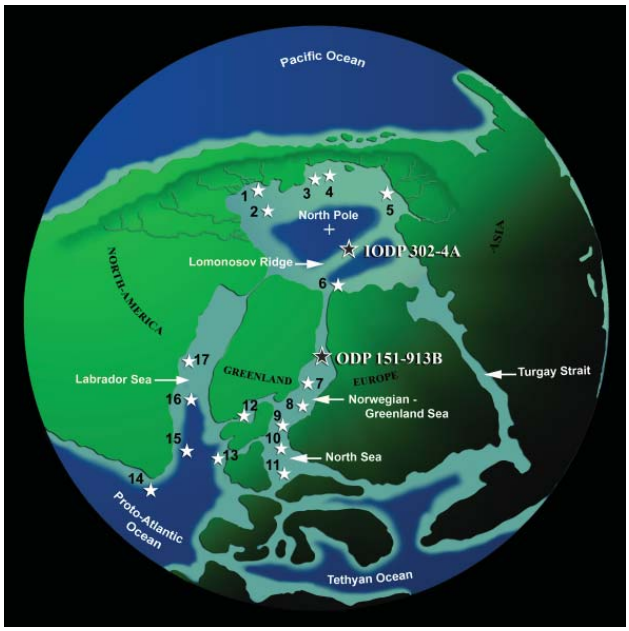

Figure 1.3: Eocene configuration of the continents. *Azolla* occurrences identified at various sites including the Mackenzie Delta & Beaufort Basin, North slope Alaska & Chukchi Sea, Siberian Shelf, Barentsz Sea, Norwegian – Greenland Sea, North Sea Basin, Faeroe-Shetland Basin, Atlantic Basin and the Labrador Sea are indicated by white stars.

warmer than today. The discovery of early Eocene remains of a varanid lizard, the tortoise *Geochelone*, and the alligator *Allognathosuchus* suggested that winter temperatures rarely dipped below freezing (Estes and Hutchinson, 1980). More recently, Arctic sea surface temperatures (SSTs) have been estimated by applying the TEX_{86} index, an organic palaeothermometer that is independent of salinity (Schouten et al., 2002; Powers et al., 2004) and calibrated to mean annual SST. TEX_{86} values suggest SSTs of ~10 °C during, and 13-14 °C immediately following, the *Azolla* phase (Brinkhuis et al., 2006). These values are similar to, or slightly higher than, other late Paleocene and Eocene floral, faunal and isotopic proxy evidence for mean annual temperatures in the Arctic (Greenwood and Wing, 1995; Jahren and Sternberg, 2003). Correspondingly, Eocene pCO_2 is believed to have been higher; up to ten times preindustrial values (Pearson and Palmer, 2000). However, proxy estimates from palaeosols (Yapp, 2004, Royer et al., 2001), marine boron isotopes (Pearson and Palmer 2000) and leaf stomatal indices (Royer et al., 2001) give estimates of Eocene atmospheric CO_2 concentrations of between 100 and 3500 ppm.

Stable oxygen isotope analyses of cellulose from middle Eocene Metasequoia wood on Axel Heiberg Island indicate that Arctic climate was not only warm (mean annual temperature of 13.2 ± 2.0 °C), but also quite humid, with an atmospheric wa-

ter content approximately twice that of today (Jahren and Sternberg, 2003). Based on modern hydrology and fully coupled paleoclimate simulations, it has been suggested that the warm greenhouse conditions characteristic of the Palaeogene period probably induced an intensified hydrological cycle, with precipitation exceeding evaporation at high latitudes (Manabe, 1997; Huber et al., 2003).

The *in situ* growth and reproduction of *Azolla,* in combination with high abundances of chrysophyte cysts (the endogenously formed resting stage of these freshwater algae), indicates that fresh- or brackish waters frequently dominated the Arctic surface water layer (Brinkhuis et al., 2006; Stickley et al., 2008). Based on qualitative data of endemic assemblages of marine diatoms and ebridians along with very high abundances of chrysophyte cysts, Stickley et al. (2008) confirmed the concomitant occurrence of lower surface water salinities and higher deeper water salinities, also suggesting episodic changes in salinity, stratification and thus trophic state. Given the limited salinity tolerance of extant *Azolla*, admixing of saline water from greater depth would quickly render the surface waters too saline for *Azolla*. Salinity stratification might thus have been a prerequisite for the development of massive *Azolla* occurrences. The, albeit incomplete, isolation of the Arctic from the worlds' oceans, together with enhanced run-off, may have favoured development of the required fresh surface water conditions.

High organic carbon fluxes, together with limited exchange with the atmosphere, partly related to the dense vegetation cover, usually renders water below extant *Azolla* mats dysoxic. In the ACEX sediments no intact vegetative *Azolla* material has been recovered (Brinkhuis et al., 2006), indicating that most of the plant tissue was decomposed in the water column or at the sediment-water interface. Based on sediment lamination (Fig. 1.1), the absence of fossil benthic organisms, high concentrations of reduced sulphur (pyrite), and organic geochemical biomarker evidence, previous reports on the Arctic region concluded that bottom waters were at least temporally devoid of oxygen (Backman et al., 2006; Brinkhuis et al., 2006; Sluijs et al., 2006; Stein et al., 2006), also during the *Azolla* interval. Salinity stratification, in combination with high riverine input of nutrients and hence increased surface water productivity and the associated enhanced export of organic matter, may have been responsible for the development of these euxinic conditions in the lower part of the water column (Stein et al., 2006).

1.5 Relevance of the Eocene *Azolla* interval

During the *Azolla* interval, tropical sea surface temperatures (SSTs) were somewhat warmer than today (with a mean annual temperature of 32 - 34 °C at 19 °S) (Pearson et al., 2007), while Arctic SSTs were substantially higher (~10 °C) (Brinkhuis et al.,

2006). At present, climate models are incapable of capturing such proxy-inferred warm high latitude temperatures, while keeping the tropics at reasonable temperatures: the (in)famous model-data mismatch (e.g. Crowley and Zachos, 2000; Huber and Sloan, 2000; Huber and Caballero, 2003; Shellito et al., 2003). From a global climate change perspective there is thus a strong need for better constraining conditions facilitating such extreme events and improving models simulating mechanisms underlying climate change.

Interestingly, the *Azolla* interval (~49 Ma) approximately coincided with the onset of a global shift towards heavier deep sea benthic foraminifera $\delta^{13}C$ values (Zachos et al., 2001) and an overall global cooling trend. This transition from a global greenhouse climate towards the modern icehouse (Zachos et al., 2008; Tripati et al., 2005) was probably heralded by decreasing atmospheric pCO_2 concentrations (Pearson and Palmer, 2000; Pagani et al., 2005). Although the total amount of carbon buried in the Arctic during the *Azolla* interval is relatively limited, the sustained occurrence of *Azolla* might have influenced local and possibly even global nutrient (nitrogen, phosphorus and carbon) cycles. Hence, unravelling the (*Azolla*) biosphere-climate interactions may shed light on the greenhouse to icehouse climate transition.

1.6 Scope and framework of this thesis

This dissertation describes the reconstruction of paleo-environmental conditions facilitating the large-scale occurrence of the freshwater fern *Azolla* in the Early/Middle Eocene Arctic and the potential impact of biosphere-climate interactions on Earth's greenhouse to icehouse transition. Hence, the aim is to explain and constrain the following four hypotheses:

(1) The presence of the freshwater fern *Azolla*, both within the Arctic Basin and adjacent Nordic Seas, suggests that at least the surface waters were frequently fresh or brackish during the *Azolla* interval.

(2) *Azolla* is known to live in symbiosis with nitrogen fixating cyanobacteria, which may have been present already in the Eocene, influencing nutrient cycling.

(3) Sustained growth of *Azolla* in the Arctic required a sustained supply of dissolved inorganic phosphorus from riverine or deepwater sources.

(4) Wide-spread occurrences of fast growing *Azolla* may have reduced atmospheric CO_2 levels during the Early/Middle Eocene.

To test these hypotheses ACEX sediments are analysed for their (organic) geochemical properties, including biomarker composition and trace metal content. Obtained proxy records are extrapolated and interpreted using numerical modelling approaches.

In **Chapter 2** the results of biomarker analyses of both extant *Azolla* species and ACEX sediments are discussed. Extant *Azolla* and the sediments from the Arctic *Azolla* interval were found to contain relatively high quantities of compounds identified as 1,ω20 C_{30}–C_{36} diols. Furthermore, structurally related mid-chain hydroxy fatty acids, long chain *n*-alkanols, keto-ols , and C_{29} ω20,ω21 diols, C_{29} 1,20,21 triols, C_{29} dihydroxy fatty acids as well as a series of wax esters containing these ω20 mono- and dihydroxy lipids were discovered. As these compounds are well preserved in the Eocene sediments, these lipids may serve as palaeo-environmental indicators of the Arctic *Azolla* interval and as markers for the past occurrence of *Azolla* in general.

In **Chapter 3** a newly developed HPLC/MS^2 method was used for the identification of heterocyst glycolipids (HGs), specific for diazotrophic cyanobacteria. Analyses of extracts of extant *Azolla filiculoides* show the presence of 1-(O-hexose)-3,25-hexacoasanediol (C_{26} HG diol) and its corresponding keto-ol, the predominant glycolipids in the family of Nostocaceae. The presence of the same HGs in ACEX sediments shows that the symbiosis between *Azolla* and *Anabaena azolla*e dates back to at least the Early/Middle Eocene. These findings indicate that heterocystous cyanobacteria, likely in symbiosis with *Azolla*, played a major role in adding newly fixed nitrogen to surface waters in the past-stratified Arctic.

Chapters 4, 5 and 6 focus on constraining water sources for the Arctic (and adjacent areas). Using the isotope-enabled version of the National Center for Atmospheric Research (NCAR) atmospheric general circulation model, Community Atmosphere Model v.3 (isoCAM3), relationships between water isotopes and past climates can be simulated. Model outcomes can be validated using the isotopic composition of leaf wax *n*-alkanes (δD). In **Chapter 4** we examine the influence of an imposed reduced meridional sea surface temperature gradient on the spatial distribution of precipitation and its isotopic composition (δD, $\delta^{18}O$) in an Early/Middle Eocene setting. The Eocene simulation accurately predicts the occurrence of less depleted precipitation, with δD values ranging only between 0 and -140‰ (compared to Present-day 0 to -300‰), supporting the prevalence of a reduced meridional temperature gradient during the *Azolla* interval.

In order to allow accurate comparison between model and proxy-data we evaluated in **Chapter 5** the hydrogen isotopic fractionation of plants using output of isoCAM3 (Chapter 4) to force the isotopic version of the NCAR Land Surface Model

(isoLSM). Model outcomes showed that the offset between δD values of precipitation and δD values of leaf wax *n*-alkanes ($\varepsilon_{w/a}$) varies in space and that the relationship was different under Eocene environmental conditions. Hence, region and time specific $\varepsilon_{w/a}$ values should be used when reconstructing δD of paleo-precipitation from measured δD of *n*-alkanes.

In **Chapter 6** we zoom in on the Eocene Arctic, using a combination of compound specific hydrogen isotope measurements and model simulations (validated in Chapter 4) to constrain Eocene Arctic surface water salinity and precipitation and runoff amounts. The hydrogen isotopic composition of biomarkers for *Azolla* encountered in Arctic Eocene sediments (Chapter 2) provide insight into the isotopic composition of Eocene Arctic surface water. Resulting reconstructed surface water δD values and precipitation δD, reconstructed using terrestrially derived *n*-alkanes extracted from ACEX sediments, combined with the $\varepsilon_{w/a}$ values computed in Chapter 5, fall in the same range. This indicates that virtually no mixing could have occurred between deeper saline waters (isotopically heavy) and the freshwater (isotopically light), thus showing that the Arctic surface waters were significantly more fresh than the underlying waters. Results of isotopically validated isoCAM3 runs show the presence of an intensified hydrological cycle, and net runoff amounting to 1700 mm/yr, confirming freshening of the Eocene Arctic surface waters.

Chapter 7 presents a high-resolution trace metal record (ICP-MS and ICP-OES) for the expanded Early/Middle Eocene section capturing the *Azolla* interval. Using trace metal budgets the inflow of saline deepwater into the Arctic is constrained. Combining sedimentary phosphorus data, freshwater fluxes from Chapter 6 and the reconstructed deepwater inflow in a new mass balance box model for the Arctic enables examining the relationships between Arctic oceanic circulation, primary productivity, and sedimentary burial and regeneration of phosphorus for the Eocene Arctic *Azolla* interval. Model outcomes showed that a combination of enhanced regeneration of P and upwelling of P-rich deepwater is needed to explain the sustained growth of *Azolla*.

In **Chapter 8** the potential role of *Azolla* as a modifier of nutrient cycles and the impact of sustained growth of *Azolla* in a major anoxic oceanic basin on atmospheric pCO_2 is investigated. Storage of 0.9 – 3.5 10^{18} g carbon in the Arctic was inferred, resulting in a 55 to 470 ppm drawdown of atmospheric pCO_2. This indicates that the Arctic *Azolla* blooms may have had a significant effect on global atmospheric pCO_2 levels through enhanced burial of organic matter.

Chapter 2

Biomarker lipids of the freshwater fern *Azolla* and its fossil counterpart from the Eocene Arctic Ocean

Eveline N. Speelman, Gert-Jan Reichart, Jan W. de Leeuw, W. Irene C. Rijpstra, and Jaap S. Sinninghe Damsté

Published in: Organic Geochemistry 40 (2009), 628 - 637.

Abstract

Eocene sediments recovered from the Lomonosov Ridge in the central Arctic Ocean during Integrated Ocean Drilling Program Expedition 302 contain high amounts of fossil remains of the free floating freshwater fern *Azolla*. Both extant *Azolla* and the sediments from the Arctic *Azolla* interval were found to contain relatively high quantities of compounds identified as 1,ω20 C_{30}– C_{36} diols. Furthermore, structurally related mid-chain hydroxy fatty acids, long chain *n*-alkanols and keto-ols were discovered. The different series have a common feature: there is always a hydroxy group at the ω20 position. In addition, structurally related C_{29} ω20,ω21 diols, C_{29} 1,20,21 triols, C_{29} dihydroxy fatty acids as well as a series of wax esters containing these mono- and dihydroxy lipids are reported. Selective extraction of *Azolla* surface lipids revealed that these compounds are most likely present in the leaf waxes of the fern. The suite of long chain, mid-chain ω20 hydroxy wax constituents is described for the first time. As they are well preserved in the Eocene sediments, these lipids may serve as palaeo-environmental indicators of the Arctic *Azolla* interval and as markers for the past occurrence of *Azolla* in general.

2.1 Introduction

Long chain, mid-chain diols were first reported as C_{30} and C_{32} 1,15 diols in marine sediments (de Leeuw et al., 1981). Subsequently, their recognition has gradually expanded via identification of new members and structurally related keto-ols, *n*-alkanols and hydroxy fatty acids present in a wide variety of marine, brackish and freshwater environments (see for a review Versteegh et al., 1997). These compounds are known to be biosynthesized by marine organisms like Eustigmatophyte microalgae (Volkman et al., 1992; Gelin et al., 1996), while diatoms of the genus *Proboscia* produce 1,14 diols and structurally related hydroxy alkanoates (Sinninghe Damsté et al., 2003; Rampen et al., 2007). Epicuticular wax crystals from different terrestrial plant species, including gymnosperms as well as angiosperms, also contain a wide variety of structurally related compounds (Jetter, 2000; Jetter and Riederer, 1999; Wen et al., 2006a,b).

Here we describe a novel series of long chain, mid-chain hydroxy compounds found in Early/Middle Eocene sediments obtained during the Integrated Ocean Drilling Program (IODP) Arctic Coring Expedition (ACEX) in 2004 at the Lomonosov Ridge in the central Arctic Ocean (Backman et al., 2006). In the same core interval fossil remains of *Azolla* have been found in high concentrations, accompanied by their morphologically intact micro- and megaspores, indicating that they grew and reproduced *in situ* (Brinkhuis et al., 2006). This suggests that these ferns may be the source of the encountered lipids.

Azolla is a genus of free floating aquatic ferns, which is presently distributed throughout tropical and temperate fresh water ecosystems (Moore, 1969). It has the tendency to form thick floating mats and is known to live in symbiosis with dinitrogen fixing cyanobacteria (Peters and Meeks, 1989). Under optimal conditions *Azolla* can double its biomass in <2 days (Peters et al., 1980). This implies that the Arctic *Azolla* blooms could have had a large impact on local, and possibly even global, carbon (C), nitrogen (N) and phosphorus (P) cycles. Both *Azolla* spores, as well as specific biomarkers for *Azolla*, can be used to provide insight into the past extent of a bloom and its influence on global C cycling. Biomarkers in immature sediments are usually not affected by diagenetic overprinting and their ^{13}C and D contents can play a crucial role in revealing information on C and water cycling during the Cenozoic in the Arctic Ocean (cf. Pagani et al., 2006). In order to assess the biomarker potential of the novel series of long chain, mid-chain hydroxy lipids encountered in ACEX sediments, we compared their distribution with those of extant *Azolla* ferns. Hence, the study describes the occurrences of these series of ω20 mid-chain hydroxy compounds in both recent *Azolla* specimens and Arctic sediments to validate the potential of these compounds as unique biomarkers applicable for palaeo-environmental reconstruction.

2.2 Materials and methods

2.2.1 Extant *Azolla* sp.

Extant *Azolla filiculoides* was collected from a trench between pastures in Elst, near Nijmegen in The Netherlands and was cultivated at the Radboud University Nijmegen, both under strictly controlled conditions in the laboratory and somewhat less controlled conditions in a greenhouse. Three fresh samples were analyzed; two were collected from the greenhouse and one from the lab.

2.2.2 ACEX core sediments

During the IODP ACEX expedition a core was taken at the Lomonosov Ridge, site 302 M0004A, at a latitude of 87.87 °N and a longitude of 136.18 °E, and at 1288 m water depth. Four different samples, all from the Eocene *Azolla* interval (Brinkhuis et al., 2006), were considered, which in total yielded sufficient organic material to allow the application of different separation techniques. The samples were taken from lithologic biogenic subunit 2 (265.01– 301.35 m coring depth), core 11x, hole 4A, which is dominated by very dark clay mud-bearing biosiliceous ooze (Backman et al., 2006). Two samples from interval 2w, section 82.5–88.5 cm (sample 1) and 126–136 cm (sample 2) and two from interval 3w, section 118–121 cm combined with 126–128 cm (sample 3) and 82–86 cm (sample 4) were analyzed. The total organic carbon (TOC) content of the samples was measured with a C, N and S analyzer (Fison NA 1500) and ranged between 3.1 and 6.0 wt%.

2.2.3 Extraction

Both the ACEX sediments and extant *Azolla* specimens were freeze dried, powdered and extracted with an accelerated solvent extractor (Dionex) using a dichloromethane (DCM)–MeOH mixture (9:1, v/v). The roots were separated from the leaves and ultrasonically extracted using DCM:MeOH (2:1, v/v). To selectively extract waxes from the outer surface of freshly sampled *Azolla* leaves, the upper surfaces were brushed gently with cotton (pre-cleaned using Soxhlet extraction) soaked with DCM. The cotton was subsequently re-extracted in an ultrasonic bath using DCM:MeOH (2:1, v/v).

2.2.4 Separation of extracts of extant *Azolla* specimen

For total lipid analysis (cf. Goossens et al., 1986) an aliquot of the total extract of extant *Azolla* was methylated with CH_2N_2, purified using SiO_2 column chromatography with ethyl acetate and silylated with bis(trimethylsilyl)trifluoroacetamide (BSTFA) and pyridine at 60 °C for 20 min. The leaf wax and root extracts were dried over a Na_2SO_4 column and derivatized using the same method. For detailed identification of lipids, another aliquot (ca. 15 mg) of the total extract was methylated with BF_3/MeOH at 60 °C for 10 min and separated using preparative thin layer chromatography (TLC) on kieselgel 60 (Merck, 0.25 mm) as described by Skipski et al. (1965). The plate was developed with di-isopropyl ether to 40% of its height,

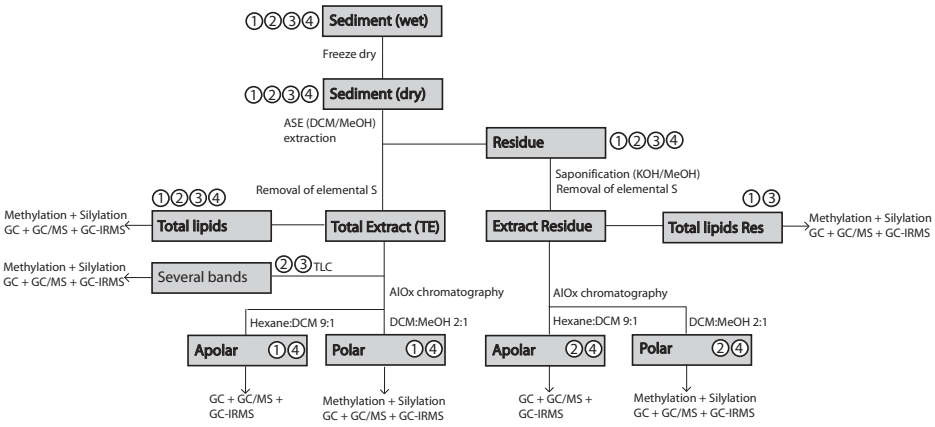

Figure 2.1: Extraction scheme for ACEX sediments. Numbers in circles correspond to sample numbers. Two samples were analyzed from interval 2w, section 82.5–88.5 cm (sample 1) and 126–136 cm (sample 2) and two from interval 3w, section 118–121 cm combined with 126–128 cm (sample 3) and 82–86 cm (sample 4).

dried, and developed with petroleum ether/diethyl ether. Nine bands, identified by spraying with rhodamine and inspection of the TLC plate under UV light, were scraped off. The two upper bands (Rf 0.8–1.0) were re-extracted using hexane and the other bands (Rf 0.1–0.8) with ethyl acetate. The polar fractions were silylated with BSTFA in pyridine to convert the alcohols to their TMS ethers.

2.2.5 Separation of sediment extracts

The extraction and separation scheme for the sediments is shown in Figure 2.1. Activated Cu was used to remove elemental S from the extracts. All residues remaining after extraction of the sediments were saponified with 1.0 M KOH in MeOH, after which elemental S was removed from the resulting extracts. Additionally, aliquots of total extracts of samples 2 and 3 (Fig. 2.1) were separated using the above TLC method. Aliquots of extracts from samples 2 and 4 obtained after saponification of the residue and the total extract of samples 1 and 4 were separated using column chromatography with activated Al_2O_3 with hexane:DCM (9:1, v/v) and DCM:MeOH (1:1, v/v) subsequently to obtain an apolar and a polar fraction, respectively. All apolar fractions were dissolved in hexane and all polar fractions in ethyl acetate after derivatization before gas chromatography (GC), gas chromatography–mass spectrometry (GC/MS) and gas chromatography–isotope ratio mass spectrometry (GC–IRMS) analyses.

2.2.6 GC and GC/MS

All fractions were first analyzed with a Hewlett Packard gas chromatograph fitted with a flame ionization detector (FID) and sulfur-selective flame photometric de-

tector (FPD). Samples were injected on-column, on a CP-Sil 5CB fused silica column (30 m x 0.32 mm i.d, film thickness 0.1 μm) with He as carrier gas set at constant pressure (100 KPa). Samples were injected at 70 °C. The oven was programmed to 130 °C at 20 °C/min and then to 320 °C (hold 20 min) at 4 °C/min. Components were identified using GC/MS (Thermo Trace GC Ultra) with a similar column and heating programme as for the GC. Concentrations were determined by integration of peak areas in the total ion currents using squalane as internal standard. Because some components of interest coeluted with sterols, relative abundances were calculated from summed mass chromatograms of the principal fragment ions, rather than from direct measurement of GC–FID peak areas.

2.2.7 Carbon isotope measurements

Compound specific $\delta^{13}C$ values were determined using GC– IRMS with a ThermoFinnigan Delta-Plus XP mass spectrometer. A similar column and oven temperature programme were used as described above, though with a constant flow of 1.2 ml/min. Co-injected squalane, whose isotopic composition was determined off line, was used as isotopic reference. Carbon isotopic compositions are reported relative to the VPDB standard and are based on duplicate analyses of well-resolved peaks and represent averaged values. Standard deviations of $\delta^{13}C$ values were usually below 0.2, but never greater than 0.35‰. The $\delta^{13}C$ values for the alcohols and fatty acids (FAs) were corrected for the isotopic composition of carbon added during derivatization. For alcohols, the $\delta^{13}C$ value of the BSTFA used for silylation was determined by derivatization of an alcohol standard (myo-inositol) with a known $\delta^{13}C$ composition. For acid moieties, a similar procedure was followed: a C_{17} FA with known $\delta^{13}C$ composition was methylated with the same batch of BF_3/MeOH as used for the extracts.

2.3 Results and discussion

In addition to C_{16} and di-unsaturated C_{18} FAs, the total lipid fraction of extant *Azolla* contains a series of uncommon lipids having a m/z 369 fragment in their mass spectra (Fig. 2.2). They were identified as mid-chain ω20 alkanols, 1,ω20 diols and ω20 hydroxy FAs (see Fig. 2.3 for examples) with chain lengths from C_{27} to C_{36} (Table 2.1). In addition, wax esters comprising a C_{16} FA esterified with a ω20 hydroxy lipid were also detected, as well as a group of structurally related ω20,ω21 dihydroxy C_{29} compounds. The total extracts of the ACEX sediments from the *Azolla* interval also contained most of these lipids, supplemented by a series of ω20 keto-1-ols (Table 2.1).

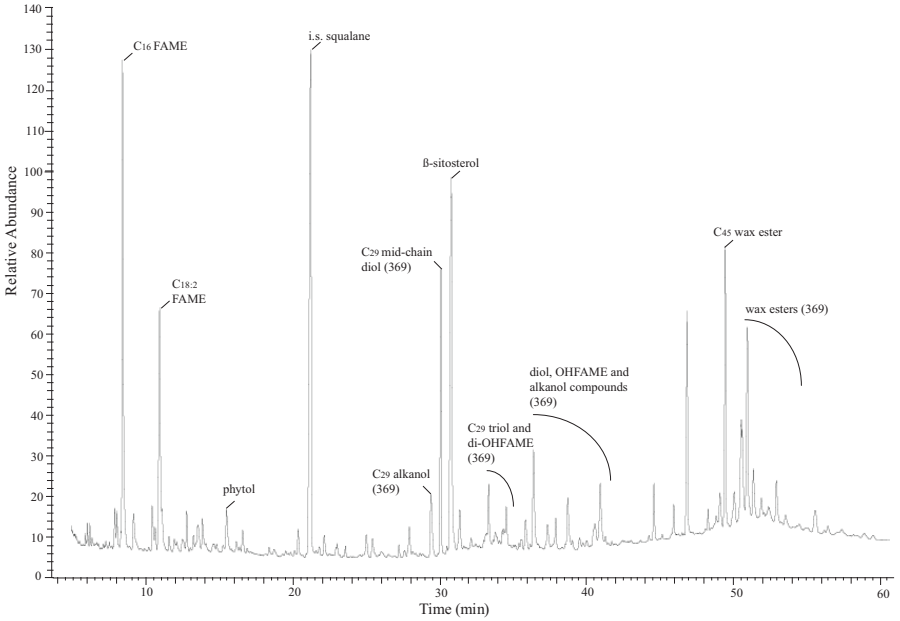

Figure 2.2: Total ion current (TIC) trace of a derivatized total extract of extant *Azolla* from a greenhouse.

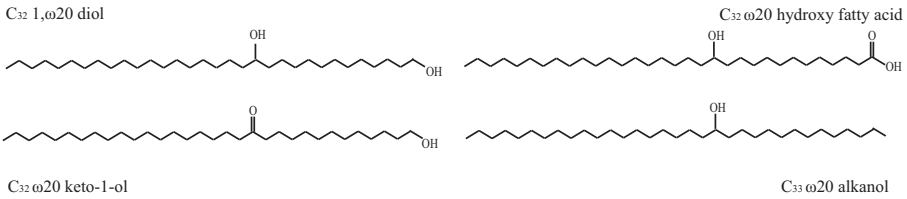

Figure 2.3: Structures of C_{32} 1,ω20 diol, C_{32} ω20 hydroxy FA, C_{33} ω20 alkanol and C_{32} keto-1-ol.

2.3.1 Identification of ω20 diols, hydroxy FAs and alkanols

The 1,ω20 diols were assigned on the basis of the mass spectra of their TMS ethers. The spectra show fragment ions at [M^+-15] (loss of methyl), [M^+-90] (loss of OTMS) and m/z 369 (base peak) and an ion at m/z 331, 359, 387 or 415 formed by cleavage around the carbon bearing the ω20 OTMS group (e.g. Fig. 2.4a). The spectra are similar to those reported for 1,ω18 diols by Xu et al. (2007), but with an ion at m/z of 369 instead of m/z 341. The diol homologous series, comprised exclusively of 1,ω20 members is composed of 1,11-triacontanediol (C_{30} 1,ω20 diol), 1,13-dotriacontanediol (C_{32} 1,ω20 diol), 1,15-tetracontanediol (C_{34} 1,ω20 diol) and 1,17-hexa contanediol (C_{36} 1,ω20 diol) (Table 2.1), and is thus dominated by even numbered

chain length (n)	diols	diols	mid-chain OHFAME	mid-chain OHFAME	*sec*-al-kanols	*sec*-alkanols	keto-ols
	Azolla	ACEX	*Azolla*	ACEX	*Azolla*	ACEX	only ACEX
C26				7 (ω20) C26 (231)		7 (ω20) C26 (187)	
C27					8 (ω20) C27 (201)		
C28			9 (ω20) C28 (259)	9 (ω20) C28 (259)	9(ω20) C28 (215)	9 (ω20) C28 (215)	
C29					10(ω20) C29 (229)	10(ω20) C29 (229)	
C30	1,11(1,ω20) C30 (331)	1,11(1,ω20) C30 (331)	11(ω20) C30 (287)	11(ω20) C30 (287)			
C31					12(ω20) C31 (257)		
C32	1,13(1,ω20) C32 (359)	1,13(1,ω20) C32 (359)	13(ω20) C32 (315)	13(ω20) C32 (315)			13 C32[ab] (537)
C33					14(ω20) C33 (285)	14(ω20) C33 (285)	
C34	1,15(1,ω20) C34 (387)	1,15(1,ω20) C34 (387)	15(ω20) C34 (343)	15(ω20) C34 (343)		15(ω20) C34 (299)	15 C34[ab] (565)
C35					16(ω20) C35 (313)	16(ω20) C35 (313)	
C36	1,17(1,ω20) C36 (415)	1,17(1,ω20) C36 (415)	17(ω20) C36 (371)	17(ω20) C36 (371)		17(ω20) C36 (327)	17 C36[ab] (593)

	chain length (C16+n)	hydroxy wax esters	hydroxy wax esters	di-hydroxy wax esters	di-hydroxy wax esters
		Azolla	ACEX	*Azolla*	ACEX
*	C45			ω9,ω10 diOH C45 623	ω9,ω10 diOH C45 (623)
	C46	ω20 C46 (497)	ω20 C46 (497)	ω20,ω21 diOH C46[ac] (483)	ω20,ω21 diOH C46[ac] (483)
	C48	ω20 C48 (525)	ω20 C48 (525)	ω20,ω21 diOH C48[ac] (511)	
	C50	ω20 C50 (553)	ω20 C50 (553)		
	C52	ω20 C52 (581)	ω20 C52 (581)		

[a] All compounds have a characteristic fragment ion at m/z 369, except
[b] which are keto-1-ols with a characteristic m/z of 130 and,
[c] which are mid-chain dihydroxy compounds characterized by loss of ω9 OTMS with m/z 215.

*	C29 diol	C29 diol	C29 triol	C29 di-OHFAME
	Azolla	ACEX	Azolla	*Azolla*
C29	9,10 (ω20,ω21) C29 diol[ac] (229)	9,10 (ω20,ω21) C29diol[ac] (229)	1,20,21 (ω1,ω20,ω21) C29 triol[ac] (457)	20,21 di-OH C29 FAME[ac] (413)

Table 2.1: Positions of OH groups in various compound classes in both extant *Azolla* and ACEX extracts, with major characteristic fragment ions also indicated[a].

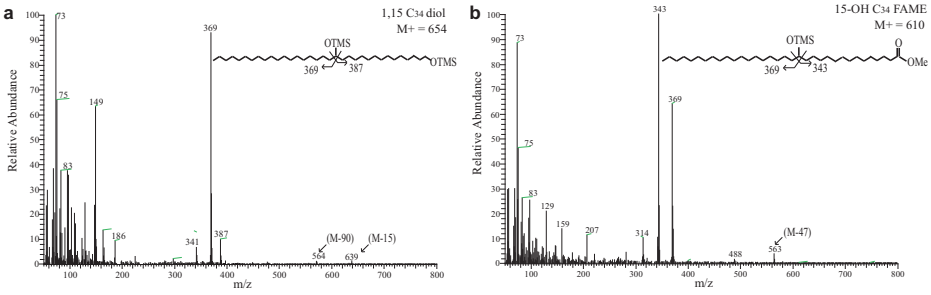

Figure 2.4: Mass spectra and structures of (a) 1,15 C_{34} diol and (b) 15 hydroxy C_{34} FA methyl ester.

homologues. In the ACEX sediments minor amounts of C_{32}–C_{38} ω20 keto-1-ols were present (Table 2.1).

FAs with an ω20 OH group and ω20 *sec*-alkanols were also identified in both extant *Azolla* specimens and the sediments from the Arctic *Azolla* interval. They eluted in the same fraction, but were fully separated from the 1,ω20 diols using TLC (Rf 0.4 and Rf 0.3, respectively). The mid-chain ω20 hydroxy FAs were identified by the dominant m/z 369 fragment, a [M^+-47] fragment (loss of OOMe) and by fragment ions consisting of the OTMS alkyl fragment including the methyl ester moiety (see Fig 2.4b for an example). They range from C_{26} to C_{36}, with only even numbered homologues (Table 2.1). The ω20 *sec*-alkanols occur primarily with odd carbon chain lengths, varying from C_{26} to C_{36}. The characteristic fragment ions of the TMS derivatives are again m/z 369 and another fragment ion (Table 2.1) also formed by cleavage around the carbon atom bearing the ω20 OTMS group.

2.3.2 Identification of 20,21 or ω20,ω21 dihydroxy compounds

In addition to the compounds with two functional groups at C-1 and ω20, compounds with an additional OH group at the ω21 position were also discovered (Table 2.1). These C_{29} compounds were identified via their common m/z 215 ions (originating from cleavage of the bond between the carbons containing the two adjacent OTMS groups; Figs. 2.5a–c) and represent the C29 ω20,ω21 diol, 1,20,21 triol and 20,21 dihydroxy FA. The C_{29} 1,20,21 triol is further characterized by a small m/z 457 ion, formed by cleavage between the 20 and 21 OTMS groups and a subsequent loss of HOTMS. The C_{29} dihydroxy FA was identified via its [M^+-31] (loss of OMe), [M^+-90] (OTMS) and m/z 413 (RCO-Me) ions. Only the C_{29} diol was also encountered in the ACEX sediments from the *Azolla* interval.

2.3.3 Identification of wax esters

Several related wax esters were discovered in extant *Azolla* and ACEX extracts. These include a series of C_{45}–C_{52} esters composed of a C_{16} FA esterified with a diol

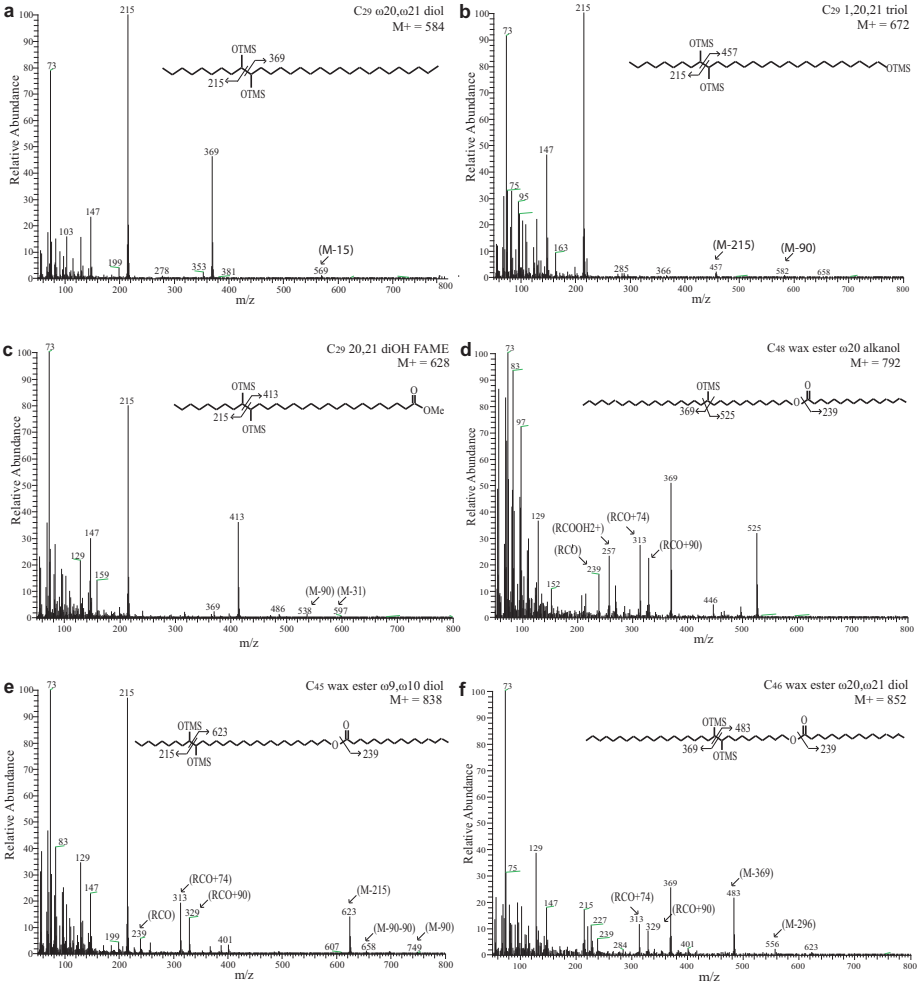

Figure 2.5: Mass spectra and structure of (a) C_{29} ω20,ω21 diol, (b) C_{29} 1,20,21 triol, (c) C_{29} 20,21 dihydroxy FA methyl ester, (d) C_{48} ω20 mono-hydroxy wax ester, (e) C45 9,10 dihydroxy wax ester and (f) C_{46} ω20,ω21 dihydroxy wax ester. NB the characteristic patterns of m/z 73, 129 and 147 for the C_{29} triol and C_{29} dihydroxy FA, respectively.

or triol. All the wax esters are characterized by an RCO fragment, reflected in m/z 239, and the corresponding RCO+74 and RCO+90 peaks, which are characteristic for wax esters (see Figs. 2.5d–f for structures and mass spectra). The wax esters with ω20 mono-hydroxy moieties correspond to the original C_{30}–C_{36} 1,ω20 diol series, where the C-1 hydroxy group is esterified with hexadecanoic acid (Table 2.1). The wax esters were thus assigned as ω20 hydroxy C_{46}, C_{48}, C_{50} and C_{52} esters. They are all characterized by a m/z 369 peak. The spectra are further characterized by an ion including the ω20 OTMS group and the other side of the chain (Table 2.1; Fig.

2.5d). Wax esters containing two OH groups were also identified and include the C_{45}, C_{46} and C_{48} wax esters. The C_{45} member is characterized by [M^+-90], [M^+-90-90] and [M^+-215] peaks and comprises the C_{29} 1,20,21 triol esterified with hexadecanoic acid. The C_{46} and C_{48} wax esters consist of a hexadecanoic acid esterified with the C_{30} 1,ω20,ω21 and the C_{32} 1,ω20,ω21 triol, respectively. They were identified by way of a minor m/z 369 peak and the ion representing M^+-369 (ω20 OTMS) group (m/z 483 and m/z 511, respectively; Table 2.1, Fig. 2.5e). In addition, the M^+-296 fragment in the spectra of both compounds is characteristic of the silyl group rearrangement from C_{20} to the carboxylic group, followed by cleavage of the C_{20}–C_{21} bond.

2.3.4 Production of ω20 hydroxy compounds by *Azolla* or *Anabaena azollae*

Long chain, mid-chain hydroxy compounds have been found extensively in plant waxes (Jetter and Riederer, 1996, 1999; Jetter, 2000; Vermeer et al., 2003; Wen et al., 2006a,b). Previous studies have investigated the composition of epicuticular waxes for a broad range of plants including needles from *Taxus baccata* to *Pisum sativum* (pea wax) and *Myricaria germanica* shrubs. With the exception of *Papaver* sp. leaves (Jetter et al., 1996; Jetter and Riederer, 1996) none of these plants had a homologous series of mono secondary alcohols, primary/secondary diols or hydroxy FAs with the mid-chain hydroxy group at a constant position relative to the end of the alkyl group (Wen and Jetter, 2007; Wen et al., 2006a,b; Jetter, 2000). The only report of a homologous series of 1,ω20 diols was for *Papaver* sp. leaves immersed in $CHCl_3$, albeit with a shorter chain length distribution than found in *Azolla* (C_{22}, C_{26}, C_{28}, C_{29} and C30; Jetter et al., 1996). No mid-chain alkanols or mid-chain hydroxy FAs with the same (ω20) configuration were reported in the *Papaver* leaf waxes. In all other plant species investigated, mainly other dihydroxy compounds were described, such as the C_{28}–C_{38} 1,5 diols in *Taxus baccata* needles (Wen and Jetter, 2007).

Recently, Xu et al. (2007) reported on the occurrence of a similar series of hydroxy compounds in sediments from a hypereutrophic freshwater lake in Venezuela, albeit with ω18 instead of ω20 functionality. They argued that cyanobacteria were the most likely source for these 1,ω18 diols, based on the composition of the planktonic community, which consisted of 90% cyanobacterial species and because of the stable carbon isotopic signatures of the compounds (Xu et al., 2007). The $\delta^{13}C$ values of the 1,ω18 diols were compared with those of β-sitosterol from the same sediment, since sterols are usually absent in cyanobacteria (Volkman, 1986). The less depleted ^{13}C content of the 1,ω18 diols (~ - 21.3‰) relative to that of β-sitosterol (-24.0‰) was interpreted to indicate an aquatic microbial origin for the diols (Xu et al., 2007). Hence, we conclude at this stage that the hydroxy compounds with their specific position(s) of the OH groups and specific chain length distributions are biosynthesized by *Azolla* species or by their cyanobacterial symbionts.

To investigate whether the compounds originate from *Azolla* or from symbionts such as *Anabaena azollae*, compound specific $\delta^{13}C$ measurements of these lipids in extant *Azolla* were undertaken, because different stable carbon isotopic compositions would be expected, depending on the origin of the ω20 compounds. Pulse-chase experiments with $^{14}CO_2$ indicate that the associated cyanobacteria themselves fix little or no CO_2 in the intact *Azolla* association (Kaplan and Peters, 1988). *A. azollae* has deferred its independent photosynthetic potential and depends on fixed carbon translocated from the photosynthetic parts of *Azolla* in the form of sucrose (Meeks and Elhai, 2002; Rai et al., 2000). In this case, the $\delta^{13}C$ values of the cyanobacterial lipids are deemed to be relatively heavy since sugars produced by the fern are relatively enriched compared to lipids (cf. van Dongen et al., 2002).

Our bulk $\delta^{13}C$ values for *Azolla* of ~-30‰ (Table 2.2) are consistent with the findings Bunn and Boon (1993) for ferns (Pterophyta) in general. The $\delta^{13}C$ values of the measured lipids ranged from -32.6‰ to -40.7‰ (Table 2.2) and were the same for the specimen from the greenhouse and the laboratory. β-Sitosterol is the most abundant sterol in extracts from *Azolla* and is produced by the fern itself. Its d13C value was -32.6‰. The diols show significantly depleted $\delta^{13}C$ values, ranging from -38.0‰ to -39.9‰. The values for the mid-chain hydroxy FAs also vary around -39‰, as do those for the C_{29} ω20,ω21 diol, the dihydroxy FA, the triol and the C_{45} wax ester.

The difference in $\delta^{13}C$ values between the β-sitosterol and all the ω20 compounds is ca. 6.5‰. Differences in the biosynthetic production pathways of isoprenoids (including β-sitosterol) and the compounds with straight chain skeletons such as the encountered ω20 compounds will influence the individual ^{13}C compositions. The $\delta^{13}C$ values of isoprenoid and acyl compounds may differ by up to 8‰, possibly as a result of the alternative pyruvate/ glyeraldehyde-3-phosphate pathway utilized in the synthesis of isoprenoid compounds (Schouten et al., 1998). This variation is sufficient to explain the observed 6.5‰ difference between the isoprenoid β-sitosterol and the straight chain ω20 hydroxy compounds, supporting the idea that the ω20 hydroxy compounds are biosynthesized by the fern and not by the endosymbiotic cyanobacteria. Since the main source of carbon for the cyanobac-

Table 2.2: The $\delta^{13}C$ values (‰ vs. VPDB) for selected lipids in extant *Azolla* extracts (values measured using selected TLC fractions).

Diols	$\delta^{13}C$ (‰)	Mid-chain OH FAME	$\delta^{13}C$ (‰)	C_{29} compounds	$\delta^{13}C$ (‰)	Other	$\delta^{13}C$ (‰)
1,11 C_{30} diol	-39.1			C_{29} diol	-39.7	ß-sitosterol	-32.6
1,13 C_{32} diol	-38.0	C_{32} OHFAME	-39.0	C_{29} triol	-37.1	C_{16} fatty acid	-34.5
1,15 C_{34} diol	-38.7	C_{34} OHFAME	-39.1	C_{29} di-hydroxy fatty acid	-38.2	C_{18} fatty acid	-36.0
1,17 C_{36} diol	-39.9	C_{36} OHFAME	-40.7	C_{45} wax ester	-38.9	TOC	-30.3

teria (i.e. sucrose supplied by *Azolla*) would be isotopically enriched relative to *Azolla* biomass (-30.3‰), it would be difficult to produce depleted acyl lipids with ~-39‰. Therefore, biosynthesis of the ω20 hydroxy lipids by the symbiont *A. azollae* is unlikely. In order to provide additional evidence for this conclusion, the roots and leaf waxes of *Azolla* were extracted separately, since the cyanobacterial symbionts are not associated with root or wax tissue in *Azolla*. Using a selective, superficial wax extraction from the fern leaves should avoid the extraction of lipids from the symbiotic bacteria living in the dorsal leaf lobes of *Azolla*. The wax extracts had relatively high amounts of ω20,ω21 C_{29} diol and C_{45} wax ester, as well as C_{16} and C_{18} FAs. Furthermore, small amounts of the C_{30}–C_{36} ω20 diols, the C_{29} triol and C_{29} mid-chain hydroxy FA, the mid-chain alkanols (ω20 C_{29} and C_{33}) and C_{48} ω20 wax ester were encountered, with much lower amounts of β-sitosterol (C_{29} ω20,ω21 diol: β-sitosterol ratio 6:1 compared to 0.25:1 in the total extract). The root extracts did not contain any of the ω20 hydroxy compounds. The C_{29} ω20,ω21 (9,10) diol is structurally very similar to the C_{29} 4,10 diol and 5,10 diol, typically found to accumulate as wax constituents of gymnosperm needle waxes (Riederer, 1989; Franich et al., 1979; Wen et al., 2006a). Hence we conclude that it is most likely that all ω20 hydroxy compounds originate from the epicuticular wax.

2.3.5 Biosynthetic pathways of ω20 hydroxy compounds

The similarity in the chain length distributions of the ω20 alkanols, the mid-chain ω20 hydroxy FA and the 1,ω20 diols, in combination with their virtually identical $\delta^{13}C$ values (Tables 2.1 and 2.2), strongly suggests that these three compound classes are formed by way of the same biosynthetic pathway. The fixed position of an OH at ω20 suggests that the series result from chain elongation of a parent secondary alcohol, rather than from hydroxylation of a range of alcohols, a process postulated by Gelin et al. (1997). The predominance of even numbered members of the homologous 1,ω20 diols further suggests that they are generated through acyl reduction after chain elongation rather than decarboxylation (Wen et al., 2006a). This mechanism is analogous to the biosynthesis of other known wax constituents. Gelin et al. (1997) had already suggested that FAs may be precursors of diols via reduction of the terminal carboxylic acid group, a pathway also supported by a labelling study of a C_{22} carboxylic acid in the freshwater alga *Ochromonas danica* (Elovson, 1974). The similar chain length distribution pattern of the mid-chain ω20 hydroxy FAs supports this idea. In contrast, the ω20 *sec*-alkanols show a strong odd/even predominance (Table 2.1). This can be explained by decarboxylation of the mid-chain ω20 hydroxy FAs. It has been found before that most wax components with two mid-chain hydroxy functional groups have alkyl chains with odd carbon numbers (e.g. Holloway and Brown, 1977), consistent with the abundant presence of C_{29} ω20,ω21 dihydroxy compounds described here. The biosynthesis of C_{29} compounds probably results from decarboxylation of the corresponding C_{30} diacids, where C_{29} triols have an additional ω1 OH group and the dihydroxy FAs an

ω1 carboxyl group. However, no C_{30} ω20,ω21 dihydroxy FA has been encountered, whereas the C_{29} FA is present. Moreover, the C_{46} and C_{48} mid-chain dihydroxy wax esters consist of an ester-bound C_{30} and C_{32} ω20,ω21 mid-chain dihydroxy compound, respectively. One could speculate that the original C_{29}, C_{30} and C_{32} triols were the product of acyl reduction rather than of decarboxylation. Most of the ω20 hydroxy compounds biosynthesized by *Azolla* have carbon isotopic compositions that are within 2‰ of the ^{13}C value of the C_{32} 1,ω20 diol. This suggests that these compounds are biosynthesized via chain elongation of the same pool, or isotopically similar pools of acetate.

2.3.6 Comparison between extant *Azolla* and Eocene samples

In both the extant *Azolla* and the ACEX sediments the 1,ω20 diols are the most abundant of the ω20 compounds. Fig. 2.6 shows the m/z 369 chromatograms for the diol fractions obtained from TLC of extant *Azolla* and ACEX sediment. Both traces display exactly the same series of C_{30}– C_{36} diols, with almost identical distributions. In both cases, the C_{32} 1,13 diol is the predominant homologue. This strongly suggest that the 1,ω20 diols in the ACEX sediments were originally biosynthesized by *Azolla* species thriving in the Eocene Arctic Ocean. In Table 2.3, concentrations and relative abundances of the 1,ω20 diols are shown for fresh *Azolla* and an ACEX sediment. In total, they comprise for *Azolla* 440 μg/g dry wt. In the ACEX sediment the concentrations are lower, with a total of 4.2 μg/g sediment, which is the equivalent to 110 μg/g TOC. After saponification of the extracted residues, additional diols are released, increasing the total amount of extracted diols, both for extant *Azolla* and ACEX sediment, indicating that they are also present as ester-bound moieties. This is consistent with the discovery of the corresponding wax esters as described above. In the saponified fractions the relative abundances of the 1,ω20 diols vary slightly. However, the C_{32} homologue is always the most abundant. Concentrations of ω20 hydroxy mid-chain FAs and ω20 alkanols are much lower and their abundances could not be determined because of co-elution with each other. Mass chromatograms of m/z 369 for a total lipid fraction of *Azolla* and an ACEX sediment are shown in Fig. 2.7. In the ACEX sediments the 15 hydroxy C_{34} and 17 hydroxy C_{36} FAs are the most abundant FA homologues (Fig. 2.7). There is little variation

Table 2.3: Comparison of concentrations and relative abundances of 1,ω20 diols for both extant *Azolla* and ACEX (sample 1) extracts.

	concentration (μg/g dry wt *Azolla*)	concentration (μg/g TOC ACEX)	rel. abundance (*Azolla*)	rel. abundance (ACEX)
1,11 C_{30} diol	14	2.9	0.1	0.06
1,13 C_{32} diol	180	51	1.0	1.0
1,15 C_{34} diol	130	31	0.6	0.6
1,17 C_{36} diol	120	21	0.5	0.4

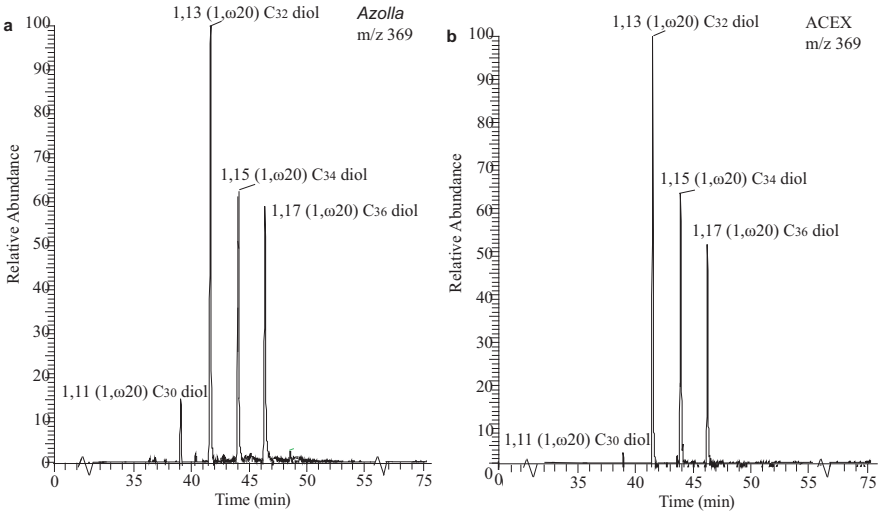

Figure 2.6: Partial mass chromatogram (35–55 min) of m/z 369 for selected TLC bands of fresh *Azolla* and ACEX extracts, displaying the distributions of the 1,ω20 C_{30}–C_{36} diols.

in total and relative abundances of the ω20 compounds amongst the total extracts from different *Azolla* samples. Between the different ACEX sediments, variations were larger. This could point to different burial conditions or varying *Azolla* species compositions. The keto-1-ols were found exclusively in the ACEX samples and not in extant *Azolla*. This suggests that the keto-1-ols may be post-depositional oxidation products of the corresponding diols (cf. Sinninghe Damsté et al., 2003; Ferreira et al., 2001). Although the biosynthesis of keto-ols has been reported for other organisms (Jetter and Riederer, 1999), they are not biosynthetically formed by *Azolla.* All wax esters encountered in extant *Azolla* specimens were also found in the Eocene Arctic sediments, except for the C48 ω20,ω21 dihydroxy wax ester (Table 2.1).

The mere presence of the highly functionalized ω20 hydroxy compounds in the Eocene ACEX samples reflects the excellent preservation potential of these relatively labile wax lipids over a period of 50 Myr. Based on their degradation rates, selected lipids from sediments were ranked according to their relative reactivity by Sun and Wakeham (1994) and Canuel and Martens (1996). They established that FAs are more prone to degradation than sterols and *n*-alkanols, which in turn are more reactive than *n*-alkanes, long-chain alkenones, long-chain alkyl diols and long-chain alkyl keto-ols. The degree of preservation for different biomarkers also depends strongly on oxygen exposure time (Sinninghe Damsté et al., 2002). It was shown for C_{30} 1,15-diols that they have lower accumulation rates under oxic conditions than under anoxic conditions (Sinninghe Damsté et al., 2002). All the compounds described seem to be equally well preserved as only the C_{29} 1,20,21 triol,

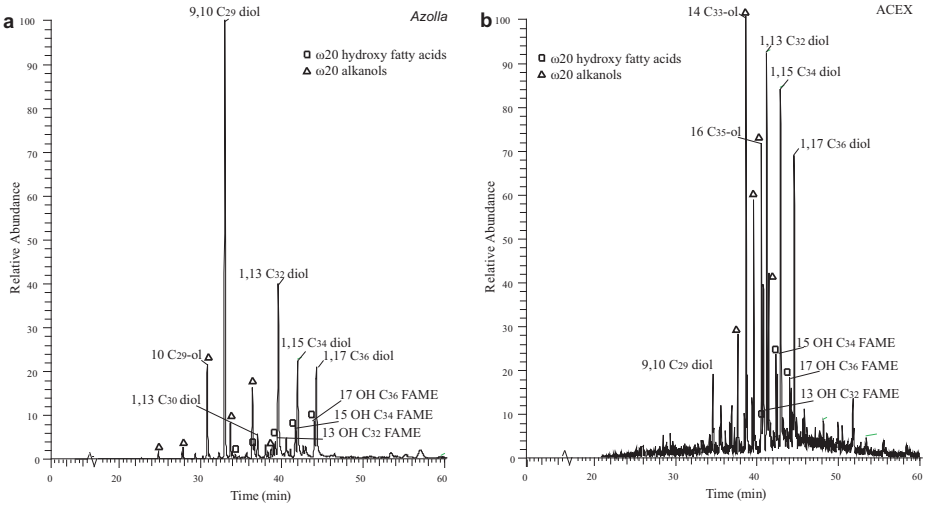

Figure 2.7: M/z 369 chromatograms for (a) total extract of extant *Azolla Filiculoides* and (b) ACEX sediment, showing distribution of ω20 hydroxy lipids. Since the ACEX extract also contains many other compounds with 369 fragments, a larger number of peaks and co-elution of some of the ω20 compounds (mainly with the ω20 alkanols) is observed.

C_{29} 20,21 dihydroxy FA and the C_{48} ω20,ω21 dihydroxy wax ester could, at least for these samples, not be found in the ACEX core sediments. Only minor amounts of ω20 diols were transformed to the corresponding keto-ols. This means that virtually all ω20 hydroxy compounds have been preserved, at least in part, over the last 50 Ma. The combination of the relative resistance to biodegradation of the compounds and the characteristic ω20 hydroxy functionality, make them highly valuable biomarkers for *Azolla*.

2.4 Conclusions

Novel and unique series of 1,ω20 long chain mid-chain diols, ω20 mid-chain hydroxy FAs and ω20 alkanols have been encountered in Middle Eocene Arctic Sediments. The same series of compounds are biosynthesized by the aquatic floating fern *Azolla filiculoides*. Furthermore, several intact wax esters, consisting of a C_{16} FA and different hydroxy compounds were present in both extant *Azolla* and in ACEX sediments. These included the ω20 mono-hydroxy C_{46}, C_{48}, C_{50} and C_{52} wax esters, the C_{46} ω20,ω21 dihydroxy wax ester and a C_{45} ω9,ω10 dihydroxy wax ester. In addition, structurally related C_{29} compounds, including the C_{29} 1,20,21 triol and C_{29} 20,21 dihydroxy FA, biosynthesized by the fern, as well as the C_{29} ω20,ω21 diol, encountered in both extant *Azolla* and ACEX samples, were found. The ω20 mid-chain keto-1-ols were only found in the ACEX sediments. The similar chain length and isomer distributions of all the ω20 hydroxy compounds encountered

suggest a common origin and biosynthetic pathway. The substantially stable ^{13}C isotope depletion of the ω20 diols and C_{29} compounds, relative to the measured β-sitosterol, can be explained by a different biosynthetic pathway for these two compound classes. Based on the selective extraction of the C_{29} compounds from the wax layers of extant *A. filiculoides*, it seems most likely that the ω20 compounds originate from the epicuticular wax layers of *Azolla* and not from endosymbiotic cyanobacteria. The total diol content of extant *Azolla* averages around 450 μg/g dry wt for the investigated samples. In the Arctic core sediments the diols were also found in exceptionally high abundance, with a maximum for the 1,13 C_{32} diol of 2.0 μg/g sediment, corresponding to 80 μg/g TOC.

Based on the uniqueness of the ω20 hydroxy compound series and the relatively low biodegradation rates, the compounds can be considered to be excellent biomarkers for *Azolla*. The presence of these ω20 compounds in both extant *Azolla* samples and in the ACEX sediments provides complementary molecular evidence for the remarkable discovery of *Azolla* blooms in a freshwater Eocene Arctic setting (Brinkhuis et al., 2006). Moreover, compound specific δD and ^{13}C measurements of these biomarkers will facilitate the reconstruction of environmental conditions and carbon and hydrogen cycling during the Eocene Arctic *Azolla* interval.

Acknowledgements

The research used samples and data provided by the Integrated Ocean Drilling Program (IODP). Funding was provided by the DARWIN Centre for Biogeology and Utrecht University. The authors specifically wish to thank M. van Kempen (MSc) for collecting and culturing the extant *Azolla filiculoides* samples and two anonymous reviewers for constructive comments.

Chapter 3

Fossilized glycolipids reveal past oceanic N_2 fixation by heterocystous cyanobacteria

Thorsten Bauersachs, Eveline N. Speelman, Ellen C. Hopmans, Gert-Jan Reichart, Stefan Schouten, and Jaap S. Sinninghe Damsté

Published in: PNAS, in press

Abstract

N_2-fixing cyanobacteria play an essential role in sustaining primary productivity in contemporary oceans and freshwater systems. However, their significance in past nitrogen cycling is difficult to establish as their preservation potential is relatively poor and specific biological markers are presently lacking. Heterocystous N_2-fixing cyanobacteria synthesize unique long-chain glycolipids in the cell envelope covering the heterocyst cell to protect the oxygen-sensitive nitrogenase enzyme. We found that these heterocyst glycolipids are remarkably well preserved in (ancient) lacustrine and marine sediments, unambiguously indicating the (past) presence of N_2-fixing heterocystous cyanobacteria. Analysis of Pleistocene sediments of the eastern Mediterranean Sea showed that heterocystous cyanobacteria, likely as epiphytes in symbiosis with planktonic diatoms, were particularly abundant during deposition of sapropels. Eocene Arctic Ocean sediments deposited at a time of large *Azolla* blooms contained glycolipids typical for heterocystous cyanobacteria presently living in symbiosis with the freshwater fern *Azolla*, indicating that this symbiosis already existed in that time. Our study thus suggests that heterocystous cyanobacteria played a major role in adding 'new' fixed nitrogen to surface waters in past stratified oceans.

3.1 Introduction

The global nitrogen cycle largely relies on biological nitrogen fixation to maintain biological productivity with some 1.4 to 2.4 Tmol of combined nitrogen being annually added to the marine nitrogen budget, counteracting the loss of bioavailable nitrogen through processes such as denitrification and anaerobic ammonium oxidation (anammox) (Deutsch et al., 2007). The filamentous cyanobacterium *Trichodesmium* sp. (Capone et al., 2005) and unicellular cyanobacteria (Church et al., 2008) are considered to be the major N_2-fixers in the contemporary open ocean. Since the nitrogenase enzyme, utilized to convert N_2 into NH_4^+, is sensitive towards molecular oxygen, some groups of N_2-fxing cyanobacteria perform photosynthesis separate in time from N_2-fixation, while another subgroup performs the fixation of N_2 in specialized cells, so-called heterocysts, to protect the oxygensensitive nitrogenase enzyme. Heterocystous cyanobacteria are often dominant diazotrophs in many freshwater and brackish environments such as the Baltic Sea (Ploug, 2008) whereas in the marine environment they mainly occur in symbiosis with diatoms (Villareal, 1992). Although the importance of N_2-fixing cyanobacteria in sustaining primary productivity in modern aquatic environments is clearly evident, their importance in ancient nitrogen cycling is less clear. Microfossils of heterocystous cyanobacteria have been found in a number of ancient rocks, documenting their evolutionary history (e.g. Tomitani et al., 2006) but their preservation potential, especially in open ocean settings, is relatively poor. Cyanobacteria have been suggested to be major primary producers during times of strong ocean stratification such as during the formation of Pleistocene Mediterranean sapropels (Sachs and Repeta, 1999) and Cretaceous black shales (Kuypers et al., 2004; Rau et al., 1987) based on the depletion of ^{15}N of bulk organic matter and chlorins, which is commonly associated with the relatively small isotopic fractionation of diazotrophs (Wada and Hattori, 1976). For the Cretaceous black shales, elevated concentrations of 2-methyl hopanes, general markers for cyanobacteria (Summons et al., 1999), have also been reported (Kuypers et al., 2004). In combination, these proxies suggest that diazotrophic cyanobacteria may have been important in replenishing the reservoir of combined nitrogen during the formation of these organic-rich marine deposits.

3.2 Materials and methods

3.2.1 Sample collection:

The heterocystous cyanobacterium *Anabaena* CCY9613 was grown as an axenic batch culture on the freshwater medium BG11 (Rippka et al., 1979). In order to induce the formation of heterocysts, combined nitrogen sources were omitted from the media. The culture was inoculated in 250 mL Erlenmeyer flasks containing 100 ml of sterile medium and maintained at an alternating 12:12 h light-dark regime

with a light intensity ranging between 5 and 30 μmol m^2/s. The culture was grown at a temperature of 14 °C. *Azolla filiculoides* was initially collected from a ditch near arable land in the surroundings of Elst, The Netherlands (N51°55'48"; E5°50'6") and further cultivated under semi-controlled conditions. Also for *Azolla* the nutrient solution used did not contain a fixed source of nitrogen.

Pleistocene sapropels (S1 and S5) were collected from the piston core MS66PC, recovered from the deep-sea Nile fan, Eastern Mediterranean (location: 33N1.9' 31E47.9') in 2004 during the MIMES MEDIFLUX program. The core was sub-sampled onboard and the 10 sediments were placed in sterile 50 ml Greiner tubes and frozen at -40 °C immediately. Sediment samples from the Eocene *Azolla* interval were obtained from lithological Unit 2, Core M0004A- 11x taken during the IODP 302 ACEX expedition at the Lomonosov Ridge, 87.87 °N, 136.18 °E (Backman et al., 2006). In this study we used sediments from 300 to 302.63 mbsf, covering part of the *Azolla* interval (Brinkhuis et al., 2006). These and sediments of other locations were generally stored at -20 °C prior to analysis.

3.2.2 Analysis of bulk geochemical parameters and isotopes.

Total organic carbon (TOC), stable carbon isotopes of organic matter (δ^{13}CTOC) and bulk stable nitrogen isotopes (δ^{15}N) were analyzed in duplicate on a ThermoScience Delta Plus isotope ratio mass spectrometer connected on-line to a Carlo Erba Instruments Flash 1112 elemental analyzer. Samples for TOC and δ^{13}CTOC measurements were treated with 2 M hydrochloric acid, neutralized and freeze-dried prior to analysis. The δ^{13}CTOC is given relative to the Vienna PeeDee Belemnite (VPDB) standard and the δ^{15}N of each sample is expressed relative to atmospheric dinitrogen. Precision is better than ±0.1‰ for carbon and ±0.2‰ for nitrogen.

3.2.3 Extraction of heterocyst glycolipids.

Heterocyst glycolipids were extracted as previously described by Bauersachs and co-workers (2009a). Briefly, freeze-dried cell material (30-50 mg) was extracted using a modified Bligh and Dyer extraction procedure (Bligh and Dyer, 1959; Rütters et al., 2002). Freeze-dried sediments (1-5 g) were extracted using the accelerated solvent extraction (ASE) technique with a solvent mixture of dichloromethane (DCM):methanol (MeOH; 3:1 v/v) at high temperature (100 °C) and pressure (20 kPa). The extraction efficiencies of the different extraction methods used in this study were found to be similar for all heterocyst glycolipids (see SI text). The bulk of the solvent was first removed by rotary evaporation under vacuum and the remaining extract was subsequently dried under a stream of nitrogen. The residue was dissolved by sonication (10 min) in DCM/MeOH (9:1, v/v) through a 0.45 μm regenerated cellulose (RC) filter (Alltech, Deerfield, IL) prior to HPLC/MS-MS analysis. Procedure blanks were produced with each extraction session and ana-

lyzed along with the samples as described below: none of the blanks showed peaks above three times the background level.

3.2.4 Development of HPLC/MS-MS method.

Normal-phase HPLC analysis of extracts was accomplished using an Agilent 1100 series LC (Agilent, San Jose, CA) coupled to a Thermo TSQ Quantum ultra EM triple quadrupole mass spectrometer with an Ion Max Source with ESI probe (Thermo Electron Corporation, Waltham, MA) operated in positive ion mode following details published earlier (Bauersachs et al., 2009a, Sturt et al., 2004) with some modifications. Briefly, separation was achieved on a LiChrospher Diol column (250 mm × 2.1 mm i.d., 5 μm: Alltech, Deerfield, IL) maintained at 30 °C. Injection volumes ranged from 1 μl for cultures to 10 μl for sediments. Heterocyst glycolipids were eluted using the following linear gradient with a flow rate of 0.2 mL/min: 90% eluent A to 70% eluent A – 30% eluent B in 10 min and held for 20 min, followed by 70% eluent A to 35% eluent A – 65% eluent B in 15 min and held for 15 min, subsequently back to 90% eluent A in 1 min and held for 20 min to re-equilibrate the column. Eluent A was composed of hexane/isopropanol/formic acid/14.8 M aqueous NH_3 (79:20:0.12:0.04, v/v/v/v) and eluent B was isopropanol/water/formic acid/14.8 M aqueous NH_3 (88:10:0.12:0.04, v/v/v/v).

HPLC/MS-MS analysis was performed in selective reaction monitoring (SRM) mode. SRM transitions were optimized by direct infusion experiments of culture extracts containing the various HGs of interest. Table S3.3 lists the protonated molecular and selected product ions and respective collision energies for maximal abundance for each of the monitored HGs. The selectivity of the newly developed SRM method was demonstrated on cyanobacterial cultures previously shown to contain HGs as dominant compounds, i.e. *Anabaena* CCY9613, *Nostoc* CCY0012 and *Calothrix* CCY9923 (Bauersachs et al., 2009a). Fig. S3.3 depicts the heterocyst glycolipid distribution of *Anabaena* CCY 9613 as analyzed in data dependend full scan mode (panel A) and under SRM conditions (panel B). Retention times of the various HGs were verified by repeated analysis of two cultures containing all analyzed HGs at the start of each analytical sequence. Solvent and procedure blanks were monitored at regular intervals to detect potential cross contamination and prevent false positive identifications of HGs.

3.3 Results

In this study, we employed biological markers specific for heterocystous N_2-fixing cyanobacteria to examine the importance of these diazotrophs in recent and ancient nitrogen cycling. In heterocystous cyanobacteria the oxygen-sensitive nitrogenase enzyme is protected by laminated layers of heterocyst glycolipids (HGs) that are

part of the heterocyst cell envelope (Walsby, 2007). These components consist of long-chain diols, triols, keto-ols and keto-diols that are glycosidically bound to hexose molecules (see Fig. S3.1) (Gambacorta et al., 1998; Bauersachs et al., 2009a). To the best of our knowledge, HGs have not been reported in any other organism and thus they represent excellent tracers not only for heterocystous cyanobacteria but also for the N_2 fixation process itself. In order to establish the applicability of heterocyst glycolipids as biological markers, we developed a sensitive HPLC-MS^2 technique based on previously published methods (Bauersachs et al., 2009a) to allow their detection in complex matrices (see 3.5 Materials and Methods). In this way, C_{26} (I; Fig. S3.1) and C_{28} HG diols (III) with distributions similar to those found in pure cultures of the heterocystous cyanobacteria *Anabaena* sp. and *Nodularia* sp. (Bauersachs et al., 2009b) were detected in microbial mats from the North Sea barrier island Schiermonnikoog (Table S3.1). We then determined the fate of HGs by screening sediments from a number of modern environments, known to host heterocystous cyanobacteria, for the presence of HGs (see SI text). Analysis of particulate organic matter from surface waters of an East African crater lake (Lake Challa), where heterocystous cyanobacteria are part of the phytoplankton community, revealed the presence of the C_{26} HG diol (I; Fig. 3.1).

This HG was also present in Lake Challa's sinking particulate organic matter collected by a sediment trap at 35 m water depth and in the upper 10 m of sediments of this lake (Fig. 3.1; Table S3.1), revealing that HGs are preserved in the sedimentary record. We also detected HGs in Baltic Sea sediments buried up to 34 m deep (Table S3.1). In this brackish coastal sea, heterocystous cyanobacteria form an important component of the phytoplankton community in present-day surface waters (Ploug, 2008). In contrast, HGs were not detected in sediments of contemporary open oceans, in agreement with the observation that heterocystous cyanobacteria represent only a small fraction of the phytoplankton assemblage in open marine environments (Hoffmann, 1999). Hence, the presence of HGs in sediments reflects the (past) presence of heterocystous N_2-fixing cyanobacteria. HGs were also detected in a number of ancient lacustrine deposits, ranging in age from Holocene to Eocene (Table S3.2), again attesting to the excellent preservation potential of these components. Sediments from all these locations accumulated under anoxic conditions in stratified freshwater lakes that were oligotrophic and likely permitted proliferation of N_2-fixing cyanobacteria. The presence of HGs in these ancient sediments is remarkable, given that glyceride lipids with glycosidic head groups are thought to be rapidly degraded and not preserved over geological time scales (Arnosti and Jørgensen, 2006). However, microbially-mediated degradation experiments and theoretical modelling shows that glycosidic ether lipids are more recalcitrant towards degradation than membrane lipids with a phospho-head group (Harvey et al., 1986; Schouten et al., 2010). Interestingly, the dominant intact polar lipids found in subsurface sediments are glycosidic derivatives of archaeol and

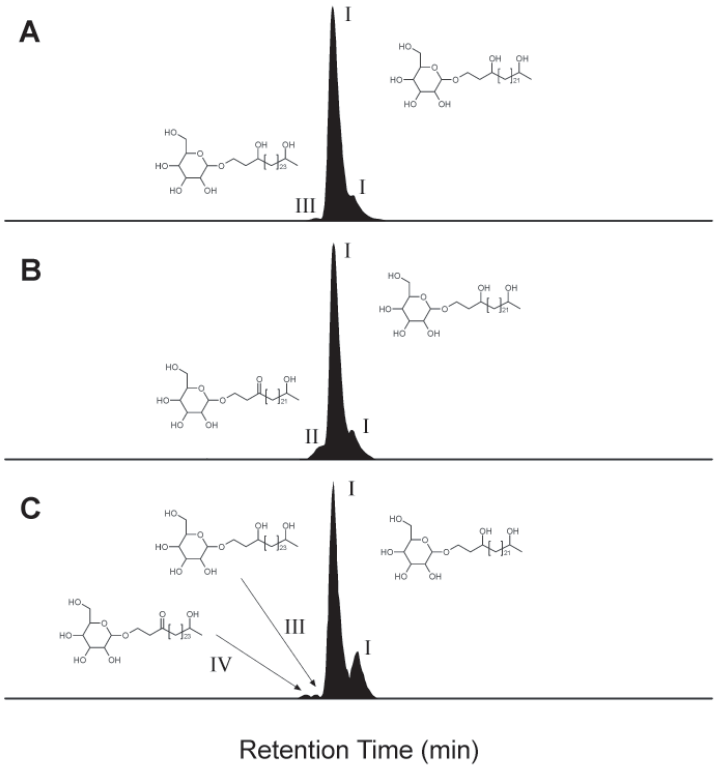

Figure 3.1: HPLC/ESI-MS/MS summed ion chromatograms of SRM transitions of heterocyst glycolipids in (A) particulate organic matter (1 m water depth), (B) sediment trap (35 m water depth) and (C) sediment (10 m depth) taken from Lake Challa. The heterocyst glycolipid distribution is dominated 1-(O-hexose)-3,25-hexacosanediol (I), while 1-(O-hexose)-3-keto-25- hexacosanol (II), 1-(O-hexose)-3,27-octacosanediol (III), 1-(O-hexose)-3-keto-27-octacosanol (IV) and an unknown isomer (possibly with a different sugar moiety) of 1-(O-hexose)-3,25- hexacosanediol (I') were detected in lower abundances. Note that the heterocyst glycolipid distribution is relatively similar in the particulate organic matter, sediment trap material and subsurface sediment suggesting no preferential degradation of individual glycolipids.

glycerol dibiphytanyl glycerol tetraether lipids (Lipp et al., 2008), which contain glycosidically bound sugar head groups similar to those in heterocyst glycolipids. The presence of fossil HGs in sediments, thus, raises the question whether certain intact polar lipids, especially those with glycosidic head groups, may be more recalcitrant than previously thought and possibly constitute a significant fossil component of the subsurface sedimentary intact polar lipid pool (Pearson, 2008).

3.4 Discussion

The ability to detect specific markers for the past presence of N_2-fixing cyanobacteria raises the exciting possibility to determine their paleoecology and their role in past nitrogen cycling. We illustrate this approach by examining the role of heterocystous cyanobacteria in the Pleistocene Eastern Mediterranean Sea and the Eocene Arctic Ocean.

3.4.1 Heterocystous cyanobacterial N_2-fixation in the Pleistocene eastern Mediterranean

During the Quaternary, the Mediterranean Sea was occasionally strongly impacted by the input of large amounts of freshwater, leading to the development of a low salinity surface layer and hence strong stratification of the upper part of the water column (Rossignol-Strick et al., 1982; Thunell et al., 1984). These conditions have led to nutrient depletion and thus possibly favoured the proliferation of N_2-fixing cyanobacteria (Sachs and Repeta, 1999). Indeed, the C_{26} (I) and C_{28} HG diols (III) were detected in sediments deposited at the onset of sapropel S1 and S5 formation, while they were either absent or only present in trace amounts in the adjacent organic-poor sediments (Table S3.2; Fig. 3.2). Maxima in the HG abundances within the S5 sapropel layer correlate well with lowest bulk nitrogen isotope values ($\delta^{15}N$ = -0.5‰), providing for the first time direct proof for past N_2 fixation by heterocyst cyanobacteria during the formation of Pleistocene sapropels. HGs were also identified within the boundaries of the S1 sapropel, albeit in lower abundances, in agreement with less depleted bulk $\delta^{15}N$ values (+0.4‰). Some differences in the distribution of the individual HGs in the S1 and S5 sapropels are noted (Table S3.2), which may either reflect adaptations to different environmental conditions, such as temperature and oxygen concentration (Bauersachs et al., 2009b), or contributions of different heterocystous cyanobacteria (Bauersachs et al., 2009b) at times of sapropel formation.

The presence of HGs in the sapropel layers is direct proof that heterocystous N_2-fixing cyanobacteria played a prominent role in the N-cycle in the eastern Mediterranean Sea during sapropel formation. These heterocystous cyanobacteria may have been free-living species as found in freshwater and brackish environments like the Baltic Sea (Villareal, 1992). Under open marine conditions, however, free-living heterocystous species have only been reported in a few occasions (Carpenter and Janson, 2001), but they can form massive blooms as endosymbionts of diatoms such as *Rhizosolenia* sp. and *Hemiaulus* sp. (Villareal, 1992). Reconstruction of the sea surface salinity of the Mediterranean Sea demonstrated that although surface salinity decreased substantially during sapropel deposition, it did not become truly brackish, remaining between 39-33‰ (van der Meer et al., 2007). Given these still typical marine salinities of the surface waters at the time of sapropel deposition, it is likely that heterocystous cyanobacteria living in association with diatoms, rather

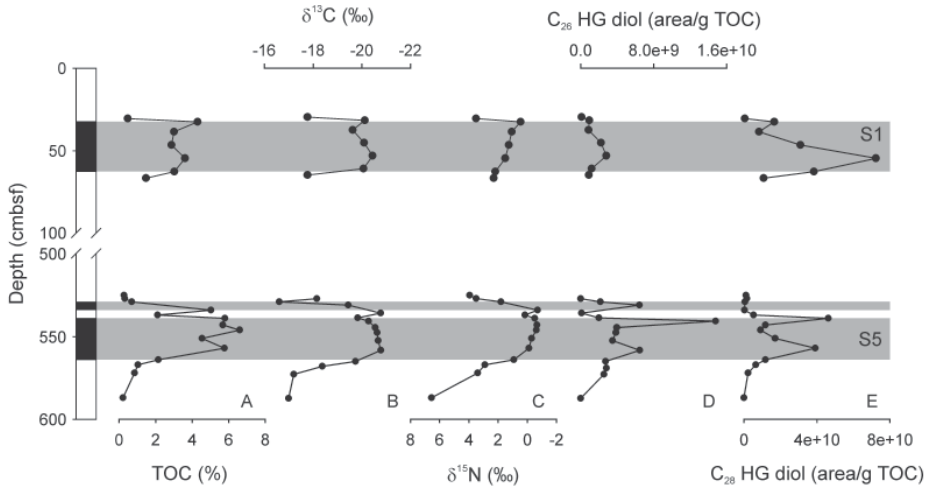

Figure 3.2: Depth profile of the Eastern Mediterranean piston core MS66PC, showing the core and stratigraphic profiles of (A) total organic carbon (TOC), (B) stable carbon isotopes or organic matter (δ^{13}CTOC), (C) bulk stable nitrogen isotopes (δ^{15}N), concentrations of (D) 1-(O-hexose)- 3,25-hexacoasanediol (C_{26} HG diol) and (E) 1-(O-hexose-)-3,27-octacosanediol (C_{28} HG diol). Grey shaded intervals represent S1 and S5 sapropel layers. The increased concentrations of the heterocyst glycolipids at times of sapropel deposition coincide with a depletion of ^{15}N suggesting enhanced dinitrogen fixation (cf. Sachs and Repeta, 1999).

than free-living heterocystous species, were the important class of N_2-fixers. High concentrations of diatoms have previously been reported from the S5 layer and invoked to explain the organic-rich nature of this deposit (Kemp et al., 1999). Therefore, it is likely that symbiotic heterocystous cyanobacteria played a major role in sustaining primary production during sapropel formation by providing a source of 'new' combined nitrogen.

3.4.2 Azolla-Nostocaceae symbiosis in the Eocene Arctic Ocean

Ocean Early/Middle Eocene sediments from the central Arctic Ocean were found to contain abundant remains of *Azolla* megaspores and microspore massulae as well as *Azolla*-specific biomarkers (Brinkhuis et al., 2006; Chapter 2). The fact that the free floating aquatic fern *Azolla* grew and reproduced in the Eocene Arctic (Brinkhuis et al., 2006) is strong evidence that the surface waters of the Arctic Basin freshened considerably as *Azolla* cannot thrive at high salinities (>3; van Kempen et al., under review). At the same time, bottom waters appear to have remained saline, facilitating deep-water anoxia and salinity stratification (Brinkhuis et al., 2006; Stickley et al., 2008; Chapter 7). The *Azolla* interval is characterized by TOC values between 3 and 6 wt%, co-varying with *Azolla* spore abundance (Fig. 3.3). Bulk sedimentary nitrogen isotope ratios are persistently low, between -0.7 and

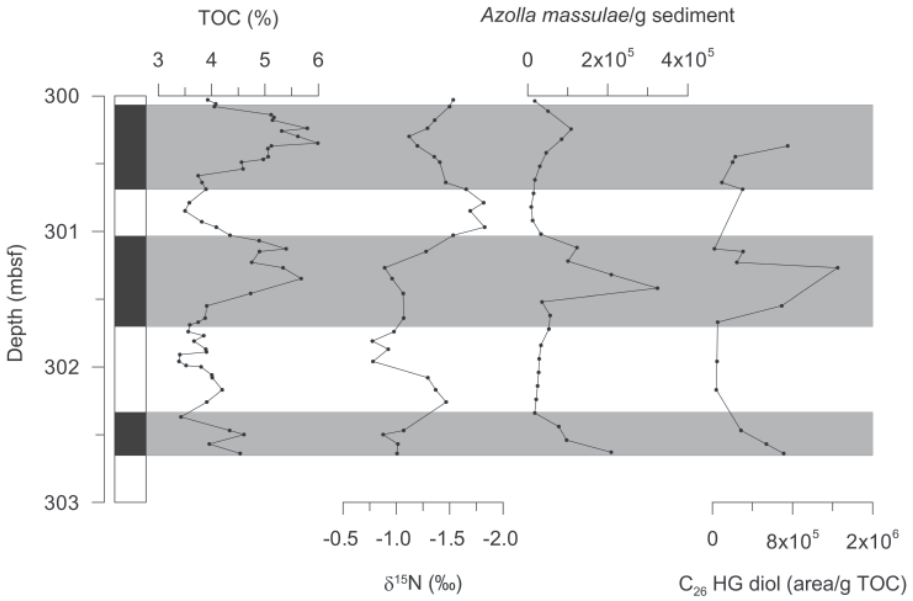

Figure 3.3: Depth profile of the Arctic Coring Expedition (ACEX), IODP leg 302 Hole 4A, Core 11x from the Middle Eocene Arctic ocean showing the stratigraphic profiles of (A) total organic carbon (TOC), (B) *Azolla* megaspore counts, (C) bulk stable nitrogen isotopes ($\delta^{15}N$), and concentrations of (D) 1-(O-hexose)-3,25-hexacoasanediol (C_{26} HG diol). Grey shaded intervals represent layers of enhanced *Azolla* abundance (see Speelman et al., 2009 for further details).

-2.4 ‰, throughout the *Azolla* interval, and average around -1‰ at peak *Azolla* occurrences (Fig. 3.3). These values are consistent with the reported nitrogen isotopic composition of diazotrophic cyanobacteria (Wada and Hattori, 1976) and cultured *Azolla* biomass with a similarly low average $\delta^{15}N$ of -1.5‰ (Chapter 8). They are also substantially lower than $\delta^{15}N$-values in the Early Eocene Arctic Ocean preceding the *Azolla* interval which range from +1 to +4‰ (Knies et al., 2008). Hence, the encountered $\delta^{15}N$ values point towards the presence of N_2-fixing organisms during the Early/Middle Eocene *Azolla* interval in the Arctic Ocean.

Extant *Azolla* species are known to live in symbiosis with N_2-fixing heterocystous cyanobacteria of the genera *Nostoc* and *Anabaena* (Braun-Howland and Nierzwicki-Bauer, 1990). These symbionts are located inside a highly specialized cavity in the dorsal leaf lobe of *Azolla* and provide the fern with fixed organic nitrogen. Through the symbiosis the aquatic fern *Azolla* is not limited by fixed nitrogen availability (Braun-Howland and Nierzwicki-Bauer, 1990), thus facilitating rapid growth (Peters and Meeks, 1989; Wagner, 1997). Indeed, analyses of extracts of extant *Azolla filiculoides* show the presence of 1-(O-hexose)-3,25-hexacosanediol (C_{26} HG diol) (I) and its corresponding keto-ol (II) (Table S1), the predominant glycolipids in the family of Nostocaceae (Bauersachs et al., 2009a). To investigate whether *Azolla*

lived already in symbiosis with N_2-fixing cyanobacteria in the Eocene, we analysed Early/Middle Eocene sediments from the central Arctic Ocean (IODP site 302, Lomonosov Ridge), containing abundant remains of *Azolla*, for their HG content. We detected the C_{26} diol HG in the sediments and found that HG concentrations co-varied with *Azolla* abundance throughout the interval (Fig. 3.3). The HGs were absent after the last occurrence of *Azolla*. The good correlation between the *Azolla* megaspore counts and HG abundance, and the similar distribution of HGs in the Eocene sediments and extant *Azolla* suggests that the symbiotic relationship between *Azolla* and diazotrophic cyanobacteria of the family of Nostocaceae was already established in the Early/Middle Eocene. Furthermore, in view of the inferred marine setting of the site during the Eocene, atmospheric nitrogen fixation by these N_2-fixing heterocystous symbiotic cyanobacteria probably played an important role in supplying fixed nitrogen and sustaining *Azolla* growth in the strongly stratified Eocene Arctic Ocean. However, negative ^{15}N-values are also observed during times of low *Azolla* counts and HG concentrations, as observed previously (Chapter 8), suggesting that N_2-fixation was a persistent feature at these times (Chapter 8; Knies et al., 2008).

3.5 Conclusions

Our results show that HGs can be preserved in ancient sediments of up to 49 Ma old where they serve as unique biomarker lipids of N_2-fixing heterocystous cyanobacteria, enabling to trace the past ecology of these microbes. Screening of ancient sediments showed that these diazotrophs have played an important role in the nitrogen cycling of past stratified marine and freshwater environments, including those in past greenhouse worlds such as the Eocene.

Examples from the Pleistocene eastern Mediterranean and the Eocene Arctic Ocean illustrate that heterocystous cyanobacteria, likely in symbiosis with diatoms and the freshwater fern *Azolla*, respectively, have played a key role in supplying newly fixed nitrogen to these past stratified marine systems.

Acknowledgements

We thank three anonymous reviewers and the Editor for comments which improved this manuscript. Financial support for this research was provided by the Darwin Center for Biogeosciences, the Royal NIOZ and the University of Utrecht awarded to JSSD and GJR. GJR acknowledges Statoil for additional financial support. Sediments were recovered from Lake Challa as part of the CHALLACEA project. Sediments from the Eocene Arctic were provided by the Integrated Ocean Drilling Program (IODP). H. Vogel, B. Wagner, M. Melles, P. De Deckker, C. Slomp, H. Mort, J. Werne, Y. van Breugel, J. Weijers, D. Verschuren, G. de Lange and L.

Schwark are acknowledged for supplying a number of the studied sediments, L. Stal and J. Campaore for providing cyanobacterial cultures and M. van Kempen for providing cultured *Azolla*.

Supplementary Information

Effects of extraction method on HG recovery

The relative extraction efficiencies of HGs using three different extraction procedures were determined, i.e. ultrasonic extraction with DCM:MeOH (2:1; ×4), Bligh & Dyer extraction (Rütters et al., 2002) and accelerated solvent extraction (ASE). Roughly equal amounts (ca. 1.5 g) of surface sediments from the North Sea barrier island Schiermonnikoog (The Netherlands) were extracted with these three techniques and identical amounts of the resulting HG fractions were injected on the HPLC/MS-MS allowing comparison of the relative amounts of HGs obtained by each extraction technique. The measured relative signal intensities per gram sediment for the individual heterocyst glycolipids of ASE extraction and ultrasonic extraction were normalized to those of the Bligh & Dyer procedure (Supplementary Fig. S3.4). This revealed that, despite the high pressure and temperature, ASE extraction yields similar or even higher recovery of HGs than the generally used procedure for IPL analysis, i.e. the Bligh & Dyer extraction. We then tested the general stability of IPLs under ASE conditions by extracting cyanobacterial biomass, containing intact polar lipids with glycosidic and phosphate head groups (Supplementary Fig. S3.5). This showed that heterocyst glycolipids are stable under ASE conditions but that the other IPLs decrease substantially using this technique. Hence, ASE extraction is a suitable technique to investigate HGs in ancient sediments.

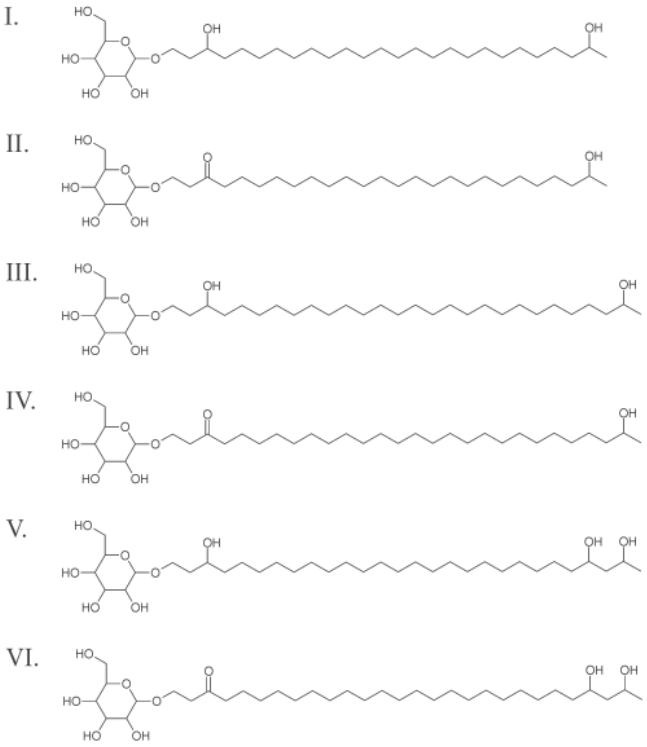

Supplementary Figure S3.1: Structures of heterocyst glycolipids detected in cultures and environmental samples.
1-(O-hexose)-3,25-hexacosanediol (I); 1-(O-hexose)-3-keto-25-hexacosanol (II);
1-(O-hexose)-3,27-octacosanediol (III); 1-(O-hexose)-3-keto-27-octacosanol (IV);
1-(O-hexose)-3,25,27-octacosanetriol (V) and 1-(O-hexose)-3-keto-25,27-octacosanediol (VI).

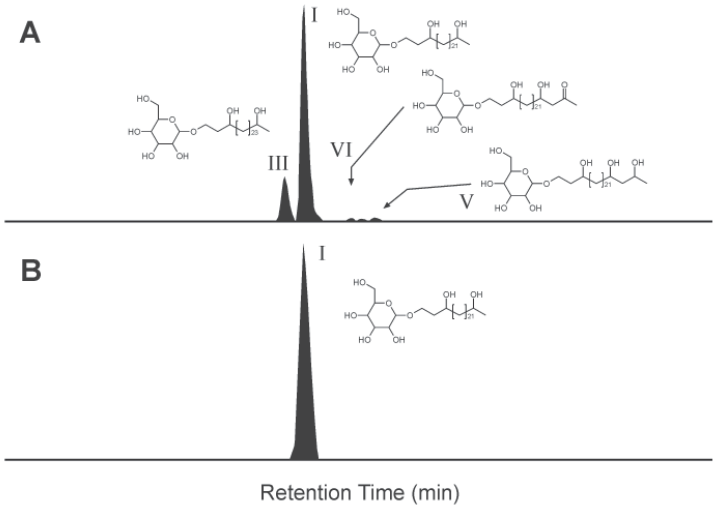

Supplementary Figure S3.2: HPLC/MS-MS chromatograms of extracts of sediments from the (A) Oligocene Lake Enspel and (B) Eocene Lake Messel. Note that the 47 Ma old sediments of Lake Messel only contained 1-(O-hexose)-3,25-hexacosanediol (I), which was also the only HG detected in the Eocene Green-River Formation. In contrast, the Oligocene sediments of Lake Enspel are characterized by six different HGs (see Table S1).

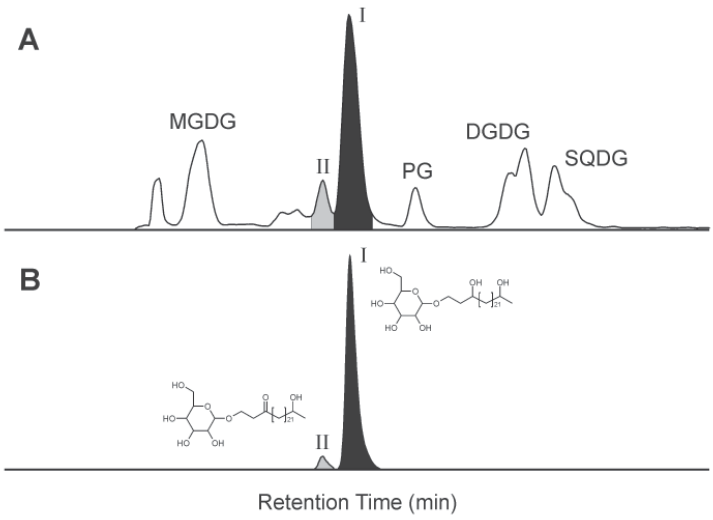

Supplementary Figure S3.3: Comparison of HG distributions in *Anabaena* CCY9613 using (A) full scan and (B) selected reaction monitoring (SRM) chromatograms. MGDG = monoglycoside diacylglycerols, DGDG = diglycoside diacylglycerols, PG = phosphoglycerol diacylglycerols, SQDG = sulfoquinosovyl diacylglycerides.

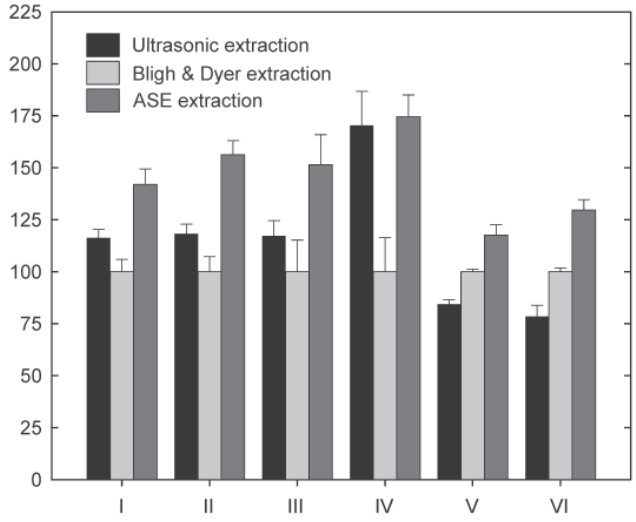

Supplementary Figure S3.4: Effect of different extraction procedures on the relative heterocyst glycolipid recovery. Accelerated solvent extraction (ASE) and ultrasonic extraction are normalized to extraction yields from the Bligh & Dyer procedure. Note that ASE yielded highest extraction efficiencies. Roman numerals refer to structures presented in Supplementary Fig. 1.

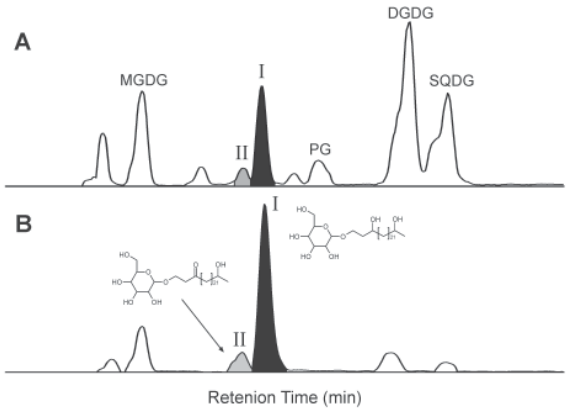

Supplementary Figure S3.5: Base peak chromatograms of full scan analysis of total lipid extracts of *Nostoc* CCY0012 extracted using (A) a modified Bligh & Dyer extraction procedure (Rütters et al., 2002) and (B) the accelerated solvent extraction (ASE) technique. Note that the diacylglycerides with phosphor polar head groups, and to a lesser extent those with a (sulphur)sugar head group, are readily degraded upon ASE extraction, while heterocyst glycolipids are seemingly not affected by the rigorous extraction procedure. MGDG = monoglycosyl diacylglycerides, DGDG = diglycosyl diacylglycerides, PG = phosphoglycerol diacylglycerides, SQDG = sulfoquinosovyl diacylglycerides.

Supplementary Table S3.1: Relative distribution of individual HGs as a percentage of total HG lipids in various cyanobacterial cultures, the freshwater fern *Azolla filiculoides* and contemporary sediments (Roman numerals refer to structures in Supplementary Fig. 3.1).

Cultures	Types	Strain	I	II	III	IV	V	VI
Anabaena sp.	Nostocaceae	CCY9402[1]	0.4	0.1	83	16	-	-
Anabaena sp.	Nostocaceae	CCY9613	95	5	0.3	-	-	-
Nostoc sp.	Nostocaceae	CCY0012[1]	97	3	0.2	0.1	-	-
Calothrix sp.	Rivulariaceae	CCY9923[1]	0.2	0.4	2	1	61	36
Azolla filiculoides	Fern		84	7	9	-	-	-
Lake/Sea	Locations	Depth/type						
Baltic Sea	Landsort Deep	Sed. (2 mbsf)	49	25	2	1	9	14
		Sed. (34 mbsf)	77	8	4	1	8	2
Black Sea		Sed. (27mbsf)	93	5	2	0.3	-	-
Kyllaren	Norway	Surface Sed.	47	40	5	8	-	-
Schiermonnikoog	The Netherlands	Intertidal flat	90	1	0.5	0.1	8	0.4
Lake Ohrid	Macedonia	Surface Sed.	10	1	66	23	-	-
Lake Malawi	Malawi	Surface Sed.	11	0.1	86	3	-	-
Lake Tanganyika	Dem. Rep. Congo	Surface Sed.	92	0.8	7	0.2	-	-
Lake Keilambete	Australia	Surface Sed.	99	0.3	0.6	0.1	-	-
Lake Challa	Kenya	POM[2]	99	<1	<1	<1	<1	<1
		Sed. Trap	91	4	3	1	<1	-
		Sediment	64	22	2	12	-	-

[1] data from Bauersachs et al. (2009b)
[2] POM = Particulate organic matter

Supplementary Table S3.2: Relative distribution of individual HGs as a percentage of total HG lipids in a number of ancient sediments (Roman numerals refer to structures presented in Supplementary Fig. S1).

Location		Age	I	II	III	IV	V	VI
Lake Enspel	Germany	Oligocene	22	1	42	27	6	2
Lake Messel	Germany	Eocene	10000	-	-	-	-	-
Green River Formation	USA	Eocene	100	-	-	-	-	-
Mediterranean Sapropel S1		Pleistocene	12	-	86	2	-	-
Mediterranean Sapropel S5		Pleistocene	22	1	75	2	-	-
ACEX core 11X		Eocene	96	4	-	-	-	-

Supplementary Table S3.3: overview of the protonated molecular and selected product ions and respective collision energies for maximal abundance for each of the monitored HGs.

Heterocyst Glycolipids	$[M+H]^+$ m/z	Product m/z	Collision Energy (V)
1-(O-hexose)-3,25-hexacosanediol (I)	577.5	379.5	15
		415.5	10
1-(O-hexose)-3-keto-25-hexacosanol (II)	575.5	377.5	15
		395.5	14
1-(O-hexose)-3,27-octacosanediol (III)	605.4	407.5	15
		443.5	10
1-(O-hexose)-3-keto-27-octacosanol (IV)	603.5	405.5	15
		423.5	14
1-(O-hexose)-3,25,27-octacosanetriol (V)	621.6	387.5	22
		405.5	18
		423.5	17
1-(O-hexose)-3-keto-25,27-octacosanediol (VI)	619.6	403.5	18
		421.5	16
		439.5	11

Chapter 4

Modeling the influence of a reduced equator-to-pole sea surface temperature gradient on the distribution of water isotopes in the Early/Middle Eocene

Eveline N. Speelman, Jacob O. Sewall, David C. Noone, Matthew Huber, Anna von der Heydt, Jaap S. Sinninghe Damsté, and Gert-Jan Reichart

Published in: Earth and Planetary Science Letters 298 (2010), 57 - 65.

Abstract

Proxy-based climate reconstructions suggest the existence of a strongly reduced equator-to-pole temperature gradient during the *Azolla* interval in the Early/Middle Eocene, compared to modern. Changes in the hydrological cycle, as a consequence of a reduced temperature gradient, are expected to be reflected in the isotopic composition of precipitation (δD, $\delta^{18}O$). The interpretation of water isotopic records to quantitatively reconstruct past precipitation patterns is, however, hampered by a lack of detailed information on changes in their spatial and temporal distribution. Using the isotope-enabled version of the National Center for Atmospheric Research (NCAR) atmospheric general circulation model, Community Atmosphere Model v.3 (isoCAM3), relationships between water isotopes and past climates can be simulated. Here we examine the influence of an imposed reduced meridional sea surface temperature gradient on the spatial distribution of precipitation and its isotopic composition in an Early/Middle Eocene setting. As a result of the applied forcings, the Eocene simulation predicts the occurrence of less depleted high latitude precipitation, with δD values ranging only between 0 and -140‰ (compared to Present-day 0 to -300‰). Comparison with Early/Middle Eocene-age isotopic proxy data shows that the simulation accurately captures the main features of the spatial distribution of the isotopic composition of Early/Middle Eocene precipitation over land in conjunction with the aspects of the modeled Early/Middle Eocene

climate. Hence, the included stable isotope module quantitatively supports the existence of a reduced meridional temperature gradient during this interval.

4.1 Introduction

The Early to Middle Eocene was one of the warmest intervals of the Cenozoic, with little or no polar terrestrial ice, global mean surface temperatures much warmer than present, deep sea temperatures 10 °C warmer than present (Sloan and Barron, 1992; Sloan, 1994; Zachos et al., 1993, 1994; Greenwood and Wing, 1995; Jahren and Sternberg, 2003), and atmospheric pCO_2 in the range of 400 - 3500 ppm (Pearson and Palmer, 2000). During a 1.2 Myr period 49 Ma ago, the free floating aquatic fern *Azolla* grew and reproduced in the Eocene Arctic (Brinkhuis et al., 2006; Chapter 1), indicating that the surface waters of the Arctic Basin freshened considerably. During this so-called *Azolla* interval, tropical sea surface temperatures (SSTs) were somewhat warmer than today (with a mean annual temperature (MAT) of 32 - 34 °C at 19 °S) (Pearson et al., 2007), while Arctic SSTs were substantially higher (with a MAT of ~10 °C) (Brinkhuis et al., 2006). The consequently reduced temperature gradient between the equator and the poles and the presence of freshwater at the North Pole (Brinkhuis et al., 2006) provide important boundary conditions for understanding the hydrological cycle and latent heat transport during this interval. While earlier in the Eocene (from 55 to 50 Ma) temperature gradients may have been even lower (e.g. Pearson et al., 2007; Sluijs et al., 2008), data coverage in the *Azolla* interval centered near 49 Ma is more complete and we thus focus on that interval.

The prevalence of a reduced equator-to-pole sea surface temperature gradient is debated as numerical climate models generally are not able to generate this proxy-inferred warm, temperate climate in the Arctic in conjunction with tropical temperatures not much warmer than modern values (e.g. Crowley and Zachos, 2000; Huber and Sloan, 2000; Huber and Caballero, 2003; Shellito et al., 2003). Additional evidence for the presence of a reduced equator-to-pole temperature gradient in the Eocene comes from the reconstructions of water isotopic signals (e.g. δD of *n*-alkanes, ^{18}O of cellulose; Feng and Epstein, 1995; Sessions et al., 1999; Fricke, 2003; Jahren, 2009; Pagani et al., 2006). As stable water isotopes (HDO and $H_2{}^{18}O$) in precipitation reflect (i) source-region, (ii) water volume loss during transport (rainout effects), (iii) local temperature, and (iv) the additive contribution of local water and mixing of different air masses (Craig and Gordon, 1965; Merlivat and Jouzel, 1979), the prevalence of a low meridional temperature gradient and associated changes in hydrological cycling should be reflected in the isotopic composition of Eocene precipitation.

The application of general circulation models (GCMs) adapted to include stable water isotope tracers allows for disentanglement of the various factors influencing the final isotopic composition of precipitation as recorded by proxy data (Joussaume et al., 1984; Jouzel et al., 1987; Noone and Simmonds, 2002; Schmidt et al., 2005; Lee et al., 2007) and provides an additional mechanism for evaluating model outcomes. Here we simulate the atmospheric response and subsequent hydrogen and oxygen isotope distributions in a world with a reduced meridional temperature gradient in an effort to enhance our understanding of the Early/Middle Eocene hydrological cycle. Model results are compared to hydrogen isotope estimates of precipitation for this interval to further evaluate proxy-based climate reconstructions that suggest the presence of a reduced meridional temperature gradient at this time.

4.2 Methods

4.2.1 Model description

To simulate the isotopic composition of precipitation and water vapor, as well as the climatological conditions during the Early/Middle Eocene, we use an adapted version (isoCAM3) of the National Center for Atmospheric Research (NCAR) Community Atmosphere model version 3 (CAM3, Collins et al., 2006). IsoCAM3 incorporates a third generation isotope tracer scheme (Noone and Sturm, 2010), which is based on the earlier isotopic scheme of Noone and Simmonds (2002) but includes a more sophisticated treatment of surface exchange and cloud processes to make use of the multiple water phases (vapor, liquid and ice) predicted by CAM (e.g. Noone, 2003; Noone and Sturm, 2010). IsoCAM3 is coupled to a dynamic land surface model (CLM3: Bonan et al., 2002; Oleson et al., 2004) in which the isotopic composition of terrestrial water and evaportranspiration is accounted for by a simple two-bucket scheme based on the model of Noone and Simmonds (2002).

4.2.2 Boundary conditions and experimental design

Using isoCAM3, we simulate global patterns of stable water isotopes for the Eocene *Azolla* interval (EO-AZOLLA) and for a modern day control case (MOD). All simulations are atmosphere only with fixed sea surface temperatures (SSTs) and simulate the H_2O, HDO and $H_2{}^{18}O$ content in all existing water phases and transitions between those phases. The modern day simulation was set up with modern boundary conditions and forcings (e.g. atmospheric pCO_2). The global mean oceanic δD and $\delta^{18}O$ isotopic composition is kept constant and was set to VSMOW. For the Early/Middle Eocene simulation, we incorporated realistic, Eocene, topography, land surface conditions, and vegetation as boundary conditions (described in Sewall et al., 2000). Orbital parameters were set to modern-day configuration. The EO-AZOLLA simulation was initialized using the atmospheric state from the

equilibrium simulation of a fully coupled CCSM1.4 Eocene run (as described in Huber and Nof, 2006). Estimates for Early/Middle Eocene atmospheric pCO_2 are uncertain, varying between ~400 and ~3500 ppm (c.f. Zachos et al., 2008; Pearson and Palmer, 2000). Here we set greenhouse gas concentrations to 2000 ppm (CO2) and 700 ppb (CH_4). Additional experiments (not shown) with higher (3000 ppm) and lower (800 ppm) CO_2 concentrations showed very minor changes in precipitation δD compared to concentrations of 2000 ppm.

Tropical Eocene sea surface temperatures simulated by the fully coupled CCSM1.4 Eocene run of Huber and Nof (2006) were found to be consistent with SST estimates of 33 °C (Pearson et al., 2007) from Tanzanian sediments from the Early/Middle Eocene. These mean annual SSTs at 19 °S paleolatitude, were reconstructed based on TEX_{86} measurements using the Schouten et al. (2003) calibration for warm SSTs. Modeled high latitude temperatures from the fully coupled CCSM1.4 Eocene run were, however, colder than available TEX_{86} SST estimates from the Early/Middle Eocene Arctic (Mean annual SST = 9.4 °C; Brinkhuis et al., 2006, using the Schouten et al., 2002 calibration) (Fig 4.1; grey dotted line). For our EO-AZOLLA simulation, we, therefore, modified SSTs from the fully coupled CCSM1.4 Eocene run, using a fixed, zonally constant, offset based on the Brinkhuis et al. (2006) TEX_{86} SST estimates from the Early/Middle Eocene Arctic. Global meridional SSTs were scaled accordingly between the Tropics and the Arctic (Fig. 4.1; red line), while preserving the spatial variability of the CCSM1.4 run. This way, we combine the modeled SST patterns with the more realistic proxy-values. The applied seasonal SST cycle smoothed the imposed offset in the model and was derived from two reconstructions based on intra-shell stable oxygen isotope profiles of shallow-water gastropods. Near Southern England, a seasonality of 10-12 °C has been suggested (Andreasson and Schmitz, 2000), while the Early/Middle Eocene US Gulf coast experienced an 8-9 °C temperature change over the year (Andreasson and Schmitz, 2000). For the Arctic, the imposed seasonal SSTs varied between 2 °C in February and 19.5 °C in September. Implied ocean heat transport produced with the simulation using this SST gradient is similar to ocean heat transport in the fully coupled simulation. Global mean δD and $\delta^{18}O$ of seawater were adjusted to reflect globally ice-free conditions (-8‰ for δD and -1‰ for $\delta^{18}O$, respectively). According to Schmidt et al. (1999), there is only a ~1.5‰ difference in $\delta^{18}O$ between low and high latitudes in the open ocean. These differences are caused by the net transport of isotopically depleted water vapor away from the tropics towards the poles, with more enriched areas where evaporation exceeds precipitation. Regional differences of ^{18}O and δD in seawater are small compared to differences in precipitation and are therefore not modeled here. The model simulations were integrated for 30 yr at a spectral resolution of T31 (~3.75 °lat. x 3.75 °lon) and results may be somewhat sensitive to resolution. The last 10 yr were averaged and used for subsequent evaluation.

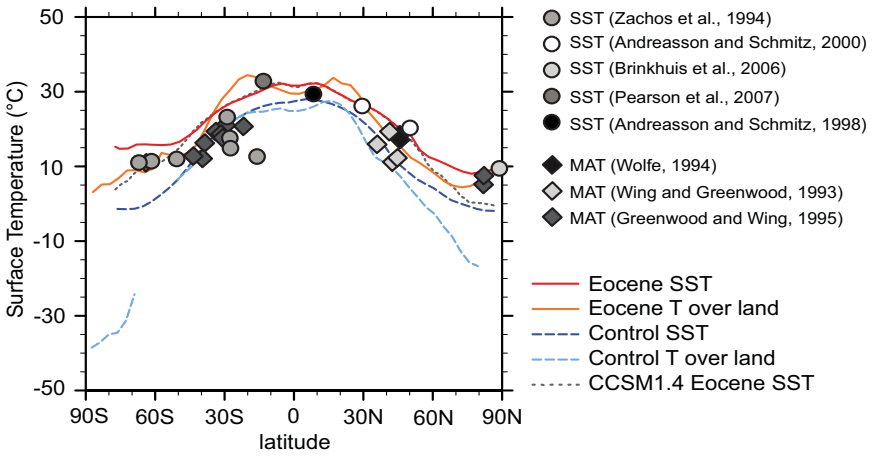

Figure 4.1: Modeled latitudinal mean annual sea surface temperatures (SST, in °C), and temperatures over land, for the Eocene (EO-AZOLLA; red/orange lines), the present-day control run (MOD; blue dashed lines) and the original fully coupled run (CCSM1.4; grey dotted line). Circles correspond to Eocene age SST proxy data, and squares correspond to various proxy-based estimates of mean annual air temperature (MAT).

4.2.3 Early/Middle Eocene *n*-alkane δD measurements

Three sediment samples from different locations from the same time interval were used to obtain measurements of δD of terrestrial C_{29} *n*-alkanes. From South to North: (1) Carcoselle Quary, Possagno, Italy (as described in Agnini et al., 2006); sample 34 3 40 (2) Danish Outcrops, Lillebælt Clay Formation, Bed L2, sample 8B (as described in Heilmann-Clausen et al., 1985) and (3) IODP Leg 151, Hole 913b, Norwegian Greenland Sea, 75°29.356'N 6°56.810'W (water depth: 3318.4 m), samples core 48x interval 1w section 20-22cm, and core 47x interval 2w, section 70-72cm.

Between 0.5 and 5 g of freeze-dried sediment was powdered and subsequently extracted with an Accelerated Solvent Extractor (Dionex) using a dichloromethane (DCM) – methanol (MeOH) mixture (9:1, v/v). The obtained lipid fractions were separated by column chromatography using an elution sequence of hexane/DCM (9:1 v/v) and DCM/MeOH (1:1 v/v). All extracts were de-sulpherized using activated Copper. To purify the apolar fraction, cyclic and branched alkanes in the hydrocarbon fraction were separated from normal alkanes by adduction with urea, using a mixture of methanol-saturated urea, pentane and acetone (200 µl each). Frozen and N_2-dried urea crystals were washed with hexane to extract cyclic/branched alkanes. Remaining urea crystals were dissolved in 500 µl of double distilled H_2O

(MiliQ) and 500 µl of methanol, and extracted with hexane to yield the purified *n*-alkane fraction.

Compounds were identified by GC/MS (Thermo Trace GC Ultra). Samples were on-column injected at 70 °C, on a CP-Sil 5CB fused silica column (30 m x 0.32 mm i.d, film thickness 0.1 µm) with Helium as carrier gas set at constant pressure (100 KPa). The oven was programmed to 130 °C at 20 °C/min and then to 320 °C at 4 °C/min, followed by an isothermal hold for 20 min.

The adducted *n*-alkane fractions were analysed for stable hydrogen isotopic compositions using isotope ratio monitoring gas chromatography-mass spectrometry (GC-IRMS). For the samples from the Danish Outcrops and IODP Leg 151 a Thermo Finnigan MAT 253 mass spectrometer was used with a J&W Scientific DB-1 capillary column (60m x 0.25 mm x 0.25 µm) at Yale University. The sample from Possagno was measured using a ThermoFinnigan Delta-Plus XP mass spectrometer at Utrecht University. A similar column and oven program were used as described above, though with a constant flow of 1 ml/min. Conversion of organic hydrogen to H_2 was conducted at 1400 °C. The H3 factor was determined daily on the isotope mass spectrometer, and was always below 5. Schimmelman Mixture A, B, and C (Schimmelmann, Biogeochemical Laboratories, Indiana University), were run twice-daily alternately to correct reference gas values. Co-injected squalane with a known δD isotopic composition (also Schimmelman) was used as internal standard to monitor performance. Hydrogen isotopic compositions are reported relative to VSMOW and are based on duplicate analyses, where possible, of well-resolved peaks (> 500 mV) and represent averaged values. The precision of isotopic measurements of H_2 reference gas after H3 correction was 0.2 or better. The average standard deviation per day for the separate *n*-alkanes was below 4‰.

4.3 Results

4.3.1 Climate output Eocene

The Early/Middle Eocene simulation (EO-AZOLLA) is largely controlled by the imposed SST gradient. Overall, EO-AZOLLA, using TEX_{86}-derived Arctic mean annual SSTs of 9.4 °C, is warmer and wetter than the present-day control run (MOD) (Fig. 4.1, Fig. 4.2). Results of the Eocene simulation show an average global surface temperature of 23.9 °C. However, simulated continental interior cold month mean (CMM) temperatures in EO-AZOLLA (not shown) dip well below freezing (down to -10 °C at certain locations) in the continental interiors of North America and Asia. Closer to the Arctic, continental CMM temperatures of 0 - 4 °C (at 79 °N) are simulated by the model. In our EO-AZOLLA simulation, evaporation (E) and precipitation (P) rates are enhanced compared to MOD and the atmospheric

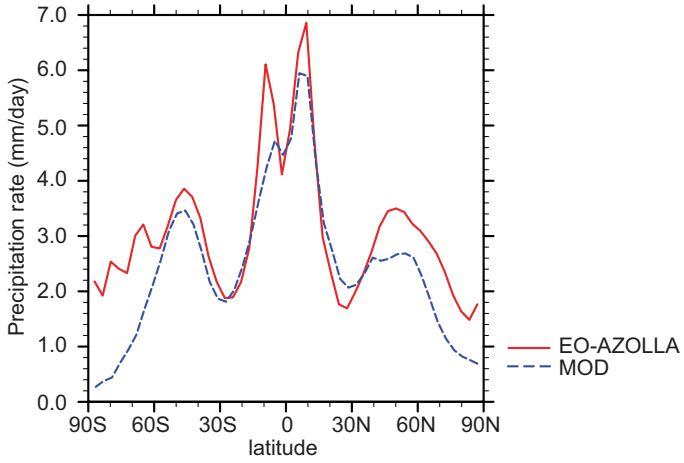

Figure 4.2: Zonal averages of mean annual precipitation rates (mm/day), for both the Eocene (red, solid line) and present-day control run (blue dashed line).

water vapor loading is higher due to lower lapse rates and higher atmospheric temperatures, with the total amount of precipitable water is higher at all latitudes (not shown) by on average 13.8 mm. In midlatitude regions, E - P values are about the same for MOD and EO-AZOLLA, but between 50 – 85 °N and 70 – 90 °S, excess precipitation is higher in the EO-AZOLLA simulation than in MOD, amounting to up to 1.6 mm/day.

Overall, annual mean meridional circulation in EO-AZOLLA is similar to present-day, with two tropical Hadley cells, the Ferrel cells at mid-latitude and the Polar cells at high latitudes. The annual mean 850 mb transient eddy kinetic energy is generally lower in the Eocene than in the modern simulation, at mid-latitudes around 20 m^2/s^2 lower than the Present-day control, reflecting weaker storm tracks (globally averaged ~7 m^2/s^2 less; not shown). Annual averaged meridional heat fluxes are also reduced in EO-AZOLLA, especially at mid-latitudes (Fig. 4.3a). Transient eddy moisture transport, on the other hand, is quite similar at low latitudes, while significantly higher (by 0.6 m/s g/kg) at higher latitudes (>50 °N and > 65 °S) in EO-AZOLLA (Fig. 4.3b).

4.3.2 Modeled isotopic composition of precipitation

4.3.2.1 Present-day control run

The modeled isotopic composition of precipitation for the present-day is shown in Figure 4.4a and b (black). In figure 4.5a, the annual global distribution of precipitation weighted δD in the MOD simulation is shown.

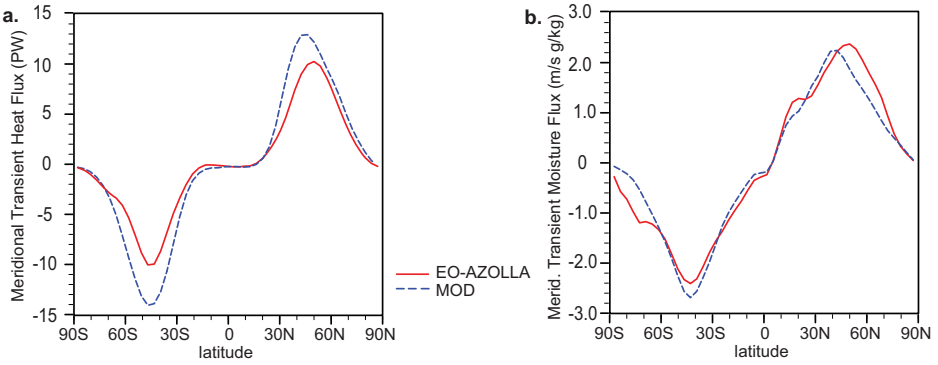

Figure 4.3: (a) Modeled zonal mean annual meridional heat transport (PW), for MOD (dashed blue) and EO-AZOLLA (red), and (b) zonal mean annual meridional moisture transport (g/kg).

4.3.2.2 Early/Middle Eocene run

The effect of an Early/Middle Eocene reduced equator-to-pole temperature gradient (as shown in Fig. 4.1) on the isotopic composition of precipitation is shown in Figure 4.4a and b, and the modeled annual global distribution of precipitation weighted δD in the EO-AZOLLA simulation is shown in Figure 4.5c. The range of absolute δD and $\delta^{18}O$ values is substantially reduced for the Eocene compared to MOD (Figs. 4.4 and 4.5; zonal mean precipitation δD red versus blue line).

4.3.3 Measured Early/Middle Eocene *n*-alkane δD

Compound specific δD of *n*-alkanes with a strong odd over even predominance from three sediment samples, specifically from the *Azolla* interval, were measured. The samples came from outcrops in Possagno, Italy, the Lillebælt Clay Formation, Denmark, and an IODP sediment core taken off the coast of Greenland (IODP Leg 913B). That the samples from Denmark and Greenland are truly synchronous with the *Azolla* interval is evident from the presence of 1,ω20 C_{32} - C_{36} diols in the sediment extracts (unpublished results), which are biomarkers for *Azolla* (Chapter 2). Measured C_{29} *n*-alkane δD varied between -130 (Possagno) to - 204‰ (Greenland). Data from contemporary environments generally suggests apparent hydrogen isotope fractionation between source water and long chain *n*-alkanes (C_{29} and C_{27}) of 96‰ to 130‰ (Sachse et al., 2004; 2006; Yang et al., 2009). These values differ between plant species and with differing environmental conditions (Liu et al., 2006; Sachse et al., 2006). Using the range of observed fractionation values, Early/Middle Eocene precipitation δD can be computed from the measured C_{29} *n*-alkane δD values (Table 1). The three samples from Western Europe show a clear latitudinal trend, with increasing depletion from South to North.

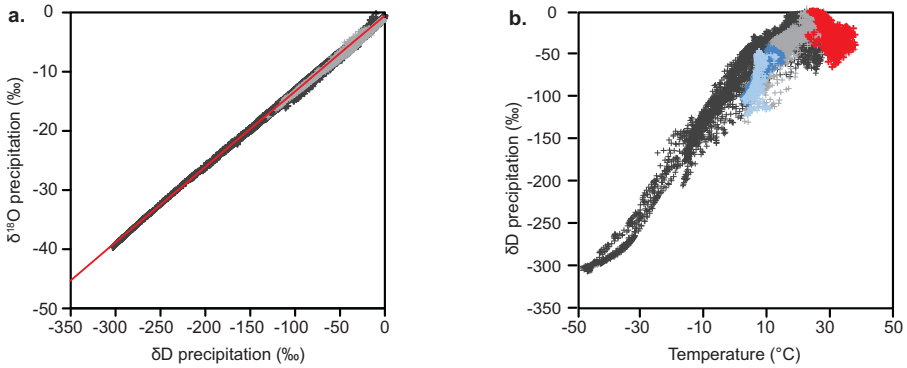

Figure 4.4: (a) Modeled mean annual isotopic composition of precipitation (‰ VSMOW) of δD versus $\delta^{18}O$, for the present-day control run (black) and for the Eocene (light grey). The dots represent the δD and $\delta^{18}O$ of precipitation for each model grid point. The red line represents the Global Meteoric Waterline (δD = 8 * δ18O + 10‰) (Craig, 1961). (b) The relationship between annual mean δD in precipitation and annual mean temperature at the surface (ºC) for model output of present-day (black) and Eocene simulations. For EO-AZOLLA regions are colored: red for the tropics (20 °S - 20 °N), grey for the mid-latitudes (20 - 70 °), light blue for the Arctic (70 - 90 °N) and blue for the Antarctic (70 - 90 °S).

Table 4.1: Comparison of modeled and reconstructed mean annual precipitation rates (mm/yr) for the Eocene *Azolla* interval (~49 Ma).

Location	Age (Ma)	Reconstructed precipitation[a] (mm/yr)	Modeled precipitation[b] (mm/yr)	Reference
US Western Interior	49-51	1040-1360	950 - 1540	Wilf et al., 1998
US Western Interior	49-51	1160-2770	950 - 1540	Wing and Greenwood, 1993
Republic, WA, US	49-50	1150	1150 (1140-1190)	Greenwood et al., 2005
Changchang, China	Early Middle Eocene	949	988 (890-1710)	Yao et al., 2009
Mahenge, Tanzania	max. 46	640-780	840 (460-840)	Jacobs and Herendeen, 2004
Yakutat, Alaska, US	Early Middle Eocene	>1500	2280 (1655-2500)	Wolfe, 1994
NW Pacific, US	Early Middle Eocene	>1500	1770 (1490-2000)	Wolfe, 1994
Axel Heiberg	49	1200	500 (450-650)	Eldrett et al., 2009

[a] Precipitation rate estimates from certain regions or locations as indicated.

[b] Modeled precipitation rate estimates of corresponding paleo-locations in the model. Values between brackets are taken from multiple surrounding grid-cells in order to characterize the uncertainty in the modelled value arising from uncertainty in paleo-location of the proxy sites and the coarse resolution of the model.

4.4 Discussion

4.4.1 Climate validation: Eocene versus proxy data and Present-day climate simulation

The EO-AZOLLA simulation is in broad agreement with proxy reconstructed environmental conditions in terms of annual mean temperature (Fig. 4.1) (but not cold month mean), humidity (not shown) and precipitation (Fig. 4.2). The imposed Early/Middle Eocene forcing thus reproduces a climate that agrees well with proxy data in locations around the globe. The Eocene simulation (EO-AZOLLA) is on average 8.5 °C warmer than the modern day control (MOD). Modeled latitudinal surface temperatures are shown and compared to various Eocene proxy-derived temperature estimates in Figure 4.1. Recrystallization of forams (as described in Pearson et al., 2007), possibly leads to underestimation of sea surface temperatures, explaining the (small) temperature offset between the modeled values and the values as inferred by Zachos et al. (1994). As observed before (e.g. Barron et al., 1995, Sloan et al., 2001), imposed warm high latitude SSTs have little impact on extratropical continental interior temperatures. Simulated continental interior cold month temperatures in EO-AZOLLA (not shown) are colder than indicated by proxy data (Greenwood and Wing, 1995; Sloan, 1994; Wolfe, 1994; Markwick 1994, Basinger, 1991). Closer to the Arctic, cold month mean estimates of 0 – 8.6 °C (cf. 0 - 4 °C Basinger, 1994; 3.3 – 8.6 °C Wolfe, 1994; -0.8 – 3.6 °C, Greenwood and Wing, 1995) do agree well with values (0 - 4 °C at 79 °N) produced by the model.

The occurrence of a fresh surface water layer in the Arctic Ocean during the *Azolla* interval (Brinkhuis et al., 2006) could be explained by an intensified hydrological cycle with precipitation exceeding evaporation at high latitudes as suggested earlier by Manabe (1997) and Huber et al. (2003), in conjunction with the very restricted connection with the open ocean dictated by the paleogeography (Brinkhuis et al., 2006). Indeed, model predicted zonal mean annual precipitation rates are notably higher in the Eocene, especially in the Arctic and Antarctic regions (Fig. 4.2). Available estimates of Early/Middle Eocene (~49 Ma) precipitation rates based on leaf-area and bioclimatic analysis of fossil floras support the modeled values (Table 4.1), except at Axel Heiberg Island where the model underestimates precipitation.

The strength of mid-latitude (eddy driven) circulation depends on mean global temperature as well as on meridional temperature differences (Caballero and Langen, 2005), and, in agreement with this, the Eocene simulation exhibits reductions in the strength of mid-latitude circulation. Weaker Eocene storm tracks are also reflected in lower transient eddy heat transport. However, at a higher global mean temperature it is possible to transport more latent heat, even with a reduced meridional temperature gradient. This is reflected in transient eddy moisture transport which is in EO-AZOLLA only slightly lower at mid-latitudes and significantly higher (~0.6 m/s g/kg) at higher latitudes (>50 °N and > 65 °S) than in MOD (Fig.

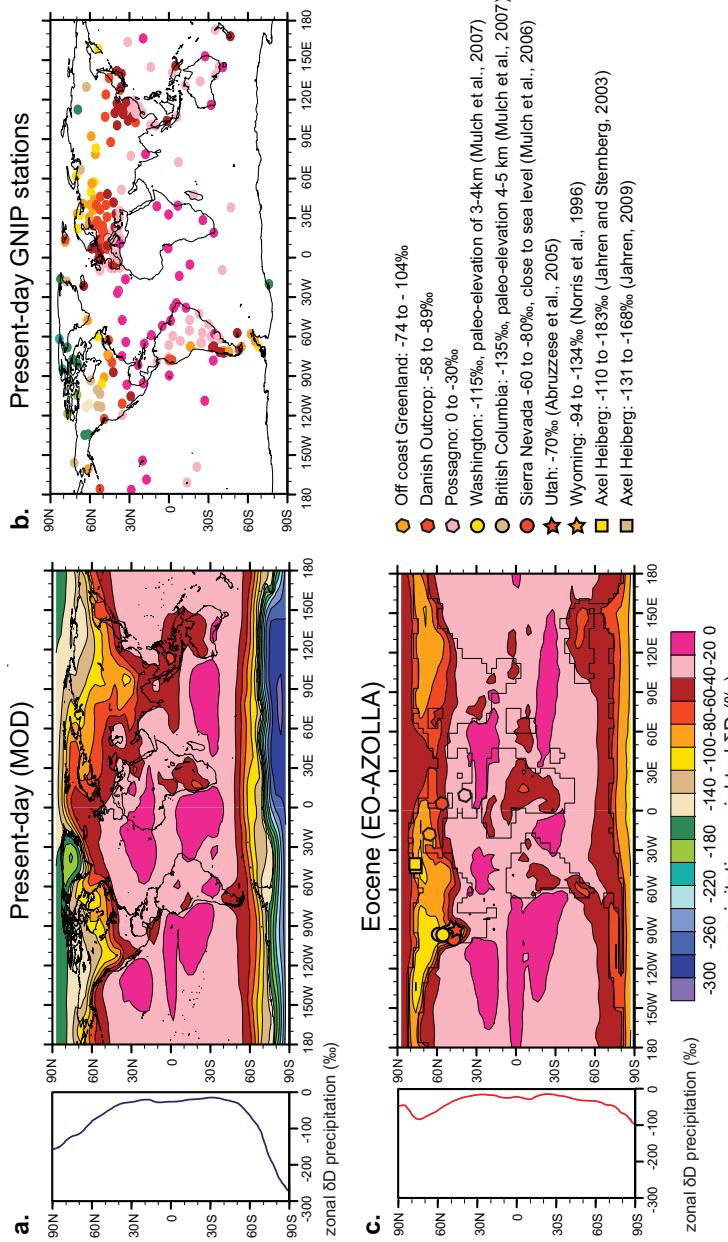

Figure 4.5: Precipitation weighted δD (using 10 year-averaged monthly means) for the present-day control run (a) and for the Eocene (c). Zonal mean precipitation weighted δD for MOD (blue) and EO-AZOLLA (red). In (b) the GNIP mean annual precipitation weighted δD station data (IAEA/WMO, 2006) are plotted for comparison with model outcomes shown in (a). (c) Model – data comparison for Eocene precipitation-weighted δD, where the colors of the symbols correspond to the color scale of the underlying plot.

4.3b). In agreement with the interpretation of Pagani et al. (2006), the simulated increase in poleward moisture transport, in EO-AZOLLA, results in enhanced high latitude precipitation as well as in a net precipitation reduction in sub-tropical areas and part of the mid-latitudes (Fig. 4.2). These changes in regional water balance are expected to significantly influence the regional and global isotopic composition of meteoric water.

4.4.2 Present-day isotope simulation versus GNIP data

Comparison of previous isoCAM3 present-day simulations to observed isotopic patterns in the Global Network of Isotopes in Precipitation (GNIP) database assembled by the International Atomic Energy Agency (IAEA/WMO, 2006) shows good agreement on global and regional scales (Noone, 2003). Our MOD simulation at T31 also captures the main features of the GNIP global distribution of $\delta^{18}O$ and δD (Fig. 4.5b) with modeled precipitation $\delta^{18}O$ and δD still following the expected linear trend known as the meteoric water line: $\delta D = 8 * \delta^{18}O + 10$ (Craig, 1961) (Fig. 4.4a). In line with the GNIP data, our MOD run describes an arcuate trend on the diagram with virtually no dependence of δD on temperature above 15 °C and a gradually increasing $\delta D/T$ slope with decreasing temperature (cf., Masson-Delmotte et al., 2008) (black crosses, Fig. 4.4b). The model also succeeds in capturing the correlation between mean annual δD and precipitation (amount effect) over warm tropical regions (black crosses, Fig. 4.4b). The latitude and continental effects (e.g. Ingraham, 1998) are clearly reproduced in the time mean statistics.

4.4.3 Model-data comparison for EO-AZOLLA isotope values

The assumption of a constant relation between δD and $\delta^{18}O$ remains valid for the Eocene simulation (as predicted from equilibrium theory; Craig, 1961), with precipitation δD and $\delta^{18}O$ from EO-AZOLLA plotting on the meteoric waterline (Fig. 4.4a). In figure 4.4, precipitation δD vs $\delta^{18}O$ values for the entire world (every grid-cell with a 10-yr average) are plotted. On a global scale, average deuterium-excess values (d-excess) in precipitation as defined by Dansgaard (1964) from the meteoric water line (Craig 1961) (d-excess = $\delta D - 8*\delta^{18}O$) end up close to 10, for both the Present-day and the Eocene.

For specific regions distinct differences, as a consequence of variation in kinetic fractionation, are observed. On average, d-excess is 6.5‰ for the Eocene Arctic. For this region, modern model and data d-excess values are higher and vary between 4 and 14‰ (Frankenberg, 2009; GNIP). Sea surface conditions that define evaporation such as relative humidity, temperature and, to a lesser degree, wind speed are key parameters for the deuterium-excess of atmospheric water vapour and precipitation (Merlivat and Jouzel, 1979). The modeled low d-excess values are consistent with higher Eocene Arctic temperatures and high relative humidity levels at a specific SST. The lowest amount weighted annual precipitation d-excess values

are found over the continents, in summer June/July (~ 2‰), coinciding with lower levels of relative humidity (60%). This indicates that, in summer, δD of precipitation is influenced by the evaporative enrichment of falling raindrops (subcloud evaporation), as described by Dansgaard (1964). Precipitation δD values decrease there from January to July, with d-excess values exhibiting strong linear correlation with precipitation δD (d-excess = - 0.13 * δD - 5.1 (r^2 0.97)). Between August and December d-excess values are higher for the same precipitation δD, coinciding with relatively higher relative humidity levels.

For verification, EO-AZOLLA results in terms of isotopic composition of precipitation can be tested against reconstructions of δD of environmental water for the Early/Middle Eocene *Azolla* interval; Figure 4.5c and Table 4.2 show the results for EO-AZOLLA precipitation weighted isotopic composition compared with proxy data estimates available for this time interval (~49 Ma). Besides the *n*-alkane inferred precipitation δD presented here, the Eocene precipitation estimates (Fig. 4.5c; Table 4.2) have been derived via a suite of different approaches and proxies,

Table 4.2: Comparison of modeled weighted (using 10 year-averaged monthly means) precipitation δD values (‰) with C_{29} *n*-alkane inferred precipitation δD and available precipitation isotopic composition estimates (‰) for the Eocene *Azolla* interval (~49 Ma).

Location	Age (Ma)	Reconstructed δD precipitation[a] (‰)	Modeled δD precipitation[b] (‰)	Reference
Possagno, Italy	Early/Middle Eocene	-0 to -34	-24 (-20 to -26)	this study
Lillebaelt, Denmark	~ 49	-59 to -93	-58 (-45 to -66)	this study
IODP 151Greenland	~ 49	-74 to -107	- 89 (-73 to -101)	this study
Kettle, WA,US	49.1	-110 to -120	-117 (-107 to -122)	Mulch et al., 2007
Shuswap, BC, US	49-47.1	-130 to -140	-107 (-107 to -116)	Mulch et al., 2007
Sierra Nevada, CA, US	50-40	-60 to -80	-78 (-51 to -100)	Mulch et al., 2006
Axel Heiberg	49	-110 to -183	-79 (-60 to -97)	Jahren and Sternberg, 2003
Axel Heiberg	49	-131 to -168	-79 (-60 to -97)	Jahren et al., 2009
Salina, UT, US	51-46.5	-70	-76 (-76 to -109)	Abruzzese et al., 2005
Lake Gosiute, WY, US	Early/Middle Eocene	-94 to -134	-80 (-76 to -94)	Norris et al., 1996

[a] Local Eocene precipitation δD/environmental water δD estimates, as well ^{18}O values converted to δD with the meteoric waterline (Craig, 1961), as cited in referenced articles.
[b] Modeled mean annual averaged weighted precipitation δD values of corresponding paleo-locations in the model. Values between brackets are taken from multiple surrounding grid-cells in order to characterize the uncertainty in the modeled value arising from uncertainty in the paleo-location of the proxy sites and the coarse resolution of the model.

including determination of hydrogen isotopic composition of kaolinite (Mulch et al., 2006), measurement of δD of *n*-alkanes from lignite layers (Jahren et al., 2009), and determination of $\delta^{18}O$ of fossil cellulose (Jahren and Sternberg, 2003). The model not only accurately captures general trends, but also absolute values are in reasonable agreement and fall well within the confidence intervals associated with the available proxy data for this specific time interval. The only region where model simulated isotopic composition of precipitation deviates from available reconstructed values is at Axel Heiberg Island, which is likely attributable to the imposed and fixed isotopic composition of the Arctic Ocean (δD = -8‰ VSMOW) in the EO-AZOLLA simulation. This imposed condition does not take into account freshening of the Arctic Ocean water (Brinkhuis et al., 2006), which would render the surface water gradually more δD depleted. Hence the δD of water evaporated from the Arctic sea surface in EO-AZOLLA is overestimated and precipitation falling in proximity of the Arctic has a δD at the high end of the proxy-defined parameter space (-168‰ to -131‰, Jahren et al., 2009). Overall, we find a good correlation between our model results, using a reduced meridional temperature gradient, and the available proxy data for the Early/Middle Eocene Azolla interval.

4.4.4 Effect of a reduced equator-pole temperature gradient on the isotopic composition of precipitation

A reduced temperature gradient dictates less isotopic distillation (Rayleigh condensation) during poleward transport. It follows from Precipitation (Fig. 4.2) and Evaporation-Precipitation (not shown) that excess precipitation at the high latitudes is higher (i.e. relatively less evaporation) in the EO-AZOLLA simulation than in MOD. As more water vapor is transported to (extreme) high latitudes along a reduced meridional temperature gradient, less rainout occurs along the airmass's trajectory (due to less cooling), which then leads to less isotopic depletion in precipitation at Eocene high latitudes relative to the modern simulation.

The major spatial relationships observed for the modern (from GNIP data (IAEA/WMO, 2006)) are retained in EO-AZOLLA (Fig. 4.5), with δD at low latitudes depending primarily on the balance between precipitation and evaporation and decreasing with decreasing temperature, poleward, with increased distance from the coast, and with increased elevation (this is especially clear in the (albeit lower) Eocene Rocky Mountains) (Fig. 4.5c). Similar to the modern situation, in the tropical regions (20 °N – 20 °S) a recycling of water through evaporation of falling rain is observed in the convective precipitation, resulting in relatively depleted isotopic values (Risi et al., 2008; Worden et al., 2007) (Fig. 4.4b; red crosses). In EO-AZOLLA, the region characterized by tropical (i.e. warmer) sea surface temperatures reaches into the mid-latitudes (Fig. 4.1). This effectively expands the region over which the moist tropical atmosphere can be considered dominated by, and in qua-

si-equilibrium with, convective storm activity. The tropical rainfall recycling effect extends, therefore, into the mid-latitudes in EO-AZOLLA.

At mid to high latitudes, EO-AZOLLA δD values are found to be more depleted than MOD δD at a certain temperature (Fig. 4.4b; grey, blue and light blue crosses). Moreover, as the model does not account for changes in surface water δD (or $\delta^{18}O$), the model possibly overestimates precipitation δD values in certain (high latitude) regions, where precipitation exceeds evaporation. The modeled offset in δD between EO-AZOLLA and MOD at a certain temperature is not due entirely to the absence of continental ice sheets (which imposes an offset of only 8‰), but is consistent with changes in mixing characteristics during the passage of vapour from warmer low latitudes to cooler high latitudes in the presence of the reduced meridional temperature gradient (Noone, 2008). As the region over which convective precipitation prevails is expanded in EO-AZOLLA relative to MOD, and the contribution of convective precipitation to total precipitation is increased (EO-AZOLLA 77% versus MOD 67%), more rain comes down in convective storms, also at higher latitudes. Since convective precipitation generally consists of larger droplets it exchanges less with near-surface moisture while falling, leading to relatively more depleted precipitation δD values.

The most depleted values (between -40 and -145‰) are observed at both poles (Fig. 4.4b; light blue and blue crosses, Fig. 4.5c). Looking at respective cells belonging to a certain region, mean annual regional δD_{precip} /T slopes at high latitudes are found to be steeper in the Eocene (Arctic: 7.3‰ /°C and Antarctic: 5.1‰ /°C) than in the present-day simulation (Arctic: 3‰ /°C and Antarctic: 3.6‰ /°C, respectively). As the reduced temperature gradient allows the moisture transport to occur with reduced interaction with the surface, it can produce a slope for Eocene high latitudes closer to that predicted from Rayleigh theory than for present-day. The differences between Eocene regional δD_{precip} /T slopes in the Arctic region (7.3‰ /°C, r^2=0.3; Fig. 4.4b; light blue crosses) and around Antarctica (5.1‰ /°C, r^2 = 0.9; Fig. 4.4b; blue crosses), further result from the imposed reduced meridional temperature gradient over the northern hemisphere, differences in the simulated cloud conditions -tied to processes that influence isotopic fractionation such as temperature dependence ice/liquid partitioning and supersaturation, and the type of clouds that prevail- and the more complex geography in the Arctic. The latter is also reflected in the more scattered relation between δD_{precip} and T in the Arctic (Fig. 4.4b; light blue crosses). Relative to present-day, these slopes in Eocene Polar Regions can be reduced because of the lack of sea ice during the Eocene, which would otherwise prevent the influence of a local source (Noone and Simmonds, 2004). This effect is probably most important in the Antarctic region, explaining in part the smaller increase in slope for Antarctica.

Despite obvious caveats related to both proxy-based reconstructions of SST and precipitation δD, connecting these independent datasets with a model evaluation shows that they are mutually consistent. This provides independent support for the long-proposed reduced meridional temperature gradient during the Early/ Middle Eocene.

4.5 Conclusion

We have shown that the integrated climate-isotope model (isoCAM3) is able to simulate the distribution of δD values in precipitation on a global scale for both the present-day and Early/Middle Eocene. The Eocene simulation, with an enforced reduced equator-to-pole temperature gradient, confirms the occurrence of enhanced moisture transport resulting in increased precipitation at high latitudes under low gradient conditions. We demonstrate that the isotopic composition of vapor and precipitation is heavily influenced by the imposed meridional temperature gradient, with δD values being appreciably more isotopically enriched in the Eocene, ranging between 0 and -140‰ compared to 0 and -300‰ in the modern day. Furthermore, Eocene model results are broadly consistent with new *n*-alkane inferred precipitation δD and a compilation of δD and $\delta^{18}O$ estimates from a suite of different proxies. The overall good correlation between our model results, using a reduced equator-to-pole temperature gradient, and annual mean temperature and precipitation proxy records independently confirms the earlier TEX_{86}-based reconstructions of reduced Early/Middle Eocene latitudinal temperature gradients. Knowledge of how SST gradients have changed over time is thus central to understanding global patterns of isotopes in precipitation.

Acknowledgements

We acknowledge Virginia Tech Advanced Research Computing and the Department of Geosciences for computation support and resources. Model runs were also sponsored by the Stichting Nationale Computerfaciliteiten (National Computing Facilities Foundation,NCF) for the use of supercomputer facilities, with financial support from the Nederlandse Organisatie voor Wetenschappelijk Onderzoek (Netherlands Organisation for Scientific Research, NWO). General project funding was provided by the DARWIN Centre for Biogeology and Utrecht University. Huber acknowledges support from the National Science Foundation funding via P2C2 0902882-OCE, and von der Heydt personal support through a VENI grant by the Netherlands Organization for Scientific Research (NWO). This research used samples and data provided by the Integrated Ocean Drilling Program (IODP). Authors thank C. Heilmann-Claussen for providing samples from Denmark, C. Agnini for sending the samples from Italy, and Mark Pagani's lab at Yale University

for assistance with compound specific δD measurements. We thank 4 anonymous reviewers for their constructive comments.

Chapter 5

Climatic controls on the modeled deuterium isotopic composition of leaf wax *n*-alkanes and implications for Eocene climate proxies

Nikolaus H. Buenning, Eveline N. Speelman, Jacob O. Sewall, Gert-Jan Reichart, and David C. Noone

under review

Abstract

The isotopic composition of leaf wax *n*-alkanes (δD_a) is often used to infer the isotopic composition of past precipitation (δD_p). Because δD_p has a strong temperature dependency outside of the tropics, δD_a values can also be used to reconstruct paleo-temperatures. Reconstructions are based on the assumption that the difference between δD_a and δD_p values ($\varepsilon_{w/a}$) and the temperature-δD_p relationship are invariable over time. However, model simulations suggest that $\varepsilon_{w/a}$ values are not spatially uniform and not constant in time. Specifically, during the Eocene (when both CO_2 concentrations and temperatures were high) modeled $\varepsilon_{w/a}$ values were consistently lower (more negative) compared to present-day values, although the underlying causes varied. Sensitivity experiments indicated that relative humidity, temperature, and radiation all contribute to a different degree in setting local $\varepsilon_{w/a}$ values. Higher growing season temperatures and differences in the seasonality of the isotopic composition of precipitation and water vapor during the Eocene have the largest impact on final $\varepsilon_{w/a}$ values. The implication of these results is that reconstructed δD_p values from δD values of leaf wax *n*-alkanes are too depleted and that, correspondingly, temperatures would be underestimated during the Eocene.

5.1 Introduction

Organic matter derived from plants has the potential to capture the deuterium/hydrogen ratio of precipitation, as meteoric water provides the hydrogen source for most plant organisms on Earth (Epstein et al., 1976). The hydrogen isotopic composition of a plant's leaf wax *n*-alkanes reflects the δD value (expressed as the deviation of the measured hydrogen isotope ratio from a standard) of a plant's source (i.e. soil) water (Sessions et al., 1999). In turn, the isotopic composition of source water is largely controlled by the δD value of local precipitation. Numerous studies have demonstrated spatial and temporal relationships between δD values of precipitation and temperature and precipitation amount (e.g., Dansgaard, 1964; Buenning and Noone, 2010). Provided that the δD values of water isotope proxies (e.g. through leaf wax derived *n*-alkanes) is preserved, past changes in local environmental conditions can be reconstructed.

Past temperature reconstructions using *n*-alkane δD values are based on a local δD-T conversion factor derived from modern observations, and is typically around 9‰/K (Jouzel et al., 1993, 1996; Petit et al., 1999). An uncertainty in proxy-derived δD values due to variable leaf water enrichment, as a consequence of evapotranspiration (e.g. Leaney et al. (1985) found deuterium enrichment ranged from 20‰ to 80‰) on the order of 50‰ results in an error in estimates of local past temperature of about 5.6 K.

In addition to the potential variations in the original δD value of source water, the final isotopic composition of *n*-alkanes found in leaf waxes is influenced by a sequence of fractionation processes prior to and during the biosynthesis of the hydrocarbons. Evaporation of soil and leaf water causes leaf water δD values to become enriched relative to precipitation (Craig and Gordon, 1965; Flanagan et al., 1991; Still et al., 2009), while fractionation during the biosynthesis of the *n*-alkanes causes depletion of δD values through preferential incorporation of the lighter isotopologue. Recent studies suggest that fractionation during biosynthesis is constant (amongst plant species and under varying environmental conditions) at a value of about -160‰ (Sessions et al., 1999; Sachse et al., 2004, 2006). Evaporative enrichment from leaf and soil water is rarely large enough to outweigh the large -160‰ fractionation from biosynthesis (Sachse et al., 2006). Consequently, the net offset between the isotopic composition of precipitation (δD_p) and that of the *n*-alkanes (δD_a) (hereafter $\varepsilon_{w/a} = \delta D_a - \delta D_p$) is almost always negative. Using $\varepsilon_{w/a}$, measured δD_a values from ancient sediments can be converted to δD_p values, which are used to infer hydrological changes and to estimate past temperatures. However, Sachse et al. (2006) and Liu et al. (2006) have shown differing $\varepsilon_{w/a}$ values between different plant species due to variations in both plant anatomy and environmental conditions.

Craig and Gordon (1965) presented a steady-state theory for approximating the isotopic composition of surface water, which has been modified by Flanagan et al. (1991) to predict the isotopic composition of leaf water (δD_L) under steady-state conditions such that:

$$\delta D_L = \varepsilon_{L-V}(T) + (1-h)(\delta D_{SW} - \varepsilon_k) + h\delta D_{CV} \quad (1)$$

where $\varepsilon_{L\text{-}V}(T)$ is the temperature (T) dependent equilibrium fractionation of HDO during the liquid-vapor phase transition, ε_k is the kinetic fractionation of HDO during the diffusion of vapor across the stomata and leaf boundary layer, h is relative humidity at the surface of the leaf, δD_{SW} is the isotopic composition of the soil water taken up by roots, and δD_{CV} is the isotopic composition of the canopy vapor. Still et al. (2009) have shown that this steady-state assumption is remarkably robust during the daytime when transpiration and photosynthetic production is high. The value of $\varepsilon_{L\text{-}V}(T)$ changes by -1.1‰/K at a temperature of about 300 K, which is typically neglected for proxy-reconstructions. Hence, equation (1) shows that the isotopic composition of leaf water is largely controlled by the δD values of soil water and canopy vapor, which in turn are set by δD values of precipitation and atmospheric vapor. Equation (1) further shows that relative humidity influences the balance between soil water and canopy vapor contributions to δD_L, as well as that it regulates the strength of the kinetic fractionation term. Indeed, equation (1) predicts that a relative humidity change of 10% units corresponds to a leaf water change of approximately 12‰.

It is likely that many of the parameters controlling δD_L were different during different periods of the past. For example, the Eocene (57.8–36.6 Ma) was characterized by high temperatures and an intensified hydrological cycle relative to today (Jahren and Sternberg, 2003), which likely modified $\varepsilon_{L\text{-}V}$, h, δD_{SW} and δD_{CV} values (Equation 1). Using a comprehensive isotopic fractionation model fitted to a detailed land surface model and atmospheric general circulation model, this study evaluates the degree to which Eocene environmental conditions cause changes in δD_L values and thus $\varepsilon_{w/a}$ as recorded in leaf wax *n*-alkanes.

5.2 Model description and experiment configuration

The H_2O, HDO, and $H_2{}^{18}O$ content of precipitation and water vapor as well as meteorological conditions for both the Eocene and the present-day were simulated using isoCAM. isoCAM is a modified version of CAM3, the National Center for Atmospheric Research (NCAR) Community Atmosphere Model (CAM) (Noone, 2003, 2006; Noone and Sturm, 2010). The fractionation scheme is based on that of Noone and Simmonds (2002) but includes a more detailed multiphase cloud

microphysical model adapted from Federer et al. (1982) and a more detailed treatment of convective transport of moisture (Noone and Sturm, 2010). Output from isoCAM was used to force the isotopic version of the NCAR Land Surface Model (isoLSM) (Bonan, 1996; Riley et al., 2002; Noone et al., 2002). isoLSM simulates the δD and $\delta^{18}O$ values in soil, xylem, and leaf waters based on modeled hydrologic and energy balance constraints. The leaf water model within isoLSM employs a time-dependent mass balance that includes a transpiration dependent leaf turnover time-scale to calculate δD_L values (Dongman 1974; Still et al., 2009). The deuterium content of leaf wax *n*-alkanes (δD_a) was then estimated by computing the photosynthesis-weighted δD value of leaf water and subtracting 160‰ to account for biosynthetic fractionation (Sessions et al., 1999; Sachse et al., 2004). Finally, $\varepsilon_{w/a}$ values were calculated by subtracting the amount weighted δD of local precipitation from local δD_a values.

Both present-day and Eocene simulations were performed with isoCAM and described in detail elsewhere (Chapter 4). For the Eocene simulations, we incorporated realistic, best guess, Eocene bathymetry, topography, land surface conditions, and vegetation as boundary conditions (described in Sewall et al. (2000)). The Eocene isoCAM simulations were initialized using the atmospheric state from an equilibrium simulation of a fully coupled CSM1.4 Eocene run (Huber and Nof, 2006). Eocene sea surface temperatures (SST) were adapted using a fixed, zonally constant, offset based on TEX_{86} SST estimates from the Early/Middle Eocene (Brinkhuis et al., 2006; Pearson et al., 2007). To evaluate the influence of vegetation type on $\varepsilon_{w/a}$ values, three separate sets of isoLSM simulations were conducted for each time period (Table 5.1). The first of these simulations sets the vegetation at each grid cell to be the type closest to the plant function type used in isoCAM. The two other sets of simulations were configured to have only 1) broadleaf evergreen trees and 2) broadleaf deciduous trees at every land grid-cell that contains vegetation. Thus, these last two sets of simulations can be used to evaluate differences irrespective of vegetation type. For similar reasons, the soil type is prescribed to be the same for all simulations and for all grid-cells (43% sand, 41% silt, and 16% clay, with 5% of the land fraction lakes and 5% wetlands). The horizontal resolution of the model is given by triangular truncation of the spherical harmonic spectrum at wave number 31, which corresponds to a Gaussian grid of about 3.75 degree longitude x 3.75 degree latitude. The isoCAM simulations ran for 30 years, with the last 10 individual years used cyclically to force isoLSM. isoLSM simulations ran for 40 years with the last 20 years averaged and used for the analysis.

This off-line model configuration did not allow feedbacks to local canopy level relative humidity and the δD values of precipitation and vapor, and there were no diurnal cycles within the CAM forcing data. These limitations should be kept in mind while considering the analysis below.

Table 5.1: Name and description of the three Eocene and three present-day simulations and the four sensitivity experiments.

Simulation	Description
PD-VAR	Forced with a present day ISOCAM simulation with varied best guess vegetation type
EOC-VAR	Forced with an Eocene-like ISOCAM simulation with varied best guess vegetation type
PD-BET	Forced with a present day ISOCAM simulation with broadleaf evergreen tress at each grid-cell
EOC-BET	Forced with an Eocene-like ISOCAM simulation with broadleaf evergreen trees at each
PD-BDT	Forced with a present day ISOCAM simulation with broadleaf deciduous trees at each grid-cell
EOC-BDT	Forced with an Eocene-like ISOCAM simulation with varied best guess vegetation type
EOC/PD-CO2	EOC-BDT with present day CO2 levels
EOC/PD-TEMP	EOC-BDT with present day temperatures
EOC/PD-RAD	EOC-BDT with present day solar radiation
EOC/PD-RH	EOC-BDT with present day relative humidity

5.3 Model Results

5.3.1 Present-day Eocene comparison

Many studies that measure δD_a values also calculate the apparent fractionation (ε'), which is slightly different than our definition of the δD_a-δD_p offset ($\varepsilon_{w/a}$). Apparent fractionation is on average 7‰ lower than $\varepsilon_{w/a}$ values and is defined as:

$$\varepsilon' = 1000\left[\frac{\delta D_a + 1000}{\delta D_P + 1000} - 1\right]. \quad (2)$$

For validation, we compared measured ε′ values with modeled values. For modeled values, single grid-cell simulations are conducted for the region where the measured values were taken from. Vegetation type was adjusted for each simulation to best reflect the plant species from which the *n*-alkanes were derived. Table 5.2 shows estimated ε′ values from these simulations, and compares them with measured present-day values. The modeled values were within the measured range for deciduous trees in Idaho (Yang and Huang, 2003), C4 grass in South Dakota (Smith and Freeman, 2006), and ferns, C3 and C4 plants in Japan (Chikaraishi and Naraoka, 2003; Chikaraishi et al., 2004). Modeled values also fell within the observed range for European deciduous trees and terrestrial lake sediments (Sachse et al., 2004, 2006). The model failed to predict ε′ values for Japanese CAM plants and European Sphagnum, though this might have been due to inadequate (or complete lack of) representation of these particular plant species in the model. Simulated values also did not agree with C3 grasses measured by Smith and Free-

man (2006), which could have been a consequence of mismatch between model conditions and their greenhouse growing conditions. Nonetheless, results in Table 5.2 demonstrate that the model does an adequate job in predicting fractionation processes that controlled δD_a values.

Figure 5.1a and 5.1b show simulated $\varepsilon_{w/a}$ values for present-day and Eocene conditions using the most realistic, "best guess", vegetation type, while Figures 5.1c-1e shows how $\varepsilon_{w/a}$ values spatially vary when the vegetation type is constant. For present-day, simulated $\varepsilon_{w/a}$ values were noticeably high (less negative) in regions in Asia and North America. However, $\varepsilon_{w/a}$ values were remarkably lower in northwest North America when the grid-cells contained broadleaf evergreen trees. Importantly, the model results demonstrate strong spatial variation in present-day $\varepsilon_{w/a}$ values, which is controlled by local meteorology and environmental conditions. For the present-day simulations, the choice of vegetation type partially affected the spatial variations in $\varepsilon_{w/a}$ values, though many features in panels 1a, 1c, and 1e are consistent across all three present-day simulations (e.g. high $\varepsilon_{w/a}$ values over most of Asia).

Compared to the present-day simulations, the Eocene spatial variations in $\varepsilon_{w/a}$ values were less dependent on vegetation type. Table 5.3 displays the global mean, the northern mid- and high-latitude mean, and the global standard deviation in $\varepsilon_{w/a}$ values for the three present-day and three Eocene simulations. The predicted global mean Eocene $\varepsilon_{w/a}$ values tend to be just slightly more negative than present

Table 5.2: Present-day model results and comparison with other studies.

Plant	Reference	Reference ε′ (‰)	Model ε′ (‰)
Quercus	Yang and Huang (2003)	-117	-110
Platanus	Yang and Huang (2003)	-93	-110
Salix	Yang and Huang (2003)	-144	-110
C3 plants	Chikaraishi and Naraoka (2003)	-117 ± 27	-130
C4 plants	Chikaraishi and Naraoka (2003)	-132 ± 12	-131
CAM plants	Chikaraishi and Naraoka (2003)	-147 ± 10	-131
Fern	Chikaraishi and Naraoka (2003)	-131 ± 6	-136
Lake sediments	Sachse et al. (2004)	-128 ± 12	-119
C3-gymnosperm	Chikaraishi et al. (2004)	-91 to -152	-128
C3 grasses	Smith and Freeman (2006)	-165 ± 12	-137
C4 grasses	Smith and Freeman (2006)	-140 ± 15	-139
Deciduous trees	Sachse et al. (2006)	-122	-121
Sphagnum species	Sachse et al. (2006)	-131	-119
Plant biomass	Sachse et al. (2006)	-118	-119

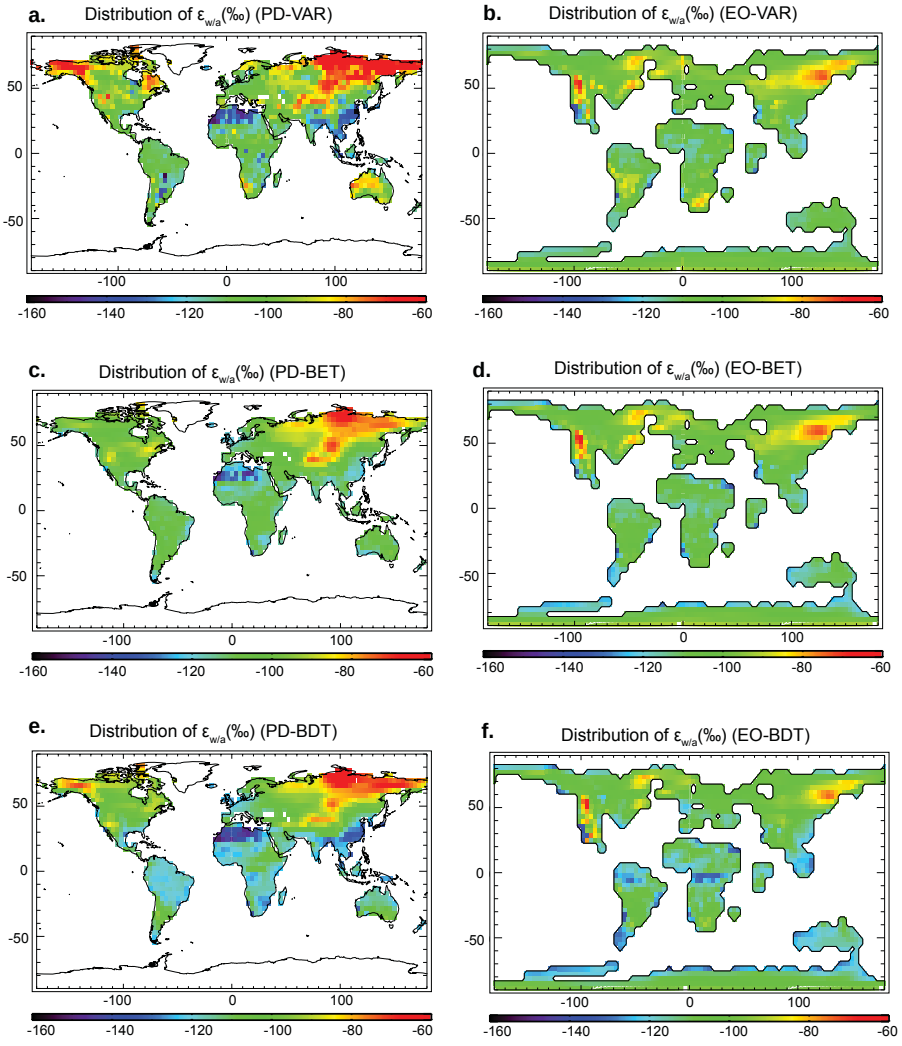

Figure 5.1: Global distribution of the offset value, $\varepsilon_{w/a}$ (‰), for the Present-day simulations (PD) and Eocene (EO) simulations, using (a,b) best guess vegetation type, (c,d) broadleaf evergreen trees, and (e,f) broadleaf deciduous trees. .

day (Table 5.3). When comparing the mean for the northern mid- and high-latitude (where most of the world's deciduous trees are found), the difference between Eo cene and present-day $\varepsilon_{w/a}$ values was much larger, however, the difference was not spatially uniform. For example, for the broadleaf deciduous tree simulations $\varepsilon_{w/a}$ values were almost the same during the Eocene compared to the present-day simulation over much of Europe (~1‰ difference) and eastern North America (~2‰ difference), whereas differences were large over Siberia (~18‰ difference),

Table 5.3: Simulated mean $\varepsilon_{w/a}$ values and the spatial standard deviation of $\varepsilon_{w/a}$ values.

Simulation	Standard Deviation $\varepsilon_{w/a}$ (‰)	Global Mean $\varepsilon_{w/a}$ (‰)	NH mid and high-lat Mean $\varepsilon_{w/a}$ (‰)[a]
PD-VAR	19.2	-102	-90.5
EOC-VAR	9.6	-103	-97.2
PD-BET	13.2	-105	-96.4
EOC-BET	10.4	-105	-98.0
PD-BDT	16.7	-109	-96.2
EOC-BDT	10.9	-110	-102.8

[a]poleward of 35 °N

central Asia (~20‰ difference), and western North America (a 22‰ difference in the Yukon and a -18‰ difference in the western U.S.). In the Eocene southwestern region of North America, $\varepsilon_{w/a}$ values were remarkably higher (less negative with a maximum value of -67‰), while values were lower to the north. Figure 5.1 clearly shows that Eocene $\varepsilon_{w/a}$ values differ from present-day values depending on location. These discrepancies have potential to bias estimates of past δD_p values and past temperature.

Assuming δD_p changes by 9‰/K (Jouzel et al., 1993; 1996; Petit et al., 1999; Noone, 2009) outside of the tropics, an average Eocene/present-day difference in $\varepsilon_{w/a}$ values of 7‰ at the northern mid- to high-latitudes would introduce a temperature estimate error of about 0.9K. However in specific regions where the difference between Eocene and present-day $\varepsilon_{w/a}$ values was relatively large reconstructed temperature errors will also be larger. In Siberia, for instance, the modeled 18‰ difference results in an error of about 2K.

5.3.2 Results from sensitivity experiments

Relative humidity and air temperature directly influence equation (1) and therefore $\varepsilon_{w/a}$. Furthermore, atmospheric CO_2 concentration and solar fluxes influence stomatal resistance indirectly and can thus change h in equation (1). All of these

Table 5.4: Values used in equation (7) for the three simulated cases.

	Case 1	Case 2	Case 3
$a\partial T/\partial(\partial D_p)$ (K/‰)	0.11	0.11	0.11
$b\Delta\delta D_a$ (‰)	-0.43	7.6	7.2
$c\Delta h_a$ (%)	1	0	1
$d\partial\varepsilon_{w/a}/\partial ha$ (‰/%)	-0.43	-0.43	-0.43
$e\partial\varepsilon_{w/a}/\partial T$ (‰/K)	-1.4	-1.4	-1.4
$f\Delta T$ (K)	0	1	1

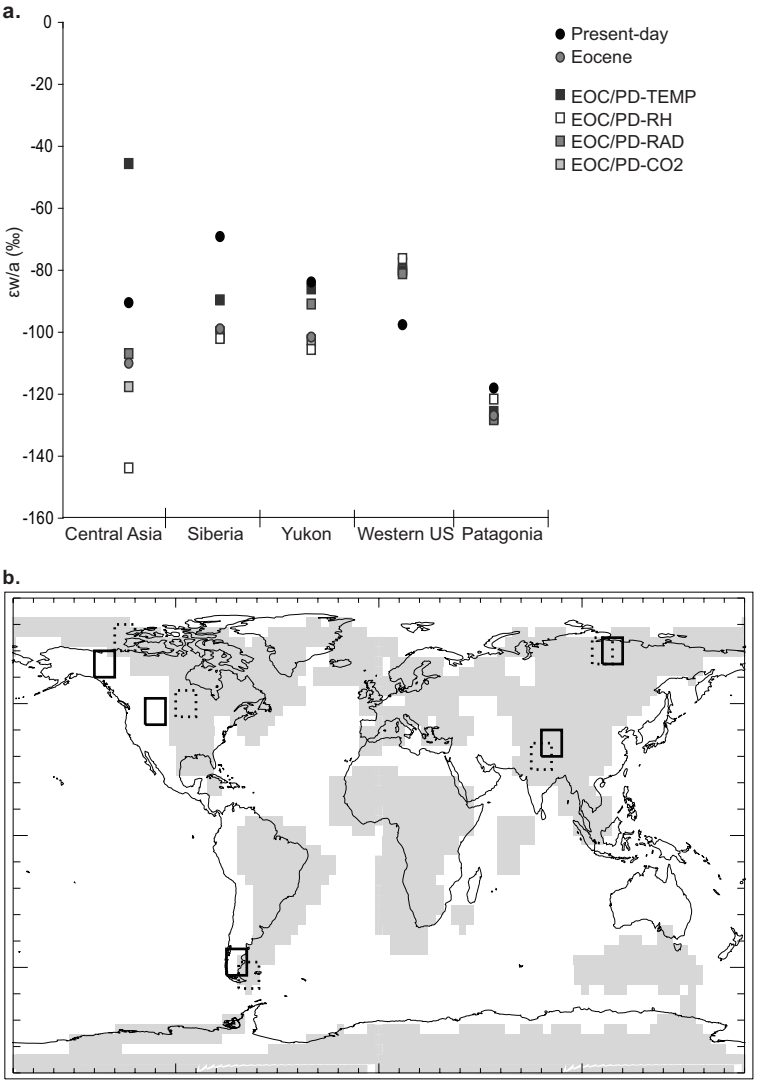

Figure 5.2: Mean $\varepsilon_{w/a}$ values (‰) for five regions for the six separate simulations listed in Table 5.1 (a). The locations of the five regions are shown in (b) as solid-line boxes for Present and dashed line boxes for Eocene. Continental locations during the Eocene are shown with light gray shading in panel b.

variables were probably different during the Eocene. Four sensitivity experiments were performed in which one of these four variables (temperature, relative humidity, solar radiation, or atmospheric CO_2 concentration) was set to present-day values, while maintaining Eocene-based values for all other variables. These sensitivity experiments were performed using only broadleaf deciduous trees to con-

trol physiologically induced differences. A list and description of each sensitivity experiment is given in Table 5.1. The influence of variables set to present-day values on Eocene model results is compared in five selected regions. The size of these regions is set to 10° of longitude by 10° of latitude, positioned at present day Central Asia, Siberia, the Yukon Territory, Western U.S., and Patagonia (shown as solid-line boxes in Figure 5.2b). To account for continental drift, Eocene results examined here are taken from regions that have been subjectively positioned at the approximate former location of these 5 areas (shown as dashed–line boxes in Figure 5.2b). Figure 5.2a compares model results for these regions that showed a clear discrepancy between the present-day and Eocene modeled $\varepsilon_{w/a}$ values.

The EOC/PD-TEMP sensitivity simulation used modern-day surface air temperatures to reveal the impact of high temperatures on latent heat fluxes, stomatal conductance, fractionation, and ultimately the value of $\varepsilon_{w/a}$. For this simulation, specific humidity was adjusted to match Eocene relative humidity, ensuring that the model's response was not associated with a vapor pressure response. The lower present-day temperatures caused $\varepsilon_{w/a}$ values to increase (less negative), which can be seen in Central Asia, Siberia, and in the Yukon regions. This temperature response was partially due to changes in the equilibrium vapor pressure offset above a liquid surface ($\varepsilon_{L\text{-}V}$). At temperatures around 300K, the fractionation factor changes by -1.1‰/K. For the Central Asia region (where the modeled response was largest) the isoCAM results suggest that the growing season temperatures were about 21 K warmer during the Eocene, which decreased the fractionation factor by 23‰. The modeled difference in $\varepsilon_{w/a}$ values between the Eocene and EOC/PD-TEMP simulations were about 64‰ for this region, so changes in the fractionation factor alone can potentially account for about one-third of the total $\varepsilon_{w/a}$ response to temperature changes.

Comparing the Eocene simulation with a simulation in which relative humidity is set to present-day values (EOC/PD-RH experiment) shows drastic changes in δD of leaf water and $\varepsilon_{w/a}$ for some regions. In general, the use of present-day relative humidity caused $\varepsilon_{w/a}$ values to be more negative (with the exception of Patagnonia). For these regions, the higher present-day relative humidity decreased leaf water isotope fractionation, due to decreased transpiration, causing δD of leaf water (and subsequently δD of *n*-alkanes) to be less enriched. The strongest isotopic response to relative humidity was found in Central Asia, where flux-weighted relative humidity was 24% lower during the Eocene. Taking the derivative of equation (1) and assuming a kinetic fractionation factor of 42‰ and an 80‰ difference between δD_{SW} and δD_{CV} values gives sensitivity: $\partial\delta D_L/\partial ha$ = -1.22‰/%. The modeled decrease in relative humidity would, therefore, cause δD_L values (and $\varepsilon_{w/a}$ values) to decrease by about 29‰ using the Craig-Gordon derived sensitivity, which is close to the modeled change of 33‰. A similar sensitivity was found by

Buenning et al. (2010a) in a set of experiments that simulated the ^{18}O content of leaf water, which was supported by observations of atmospheric $CO^{18}O$ (Buenning et al., 2010b). For Patagonia, the lower present-day relative humidity does bring $\varepsilon_{w/a}$ values closer to present-day simulated values, which indicates relative humidity is one of the variables that contributed to higher $\varepsilon_{w/a}$ values during the Eocene. For the other four regions, however, the model results suggest that relative humidity was not the main driver for the difference in $\varepsilon_{w/a}$ values between the two climatic states. In fact, in most regions humidity kept present day and Eocene $\varepsilon_{w/a}$ values from becoming too dissimilar by opposing changes associated with temperature and other factors (Figure 5.2a).

The Eocene simulations using modern-day radiation and modern-day CO_2 concentration only slightly altered δD and $\varepsilon_{w/a}$ values relative to the Eocene base simulation. In the Yukon region, however, radiation did appear to play a role as the region was at higher latitudes during the Eocene. The drastically lower solar energy input would have limited photosynthesis (Figure 5.1a in Nemani et al. (2003)), and caused both stomatal conductance and isotope fractionation to decrease.

To quantify the sensitivity of $\varepsilon_{w/a}$ to the parameters that showed the strongest impact, small perturbations were applied to both atmospheric temperature (T in units of K) and atmospheric relative humidity (ha in units of %). Additional simulations were performed to test the sensitivity of the global mean $\varepsilon_{w/a}$ value to small global perturbations in temperature and relative humidity. Sensitivities are thus approximated in terms of partial derivatives ($\partial\varepsilon_{w/a}/\partial T$ and $\partial\varepsilon_{w/a}/\partial ha$). These sensitivities can be written as partial derivatives (rather than total derivatives) since the change in the forcing is on that of the parameter of interest (i.e., all other forcing terms held fixed). The sensitivities can be used to construct a prediction model where deviations from the global mean value can be estimated as:

$$\Delta\varepsilon_{w/a} = \Delta T \frac{\partial \varepsilon_{w/a}}{\partial T} + \Delta h_a \frac{\partial \varepsilon_{w/a}}{\partial h_a} . \tag{3}$$

The resulting modeled sensitivities were approximately: $\partial\varepsilon_{w/a}/\partial T$ = -1.4‰/K and $\partial\varepsilon_{w/a}/\partial ha$ = -0.43‰/%. Consequently, these values can be used together with equation (3) to better estimate the $\varepsilon_{w/a}$ value to apply for any δD_a given known temperature and relative humidity anomalies. Because ΔT appears on the right, (3) must be modified to be useful for paleo-temperature reconstructions. Specifically, the reconstruction problem is posed as TEocene = TPresent + ΔT. Noting that one can write:

$$\Delta(\delta D_P) = \Delta(\delta D_a) - \Delta\varepsilon_{w\,a} \tag{4}$$

$$\Delta T = \Delta(\delta D_P)\frac{\partial T}{\partial(\delta D_P)} . \tag{5}$$

Substituting equation (3) into (4) gives

$$\Delta(\delta D_P) = \Delta D_a - \Delta T \frac{\partial \varepsilon_{w/a}}{\partial T} + \Delta h_a \frac{\partial \varepsilon_{w/a}}{\partial h_a} \quad (6)$$

which can be combined with equation (5) and rearranged to find an expression for the change in temperature:

$$\Delta T = \frac{\partial T}{\partial(\delta D_P)}\left(\Delta \delta D_a - \Delta h_a \frac{\partial \varepsilon_{w/a}}{\partial h_a}\right)\left[1 + \frac{\partial T}{\partial(\delta D_P)}\left(\frac{\partial \varepsilon_{w/a}}{\partial T}\right)\right]^{-1}. \quad (7)$$

The value of $\Delta\delta D_a$ is derived from analysis of deuterium in leaf wax *n*-alkanes from present-day and from those found within Eocene sediments. With the temperature isotope relationship specified by others (e.g. $\partial T/\partial(\delta D_P)$ (Jouzel et al., 1993, 1996; Petit et al., 1999)) and $\partial\varepsilon_{w/a}/\partial T$ and $\partial\varepsilon_{w/a}/\partial ha$ derived here, equation 7 provides a more accurate estimate of past temperatures given a known difference in δD_a values and an assumed change in ha, which could be difficult to estimate.

To demonstrate the usefulness of equation (7), three additional isoLSM simulations were conducted to validate the reconstruction. The three scenarios considered here were 1) a 1% increase in relative humidity; 2) a 1 K increase in global temperatures; and 3) both a 1 K increase in temperature and a 1% increase in relative humidity. For the last two additional simulations, the δD values of precipitation and atmospheric vapor were also increased by 9‰. The values used in equation 7 and the simulated change in global mean δD_a values are shown in Table 5.4. There was no temperature change in case 1, only a 1% increase in relative humidity, which caused the simulated global δD_a value to decrease by 0.43‰. Evaluating equation (7) with this change in δD_a values and the other values listed in Table 5.4 results in an estimated temperature change of 0 K, which was the expected result. For the 2nd case, the 1K increase in temperature and the 9‰ increase in the δD values of precipitation and vapor caused global δD_a values to increase by 7.6‰, yielding a predicted temperature change of 1.0 K (Table 5.4). When both changes are applied (case 3) isoLSM simulates a 7.2‰ increase to global δD_a values, which also predicts a 1 K increase in global temperatures. Thus, all 3 simulations demonstrate the ability of equation 7 to estimate temperature changes given differences in δD_a values and relative humidity.

Comparing Eocene and present-day simulations, equation (7) works remarkably well for some locations but poorly for others. For example, in Siberia, relative humidity and δD_a values were simulated to be about 10% and 25‰ higher during the Eocene, respectively, and equation (7) accurately backs out the 4K temperature difference. On the other hand, in the western U.S., equation (7) only predicts temperatures to be 1 K higher during the Eocene, whereas the set temperature difference was 9 K. The reason why equation (7) did not work for certain locations is that it

relies on the seasonality of the growing season, precipitation amount, and the δD value of precipitation to be constant in time.

5.3.3 Validity of annual mean proxy estimates

In addition to environmental controls on the biophysics, the premise that the *n*-alkane δD values can be used as a proxy for annual mean δD of precipitation (δD_P) rests on the stability in the seasonality of δD of precipitation relative to the growing season in which the leaf wax *n*-alkanes are produced. To evaluate these influences, the processes resulting in the final $\varepsilon_{w/a}$ value were broken down into three separate fractionation steps, including (1) precipitation to plant xylem water, (2) xylem water to leaf water, and (3) leaf water to leaf wax *n*-alkanes. The focus here is on the isotopic fractionation within the first two processes, assuming as before, the fractionation in the final step is approximately constant at –160‰.

Simulated amount-weighted δD_P values were subtracted from the photosynthesis weighted xylem δD_X values (1st component), and the same δD_X values were subtracted from photosynthesis weighted δD_L values (2nd component). Results are shown in Figure 5.3 for both present-day and Eocene broadleaf deciduous tree simulations. For the present-day simulation, the δD_P and δD_X difference exerted a minor influence on $\varepsilon_{w/a}$ values, with an exception for Patagonia and parts of Asia where it acts to keep $\varepsilon_{w/a}$ values relatively high. On the other hand, much of the spatial variation in $\varepsilon_{w/a}$ values was a consequence of the differences between δD_X and δD_L values. For instance, in the Siberian and Yukon regions the high simulated $\varepsilon_{w/a}$ values (Figure 5.1e) largely reflect the δD_L-δD_X difference (Figure 5.3c). These findings suggest that present-day $\varepsilon_{w/a}$ values are largely influenced by the δD_L-δD_X difference (as modeled by equation 1), with the exception of some locations (Patagonia and Central Asia) where water isotope seasonality appears to play some role.

Compared to the present-day simulation (Figures 5.3c and 5.3d), the Eocene simulation predicted less enrichment from xylem to leaf water (with an exception to a broad region in western North America). As shown through the sensitivity experiments, this was largely a result of higher temperatures during the Eocene growing season, causing $\varepsilon_{w/a}$ values to become relatively low. Additionally, the influence of the δD_X-δD_P difference was not the same during the Eocene. Particularly, in Patagonia the δD_X-δD_P difference (Figure 5.3b) decreased $\varepsilon_{w/a}$ values on average by 14‰, in contrast to the present-day simulation, which increased $\varepsilon_{w/a}$ values by about 2‰. This decrease in δ values seems to primarily reflect seasonality in the isotopic composition of precipitation relative to the growing season and is partially responsible for the lower $\varepsilon_{w/a}$ values during the Eocene in this region. These results suggest that differences or changes in the seasonality of precipitation and/or the isotopic com-

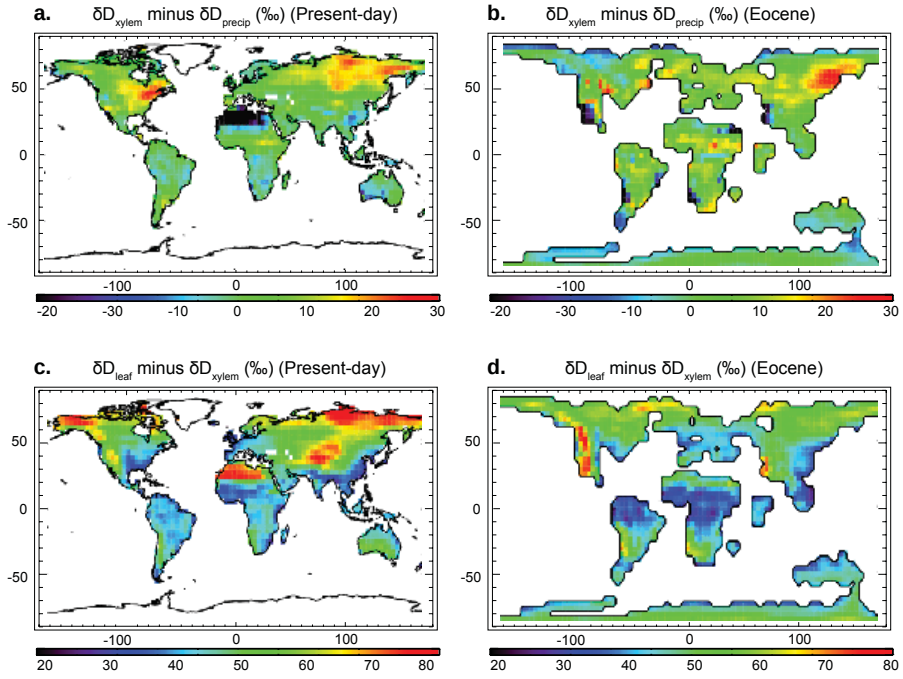

Figure 5.3: Photosynthesis weighted δ*D* of xylem water minus amount weighted annual mean δD of precipitation (‰) for both Present and Eocene simulations (a and b). Also plotted are photosynthesis weighted mean δD of leaf water minus photosynthesis weighted mean δD of xylem (‰) (c and d).

position of precipitation can potentially change the values of $\varepsilon_{w/a}$, which is a factor that has not previously been accounted for in *n*-alkane proxy reconstructions.

5.4 Conclusion

This study showed that the offset between δD values of precipitation and δD values of leaf wax *n*-alkanes ($\varepsilon_{w/a}$) varies in space and that the relationship was different under Eocene environmental conditions. Results from model simulations suggest that in the northern mid- to high-latitudes $\varepsilon_{w/a}$ values were on average 6‰ lower during the Eocene. Sensitivity experiments showed temperature and relative humidity exert a large influence on $\varepsilon_{w/a}$ values, where the influence of temperature is partially associated with the temperature dependence of equilibrium fractionation. Over Siberia and Central Asia the lower $\varepsilon_{w/a}$ values found for the Eocene simulation were largely a result of the higher growing season temperatures, which reduced the efficiency of fractionation during evaporation from leaves. Over the Yukon differences in $\varepsilon_{w/a}$ values resulted from changes in solar radiation and temperature,

while the differences in Patagonia were driven by a combination of relative humidity and the seasonal timing of the isotopic composition of precipitation.

Model results suggest that using a constant $\varepsilon_{w/a}$ value for reconstructing δD of paleo-precipitation from measured δD of *n*-alkanes is inaccurate. For the Eocene, the offset should be more negative than $\varepsilon_{w/a}$ values typically found today. This holds for many regions outside of the tropics (with the large exception in the western U.S.). Hence, when modern-day $\varepsilon_{w/a}$ values are used to reconstruct δD of paleo-precipitation, the reconstructed values will be skewed towards lower values, which in turn will lead to inaccurate interpretations of the paleo-hydrological cycle. Similarly, when using modern-day $\varepsilon_{w/a}$ values to estimate Eocene temperatures based on the δD of *n*-alkanes, the reconstructed values will be biased towards lower temperatures. This would suggest that the Eocene epoch might have been warmer than suggested by temperatures previously derived from *n*-alkane proxies. Differences in leaf water enrichment introduce an uncertainty in temperature reconstruction from δD values of leaf wax *n*-alkanes and should be taken into account when using δD_a values as a temperature proxy.

Acknowledgements

We thank Matt Huber for providing boundary data sets for ISOCAM simulations and Jaap Sinninghe Damsté for support. We acknowledge Virginia Tech Advanced Research Computing and the Department of Geosciences for computation support and resources. ENS acknowledges funding provided by the DARWIN Centre for Biogeology and Utrecht University. NHB and DCN were supported by an award from the NOAA Paleoclimatology Program.

Chapter 6

Reconstruction of Eocene Arctic hydrology using proxy data and isotope modeling

Eveline N. Speelman, Jacob O. Sewall, David C. Noone, Monique M.L. van Kempen, Jaap S. Sinninghe Damsté, and Gert-Jan Reichart

under review

Abstract

With the realization that both the Eocene Arctic Ocean and the Nordic Seas were covered with enormous quantities of the free floating freshwater fern *Azolla* (Brinkhuis et al., Nature, 2006), new questions regarding the Eocene conditions facilitating these blooms arose. Our present research focuses on constraining the sources and salinity of Eocene Arctic surface water through the application of compound-specific hydrogen isotope measurements and climate model simulations. The δD of long chain higher plant derived *n*-alkanes present in the Eocene Arctic sediments, in combination with a known fractionation during biosynthesis, provided an estimate of the δD of continental precipitation. Biomarkers specific for *Azolla* (i.e. 1,ω20 C_{32} – C_{36} diols) were encountered in Eocene Arctic sediments. Through culture experiments with extant *Azolla*, the δD fractionation of these diols relative to the culture water was determined (~100‰) and the δD of the Eocene diols can now provide insight into the isotopic composition of Eocene Arctic surface water. These reconstructed δD values of Arctic surface waters and precipitation fall in the same range, indicating that virtually no mixing between deeper saline waters (isotopically heavy) and the incoming freshwater (isotopically light) occurred. It is thus likely that the Eocene Arctic surface waters were significantly more fresh than the underlying waters. The Community Atmosphere Model v.3 combined with an integrated isotope tracer code (isoCAM3) was used to quantify the moisture path-

ways and runoff responsible for freshening of the Eocene Arctic surface waters. Results of model simulations with Eocene boundary conditions show increased moisture transport towards the Northern high latitudes. Net runoff and precipitation entering the Arctic amounted to 1.5 x 10^{13} m^3/yr, which is the equivalent of ca. 1700 mm/yr. Overall, model results and compound-specific δD measurements show precipitation pattern changes and confirm the extreme freshening (up to 0) of the Eocene Arctic surface waters that allowed *Azolla* blooms to develop.

6.1 Introduction

The Eocene *Azolla* interval (~49 Ma) represents a period of substantial freshening of Arctic surface waters during an estimated period of 0.16 – 1.2 Ma (Brinkhuis et al., 2006; Chapter 1). The freshening of the surface waters of the Arctic Ocean is associated with *in situ* growth and reproduction of the freshwater floating fern *Azolla*, in combination with high abundances of chrysophytes (Brinkhuis et al., 2006). The *Azolla* remains have been found in locations all around the Arctic Basin and in both Nordic Seas, including sites off the coast of Greenland and in Denmark (Brinkhuis et al., 2006; Heilmann-Clausen et al., 1985; Chapter 1; and references therein). In the Early/Middle Eocene the Arctic Ocean was almost completely enclosed (Scotese, 1988), with the still shallow proto-Fram Strait (Jakobsson et al., 2007) and epicontinental West Siberian Sea Strait/Turgai Strait (Akhmetiev, 2009) forming the only, probably intermittent, connections between the Arctic Basin and the open ocean. The continued presence of marine diatoms indicates that the deeper water must have remained more saline than the surface waters (Stickley et al., 2008). A quantitative salinity estimate of ~ 21 for deeper waters comes from Waddell and Moore (2008), based on oxygen isotope analyses of fish bones recrystalized in these deeper waters. During the *Azolla* interval, the Arctic was warm, with sea surface temperatures (SSTs) between 8 and 12 °C (Brinkhuis et al., 2006) and air temperatures up to 20 °C (Barke et al., in prep.). Also, tropical SSTs were higher than present (32 – 34 °C at 19 °S; Pearson et al., 2007).

The rainfall response to these Eocene sea surface temperature (SST) conditions is two-fold: 1) enhanced global precipitation as a direct consequence of higher tropical temperatures and 2) changing precipitation patterns resulting from a decreased equator-to-pole SST gradient. An increase in tropical SSTs leads to lower tropical lapse rates, driven by the moist adiabatic response in the tropics. Due to the lower lapse rates and higher atmospheric temperatures, water vapour loading is higher in the Eocene (Pagani et al., 2006; Chapter 4). In contrast to the amount, the rainfall patterns as a function of latitude are not associated with the global mean temperature, but only with the latitudinal temperature gradient. A prevailing decreased equator-to-pole gradient leads to a decrease in both eddy and total transport (e.g.

Rind, 1998). However, higher global mean temperatures for the Eocene drive overall increased transport of latent heat and increased divergence of water (Chapter 4). Changes in water vapour flux convergence and precipitation minus evaporation (P - E) may have altered river runoff into the Arctic Ocean, potentially influencing its density structure and stratification through freshening of the surface waters. However, where the moisture came from, how much runoff entered the Arctic Basin and to which degree the Arctic surface waters became fresh (i.e. how much mixing between fresh surface and saline deep water still may have occurred) is still largely unknown.

The hydrogen isotopic composition of precipitation reflects the combined influence of source-region δD, water mass loss during transport, local temperature, and the additive contribution of local water (Craig and Gordon, 1965; Merlivat and Jouzel, 1979). Hence, differences in hydrological cycling should be reflected in the isotopic composition of Eocene precipitation, which can be captured in organic matter (Epstein et al., 1976). Sediments from the *Azolla* interval, recovered from the Lomonosov Ridge in the central Arctic Ocean during Integrated Ocean Drilling Program Expedition 302 (ACEX), contain high amounts of well-preserved organic compounds, including long chain *n*-alkanes and specific biomarkers for *Azolla* (e.g. 1,ω20 C_{32} – C_{36} diols, 9,10 C_{29} diol; Chapter 2). Long chain *n*-alkanes with an odd-over-even predominance are typically derived from the waxes of higher plants (Eglinton and Hamilton, 1967) and can be used to reconstruct (palaeo)precipitation δD over land (Sessions et al., 1999; Sachse et al., 2004; Pagani et al., 2006). Determination of the hydrogen isotopic composition of the biomarkers for *Azolla* from the Eocene Arctic, compared to the δD of extant *Azolla* cultured in water with known isotopic composition, potentially provides insight into the isotopic composition of Eocene Arctic surface water. An isotope enabled climate model has been calibrated for the Eocene (Chapter 4), comparing available precipitation δD proxy values with modeling experiments. As the model seems capable of capturing precipitation amounts and distribution accurately for both the Eocene and the present, it can now be specifically applied to interpret the Eocene Arctic hydrological budget.

Here we determine the hydrogen isotopic fractionation of terrestrially derived *n*-alkanes and compare this δD proxy data with new isotope model simulations to identify the precipitation source regions and prevailing meteorological conditions acting to freshen Eocene Arctic surface waters. Furthermore, we determine the hydrogen isotopic fractionation between the *Azolla*-specific biomarkers and the water it grows in. Combining the δD measurements on *n*-alkanes and *Azolla* 1,ω20 C_{32} diols (both extracted from ACEX sediments), with modeled runoff will provide additional constraints on Eocene Arctic surface water salinity.

6.2 Materials and Methods

6.2.1 Sample material

6.2.1.1 Extant Azolla

Azolla filiculoides was collected from an arable land ditch in the surroundings of Elst, The Netherlands (N51°55'48"; E5°50'6") and was cultivated in the laboratory for approximately 4 months. In the experiment the plants were grown in nutrient solutions to which different amounts of a 5M NaCl stock solution were added (0 and 60 mM, respectively). At the start of the experiment 4 g of fresh *Azolla* was introduced into separate aquaria, with three replicates per treatment (detailed description in van Kempen et al., under review). Subsamples of the different nutrient solutions were stored for later stable hydrogen isotopic analyses. *Azolla* samples were dried at 70 °C for subsequent biomarker extraction and compound specific hydrogen isotope analyses.

6.2.1.2 Sediment samples

During the IODP 302 ACEX expedition, a core was taken at the Lomonosov Ridge, Site 302, Hole M0004A, 87.87 °N, 136.18 °E (Backman et al., 2006). After extraction and screening of circa 80 samples, we selected three sediment samples in which biomarker concentrations were high enough to allow compound specific hydrogen isotopic analyses. All three samples are from lithologic biogenic subunit 2 (265.01 – 301.35 meter coring depth), Core 11x, Hole 4A. One sample from interval 2w, section 121 – 122 cm (300.01 mbsf), one sample from interval 3w, section 118-121 cm combined with 126-128 cm (301.49 mbsf), and one from interval 4w, section 25-29 cm (302.65 mbsf) were extracted for biomarkers. All samples were taken from depths at which *Azolla* microspore massulae abundance and correspondingly organic carbon content were intermediate (4.0, 4.3 and 4.0 wt% Corg, respectively; Chapter 8).

6.2.2 Sample preparation and biomarker identification

6.2.2.1 Biomarkers

Between 0.5 and 5 g of freeze-dried sediment or extant *Azolla* specimens was powdered and subsequently extracted with an Accelerated Solvent Extractor (Dionex) using a dichloromethane (DCM) – methanol (MeOH) mixture (9:1, v/v). The lipid fractions obtained during accelerated solvent extraction were separated by column chromatography using an elution sequence of hexane/DCM (9:1 v/v) and DCM/MeOH (1:1 v/v). All extracts were de-sulphurized using activated Copper. Urea adduction was used on the apolar fraction to separate the normal alkanes from cyclic and branched alkanes, using a mixture of methanol-saturated urea, hexane and acetone (200 µl each). The resulting urea crystals were extracted with hexane and subsequently dissolved in 1 ml of double distilled H_2O (MiliQ)/methanol (1:1 v/v), and extracted with hexane to yield the purified *n*-alkane fraction. To remove methylated fatty acids, the obtained *n*-alkane fraction was further purified using

column chromatography using $AgNO_3$-impregnated silica as the stationary phase and hexane, hexane/DCM (9:1, v/v) and hexane/DCM (1:1, v/v) as eluents, where the *n*-alkanes elute in the hexane fraction.

From selected other sediment samples and extracts of extant *Azolla*, total lipid fractions were de-sulphurized (sediment extracts only) and methylated with BF_3/MeOH at 60° for 10 min. A purified fraction containing only 1,ω20 diols was obtained using TLC (as described in Chapter 2). Polar compounds containing an alcohol moiety (sample 11x3w 118-121,126-128 cm and the *Azolla* extract) were silylated using BSTFA/pyr (1:1) and heated at 60 °C for 20 minutes. For comparison, the TLC fractions of sample 11x4w 25-29.5 and also the *Azolla* extract were acetylated using acetic anhydride and pyridine (200 µl each) and heated at 75 °C for 30 minutes.

Compounds were identified by GC/MS (Thermo Trace GC Ultra). Samples were injected on-column at 70 °C (CP-Sil 5CB fused silica column (30 m x 0.32 mm i.d, film thickness 0.1 µm)) with Helium as carrier gas set at constant pressure (100 KPa). The oven program was set to a rate of 20 °C/min to 130 °C, followed by 4 °C/min to 320 °C, and an isothermal hold for 20 min.

6.2.2.2 Compound specific δD analyses

The adducted *n*-alkane fractions and the TLC isolated 1,ω20 C_{32} - C_{36} diol fractions were analysed for their stable hydrogen isotopic compositions using isotope ratio monitoring gas chromatography-mass spectrometry (GC-IRMS; ThermoFinnigan Delta-Plus XP mass spectrometer). A similar column and oven program were used as described above, though with a constant flow of 1 ml/min. Pyrolytic conversion of organic hydrogen to H_2 was conducted at 1400 °C. The H3 factor was determined daily, and was always below 5. Schimmelmann Mixture A and B (Schimmelmann, Biogeochemical Laboratories, Indiana University) were run twice-daily alternately to correct reference gas values. Performance during analysis was monitored using a co-injected standard (squalane) with a known δD isotopic composition (also Schimmelmann). Hydrogen isotopic compositions are reported relative to VSMOW and are based on duplicate analyses, where possible, of well-resolved peaks (> 400 mV); representing averaged values. The δD of the used BSTFA (-60 to -80‰) was determined offline using butanol with a predetermined δD (-110‰), introducing an uncertainty of 3‰ to the overall measurements. The hydrogen isotopic composition of acetic anhydride used for acetylation was determined (-34.9‰) at the Royal Netherlands Institute for Sea Research (NIOZ) by direct injection on the Elemental Analysis (EA)/Thermal Conversion (TC)/IRMS with a Thermo Electron EA/TC coupled to a Thermo Electron DELTAPlus XL mass spectrometer. In the case of alcohol moieties, the δD values were corrected for the BSTFA and acetanhydride, respectively. The precision of isotopic measurements of H_2 reference gas

was 0.2 or better. The average standard deviation per day for separate *n*-alkanes in the Schimmelmann standards was below 4‰.

6.2.3 Analyses of water δD

Water samples from the culturing experiment were analysed for their hydrogen isotopic composition. 5 µl of water was injected on a Cr-oven at 900 °C and reacted for 10 minutes. The generated H_2 was subsequently captured using liquid nitrogen and measured on a dual inlet Mass spectrometer (Delta Plus, Thermo). Values are reported with respect to the VSMOW scale, using three laboratory standards (RZW and RMW (in-house standards) and Greenland Ice Sheet Precipitation (GISP)). Precision of the analyses was ~3‰.

6.2.4 Model description and boundary conditions

The Community Atmosphere Model v.3 (CAM3, Collins et al., 2006), developed by the National Center for Atmospheric Research (NCAR), combined with an integrated isotope tracer code (isoCAM3; Noone, 2003; Noone and Sturm, 2010) is used to simulate climatological conditions as well as the isotopic composition of precipitation for both the Eocene *Azolla* interval and a modern-day control run. IsoCAM3 is coupled to a dynamic land surface model (CLM3: Bonan et al., 2002; Oleson et al., 2004). The isoCAM3 runs are set up to simulate the H_2O, HDO, and $H_2{}^{18}O$ content in both precipitation and water vapor (Noone, 2003; Noone and Sturm, 2010). The modern day simulation (MOD) was set up with modern boundary conditions and forcings (e.g. atmospheric pCO_2) and is described in detail elsewhere (Chapter 4). Outcomes of the first Eocene simulation (EO-AZOLLA) broadly agree with climate proxy data from around the globe and accurately capture the global isotopic composition of precipitation for the Early/Middle Eocene (Chapter 4). However, close to the Arctic, the model was found to overestimate precipitation δD as compared to proxy data (Chapter 4). In the new Eocene simulation (EO-AZOLLA-FRESH) global mean δD and $\delta^{18}O$ (VSMOW) of seawater is set to reflect ice-free conditions (-8‰ for δD and -1‰ for $\delta^{18}O$, respectively), and Arctic seawater is set to -82.8‰ (δD) and -11.3‰ ($\delta^{18}O$), respectively. We thus still prescribe a constant isotopic composition for ocean surface water, but now with the composition of the Arctic surface waters being based on the isotopic composition of runoff entering the Arctic in the EO-AZOLLA model experiment. This specification is consistent with the Arctic being capped by fresher and less dense water derived from river outflow. All Eocene simulations are driven by fixed, zonally constant, sea surface temperatures (SSTs), modified from a fully coupled CCSM1.4 Eocene run (Huber and Nof, 2006; Chapter 4). In EO-AZOLLA-FRESH, Arctic SST is set to 9.4 °C, based on TEX_{86} temperature estimates for the *Azolla* interval. To investigate the effect of changes in the SST gradient on the hydrogen isotopic composition of Arctic sea surface water, we conducted two additional experimental runs. The first one is slightly warmer with a mean annual Arctic SST of 11.8 °C (EO-WARM) and the sec-

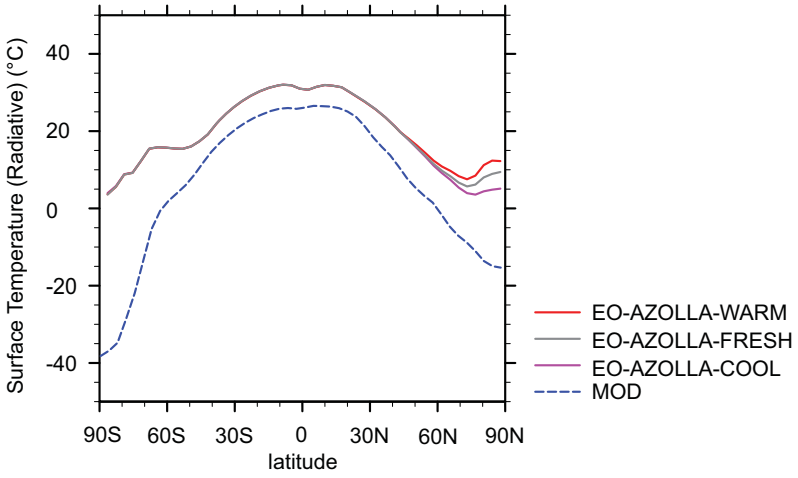

Figure 6.1: Modeled latitudinal mean annual sea surface temperatures (SSTs, in °C), for both the EO-AZOLLA-FRESH (pink), EO-AZOLLA-WARM (red) and EO-AZOLLA-COOL (blue) runs.

ond run sets mean annual Arctic SST to 7.2 °C, where TEX_{86} values are taken as being representative of Arctic summer SST (EO-COOL), while keeping temperatures below 45 °N constant. EO-COOL also contained a pre-described fixed amount of perennial sea-ice, where sea ice exists where T < 0 °C. The resulting latitudinal gradients are presented in Figure 6.1. The isotope-enabled CAM3 simulations ran for 30 years at a spectral resolution of T31 (~3.75 °lat. x 3.75 °lon), with the last 10 years averaged and used for subsequent evaluation. In total 3 new simulations were run. Boundary conditions applied in all 5 simulations, including the original EO-AZOLLA and MOD runs (Chapter 4), are presented in Table 6.1.

Table 6.1: Overview of the set-up of the different model simulations.

	Arctic SST (°C)	pCO_2 (ppm)	Arctic Sea Ice	δD Arctic surface water (‰)	$\delta^{18}O$ Arctic surface water (‰)
MOD	-2	365	Y	0	0
EO-AZOLLA	9.4	2000	N	-8	-1
EO-WARM	11.8	2000	N	-8	-1
EO-COOL	7.2	2000	Y	-8	-1
EO-AZOLLA-FRESH	9.4	2000	N	-82.8	-11.3

6.3 Results and Discussion

6.3.1 ACEX proxy data for Eocene Arctic precipitation

Whereas in ACEX sediment samples long chain *n*-alkanes are present, only in one sample (11x 2w 121 - 122 cm) were they present in high enough concentrations to allow compound specific hydrogen isotope analyses. These *n*-alkanes, with a clear odd over even predominance, are derived from higher plant waxes (Eglinton and Hamilton, 1967) and were probably transported to the Lomonosov Ridge by either river runoff or on dust particles, since extracts of extant *Azolla* do not contain these compounds. Compound specific hydrogen isotope analyses showed that the C_{27} and C_{29} *n*-alkane δD values were -210 and -238‰ (VSMOW), respectively. For reconstruction of precipitation δD values, measured compound specific *n*-alkane δD values should be corrected for isotopic fractionation during biosynthesis (160‰) and fractionation resulting from evaporative enrichment. Apparent fractionation factors of 86 to over 130‰ have been reported (Sachse et al., 2004; 2006; Yang et al., 2009). However, apparent fractionation varies with humidity, temperature, and pCO_2 and was thus likely different for the Eocene (Liu et al., 2006; Chapter 5). Using similar boundary conditions as described above and modeled precipitation and humidity, apparent fractionation factors ($\varepsilon_{w/a}$ values) were calculated specifically for the Early/Middle Eocene *Azolla* interval (Chapter 5). For deciduous trees surrounding the Arctic, the computed average apparent fractionation factor ($e_{w/a}$) is 105‰ (Chapter 5). This gives a C_{27} and C_{29} *n*-alkane derived δD of -105 to - 133‰ for precipitation (δD_{precip}) falling in proximity of the Eocene Arctic Ocean. These values agree with the high end of reconstructed δD of environmental water of -110 to -183 (Jahren and Sternberg, 2003) and -131 to -168‰ (Jahren et al., 2009) for Axel Heiberg Island and are in the same range as δD_{precip} reconstructed by Pagani et al. (2006) for the Arctic after the Paleocene Eocene Thermal Maximum (-105 to -145‰). These values for high latitude δD_{precip} are also in line with increased high latitude precipitation resulting from enhanced moisture transport as a consequence of warm climatic conditions and prevalence of a reduced equator-to-pole SST gradient. Still, this δD_{precip} value represents only a single geographical location. Hence, a numerical modeling approach is needed to quantify fresh water fluxes and to calculate weighted averages of δD_{precip} over the Arctic drainage basin as preferential moisture pathways could have a large impact on the overall isotopic composition of the integrated freshwater budget.

6.3.2 Model Outcome

6.3.2.1 Model outcome with adapted Arctic surface water δD

Proxy-inferred and modeled Arctic precipitation for the Eocene *Azolla* interval show that precipitation δD was substantially enriched relative to today, with δD_{precip} values of -105 to - 133‰ (proxy-based) and -40 to -130‰ (modeled), respectively. Comparison between EO-AZOLLA and EO-AZOLLA-FRESH shows that the isotopic composition of the runoff, mass weighted by mean monthly precipitation,

entering the Arctic became slightly more depleted: -79.1‰ for δD and - 10.7‰ for $\delta^{18}O$ for the EO-AZOLLA versus -86‰ δD -11.7‰ $\delta^{18}O$ for the EO-AZOLLA-FRESH simulation (Fig. 6.2b; within area indicated by the black line). No substantial differences were observed below 60 °N, indicating that the original results (EO-AZOLLA; Fig. 6.2a) for the continental regions surrounding the Arctic (above 60 °N) were, indeed, somewhat influenced by evaporation of relatively enriched Arctic Ocean surface water. The δD of the precipitation falling directly over the Arctic Ocean shows a significant decrease, from -54‰ (EO-AZOLLA) to -100‰ (EO-AZOLLA-FRESH). However, modeled mean annual precipitation weighted δD summed over the entire Arctic catchment and ocean areas (-89‰) is still less depleted than the δDp reconstruction based on the ACEX data and existing proxy-based estimates from this region (e.g. Jahren et al., 2009), but overlap with values simulated by Roberts et al. (2009) for Eocene Arctic surface water δD. These data are not mutually exclusive since the mean annual precipitation weighted average δD_{precip} of the Arctic basin is based on the basin as a whole, whereas the proxy-based values represent single geographical locations and timing (e.g. seasonal bias of the growth season).

For validation of our new modeling approach we compare available, proxy-derived δD_{precip} values for the *Azolla* interval with modeled δD_{precip} from both the original run (EO-AZOLLA) and the new simulation (EO-AZOLLA-FRESH), with a special focus on the area influencing Arctic runoff (Fig. 6.2). Proxy-based reconstructions of δDp encountered within this area come from samples from Axel Heiberg Island (Jahren et al., 2009), the Lillebælt Clay Formation, Denmark, and a sediment core taken off the coast of Greenland (IODP 151, 913B) (Chapter 4). The measured δD of C_{29} *n*-alkanes from the latter two are now, like for the Arctic, corrected using apparent fractionation factors of -119‰ (Danish Outcrop) and -100‰ (Greenland), respectively, based on the in Chapter 5 computed $e_{w/a}$ values. The δD of precipitation from the EO-AZOLLA-FRESH simulation more closely resembles proxy-derived δD_{precip} in the regions where *Azolla* thrived: for both the Danish Outcrop and Greenland samples, reconstructed and modeled δD_{precip} show a better match with EO-AZOLLA-FRESH (Fig. 6.2b). Also, modeled δD_{precip} values at Axel Heiberg Island are closer to reconstructed values in EO-AZOLLA-FRESH than they are in the original EO-AZOLLA experiment (Fig. 6.2b). Differences may be explained by the fact that proxy-derived δD_{precip} probably represents seasonal precipitation. For example, modeled δD of Eocene precipitation in the Axel Heiberg region varies between -82‰ (June) and -163‰ (February). A strong contribution of recycled water to local rainfall (50% in the model) enriches precipitation isotopically and thus amplifies the seasonal amplitude of the water isotopes (as reflected in relatively high summer δD_{precip} values). Jahren et al. (2009) argue that *n*-alkanes in Middle Eocene sediments from Axel Heiberg Island recorded environmental water δD early in the short growing season (−168 to −131‰). These values overlap with our mod-

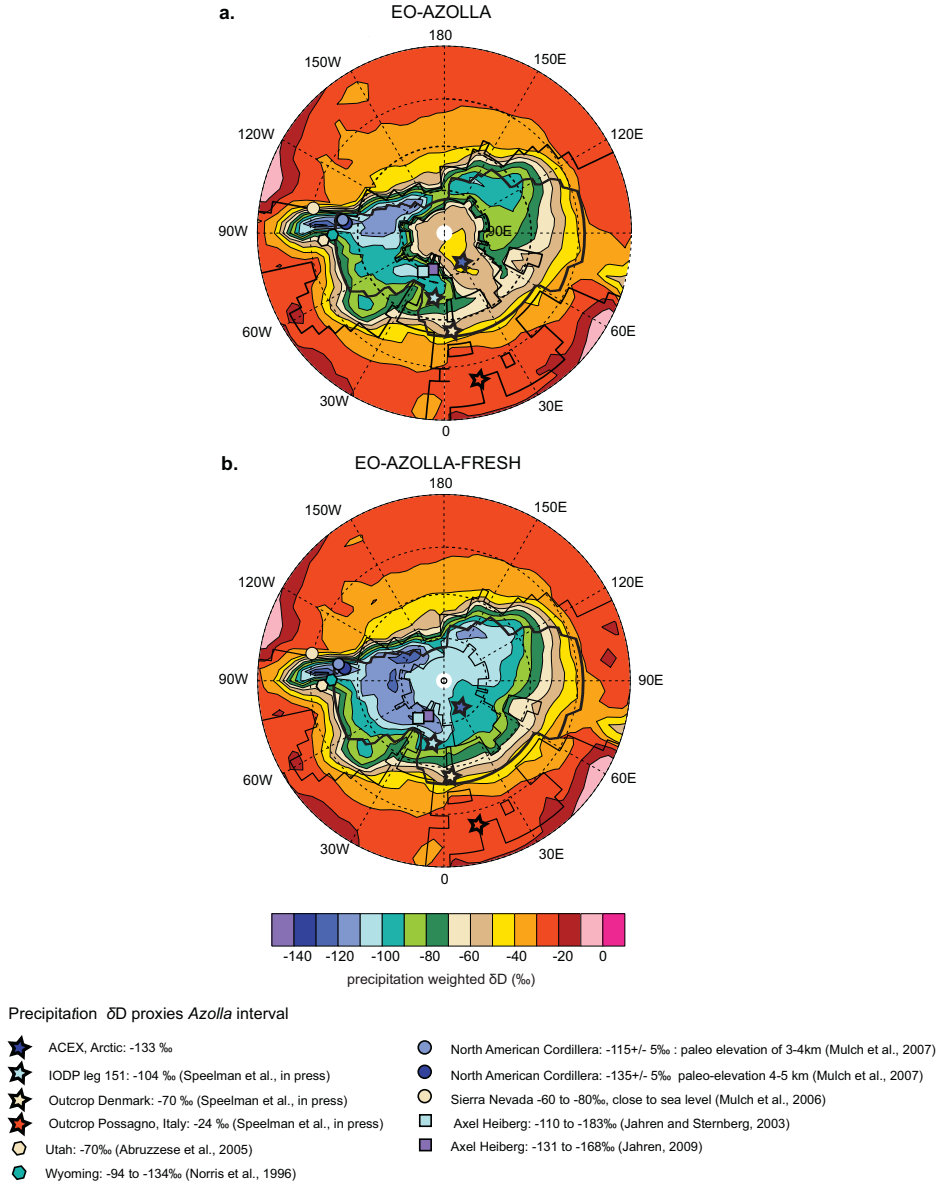

Figure 6.2: (a) Precipitation δD for the Northern Hemisphere (>30 °N) for EO-AZOLLA and (b) Precipitation δD for the Northern Hemisphere (30 °N onwards) for EO-AZOLLA-FRESH, with the borders of the Eocene Arctic catchment area indicated with a black line. Model – data comparison for Eocene precipitation-weighted δD, where the colors of the symbols correspond to the color scale of the underlying plot.

eled winter/spring δD_{precip} values for this region and C_{29} *n*-alkane derived δD_{precip} estimates from the ACEX sediments (of -105 to -133‰). In addition, in the same study δD estimates of environmental water were made using the $\delta^{18}O$ of phenylglucosazone (a product of wood synthesis), where wood construction is performed relatively late in the growing season, and at a more constant rate year round. The wood compounds indicate less depleted δD_{precip} of ~-125 to -145‰ (Jahren et al., 2009). Modeled mean annual precipitation weighted δD_{precip} is slightly less depleted for this specific region (-102‰; EO-AZOLLA and -111‰; EO-AZOLLA-FRESH) potentially indicating that the contribution of summer precipitation with a high δD_{precip} is overestimated in our simulations. Overall isotopic composition of precipitation as modeled in EO-AZOLLA-FRESH gives a more accurate representation of δD_{precip} than EO-AZOLLA for this region during the *Azolla* interval. Moreover, the fact that EO-AZOLLA-FRESH gives a better match with the proxy-data lends support to the idea that the Arctic surface waters were indeed (more) isotopically depleted and, therefore, fresh(er).

6.3.2.2 Arctic water budget

The net Arctic atmospheric water budget is determined by meridional water transport. Higher global mean temperatures for the Eocene drive increased transport of latent heat and increased divergence of water (Chapter 4). Figure 6.3a shows the vertically integrated mean annual northward moisture transport ($\overline{vq}$), mean meridional moisture circulation ($\overline{v}\,\overline{q}$), and moisture transport due to transient perturbations ($\overline{v'q'}$), across the southern-most boundary of the defined drainage area of the Arctic (Fig. 6.3b) for the Eocene run (EO-AZOLLA-FRESH). The area from which runoff drains into the Eocene Arctic Ocean is based on Eocene topography (Sewall et. al., 2000) and is shown in Figures 6.3b and 6.4 (black lines). Overall, there is a net northward-directed flux of water vapor into the basin (Fig. 6.3a). In fact, only between 65 - 100 °W (central North America) southward moisture transport (negative values) prevails. Peak pole-ward transport occurs at the Atlantic side of the Arctic (~15 °W), reflecting the combined effects of high vertically integrated available moisture (> 2g/kg) and high mean values of v (6 m/s). Eddy meridional transport of water vapor, as typically seen along the polar front and in the intertropical convergence zone, also shows a predominant flow directed northward (Fig. 6.3a). In contrast, mean meridional circulation ($\overline{v}\,\overline{q}$) is only directed into the basin between 60 - 100 °E (Central Asia), 170 °E - 110 °W (Pacific Ocean) and 60 °W - 20 °E (Atlantic Ocean). As is evident from figure 4b, mean annual precipitation excess (P-E) over the Eocene Arctic basin ranges widely. The mean annual amount of precipitation falling over the Arctic Basin is 620 mm/yr. The amount of computed mean annual runoff in the indicated Arctic catchment area (Fig. 6.4) of 23×10^6 km2 sums up to 2.5×10^{13} m^3 /yr or 906 mm/yr, which is more than four times the currently recorded river runoff into the Arctic of 0.513 10^{13} m^3/yr or 212 mm/yr averaged across the drainage basin (Lammers, 2001). Total modeled evaporation is 1.54

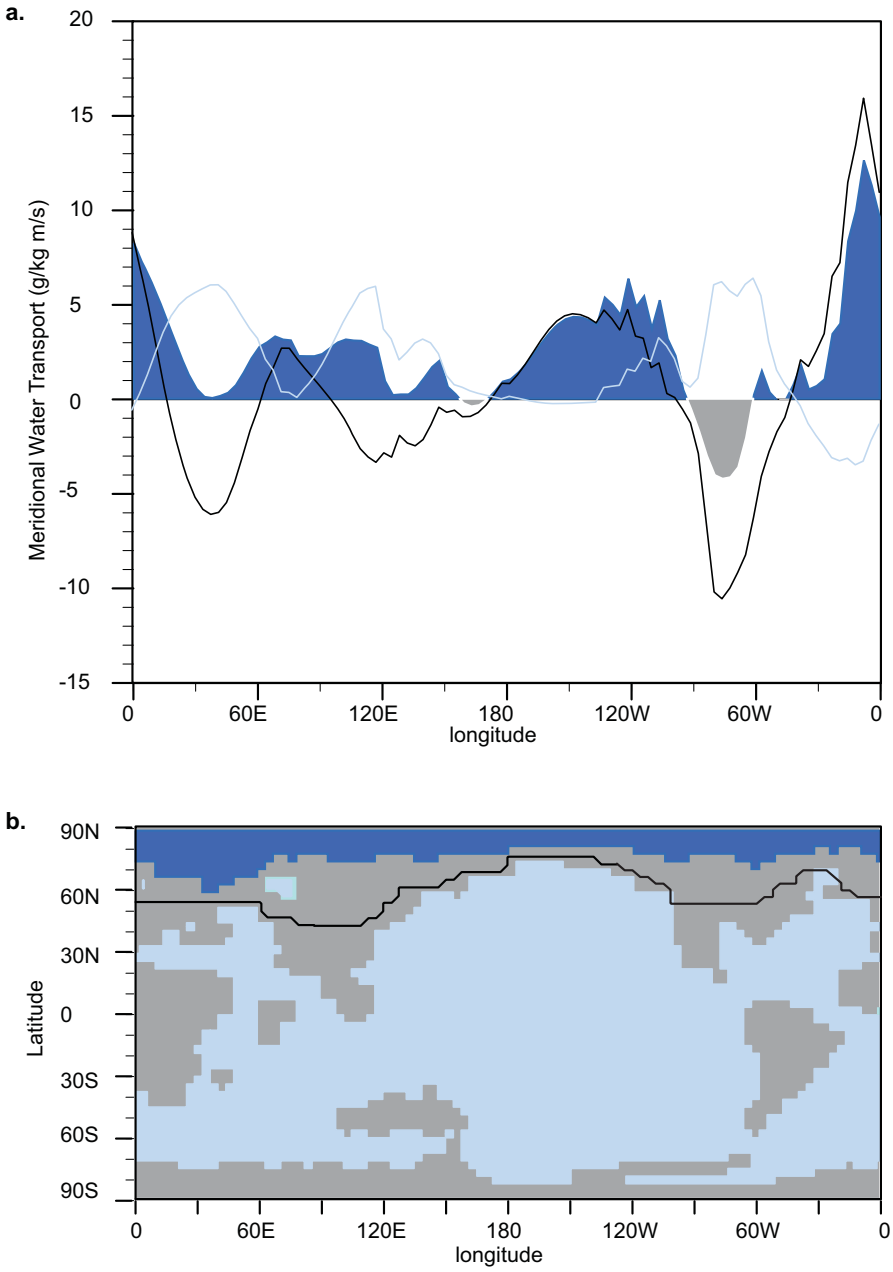

Figure 6.3: (a) long-tem (10 year) longitudinal distribution of vertically integrated (from p = surface pressure to p = 1mb, in g/kg m/s) averages of total mean meridional vapour transport (blue area), mean meridional vapour transport (black line) and transient meridional vapour transport (light blue line) for EO-AZOLLA simulation. (2) Plot of configuration of Eocene continents (grey). Area from which runoff drains into the Arctic Ocean is indicated by the black line.

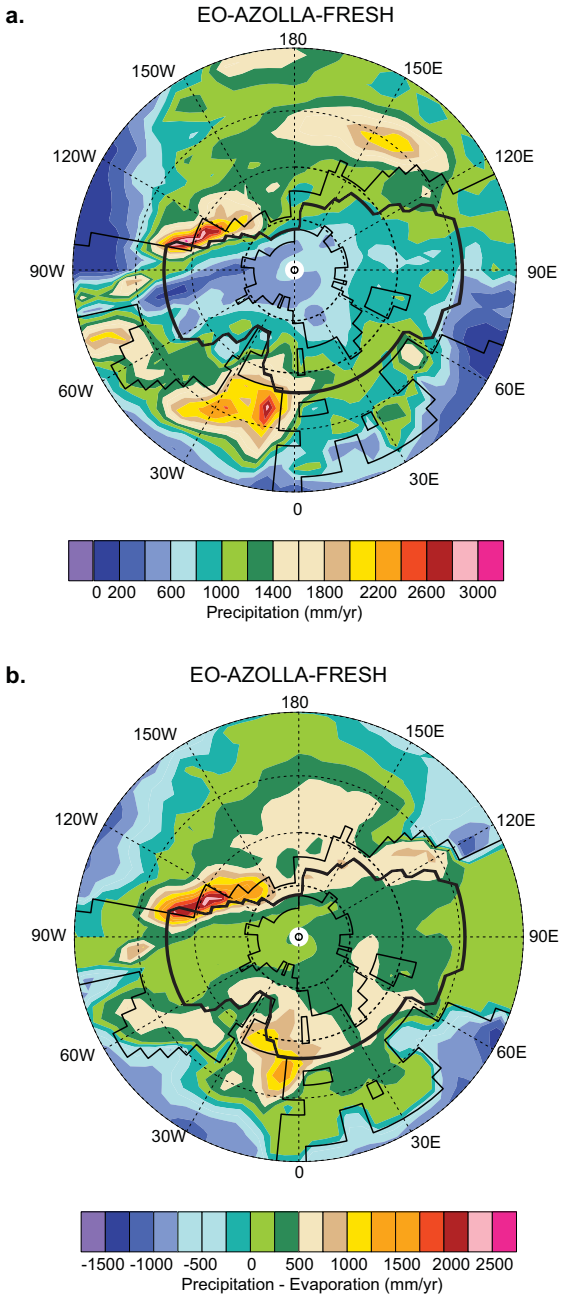

Figure 6.4: (a) Modeled net precipitation (precipitation - evaporation) over the Northern Hemisphere for EO-AZOLLA-FRESH, with the Eocene Arctic Ocean and the corresponding runoff area surrounded by black line. (b) Modeled net precipitation (precipitation - evaporation) over the Northern Hemisphere for EO-AZOLLA-FRESH.

x 10^{13} m^3, of which 16% originates from within the Arctic Basin. Hence the summed net amount of freshwater entering the Arctic Basin (Precipitation + Runoff - Evaporation) is 1.45 x 10^{13} m^3, which is the equivalent of 1700 mm/yr (based on area of the model Eocene Arctic basin of 8.55 x 10^{12} m^2). Overall, about 50% of the precipitation in the drainage basin is advected precipitation and the remainder of precipitation falling in the Eocene Arctic is associated with locally derived precipitation (precipitation associated with water evaporated from the surface within the region). As indicated in Figure 6.3a, the net advective moisture flux, calculated as the line integral of the vertically integrated moisture flux directed into the region, sums up to ~26.9 kg/m/s (~1.45 x 10^{13} m^3) (vs 11.5, or 6.1 x 10^{12} m^3 for MOD along the same shell), highlighting the net influx of freshwater into the Eocene Arctic catchment area. Both the enhanced freshwater influx and isotopically depleted precipitation suggested by the model simulation are in line with the occurrence of *Azolla* in the Arctic.

6.3.3 Arctic surface water salinity reconstruction

To investigate the hydrogen isotopic composition of the Eocene Arctic surface waters and thence their salinity, we analyzed *Azolla* biomarkers for their compound specific δD isotopic composition. Analyses of the δD of 1,ω20 C_{32}, C_{34}, C_{36} diols produced by the cultured *Azolla filiculoides* showed values between ~ -151 to -163‰ (stdev 5‰). Using the measured δD of the water in which the *Azolla* was grown (-50‰), we calculate that the overall fractionation factor for δD in extant *Azolla filiculoides* is -101 to - 113‰. Addition of 60 mM NaCl to the nutrient solution of *Azolla filiculoides* did not affect fractionation of δD in the 1,ω20 C_{32} - C_{36} diols. The same 1,ω20 C_{32} – C_{36} diols, were extracted from two ACEX *Azolla*-containing sediment samples. Only concentrations of C_{32} diols, of which the abundance in ACEX sediments is higher than that of the 1,ω20 C_{34} or C_{36} diols (Chapter 2), were sufficiently high enough to allow accurate measurement of δD and were found to have a δD of between -229 and -234‰. Both the acetylated and the silylated sample, after correction for the isotopic values of the added hydrogen atoms, showed δD values for these diols within this narrow range. This is quite remarkable as the samples come from two different stratigraphic levels. However, *Azolla* spore abundances and organic carbon content are similar (35.000 counts and ~ 4 wt%, respectively) for the two sampling depths, one depth before and one immediately after an *Azolla* abundance peak, possibly indicating a similar precipitation and, thus, surface water salinity regime at these times. Assuming the overall fractionation of δD prior and during biosynthesis of the 1,ω20 C_{32} diols was the same for the Eocene Arctic *Azolla* and the cultured *Azolla*, the δD of the Eocene Arctic surface waters can be computed. The reconstructed Eocene Arctic surface water composition then lies between -116 and -133‰ (δD).

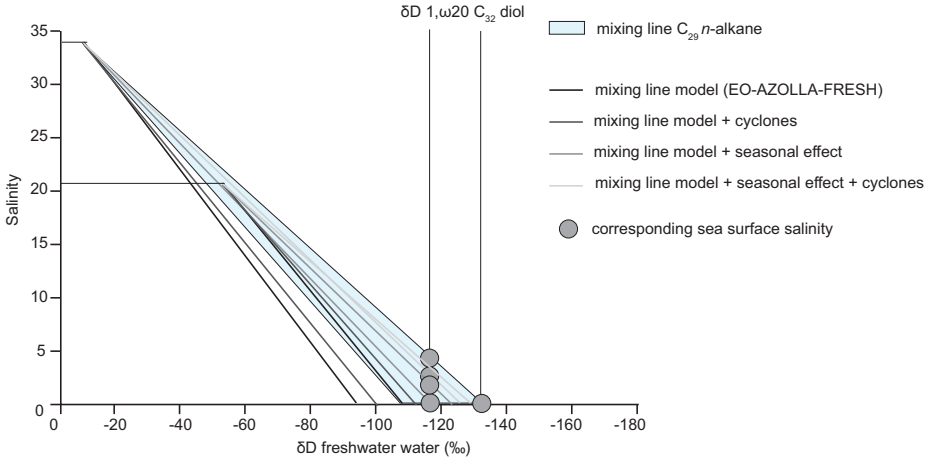

Figure 6.5: Graph showing various mixing lines between (deeper) saline and surface fresh water, based on Azolla-biomarker based estimates of surface water δD in combination with precipitation/ runoff δD inferred from *n*-alkane (light blue) and model data (different grey lines).

These values are remarkably similar to δD_{precip} of the C29 *n*-alkanes (-105 to - 133‰) encountered in the samples from the same ACEX core (11x). The fact that the long chain mid-chain diols produced by *Azolla* and the *n*-alkanes synthesized by higher plants point to similar source water hydrogen isotopic signatures suggests they potentially used the same source waters. The sediment containing the C_{29} *n*-alkanes from which δD_{precip} could be inferred, contained ~ 21000 spore counts/g and was also located right after an *Azolla* abundance peak, potentially indicating prevalence of similar hydrological conditions as during deposition of the diols. However, this sample is located upcore (48, respectively 164 cm from the analysed diol-bearing sample (300.01 mbsf versus 300.49 and 301.65). Pollen analysis suggests that the circum Arctic might have been somewhat drier at that time (Barke et al., in prep), in which case the *n*-alkane δD would be relatively isotopically enriched. Combining results from the hydrogen isotopic analyses of the C_{27} and C_{29} *n*-alkanes (δD precipitation: -105 to -133‰) and 1,ω20 C_{32} diols (δD surface water: -116 and -133‰) allows computation of the degree of mixing between fresh surface waters (i.e. precipitation, with a salinity of 0) and deeper saline waters. First we assume the isotopic δD composition of the Eocene global ocean to have been -8‰, reflecting ice-free conditions. Following a similar reasoning we use a salinity of 34 as the estimate of the high salinity end member. It quickly follows that only limited mixing occurred between the deeper and surface waters, up to 14%. This implies that surface waters were indeed fresh, at least during times *Azolla* was abundant, with a calculated salinity between 0 and 6 salinity units (Fig. 6.5).

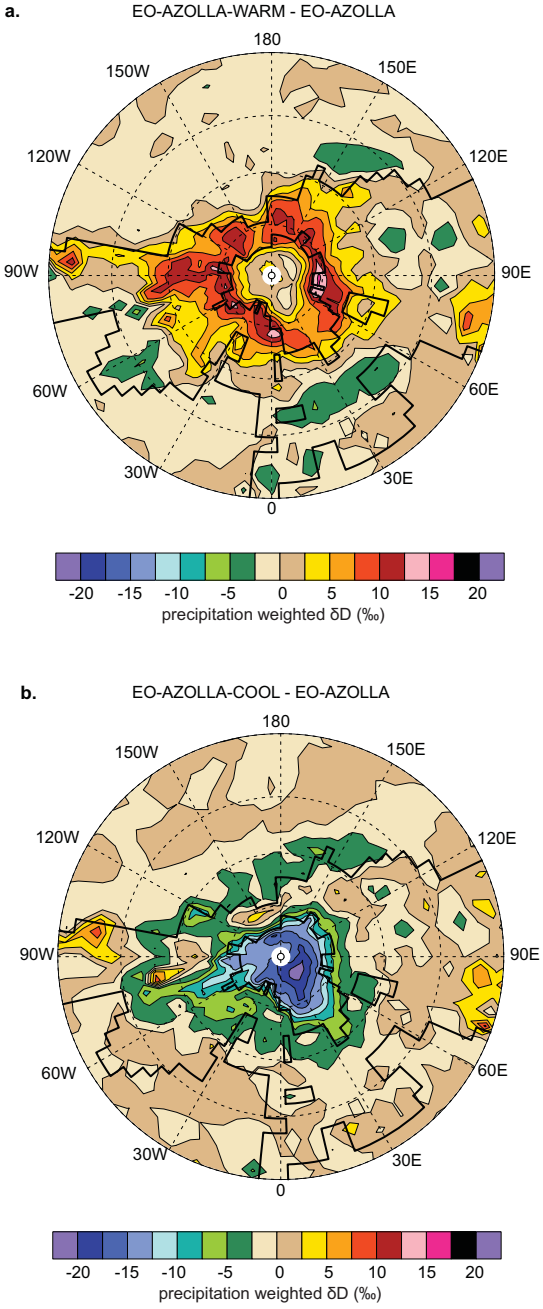

Figure 6.6: (a) Difference plot of modeled mean annual isotopic composition of precipitation (‰ VSMOW) comparing EO-AZOLLA and EO-AZOLLA-WARM. (b) Difference plot for EO-AZOLLA minus EO-AZOLLA-COOL.

The computed mixing gradient between freshwater input and open ocean saline water can be applied to the deep Arctic basin water $\delta^{18}O_w$ estimate by Waddell and Moore (2008), which is -8.1‰. Converted to δD_w this is -54‰, which then corresponds to a salinity of 18 tot 21.5, in line with their original estimate of 15 to 21. Hence, consistent with previous reports (i.e. Stein et al., 2006; März et al., 2009) our results support the existence of a stratified water column, with sea surface salinities of at most 6 salinity units, and a deeper water salinity of about 20.

The high end of our surface salinity estimate is comparable to sea surface water salinity simulated by Roberts et al. (2009) (also 6) based on modeling experiments with a restricted Arctic seaway connection. However, the SST gradient used in their model is probably too steep (Arctic Eocene mean annual SST of 2 instead of 9.4 °C), thereby possibly underestimating precipitation and, thus, freshening of the Arctic and, thence, overestimating Arctic surface water salinity. Other support for *Azolla* interval Arctic surface water salinities closer to 0 comes from comparison of the modeled and *Azolla* biomarker-inferred δD of Arctic surface water. The mean annual precipitation weighted modeled Arctic surface water δD is -89‰ ($\delta^{18}O$; -10.2‰), consisting of a volume weighted combination of runoff δD (-86; $\delta^{18}O$ -11.7‰) and precipitation δD (-100; $\delta^{18}O$ -13.8‰) over the Arctic. The modeled, summed average, Arctic surface water δD is thus less depleted by at least 16‰ than the δD inferred from the biomarkers for *Azolla* (-116 and -133‰). This offset could result from a number of factors acting in concert or independently, e.g. i) the TEX_{86}-based reconstructed sea surface temperature for the Eocene *Azolla* event is too high, resulting in isotopic predictions from the model that are too high (less depleted), ii) depleted rainfall as a result of (tropical) cyclones is not incorporated accurately enough in the model, leading to underestimation of δD_p depletion, iii) the mean annual runoff δD is not representative of Arctic surface water composition during (seasonal) *Azolla* growth), iv) the lower latitude areas have been overrepresented in the integrated drainage basin averages.

Results of runs with slightly higher (EO-WARM; 11.8 °C) and lower (EO-COOL; 7.2 °C) Arctic SSTs, compared to the standard run (Chapter 4, 9.4°C) show that within this temperature range different imposed Arctic Eocene SSTs only exert a minor influence on the summed amount and isotopic composition of runoff flowing into the Arctic (-82‰ for EO-AZOLLA-COOL and -75‰ for EO-AZOLLA-WARM, respectively) (Fig. 6.6). Locally, the maximum difference amounts to + 15‰ (Siberia; EO-WARM), and -20‰, due to sea-ice cover (EO-COOL) (Fig. 6.6). Hence, only substantially cooler Arctic SSTs including a seasonal sea-ice cover could explain the observed offset. However, based on abundant floral evidence (Greenwood and Wing, 1995; Jahren and Sternberg, 2003), lack of proof for sea-ice occurrence (Stickley et al., 2009), and correspondence of global δD patterns (Chapter 4), during this interval (~49 Ma), this seems unlikely.

Possibly the model underestimates Eocene cyclonal moisture transport, and rain-out, at the T31 resolution (e.g. Jouzel, 2000) especially as we use the uncoupled atmospheric model (Yeager et al., 2006). Assuming tropical cyclone activity would have been responsible for transport of an additional 10% of precipitation to the Arctic, with an isotopic composition of ~ -96‰ lighter (Lawrence and Gedzelman, 1996; Lawrence et al., 2004), the δD values of runoff would decrease to -99‰ (Fig. 6.5; medium grey line). This decreases the overall mismatch between modeled and proxy-inferred runoff δD from 27 to 17‰. Given the warm Eocene (tropical) sea surface temperatures, in combination with decreased wind surface stress (not shown), tropical cyclone activity could increase and extend to higher latitudes, thus transporting depleted water into the Arctic region. In fact, increased tropical cyclone activity has been used to explain the prevalence of low meridional temperature gradients through increased northward heat transport via tropical cyclones (Emanuel, 2001; Korty et al., 2008).

Seasonal contrast in the isotopic composition of both local precipitation and runoff is large. Whereas modeled basin averaged summer (June July August) precipitation and runoff have δD values of about -61 and -76‰, winter (December, January, February) δD_p and runoff both have values of -116‰. Hence, the entire difference of 27‰ between modeled mean annual surface water δD and δD of *Azolla* 1,ω20 C_{32} diols, can be explained by seasonality (Fig. 6.5; light grey lines). Since *Azolla* could only photosynthesize during the light summer season, this would imply that the more depleted winter precipitation arrived at the Arctic Ocean Lomonosov Ridge in spring/summer. Hence it could be that Arctic surface water isotopic composition exhibited a time lag-effect, thus mainly recording winter precipitation over land.

Runoff entering the Arctic Basin can be less depleted depending on its source area. A smaller relative contribution from lower latitudes, now included in the drainage basin shell used to calculate the integrated runoff, would increase the basin wide δD depletion. However, high contents of smectite encountered in the ACEX sediments reflect fine material, which was probably delivered from the Barents-Kara-western Laptev Sea (Krylov et al., 2008). Within that specific region the isotopic composition is, relatively enriched, with a mean annual average δD_{precip} of -40 to -80‰ (Fig. 6.2). This implies that isotopically other areas must have supplied appreciable amounts of more depleted runoff as well.

Regardless of the cause of the offset, the greater surface depletion in the biomarker-inferred δD implies even less mixing with deeper, heavier, and more saline waters. The comparison of modeled and biomarker δD results thus suggests that virtually no mixing of surface and deeper saline waters could have occurred, and the salinity of the *Azolla* Interval Arctic Ocean surface must have been very close to 0.

6.4 Conclusion

Enriched precipitation δD values inferred from *n*-alkanes (-105 to - 133‰), extracted from Eocene Arctic sediments, indicate prevalence of enhanced moisture transport from lower latitudes towards the high latitudes. The modeled summed net amount of freshwater entering the Arctic Basin (Precipitation + Runoff - Evaporation) is 1.45 x 10^{13} m^3, for EO-AZOLLA-FRESH (Fig. 6.4). About 50% of this precipitation is fluxed into the Arctic drainage area, and 50% consists of recycled precipitation (resulting from local evaporation). New model outcomes are found to be broadly consistent with proxy-derived high-latitude δD_{precip} estimates for the *Azolla* interval (~49 Ma). Terrestrial *n*-alkane derived estimates for δD_{precip} and our model results thus suggest freshening of the Arctic surface waters was a result of enhanced precipitation and runoff.

Through culture experiments with extant *Azolla*, the δD fractionation of biomarkers specific for *Azolla* (i.e. 1,ω20 C_{32} – C_{36} diols), relative to the source water was determined (~100‰). The δD of these diols encountered in Eocene Arctic sediments now provide insight into the isotopic composition of Eocene Arctic surface water. According to the 1,ω20 C_{32} diols Eocene Arctic surface waters had a δD of -116 to -133‰. These values fall in the same range as δD_{precip} inferred from the C_{27} and C_{29} *n*-alkanes for this interval, indicating that only limited mixing (up to 14%) occurred between the deeper saline waters (δD -8‰; salinity 34) and surface waters (-105 to -133‰; salinity 0). Model outcome and proxy data together thus confirm Arctic surface water freshening (0 – 6) during the *Azolla* interval, with little to no mixing between the abundant runoff and precipitation (surface waters) and deeper saline (~20) waters in the Arctic basin.

Acknowledgements

We thank the DARWIN Centre for Biogeology, Utrecht University and Statoil-Hydro for their financial support. We acknowledge Virginia Tech Advanced Research Computing and the Department of Geosciences for computation support and resources. Model runs were also sponsored by the Stichting Nationale Computerfaciliteiten (National Computing Facilities Foundation, NCF) for the use of supercomputer facilities, with financial support from the Nederlandse Organisatie voor Wetenschappelijk Onderzoek (Netherlands Organisation for Scientific Research, NWO). Development of the isotopic version of CAM was supported by the NOAA Paleoclimate program. This research used samples and data provided by the Integrated Ocean Drilling Program (IODP). We're grateful for laboratory assistance by A. van Dijk (UU) and M. van der Meer and E. Hopmans (NIOZ).

Chapter 7

Geochemical constraints on Arctic Ocean ventilation and phosphorus cycling during the *Azolla* interval

Eveline N. Speelman, Caroline P. Slomp, Judith Barke, Henk Brinkhuis, Jaap S. Sinninghe Damsté , and Gert-Jan Reichart

in prep.

Abstract

Here we present a high-resolution trace metal record for the expanded Early/Middle Eocene section capturing the *Azolla* interval from Integrated Ocean Drilling Program (IODP) Expedition 302 (ACEX) drilled on the Lomonosov Ridge, central Arctic Ocean. During the *Azolla* interval (~49 Ma) Arctic surface waters freshened, while at the same time bottom waters remained saline, indicating that the Arctic was highly stratified. The restricted ventilation and stratification in concert with ongoing export of organic matter most likely were responsible for the development of anoxic conditions in the lower part of the water column. Whereas the excess precipitation over evaporation maintained the freshwater lid, sustained input of open ocean water was needed to keep the deeper waters saline. High sulphur concentrations (~ 6 wt%) and depleted sulphur isotopes (~ -35‰ VCDT) in combination with trace metal enrichments indicate that euxinic conditions resulted in the efficient removal of redox sensitive trace metals from the water column throughout this period. Using the sedimentary trace metal record we constrained circulation in the Arctic Ocean by assessing the relative importance of trace metal input sources (i.e. fluvial, eolian, and seawater inflow). Excess vanadium accumulation during the *Azolla* event requires an inflow of open ocean water between 8 and 20 x 10^{12} m^3/yr to sustain vanadium levels, depending on the river water V-concentration. Excess molybdenum accumulation rates suggest an inflow of only 1.4 x 10^{12} m^3/yr. These

inflow rates imply Arctic Ocean (deep) water residence times of 650 - 9500 years, respectively. Using these constraints, a box model for the coupled cycles of water, salt, carbon, phosphorus and oxygen in the Arctic Ocean was defined and used to show that ventilation must have been restricted to keep surface waters fresh and deeper waters saline. However, under these conditions, upwelling from the deep basin still accounted for up to 70% of the total phosphorus supply to the surface waters. High productivity rates were thus sustained by efficient nutrient regeneration in surface and deep waters.

7.1 Introduction

According to plate tectonic, bathymetric, and paleogeographic reconstructions, the Early/Middle Eocene Arctic Ocean was a virtually isolated relatively shallow basin (Jakobsson et al., 2007), with the still shallow Fram Strait (Jakobsson et al., 2007) and epicontinental West Siberian Sea Strait/Turgai Strait (Akhmetiev, 2007; 2009) probably forming the only, perhaps even intermittent, connections between the Arctic Basin and the open ocean. During an estimated period of between 160 kyr and 1.2 Myr (Chapter 1), an aquatic floating fern, *Azolla*, grew and reproduced all around the enclosed Arctic Basin and in adjacent seas (Brinkhuis et al., 2006). Extant *Azolla* currently grows in tropical and temperate freshwater systems and lives in symbiosis with nitrogen fixating cyanobacterial symbionts. These heterocystous cyanobacteria provide the fern with a source of fixed nitrogen, fulfilling its entire nitrogen demand. Recently, Bauersachs et al. (Chapter 3) found biomarker evidence for the occurrence of these heterocystous cyanobacteria and their possible symbiotic relationship with *Azolla arctica* (Collinson et al., 2009) in the Early/Middle Eocene. In order to sustain *Azolla* growth during this interval (~ 49 Ma), surface waters must have freshened and, with the nitrogen demand fulfilled, enough phosphorus (P) must have been available.

Recently, simulations with an atmospheric general circulation model (isoCAM3) in combination with compound specific hydrogen isotope analyses of *Azolla*-specific biomarkers (Chapter 2) showed that indeed Eocene Arctic surface waters freshened substantially through an enhanced flux of runoff and precipitation into the basin (Chapter 6). Meanwhile, Arctic deeper waters remained saline (Waddell and Moore, 2008; Brinkhuis et al., 2006; Onodera et al., 2008; Stein et al., 2006; Stickley et al., 2008). Whereas enhanced precipitation and river runoff facilitated the occurrence of a freshwater lid (Chapter 6), sustained input of seawater from adjacent seas is needed to keep the deeper waters saline. To which degree the restricted Arctic Ocean exchanged with the open ocean is, however, still largely unknown. At the same time, inflow of deep water and river water together controlled phosphorus input and thus *Azolla* production. Consequently, quantitative insight into the cou-

pled cycles of water and phosphorus in the Arctic basin is required to understand the persistent occurrence of *Azolla* in the Early/Middle Eocene Arctic Ocean.

The phosphorus input needed to explain the prolonged occurrence of *Azolla* in the Arctic over a 1.2 Myr period, can be attributed to: 1) inflow of deeper waters with -relatively high- phosphorus concentrations from the open ocean (Atlantic), 2) -enhanced- phosphorus input from rivers, 3) phosphorus release from flooded shelf areas and, 4) efficient phosphorus recycling in the basin. Here we investigate the role of these factors in two steps. First, we assess freshwater input, and cyclic changes therein, using elements characteristic of river discharge and the magnitude of the deepwater inflow, based on analyses of the distribution of redox sensitive elements in the sediment record. Second, the estimated fluxes are used to constrain a new mass balance model for the coupled marine cycles of water, salt, phosphorus, carbon and oxygen. This box model is then used to examine the relationships between Arctic Ocean circulation, primary productivity, and sedimentary burial and regeneration of phosphorus and particulate organic C (POC), for the Eocene Arctic *Azolla* interval.

7.2 Materials and Methods

7.2.1 Trace metal analyses

7.2.1.1 Sample material: IODP 302 (ACEX) sediments

During the IODP 302 ACEX expedition, cores were taken at 1288 m water depth at the Lomonosov Ridge, Expedition 302, Hole M0004A, 87.87 °N, 136.18 °E (Backman et al., 2006). The high-resolution data set presented here focuses specifically on the *Azolla* interval and overlaps with a larger interval previously analyzed by core scanning (Spofforth et al., 2008) and discrete sample XRF analyses (März et al., 2010). We used sediments from lithological Unit 2, Core M0004A-11x 297.31 to 302.63 mbsf covering the *Azolla* interval as encountered in the core (Brinkhuis et al., 2006). In addition, several samples from cores 19x (320.93 - 322.43 mbsf) and 10x (291.91 - 297.34 mbsf) were included, from before and after the *Azolla* interval, respectively. Core 11x has pale-grey dark-grey laminations, where the *Azolla* remains are associated with the light layer in the SEM pictures (Brinkhuis et al., 2006). The recovery within section 11x was good and includes the end of the *Azolla* interval. The overall sample resolution was up to one sample every 4 cm. Results are compared to previously reported values for bulk geochemical analyses (TOC, 112 samples) and palynological analyses (54 samples) (Chapter 8).

7.2.1.2 ICP-OES/MS

Sediment samples were freeze-dried and thoroughly ground in an agate mortar prior to digestion in a HF, HNO_3, and $HClO_4$ mixture. After evaporation the resi-

due was taken up in 1M HCl. Total concentrations of major (e.g. Al, Ca, Fe, K, Mg, Na, P, S, Ti) and minor (e.g. Ba, Co, Cu, Mn, Mo, Ni, V, Zn, Zr) elements were determined via ICP-OES (Perkin-Elmer Optima 3000). The same total destructions were analyzed by ICP-MS (Agilent 7500 and Thermo Finnigan X-series) to quantify trace elements such as As and U. The accuracy and precision of the measurements were monitored by including international and in-house standards and were both better than and 3% for ICP-OES, and 7% for ICP-MS, respectively.

Element concentrations are Al-normalized to correct for variable dilution by biogenic (e.g. carbonate, opal) or diagenetic (e.g. pyrite, barite, apatite, siderite) components (van der Weijden, 2002). In this way, variations of the major elements in the system are distinguished as previously done by Backman et al. (2006), Martinez et al. (2009), and März (2010) for ACEX sediments. We further use an average shale approach to deconvolve the respective contributions of authigenic and detrital metal inputs and to consider enrichment of individual elements (Wedepohl, 1971). The authigenic metal concentration, [Me]auth, is calculated from the bulk sample concentration, [Me]total, as: [Me]auth = [Me]total - {([Me]detrital/[Al]detrital) * [Al]total}, where the detrital concentrations, [Me]detrital and [Al]detrital, are average shale values from Turekian and Wedepohl (1961).

7.2.1.3 Sulphur isotopes

Sulphur isotopes have been measured on bulk sediments of three samples of core 11x: section 1w: 28-30 cm (297.58 mbsf), section 3w, 48-50cm (300.79 mbsf), and section 3w, 104-107cm (301.35 mbsf). Bulk $\delta^{34}S$ was measured using an elemental analyzer (NA 1500NCS) coupled online to an IRMS (Thermo Delta plus). Results are reported against the Vienna Canon Diablo Troilite (VCDT) standard.

7.2.1.4 Sequential P extraction

The various sedimentary forms of P, which include exchangeable, Fe-bound, authigenic, biogenic, detrital and organic P, can be determined using a multi-step phosphorus extraction procedure (c.f. Ruttenberg, 1992). Unfortunately, consistent with results obtained by Kraal et al. (2009) for ACEX Paleogene-Eocene Thermal Maximum samples (PETM, ~55 Ma) analysis of this carbonate-poor part of the ACEX record (following the extraction procedure by Ruttenberg (1992) as modified by Slomp et al. (1996)) also showed evidence of post-recovery pyrite oxidation. The associated alteration of P speciation (results not shown) involved a conversion of authigenic Ca- into iron oxyhydroxide bound P (Fe-bound P). Hence, Fe-bound P now accounts for 97% of total P, and erroneously appears to be the major P phase in these laminated sediments deposited under euxinic conditions. Therefore we only use the organic P contents and ICP-OES total P data for further interpretation.

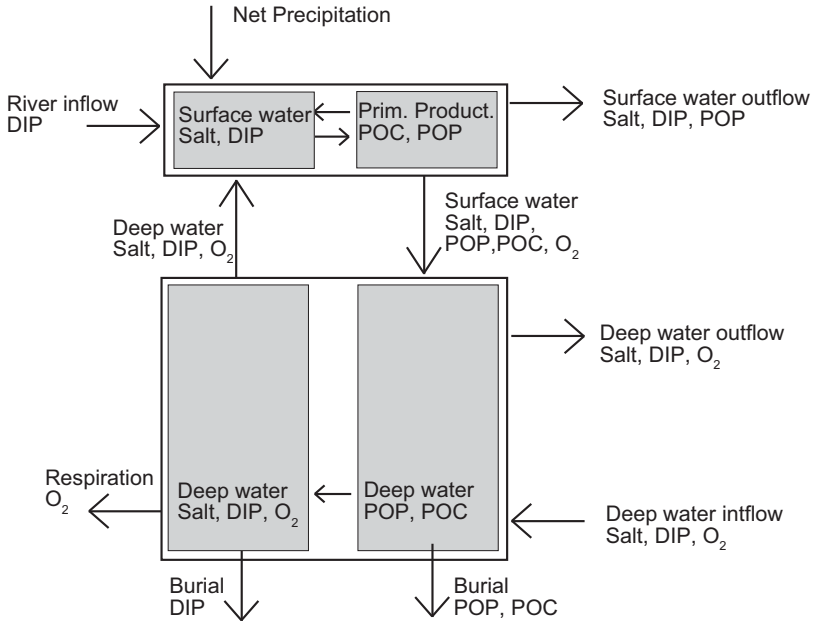

Figure 7.1: Schematic overview of the reservoirs and fluxes in the mass balance model.

7.2.1.5 Time series analyses

Time series analysis was performed on TOC and the element over aluminum ratio records in the depth domain. For this analysis Analyseries version 1.1.1 (Paillard et al., 1996) was used, applying the Blackman-Tukey spectral analysis, using compromise settings and a 90% confidence interval. Power spectra were calculated and a Gaussian bandpass filter was plotted with the data.

7.2.2 Box Model Description

The box model represents the cycling of phosphorus and includes the relevant parts of the water, salt, carbon and oxygen cycles in the Eocene Arctic Ocean (Fig. 7.1). The model uses concepts of previous modeling studies on oceanic nutrient cycling (Van Cappellen and Ingall, 1994, Slomp and Van Cappellen, 2007). The differential equations describing mass conservation in the model are solved using R software (R Development Core Team, 2010; Soetaert and Herman, 2009; Soetaert et al., 2010).

7.2.2.1 Water and salt fluxes

The model consists of two physical boxes: the first box comprises the upper part of the Eocene Arctic Ocean that supposedly freshened enough to sustain *Azolla* growth, and was directly influenced by river input and upward mixing, while the second box represents the saline deep ocean, which is influenced by lateral advec-

Table 7.1: Reservoir sizes and fluxes of the steady-state water cycle in the Arctic Ocean during the Eocene *Azolla* interval. The mean depths of the surface and deep layers are 50 and 1450 m, respectively. The surface area of the Arctic Ocean is 8.55 Tm^2.

Reservoirs	Value	Unit	Source
Surface water volume	700	Tm^3	Depth x area
Deep water volume	20300	Tm^3	Depth x area
Fluxes	Value	Unit	Source
River runoff	12.1	Tm^3/yr	[1]
Net precipitation	2.5	Tm^3/yr	[1]
Surface water outflow	14.6	Tm^3/yr	Mass balance
Deep water inflow	5	Tm^3/yr	See text
Deep water outflow	5	Tm^3/yr	Mass balance
Upwelling	4.8	Tm^3/yr	See text
Downwelling	4.8	Tm^3/yr	See text

[1] Chapter 6.

tion of deep ocean water and mixing as well. Reservoir sizes (Table 7.1) are best guess estimates, fitted to match the Eocene basin configuration. Freshwater fluxes (Fig. 7.1; Table 7.1) are taken from outcomes of a general circulation model (Chapter 6) and saline water influxes are estimated using trace metal accumulation, as explained below. Freshwater input is the sum of direct net rainfall over the basin and river runoff, with only the latter supplying P. Surface and deep-water outflow are defined by mass balance constraints only.

Changes in circulation between surface and deepwater are imposed by multiplying the up- and downwelling flux of water with a dimensionless mixing parameter. The up- and downwelling fluxes are constrained by the maximum allowed surface water salinity and the minimum salinity of the deep water. Extant *Azolla* can only survive in water with salinities up to 90 mM (or 5 salinity units) (van Kempen et al., under review). Compound specific hydrogen isotope analyses for the Eocene Arctic showed that the surface waters were indeed fresh (Chapter 6). Hence, surface water salinity in the box model should remain below 5. Similarly, the deeper water must have maintained a salinity of at least 15 to 21, based on stable oxygen isotope analyses on recrystallized fish bones (Waddell and Moore, 2008). Salinity in the surface and deep ocean boxes is influenced by river runoff (with a salinity of 0), inflow of deeper ocean water (with a salinity of 35) and mixing between the two reservoirs. Steady-state fluxes for maximum mixing for the Eocene Arctic are shown in Table 7.1.

7.2.2.2 Nutrients, productivity and bottom water oxygenation

The model only contains P as a nutrient, since the ubiquitous presence of nitrogen fixating cyanobacteria ensures production of all fixed nitrogen needed to sustain

Table 7.2: Reservoir sizes and fluxes of the steady-state carbon and phosphorus cycles in the Arctic Ocean during the Eocene.

	Value	Unit	Source
Surface water POC	8.55	Tmol	Surface POP x C/P ratio *Azolla* [1]
Deep water POC	85.5	Tmol	Deep POP x C/P ratio *Azolla* [1]
Surface water POP	0.342	Tmol	Equal to POP produced yearly
Deep water POP	3.42	Tmol	10 x surface POP
Surface water DIP	0.49	Tmol	Surface water volume x [DIP] surface [2]
Deep water DIP	38.48	Tmol	Deep water volume x [DIP] deep [3]
Fluxes	Value	Unit	Source
Primary productivity (POC production)	85.5	Tmol/yr	Primary productivity in g C/m^2/y x area x 1/Molar weight C (12) [4]
POC mineralization surface waters	80.5	Tmol/yr	94.2% of POC production
POC export surface to deep waters	5.0	Tmol/yr	5.8% of POC production
POC burial flux	1.0	Tmol/yr	POP burial x average C/P ratio sediment [5]
POC mineralization deep waters	4.0	Tmol/yr	Mass balance
Primary productivity (POP production)	0.342	Tmol/yr	POC production x C/P ratio *Azolla* [1]
POP mineralization surface waters	0.322	Tmol/yr	POC mineralization x C/P ratio *Azolla* [1]
POP export surface to deep waters	0.020	Tmol/yr	POC export x C/P ratio *Azolla* [1]
POP burial	0.0035	Tmol/yr	Sediment P conc. x MAR, 50% buried as POP [6]
POP mineralization deep waters	0.016	Tmol/yr	Mass balance
River input of DIP		Tmol/yr	River runoff x [DIP] river [7]
DIP input precipitation	0.0	Tmol/yr	Precipitation x [DIP] rain [8]
Deepwater inflow of DIP	0.0025	Tmol/yr	Deepwater inflow x [DIP] seawater [9]
Deepwater outflow of DIP	0.0025	Tmol/yr	Deepwater outflow x [DIP] deep water
DIP burial	0.0035	Tmol/yr	50% of total P burial, see POP burial
Downwelling of DIP	4.8	Tmol/yr	See text

[1] molar C/P ratio of *Azolla* of 250; may vary between 100 and 1300 (van Kempen et al., in prep.); [2] [DIP] surface equal to 30% of river concentration [3] [DIP] deep = 1.9 μM [4] 120 g C/m^2/yr; Knies et al. (2007) [5] see Figure 1 [6] sediment P concentration measured 23.4 μmol/g, MAR = mass accumulation rate (35g/m^2/yr) [7] [DIP]river = 2.0 μM based on Meybeck (1982) [8] [DIP] rain = 0 μM [9] [DIP] deepwater = 0.5 μM.

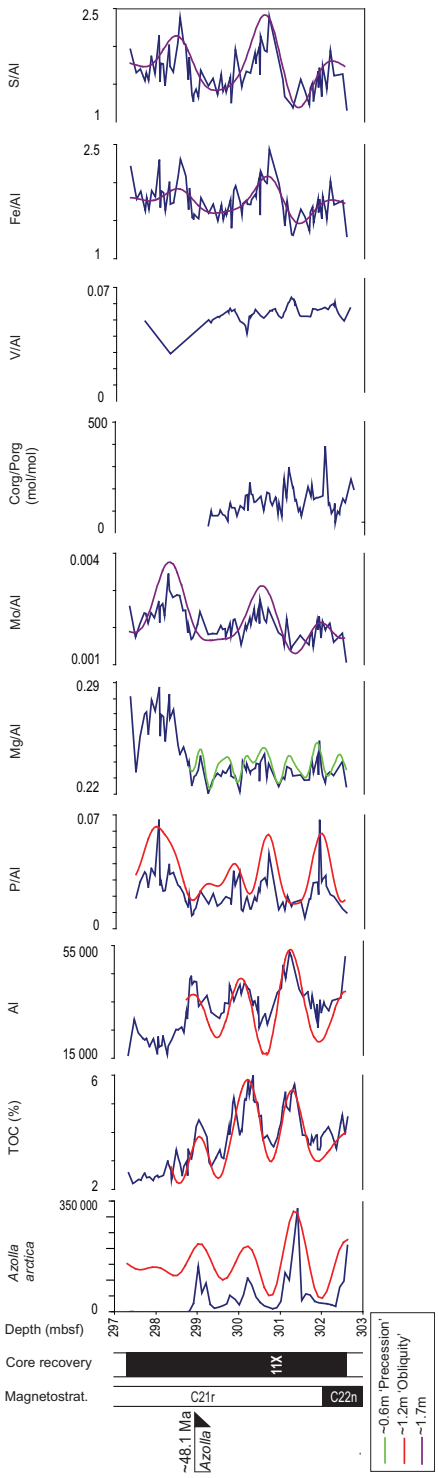

Figure 7.2: Al-normalized element concentrations (mg/kg mg/kg) in ACEX core 11x. C_{org} over P_{org} is given in mol/mol.

growth of *Azolla*. Phosphorus is assumed to be present in the water column as dissolved inorganic phosphorus (DIP). Particulate organic phosphorus (POP) is associated with (living) organic biomass or detritus. The processes affecting concentrations of dissolved and organic phosphorus are river input, deep water inflow, primary production, remineralization (both in the surface waters and the deep waters), transfer between the two boxes and burial of inorganic and organic phosphorus. The latter are estimated from total P concentrations and sediment accumulation rates in Arctic sediments, but may vary with deepwater oxygen concentration (Table 7.2). All applied steady-state P fluxes are shown in Table 7.2. First-order rate expressions were derived for all processes that are not explicitly linked to the water cycle. Where such a link is present, fluxes were modeled as the product of the water flux and the concentration in the source reservoir (Slomp and Van Cappellen, 2007). Depletion of bottom water oxygen leads to reductive dissolution of Fe oxyhydroxides and release of associated P as DIP. In addition, the burial efficiency of POP is reduced under anoxia. Both effects of low oxygen conditions are included in the model by assuming simple linear corrections of P burial for changes in bottom water oxygen (Slomp and Van Cappellen, 2007). In this case, PIP and POP burial are defined for anoxic conditions in the steady-state model (Table 7.2) and are assumed to increase with progressive deep water oxygenation to a given maximum P burial.

The only carbon phase represented in the model is particulate organic carbon (POC). The processes affecting POC are primary production, mineralization, export from surface waters to the deep ocean and burial in the sediment (Table 7.2). Primary production is set to match primary productivity as reconstructed by Knies et al. (2007) for the Early/Middle Eocene Arctic and follows phosphorus via the C/P ratio of *Azolla* and the encountered C/P ratios in the ACEX sediments (Table 7.2).

For dissolved oxygen only changes in the deep reservoir are considered, implying that surface waters are assumed to have remained fully oxic (at a concentration of 325 μM). The oxygen concentration in the deep water inflow is set at 100 μM. The dependence of the rate of aerobic respiration in the deep waters on oxygen and organic matter availability in the deep ocean is modeled as described in Slomp and Van Cappellen (2007). The salinity of precipitation and runoff is assumed to be zero. The deep water inflow, in contrast, is assumed to have a salinity of 35.

7.3 Results and discussion

7.3.1 Element distribution, cyclicity

Our Al-normalized data compare well to results of analyses of major elements for ACEX sediments as previously published by Backman et al. (2006), Martinez et

al. (2009), and März et al. (2010). Al2O3 contents vary between ~ 5 and 9 wt%. Although it is not possible to analyze Si using our analytical approach, since Si evaporates as an HF-Si azeotrope during the drying of the dissolved sediments, taking 100% minus the sum of oxides from our analyses agrees well with the high 50 – 60% biogenic silica calculated by Spofforth et al. (2008).

Azolla massulae counts show a cyclic signal (1.2 m), presumably reflecting obliquity cycles (Chapter 8). A similar cyclicity is observed in the organic carbon content (TOC) record as well, with *Azolla* massulae counts co-varying with TOC (Brinkhuis et al., 2006). This suggests that the organic carbon content of the sediment is largely controlled by *Azolla* production (Chapter 8). For some major elements also distinct cyclicity is observed, Al and Na showing a 1.25 meter periodicity (Fig. 7.2; red line). Mg/Al ratios show higher frequency cyclicity, with a period of around 0.6 meter (Fig. 7.2; green line). Looking at elemental records including the interval following the *Azolla* interval suggests a 1.7 m cyclicity for Fe/Al, S/Al, Cu/Al, Mo/Al, Ti/Al (Fig. 7.2; purple line). Although these cycles are quite obvious in the records, the periodicity should be interpreted with caution as the length of the available record only spans 2.5 cycle of 1.7 meter.

7.3.2 River transport

Rivers transport both sediments and nutrients into the basin. *Azolla* maxima have been associated with obliquity maxima, which in turn are interpreted to reflect humid conditions on land and enhanced freshwater runoff to the Arctic Ocean (Barke et al., under review). Since the cyclic signal observed in Al concentrations closely follows *Azolla* megaspore abundances and organic carbon content, increases in Al content probably reflect increased Al-rich clay input through enhanced runoff.

The composition of the terrigenous input is primarily reflected in the major element distribution of the clay minerals. Different clay minerals have different element to aluminium ratios and changes therein thus also affect these elemental ratios. Terrigenous elements are all strongly positively correlated with each other (Fig. 7.3: Al-Ti; r^2=0.94, Al-K; r^2 =0.97, and Al-Mg; r^2 =0.98). In general, K/Al and Ti/Al ratios are fairly constant throughout core 11x and average around 0.2 and 0.045, respectively. Also Mg/Al is rather constant with an average value of 0.23. Although Mg/Al shows a weak periodicity of 0.6m, possibly reflecting a long distance runoff signal related to precession (Barke et al., under review), Mg versus Al slopes are fairly constant throughout the interval and thence the source region probably remained the same. The only appreciable change in major element composition is observed at the end of the *Azolla* interval, showing a small but distinct increase in Mg/Al (Fig. 7.2). Comparing element ratios (Ti/Al, K/Al, and Mg/Al) from before, during and after the *Azolla* interval, shows that no obvious changes in sediment provenance occurred before or upon ending of the *Azolla* phase (Fig. 7.3). The K/Al

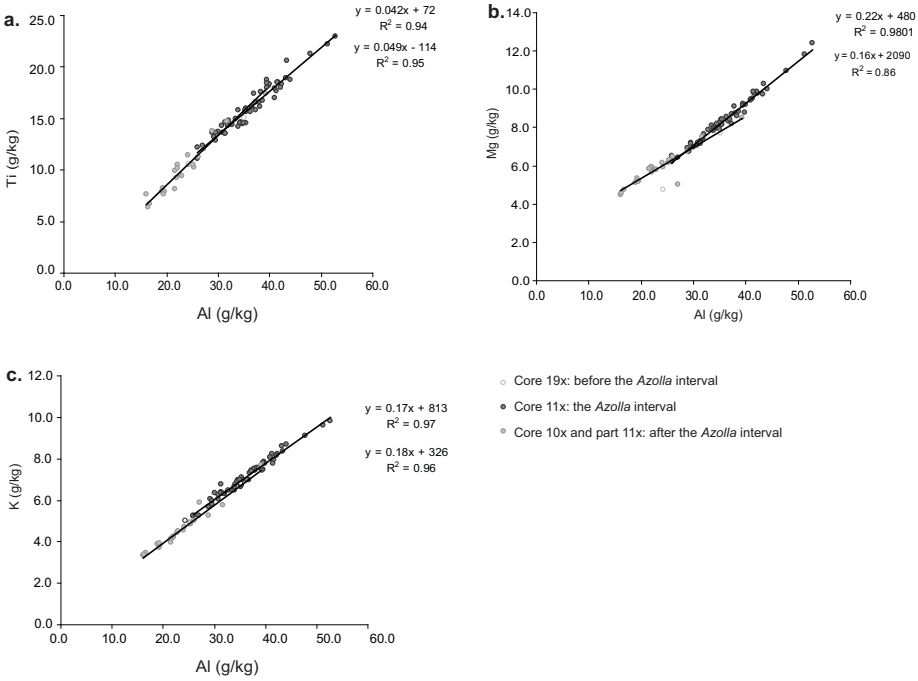

Figure 7.3: Correlation of terrigenous elements: (a) Ti vs Al, (b) Mg vs Al, and (c) K vs Al.

and Mg/Al ratios mirror each other in Unit 2 of the ACEX record (Fig. 7.2; März et al., 2010). The *Azolla* interval corresponds with highest Mg/Al and thus lowest K/Al values. This anti-correlation between K/Al and Mg/Al probably reflects changes in the relative contribution of two end members with contrasting compositions. Such a change could be either due to a shift between rivers draining into the basins or a change in the composition of the material eroded by the same river. In both cases this change might be accompanied by a change in the input of nutrients to the basin as well. However, as during the *Azolla* interval itself no such changes are observed, no major variability in river input and thus nutrient supply is expected.

The mean Ti/Al ratio is slightly lower than the overall ACEX mean, but gradually increases up core from ~0.04 to ~0.06. Similarly, although highly variable, the Zr/Al ratio is relatively low from ~0.0013 – 0.0020 for the *Azolla* interval, while values are higher (~15 to ~30) in the upper part of the core (März et al., 2010). Although these elemental ratios are also often interpreted as proxies for wind driven deposition (Reichart et al., 1997), this is unlikely for the Arctic, because of the general high humidity levels (Jahren et al., 2009), hampering appreciable dust transport. More likely, the lower Ti/Al ratios might be attributed to a lower energy depositional environment, as a sea level rise during the *Azolla* interval (Haq et al., 1987) would move the depositional locus to a more in-land position. This also potentially affects

how much riverine P reaches the study site. A transgression may at the same time lead to release of additional P upon erosion (Bjerrum et al., 2006) and salinization (Canavan et al., 2006) of newly flooded shelf areas.

7.3.3 Bottom water oxygenation

Previous trace metal-based studies suggest the prevalence of persistent (Stein et al., 2006) to possibly intermittent bottom water dysoxia in the Early/Middle Eocene Arctic (März et al., 2010), which is in line with the continuous laminations, absence of fossil benthic organisms, the presence of pyrite, and evidence from organic geochemical biomarkers (Chapter 2; Knies et al., 2008; Spofforth et al., 2008; Stein et al., 2006).

Trace elements are either enriched or depleted under oxygen poor conditions, depending on their redox sensitive behavior. Typically Mo, U, V and Ni are enriched under dysoxic bottom water conditions, whereas Mn and Co are often depleted. The elements Cu and As (Table 7.3) are incorporated in sulphides and enriched under euxinc conditions. Some of these elements are transported to the sediment, scavenged on organic matter, and can be trapped in the sediment under oxygen depleted conditions. Iron can be both enriched under well oxygenated conditions as Fe-(hydr)oxides, or under oxygen limited conditions in the form of pyrite. This way each specific element has a range of enrichment factors depending on the depositional environment in general and the degree of oxygen deficiency. Most trace metals are enriched in the Arctic sediments compared to average shale (Turekian and Wedepohl, 1961) before, within, and after the *Azolla*-containing interval. Fe, S, Ba, Sc, V, Mo, Co, Cr, Cu, Ni, Y, Zn, U are all enriched, with highest enrichments recorded for Co, Cu, V and U (Table 7.3). Still, compared to open ocean sediments deposited under anoxic/sub oxic conditions or even sediments deposited in a restricted oxygen depleted basin such as Mediterranean sapropels (Brumsack, 2006), enrichment is relatively limited. This implies that either the bottom waters were not truly, continuously, anoxic or that the influx of redox sensitive elements to the basin was restricted.

Based on the sulphur isotopic data, however, bottom waters must have been anoxic, although not necessarily continuously. Sulphur concentrations are high throughout the interval (ca. 3 - 7 wt%) and correlate with Fe, indicating that S is predominantly present in the form of pyrite (Chapter 8). However, part of the S present is organically bound (unpublished results). Sulphur isotopes (-34.5 (297.58 mbsf), -35.6 (301.35 mbsf), and -38.2 (300.79 mbsf)‰ (VCDT), respectively) are considerably depleted compared to sea water sulphate (ca. +20‰). This implies that sulphate reduction occurred in the water column and that not all available sulphate was reduced, as both processes would have returned bulk isotope values to their original oceanic isotopic sulphate value (Passier and de Lange, 1998). Hence there

Table 7.3: Overview of element enrichments in ACEX core 11X, during and after the *Azolla* interval.

	Azolla interval[a] (mg/kg mg/kg)	After[b] (mg/kg mg/kg)	Average Shale[c] (mg/kg mg/kg)	Enrichment *Azolla*	Enrichment After
Major elements					
Fe/Al	1.693	1.86	0.59	2.87	3.153
K/Al	0.1972	0.1962	0.3325	0.593	0.5902
Mg/Al	0.04446	0.04316	0.1875	0.2371	0.2302
P/Al	0.02119	0.02655	0.00875	2.421	3.034
S/Al	1.575	1.759	0.03	52.49	58.63
Ti/Al	0.04443	0.04347	0.0575	0.7727	0.756
Minor elements					
Ba/Al	0.003166	0.002716	0.00725	0.4367	0.3746
Co/Al	0.000943	0.001023	0.0002375	3.97	4.307
Cr/Al	0.00148	0.001436	0.001125	1.316	1.276
Cu/Al	0.001898	0.002182	0.0005625	3.374	3.879
Ni/Al	0.001442	0.00182	0.00085	1.697	2.141
Mn/Al	0.02335	0.02706	0.010625	0.176	0.2061
Mo/Al	0.2333	0.02045	0.0000325	57.54	67.39
Sc/Al	0.000294	0.000287	0.0001625	1.809	1.766
V/Al	0.005681	0.005316	0.001625	3.496	3.271
Y/Al	0.000822	0.000684	0.000325	2.529	2.105
Zn/Al	0.003165	0.003237	0.001188	2.665	2.726
Zr/Al	0.001666	0.001486	0.002	0.833	0.743
Trace elements					
As/Al	0.001212	0.001748	0.0001625	7.459	10.76
U/Al	0.000397	0.00043	0.00004625	8.584	9.297

[a] Samples 11x 2w|3-5 - 11x5w| 7-9 (298.83 - 302.57 mbsf)
[b] Samples 10x 3w|70-72 - 11x1w|144-146 (295.05 - 298.76 mbsf)
[c] Average shale (Turekian and Wedepohl, 1961)

was a deeper water supply of sulphate (saline deep water) during the interval and at least the deeper water was euxinic, albeit not necessarily continuously.

In addition to the fact that the elements enriched under oxygen-depleted conditions are enriched less than expected, Mn is not depleted as much as expected. The relatively high Mn concentrations compared to sediments deposited under continuously anoxic conditions has been suggested to reflect periodical reoxygenation (März et al., 2010). Episodic, but short-termed reventilation of the deep Arctic Ocean during Eocene times, through enhanced influxes of saline marine waters from the Atlantic is supported by Nd isotope data from fish bones (Waddell and Moore, 2008; Gleason et al., 2009) and by silicofossil preservation (Stickley et al., 2008). These events could, however, not have been long enough to allow recolonization of the benthic environment, as this would have destroyed the laminations

present throughout. Alternatively, elements remobilized under anoxic bottom water conditions potentially become relatively enriched through leaching from suboxic slope sediments (Schenau et al., 2002). Highest Mn concentrations, and similarly Fe, would in that case be related to the maximum extent of dysoxia in the water column (März et al., 2010). A sea level rise during, or prior to, the *Azolla* event would increase the slope area subject to bottom water anoxia, thus facilitating transport of Mn and Fe to the deeper parts of the basin (Mangini et al., 1990; Schenau et al., 2002). The higher Mn concentrations are thus not necessarily indicative of less severe oxygen depletion, but may rather reflect changes in sea level.

As the Arctic was a restricted basin, over time, the stagnating water mass was susceptible to depletion of its dissolved trace elements if these were removed to the sediments faster than that they were replenished by ventilation (e.g. Colodner et al., 1995). Hence, the elements enriched in the sediments possibly became scarce in the overlying seawater under (semi-) continuously anoxic-sulphidic conditions. The degree of restriction of the Arctic basin is potentially reflected in the enrichment factor of those elements whose inflow was limited.

7.3.4 Inflow of deep water

The fact that both V and Mo enrichment in the Arctic Basin was relatively limited during the *Azolla* interval indicates that the supply of both elements was limited. Both elements are present in seawater in relatively high concentrations (10.6 and 1.8 ppb, respectively) and are usually enriched in sediments deposited under anoxic conditions (e.g. Shaw et al., 1990; Van Bentum et al., 2009). The bottom water anoxia will have resulted in all Mo and V entering the basin with deeper water being (almost) instantaneously retained in the accumulating sediment. The supply of redox sensitive trace elements, including V and Mo, to the seawater depends primarily on five sources: (1) regeneration from sediments, mostly at suboxic shelf and slope sediments, (2) hydrothermal input; (3) aeolian input; (4) fluvial runoff and (5) seawater inflow from adjacent basins.

Not all of these sources are, however, relevant for V and Mo burial in the Arctic Basin during the *Azolla* interval. (1) *Azolla* growing in floating mats is known to hamper oxygen diffusion into the water, rendering the waters (often including surface waters) dysoxic. In contrast to Mn and Fe, under continuously oxygen depleted conditions Mo and V would rather remain fixed in the slope sediment and not be regenerated. (2) Enhanced hydrothermal activity would be reflected by an increase in especially those elements associated with it, such as Zn (Arthur et al., 1988). The enrichment factor for Zn is, however, only 2.8, which is much lower than would be expected in case of significant hydrothermal input. (3) The overall humid conditions on the landmasses surrounding the Arctic basin (Jahren et al., 2009) prevented appreciable inputs of dust and thus of associated trace elements.

(4) An estimate of river runoff into the Eocene Arctic during the *Azolla* interval has been obtained through modeling (Chapter 6). Hence, (enhanced) riverine input of V and Mo can be computed. Therefore, (5), Mo and V excess accumulation rates enable reconstruction of water exchange between the Arctic Ocean and the open ocean.

To investigate if indeed all V and Mo had to be stripped from the water column during the *Azolla* interval, we adopted a budget calculation approach (Nijenhuis et al., 1999). As Eocene seawater concentrations are not known, we assume present-day values. Vanadium presently has an average seawater concentration of 1.8 ppb (Bruland, 1987; Collier, 1984) and its current world river water concentration ranges from 0.5 to 1.0 ppb (Shiller and Boyle, 1987; Nijenhuis et al., 1999). For Molybdenum sea and river concentrations are 10.6 and 0.5 ppb, respectively (Broecker and Peng, 1982; Martin and Whitfield, 1983). Because *Azolla* occured all around the basin (Brinkhuis et al., 2006; Chapter 1) we assume that there is no significant lateral variability in overall sediment chemistry. We thus extrapolate the measured trace element concentrations over the entire basin, calculating integrated trace metal burial rates. On average, the V concentration in the *Azolla*-bearing sediments was 200 ppm and Mo averaged around 70 ppm. Hence, V and Mo are enriched by 138.5 and 68.8 ppm, respectively, compared to average shale (Turekian and Wedepohl, 1961).

Modeled annual averaged river runoff into the Eocene Arctic basin amounted to 12.1×10^{12} m^3/yr (Chapter 6). Hence for computation of total riverine trace metal supply the modeled river runoff can be multiplied by the average V and Mo river water concentrations. Given the average accumulation rate of 24.3 cm/kyr during the *Azolla* interval (Backman et al., 2008), in combination with a measured dry bulk density of the sediment of 1.45, the Mass Accumulation Rate (MAR) can be calculated for the Eocene Arctic: 35 g/m^2/yr. Combining encountered V enrichment with a the reconstructed MAR, an Eocene Arctic Basin volume of 1.3×10^{16} m^3 and modeled river runoff of 12.1×10^{12} m^3 /yr, it follows that about 14 to 29% of the V encountered in the sediments is accounted for by river runoff. The same calculation using Molybdenum shows that about 29.4% of Mo can be accounted for by river runoff. Hence, the remaining between 71 - 86% of V and 70.6% of Mo had to originate from seawater. Given the average concentrations of V (1.8 ppb) and Mo (10.6 ppb) in seawater, the amount of seawater needed to sustain the observed burial flux of trace metals can be computed. This implies an influx of seawater between 2.0×10^{13} and 8×10^{12} m^3 /yr (based on V) and 1.37×10^{12} m^3 /yr (based on Mo), respectively. Consequently Arctic Ocean (deep) water residence times must have been between 650 - 9350 years.

The summed net amount of precipitation (river runoff + precipitation) entering the Arctic Basin (P-E) is 1.45 10^{13}/yr (Chapter 6). This implies that a compensating inflow of saline North Atlantic water must have occurred, resulting in a bi-directional, two-layer flow through the (proto-) Fram strait. A steady-state situation requires conservation of water fluxes into and out of the basin, where deepwater inflow plus net precipitation equals outflow. At the same time the salt budget requires that inflow (1.37 or 20 x 10^{12} m^3 /yr) times the salinity of the open ocean (34) equals outflow (14.5 x 10^{12} m^3 /yr + 1.37 or 20 x 10^{12} m^3/yr) times the salinity of the (surface) water flowing out of the basin. This suggests salinities of 20, respectively 3 for the combined outflow. Surface water salinity reconstructed using compound specific hydrogen analyses of biomarkers specific for *Azolla*, is 0 – 6 (Chapter 6). The salinity of water flowing out of the basin based on Mo corresponds well to these reconstructed values. Overall, these reconstructed residence times of the deep Eocene Arctic water are high compared to most deeper water masses, facilitating oxygen depletion.

7.3.5 Phosphorus budget

In Unit 2, of which the *Azolla* rich section is a small part, variability of P/Al is highest (März et al., 2010). Phosphorus concentrations range between 5.1 and 57.5 μmol/g, averaging around 23.1 μmol/g for the *Azolla* interval. Molar organic carbon phosphorus ratios average around 160 and vary between 50 and 300 (Fig. 7.2). Sediment P/Al ratios are highest when *Azolla* megaspore abundances are lowest. This indicates either enhanced P recycling during extensive *Azolla* growth, or relatively high C/P ratios of *Azolla* compared to other biomass produced in the Arctic. Molar C_{org}/P_{org} ratios in extant *Azolla* are generally higher, varying between ~110 to up to ~1290 (van Kempen et al., in prep), with *Azolla* C_{org}/P_{org} with C_{org}/P_{org} ratios being negatively correlated to dissolved phosphate concentrations (between 20 and 0.1 μmol/L, respectively). Sedimentary organic phosphorus estimates for the Arctic *Azolla* interval, based on sequential phosphorus extraction, vary around 1.3 μmol/g or 8% of total P content. Sedimentary molar organic carbon to organic phosphorus ratios thus vary within a wide range of ~550 and 3300.

Assuming phosphorus is buried equally all over the basin with a concentration of 23 μmol/g sediment, 7 x 10^9 mol P is buried annually in the Eocene Arctic basin (Table 7.2). Based on minimum and maximum deep water influxes of 1.4 x 10^{12} and 20 x 10^{12} m^3 /yr inferred from V and Mo budgets, and a (modern-day) North Atlantic deep water phosphorus concentration of 0.5 μmol/l, about 0.68 to 10 x 10^9 mol P enters the basin per year. Hence, the maximum deep water influx of 20 x 10^{12} m^3/yr would potentially have supplied enough phosphorus to the Arctic Basin to fully explain the reconstructed phosphorus burial rate. However, the low salinity of the Arctic surface water dictates that mixing between inflowing deeper saline water and surface water was rather limited, which also limits the upward flux of P-rich

deepwater. Hence specific combinations of external riverine P input, upwelling of DIP and regeneration are needed to sustain primary productivity.

7.3.6 Model application

Using the range of inflow rates of deep saline waters calculated above and the restrictions on the oxygen conditions in the deep basin and surface water and deep water salinity (<5 and >15 - 21, respectively), we can constrain Arctic Basin ventilation during the Eocene *Azolla* interval. When all (water) fluxes are known, the relative contributions of the different sources to surface water P can be assessed.

7.3.6.1 Constraining water cycling

First, ventilation rates between surface and deep waters were constrained using the given upper salinity limit of 5 for the surface waters and using lower limits of 21 and 15 for the deeper waters. Riverine inflow was kept constant at 12.1 x 10^{12} m^3/yr (Table 7.1), while deepwater inflow (and thus indirectly residence time) was varied between 1 and 25 x 10^{12} m^3/yr, encompassing the Mo and V inferred deepwater inflow rates. In Figure 7.4a the effect of these changes in deepwater inflow (i.e. residence time) on up-and downwelling fluxes, within the given salinity constraints for the model, is shown. As less saline deep water enters the basin, more mixing can occur without surface water salinities exceeding values > 5 (Figure 7.4a; left hand side). However, slowing down the influx of saline (deep) water eventually limits the possibility for mixing between the two reservoirs, since deepwater salinity should stay above 15 to 21 (Figure 7.4a; right hand side). Hence, given these constraints on salinity (15), the highest upwelling and downwelling flux (~7.2 x 10^{12} m^3/yr) is associated with a residence time of ~3700 years. This also implies that if mixing increases above this value, low surface water salinity (<5) can no longer be maintained.

Using up- and downwelling fluxes of 4.8 x 10^{12} m^3/yr (based on a deep water salinity of 20; Chapter 6), and a corresponding seawater influx of 5 x 10^{12} m^3/yr (Table 7.1), model results indicate freshening of the deep and surface waters when using marine conditions as a starting point. Figure 7.5 shows the results of such a transient model scenario in which both deep and surface waters are initially fully saline (salinity of 35). It follows that surface and deepwater salinities of 5 and 20, respectively, are reached within 10 kyr. This implies that the mixing constraints on up and downwelling still allow that within an obliquity cycle the surface water can freshen and re-salinify in response to changes in water input. Using the steady state fluxes as described in Table 7.1, deep waters in the Arctic become anoxic within less than 1000 yrs (not shown).

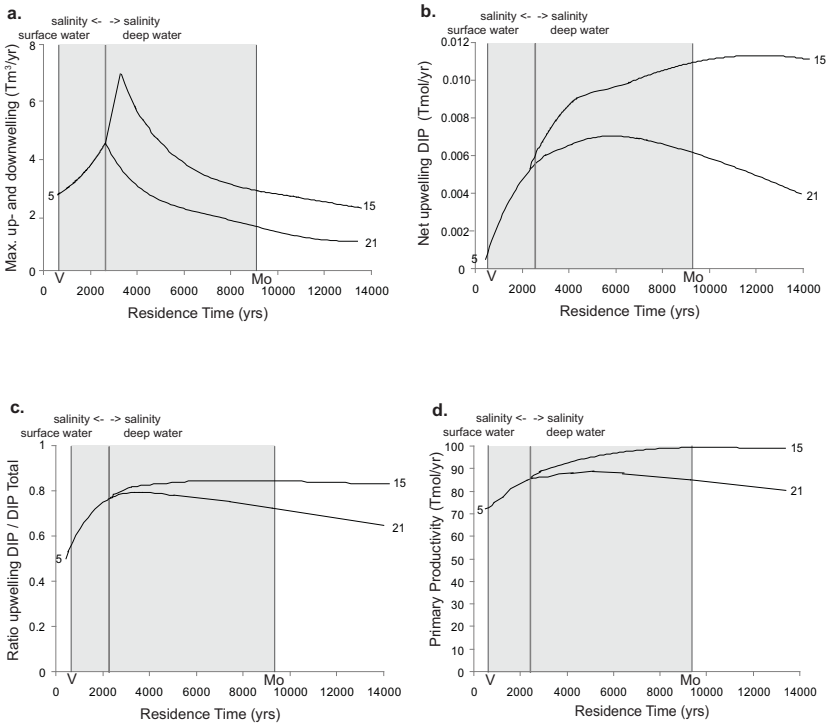

Figure 7.4: (a) Inferred up- and downwelling water fluxes for different deepwater inflow rates (ocean residence time) and constant riverine inflow. Lines indicate maximum fluxes for imposed salinity constraints (surface water < 5, deep water > 15 or 21). (b) Net deepwater DIP upwelling given the up-and downwelling water fluxes displayed in a. (c) Contribution deepwater DIP upwelling to total surface water DIP for fluxes of a. (d) Corresponding response primary productivity to surface water DIP concentrations.

7.3.6.2 Phosphorus cycling

With the freshwater, deepwater and up- and downwelling fluxes reasonably well-constrained, model simulations can now be used to look at phosphorus cycling. A primary productivity estimate of 120 g C/m^2/yr, or 85.5 x 10^{12} mol/yr for the entire basin has been determined by Knies et al. (2008) for the *Azolla* interval (Table 7.2). In order to ensure sustainment of this primary productivity, given the water (and thus DIP and POP) fluxes as shown in Table 7.2, C and P steady-state regeneration rates of ~94% are needed. This shows that in order to sustain primary productivity, intense recycling of organic matter must have taken place in the surface waters. This is in line with the inferred low burial efficiency of organic carbon of 1.2% for the Eocene Arctic during this interval (Chapter 8) and the fact that floating mats of *Azolla* hamper oxygen diffusion, rendering surface waters anoxic, thus facilitating enhanced recycling of organic matter in the surface waters.

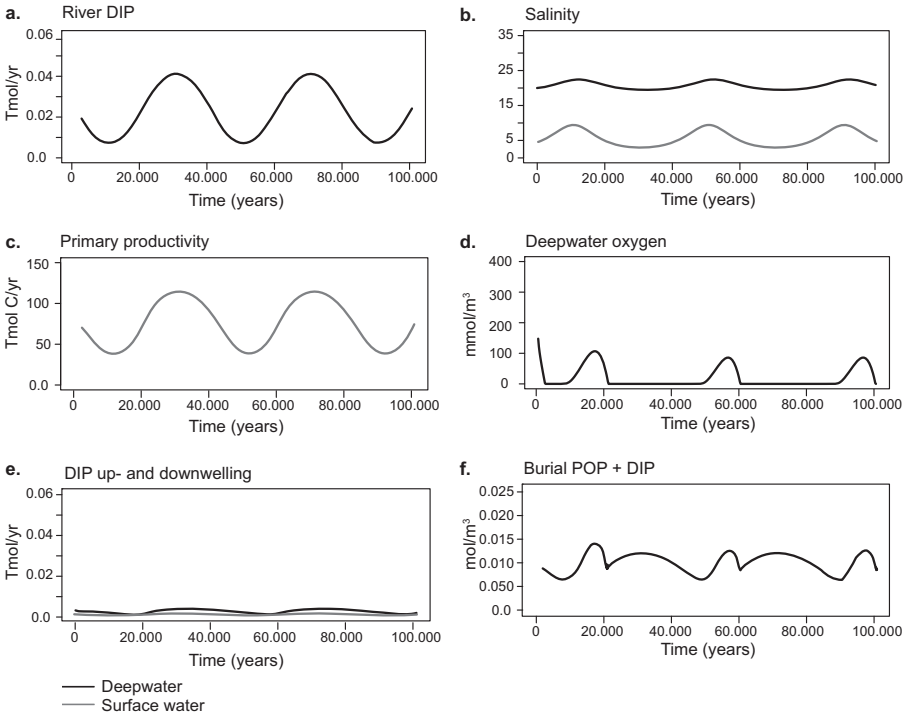

Figure 7.5: Box model simulations using an obliquity-paced river runoff scheme. (a) river DIP, (b) salinity response in the surface and deepwater, (c) primary productivity, (d) deepwater oxygen concentration response, (e) up-and downwelling DIP in response to varying surface DIP and deep DIP concentrations, (f) (oxygen-dependend) burial of POP and DIP.

Model simulations can further be used to assess the sensitivity of P supply to the surface waters to different assumptions about water cycling in the Arctic Ocean during the Eocene. When changing the seawater inflow (residence time) and up- and downwelling fluxes within the constraints imposed by salinity, while keeping all else constant, significant changes in DIP supply are observed in the model results. Corresponding up- and downwelling fluxes of water are shown in figure 7.4a. If the seawater influx decreases (i.e. increasing residence time), the upwelling of deep DIP will initially increase (Fig. 7.4b). Correspondingly, at low residence times (higher deep water inflow rates) primary production increases with increasing residence time due to enhanced DIP upwelling of DIP rich deeper waters (Fig. 7.4d). Under the set boundary conditions for the Eocene Arctic, optimum primary production occurs with an approximate residence time of 6500 years. Here the DIP concentration in the surface waters is highest, as the net DIP upwelling flux (DIP upwelling – DIP downwelling) reaches its highest value. At higher residence times (lower inflow rates), DIP upwelling decreases again as the mixing must decrease in

order to maintain the required deepwater salinity (Fig. 7.4c). The relative contribution of upwelling DIP versus riverine DIP influx is greatest for a sea water influx of ~ 4.8 x 10^{12} m^3/yr. The net DIP upwelling flux then contributes approximately 70% (deepwater salinity 21), respectively 85% (deep water salinity 15) of the total influx of DIP (sum of riverine DIP and net upwelling of DIP).

7.3.6.3 Simulating obliquity paced river inflow

Phosphorus fluxes into the basin are expected to co-vary with runoff, assuming river water P concentrations stay constant. Hence, during *Azolla* maxima, when runoff peaks, riverine P input supposedly is highest. To investigate the effect of these changes in riverine P input on primary productivity, degradation and bottom water conditions, a model scenario with a sinusoid function for river water inflow was defined. Using the steady-state as described in Tables 7.1 and 7.2 as a starting point, with up- and downwelling fluxes of 4.8 x 10^{12} m^3/yr (equivalent to a residence time of 4300 yrs), an obliquity-paced river runoff scheme (following *Azolla* spore abundances and Al sediment concentrations) with an amplitude of 0.5 was imposed. It follows from figure 7.5 that DIP uptake and primary productivity indeed increases with increasing runoff. Hence, modulation of river runoff provides a mechanism to increase and decrease *Azolla* growth through varying P supply in the Eocene Arctic, even though the majority of the DIP might be supplied by upwelling (Fig. 7.4c).

When river runoff falls below 3.6 x 10^{12} m^3/yr (down to 30% when compared to the steady state value) surface water salinity rises up to 10 (Fig. 7.5b), and deep waters become oxygenated (100 μmol/l) (Fig 5.d), which then leads to enhanced burial of DIP and POP (Fig. 7.5f). In the sediments, P/Al ratios are indeed higher during *Azolla* minima, potentially indicating that P burial was higher during times with decreased river runoff (Fig. 7.2). Turning it around, lower P/Al during *Azolla* maxima, could indicate enhanced P recycling during these episodes.

At the end of the *Azolla* interval, freshwater pulses continue, as indicated by continued presence of freshwater crysophytes (Stickley et al., 2008). Still, the lower input of Al indicates a reduction in riverine sediment input. A reduced input of riverine DIP then leads to a decrease in primary productivity. Due to a decrease in primary productivity and subsequent reduced export productivity, deep water could be become oxygenated, which is reflected in e.g. slightly lower Mo/Al and V/Al ratios. This potentially enhances P burial -reflected in higher P/Al ratios immediately following the *Azolla* interval-, reducing upwelling of deep DIP. This –temporary- dip in DIP may thus have contributed to the demise of *Azolla* in the Eocene Arctic.

7.4 Conclusion

Redox sensitive trace metal enrichment in Eocene Arctic sediments is relatively limited compared to open ocean sediments deposited under anoxic/suboxic conditions. This implies that either bottom water were not continuously anoxic or that the inflow of redox sensitive elements to the basin was restricted. Depleted sulphur isotopes and continuous laminations indicate that deeper waters were euxinic and that deeper waters remained saline. Whereas the excess precipitation over evaporation maintained the freshwater lid, sustained input of open ocean water is needed to keep the deeper waters saline. Using trace metal budgets (V and Mo) the influx of saline waters is constrained. An influx of 1.3 - 20 x 10^{12} m^3/yr was found to be necessary to sustain sedimentary V and Mo levels. A newly developed mass balance model for the Eocene Arctic was used to quantitatively assess the salt, oxygen, carbon and P cycling within the basin. Given a freshwater influx of 12.1 x 10^{12} m^3/yr (Chapter 6) and deepwater influx of 1.3 to 20 x 10^{12} m^3/yr (salinity 35), and the restrictions on the oxygen depleted conditions in the deep basin and surface water and deep water salinity (<5 and 15 to 21, respectively), allows for maximum up- and downwelling fluxes of ~ 5 x 10^{12} m^3/yr. Calibration of the steady-state of the model shows that extensive recycling of DIP in the surface waters is needed to sustain *Azolla* productivity. In addition, with the relatively limited mixing between the surface and the deeper waters, the relative importance of upwelling of deep water DIP to the total DIP available in the surface water still reaches values of ca. 70%, thus upwelling contributes to the high primary productivity. Similarly, changes in river runoff (and DIP supply) affect primary productivity and thus deepwater oxygenation, changing POP and DIP burial rates. Overall, high P recycling in surface waters in combination with upwelling of (deep water) DIP is needed to sustain *Azolla* growth in the Eocene Arctic.

Acknowledgements:
We thank the DARWIN Centre for Biogeology, Utrecht University and Statoil-Hydro for their financial support. This research used samples and data provided by the Integrated Ocean Drilling Program (IODP). CPS acknowledges funding by the Netherlands Organisation for Scientific Research (NWO Vidi-grant).

Chapter 8

The Eocene Arctic *Azolla* bloom: environmental conditions, productivity and carbon drawdown

Eveline N. Speelman, Monique M.L. van Kempen, Judith Barke, Henk Brinkhuis, Gert-Jan Reichart, Alphons J.P. Smolders, Jan G.M. Roelofs, Francesca Sangiorgi, Jan W. de Leeuw, Andy F. Lotter, and Jaap S. Sinninghe Damsté

Adapted from: Speelman et al. Geobiology 7, 155 – 170 (2009)

Abstract

Enormous quantities of the free floating freshwater fern *Azolla* grew and reproduced *in situ* in the Arctic Ocean during the middle Eocene, as was demonstrated by microscopic analysis of microlaminated sediments recovered from the Lomonosov Ridge during Integrated Ocean Drilling Program (IODP) Expedition 302. The timing of the *Azolla* phase (~49 Ma) coincides with the earliest signs of onset of the transition from a greenhouse towards the modern icehouse Earth. The sustained growth of *Azolla*, currently ranking amongst the fastest growing plants on Earth, in a major anoxic oceanic basin may have contributed to decreasing atmospheric pCO_2-levels via burial of *Azolla*-derived organic matter. The consequences of these enormous *Azolla* blooms for regional and global carbon cycling are still largely unknown. Cultivation experiments have been set up to investigate the influence of elevated pCO_2 on *Azolla* growth, showing a marked increase in *Azolla filiculoides* productivity under elevated (760 and 1910 ppm) pCO_2 conditions. The combined results of organic carbon, sulphur, nitrogen content and ^{15}N and ^{13}C measurements of sediments from the *Azolla* interval illustrate the potential contribution of nitrogen fixation to productivity in a euxinic stratified Eocene Arctic. Organic carbon analyses and burial flux calculations were used to quantitatively estimate storage of carbon (0.9 – 3.5 10^{18} gC) in the Arctic during the *Azolla* interval. Storing 0.9 10^{18}

to 3.5 10^{18} g carbon would result in a 55 to 470 ppm drawdown of pCO_2 under Eocene conditions, indicating that the Arctic *Azolla* blooms may have had a significant effect on global atmospheric pCO_2 levels through enhanced burial of organic matter.

8.1 Introduction

A reconstructed mean annual sea surface temperature of ~10 °C in the Eocene Arctic during the *Azolla* phase prevailed in absence of oceanic heat transport (Brinkhuis et al., 2006). This implies that increased greenhouse gas concentrations and associated feedbacks must have been the dominant factor in keeping high latitudes warm (Huber et al., 2003). Changes in the carbon dioxide concentrations in the atmosphere are commonly regarded as likely forcing mechanism of global climate on geological time scales because of the large and predictable effect of CO_2 on temperature (Pearson and Palmer, 2000). The exact relation between atmospheric CO_2 concentration and the greenhouse climate of the early Eocene is uncertain because proxy measurements from palaeosols (Yapp, 2004; Royer et al., 2001), marine boron isotopes (Pearson and Palmer 2000) and leaf stomatal indices (Royer et al., 2001) give extremely variable estimates of atmospheric CO_2 concentrations of between 400 and 3500 ppmv. In the middle Eocene pCO_2 is assumed to have been up to ten times preindustrial values (Pearson and Palmer, 2000). It is well known that high pCO_2 may stimulate growth of *Azolla* species (Allen et al., 1988; Idso et al., 1989; Koizumi et al., 2001). Moreover, there are indications that at higher CO_2 concentrations plants generally cope better with environmental stresses such as high salinity levels (Reuveni et al., 1997).

The *Azolla* phase in the Eocene Arctic, during which the organic carbon content of the sediment reaches a maximum (Moran et al., 2006), coincides with a global shift towards heavier $\delta^{13}C$ values in benthic foraminifera (e.g., Zachos et al., 2001), suggesting enhanced global sequestration of organic matter. Waddell and Moore (2008) also found a positive $\delta^{13}C$ excursion in fish bone remains and speculated that during a period of extreme primary productivity the Arctic surface waters became depleted in ^{12}C, which subsequently resulted in burial of the fish bones with ^{13}C enriched organic matter. The combination of extremely high primary production by *Azolla* on a freshwater surface, together with the anoxic and saline nature of Eocene Arctic deep waters makes the Arctic Basin ideally suited as an important carbon sink. In addition, like extant *Azolla*, Eocene *Azolla* lived in symbiosis with a nitrogen fixating cyanobacterial symbiont (Chapter 3). These nitrogen-fixing bacteria play a key role in global biogeochemical cycles as availability of fixed nitrogen and dissolved phosphorus together limit primary productivity and thus CO_2 fixation. In anoxic environments a substantial loss of fixed nitrogen occurs through

denitrification or anaerobic ammonia oxidation activity (Kuypers et al., 2003) and on shorter timescales fixed nitrogen is often a limiting nutrient. During growth of *Azolla*, however, this loss of fixed nitrogen may be compensated by symbiotic nitrogen fixating bacteria. Sustained growth of *Azolla* in a major anoxic oceanic basin may thus have contributed significantly to reducing atmospheric CO_2 levels, either directly by the storage of large amounts of organic carbon or/and indirectly through enhanced nitrogen fixation.

Here we discuss the potential role of *Azolla* as a modifier of nutrient cycles and evaluate if and how that role was instrumental for Earth's greenhouse to icehouse transition. *Azolla* cultivation experiments were set up to elucidate the potential impact of elevated pCO_2 levels on the growth of *Azolla*. Results of these experiments are used to further constrain knowledge of *Azolla* growth rates, productivity and potential carbon drawdown in the context of reconstructed Eocene Arctic environmental conditions.

8.2 Materials and Methods

8.2.1 Sample material: extant *Azolla*

Azolla filiculoides was collected from an arable land ditch in the surroundings of Elst, The Netherlands (N51°55'48"; E5°50'6"). Two fresh *Azolla* samples were used for biomarker and compound-specific isotope analysis. Bulk *Azolla* and manually picked megaspores were analysed for their $\delta^{13}C$ and $\delta^{15}N$ isotopic composition.

8.2.2 Sample material: IODP 302 (ACEX) sediments

During the IODP 302 ACEX expedition, cores were taken at 1288 m water depth at the Lomonosov Ridge, Expedition 302, Hole M0004A, 87.87 °N, 136.18 °E (Backman et al., 2006). In this study we used sediments from lithological Unit 2, Core M0004A-11x 297.31 to 302.63 mbsf covering the *Azolla* interval as encountered in the core (Brinkhuis et al., 2006). This unit is dominated by very dark clay mud-bearing biosiliceous ooze. Paleowater depths are estimated to be shallow, perhaps on the order of ~200 m (Moran et al., 2006). The entire core 11x has pale-grey dark-grey laminations. The *Azolla* remains are associated with the light layer in the SEM pictures (Brinkhuis et al., 2006). The recovery within section 11x was good, including the end of the *Azolla* interval. Fifty-four samples were used for palynological analyses, giving a sample resolution of one sample every 10 cm. In total, 90 samples were used for bulk geochemical analyses and two for biomarker and compound-specific isotope analyses. *Azolla* megaspores from the ACEX core were manually picked for the determination of $\delta^{13}C$ values.

8.2.3 Pilot experiment: Growth of *Azolla* at elevated atmospheric CO_2 concentrations

To study the influence of different atmospheric carbon dioxide concentrations on *Azolla* growth, *Azolla filiculoides* was grown in glass aquaria with a water volume of 15.6 l and headspace of 3.4 l. The aquaria were made air-tight except for a gas overflow outlet. The aquaria were placed in a water bath with a controlled mean temperature of 15 °C. At the start of the experiment 4 g of fresh *Azolla* was introduced in each aquarium. Three different treatments with specific atmospheric CO_2 concentrations were completed, with eight replicates per treatment (Fig. 8.1). At the start of the experiments the measured CO_2 concentrations in the headspaces of the different aquaria amounted to 340, 760 and 1910 ppm, respectively. Appropriate atmospheric CO_2 concentrations were attained by mixing compressed air with custom-made mixtures of various concentrations of CO_2 in synthetic air (Air Liquide, Eindhoven, the Netherlands), using mass flow controllers and gas blenders (Bronkhorst Hi-Tec, Veenendaal, the Netherlands). Per treatment the gas mixture was uniformly distributed between the headspaces of the eight aquaria, refreshing the air volume within each aquarium every 5 min. The nutrient solution in the aquaria contained 1.75 mmol/l NaHCO3, 1.75 mmol/l $CaCl_2 \bullet 2H_2O$, 0.025 mmol/l NaH_2PO_4 • H2O, 1 mmol/l K_2SO_4, 1 mmol/l $MgSO_4$ • 7H2O, 0.01 mmol/l Fe-EDTA, 0.001 mmol/l $CuSO_4$ • $5H_2O$, 0.02 mmol/l $MnCl_2$ • $4H_2O$, 0.01 mmol/l $ZnSO_4$ • $7H_2O$, 0.003 mmol/l $Na_2MoO_4 \bullet 2H_2O$, 0.02 mmol/l H_3BO_3 and 0.004 mmol/l $CoCl_2 \bullet 6H_2O$ and was adjusted to a pH of 7.5 using 30% HCl. Fresh nutrient solution was supplied at a rate of 0.2 l/h from containers using peristaltic pumps, the water level being held at a constant level by means of an overflow outlet (Fig. 8.1). Since no nitrogen was added to the nutrient solution, *Azolla* completely depended on its cyanobacterial symbionts for nitrogen supply. The experiments were performed in a greenhouse where the light flux amounted to at least 150 μmol/m/s at vegetation level, supplemented by 600 watt HDN lamps set to a day: night rhythm of 16:8 h.

The CO_2 concentrations in the headspaces above each aquarium were monitored. Air samples were taken with a syringe at the gas overflow outlet and CO_2 concentrations were measured directly using an Infrared Gas Analyzer (IRGA, type ABB Advance Optima). Nutrient solutions of all aquaria were sampled weekly for nutrient analyses with the aid of rhizons. The solutions were analysed for pH, total inorganic carbon using an Infrared Gas Analyzer (IRGA, type ABB Advance Optima), and total concentrations of Al, Ca, Fe, K, Mg, Mn, Na, P, S, Si and Zn using inductively coupled plasma emission spectrometry (ICP-OES). To avoid contamination all used glassware was immersed in acid (30% HCL) for 24 hours after which it was rinsed three times with demineralised water. Total inorganic carbon content in the nutrient solution was measured by injection of 0.2 ml of the nutrient solution into a concentrated H_2PO_4 solution of 2.1% in a glass reservoir that was directly coupled to an infrared gas analyser to ensure direct measurement of released

Figure 8.1: The experimental set-up in the greenhouse.

dissolved carbon. Plants were harvested on days 0, 10, 17 and 23. At harvest total fresh weight of the cultured *Azolla* was determined for each aquarium after which 4 g of fresh *Azolla* was put back into the aquaria while the rest was dried at 70 °C for 48 h to determine the element composition of the biomass. The total dry weight at a specific sampling time was calculated using the dry weight to fresh weight ratio from the sub-sample. Cumulative dry weights were based on using these dry weight ratios, adding them up to the total dry weight calculated for the previous time intervals. To analyse nutrient contents of plant tissue, dried samples were ground in liquid nitrogen. Nitrogen and carbon were subsequently measured with a CNS analyzer (type Fisons NA1500). 200 μg plant material was digested using a acid mixture (4 ml HNO_3 (65%) and 1 ml H_2O_2 (30%) (Kingston and Haswell, 1997) in Teflon vessels heated in a Milestone microwave oven. Total concentrations of Al, Ca, Fe, K, Mg, Mn, Na, P, S, Si, and Zn were measured in diluted digestates.

8.2.4 Palynology

Sub-samples were first cleaned by removing the top part and oven dried at 60 °C overnight. Agepon (Agfa-Gevaert, art Nr AKX2P) wetting agent was added. Precisely weighted sediment samples were then treated with HCl and HF in standard palynological treatment. Residues were sieved retaining the fraction size between 15 and 250 μm. Lycopodium clavatum tablets containing a known amount of spores were added to the samples to calculate the concentrations of *Azolla* massulae per gram of sediment. The samples were then examined under a binocular microscope at a magnification of 400x.

8.2.5 Bulk TOC, N, and isotope measurements on extant *Azolla*

Extant *Azolla* samples were oven dried at 70 °C for 24 hours. Total organic carbon (TOC), δ^{13}CTOC, total nitrogen content (N_{tot}) and bulk δ^{15}N were measured using an elemental analyser (Fison NA 1500 CNS), connected to a mass spectrometer (Finnigan Delta Plus). δ^{13}CTOC values are reported against VPDB. δ^{15}N values are calculated as per mille excess above their natural abundance in air. Analytical precision and accuracy were determined by replicate analyses and by comparison with international and in-house standards. Precision was better than 0.1% for TOC, N_{tot}, and 0.1‰ for δ^{13}CTOC, and 0.15‰ for δ^{15}N.

8.2.6 Sediment bulk TOC, N, S, and isotope measurements

Total organic carbon (TOC), total nitrogen content (N_{tot}), total nitrogen isotopic composition ($\delta^{15}N_{tot}$) and total sulphur content of bulk sediment samples were determined, with a sampling spacing of 10 cm for the *Azolla* interval. All sediment samples were freeze-dried and subsequently grounded in an agate mortar. Prior to the determination of organic carbon content and δ^{13}CTOC inorganic carbon was removed. Samples were treated with 10% HCl, rinsed with demineralized water to remove $CaCl_2$, and dried. TOC, δ^{13}CTOC, N_{tot} and $\delta^{15}N_{tot}$ were measured using the same procedure, with similar precision and accuracy, as described above in par 3.5. Total concentrations of S were determined after digestion in a mixture of HF, HNO_3, and $HClO_4$ and final solution in 1M HCl via ICP-OES (Perkin-Elmer Optima 3000). The accuracy and precision of the measurements were monitored by including international and laboratory standards and were better than 3%.

8.2.7 Compound-specific isotope analyses ACEX sediments and extant *Azolla*

Both ACEX sediments and extant *Azolla* specimens were freeze-dried, powdered and subsequently extracted with an Accelerated Solvent Extractor (Dionex) using a dichloromethane (DCM) – methanol (MeOH) mixture (9:1, v/v). To separate the compounds of interest an aliquot (ca. 15 mg) of the total extract was methylated with BF_3/MeOH at 60°C for 10 min and subsequently separated by preparative thin layer chromatography (TLC) on kieselgel 60 (Merck, 0.25mm) as described by Skipski et al. (1965). The lower, more polar, bands were silylated with BSTFA in pyridine to convert the alcohols into the corresponding TMS-ethers. Components were identified by GC/MS (Thermo Trace GC Ultra). Samples were on-column injected at 70 °C, on a CP-Sil 5CB fused silica column (30 m x 0.32 mm i.d, film thickness 0.1 μm) with Helium as carrier gas set at constant pressure (100 KPa). The oven was programmed to 130 °C at 20 °C/min and then to 320 °C at 4 °C/min, followed by an isothermal hold for 20 min. Compound specific δ^{13}C values were determined using isotope ratio monitoring gas chromatography-mass spectrometry (GC-IRMS), using a ThermoFinnigan Delta-Plus XP mass spectrometer. A similar

column and oven program were used as described above, though with a constant flow of 1.2 ml/min. Co-injected squalane, with a known, offline determined, isotopic composition was used as internal standard. Carbon isotopic compositions are reported relative to the VPDB standard and are based on duplicate analyses of well-resolved peaks and represent averaged values. In the case of alcohol moieties, the $\delta^{13}C$ value of the BSTFA used for silylation was determined by derivatization of an authentic alcohol (myo-inositol) standard with a known $\delta^{13}C$ composition. Standard deviation of co-injected squalane was 0.2‰. Duplicates had a standard deviation better than 0.5‰.

8.3 Results and Discussion

In order to further constrain the exact environmental conditions facilitating the Eocene Arctic *Azolla* blooms a suite of geochemical and palynological analyses are performed. Furthermore, the influence of these Eocene conditions is investigated using *Azolla* cultivation experiments, focusing on elevated pCO_2 conditions. Finally, the combined results will shed light on *Azolla* occurrence, productivity and potential atmospheric CO_2 drawdown.

8.3.1 Pilot cultivation experiments with extant *Azolla*: a key to the past.

During the middle Eocene atmospheric CO_2 levels were much higher than today (Pearson and Palmer, 2000). To investigate the influence of elevated atmospheric CO_2 concentrations on *Azolla* growth rates, CO_2 concentrations in the headspaces of the cultivation aquaria were set to values of 340 ppm (control), 760 ppm and 1910 ppm, respectively. Distinct increases in biomass production in response to elevated carbon dioxide concentrations were evident (Fig. 8.2). After 23 days the total dry biomass amounted to 3.92±0.37, 5.98±0.47 and 7.87±1.04, respectively. The amount of biomass produced in the high (1910 ppm) CO_2 treatment was twice that of the biomass produced in the control treatment at 340 ppm. The experiment using an intermediate CO_2 concentration (760 ppm) yielded 1.5 times more biomass (Fig. 8.2). During growth in the light period (16 h/d) the preset CO_2 concentrations within the headspaces dropped appreciably. Lowest CO_2 concentrations in headspaces were measured just before harvest, when *Azolla* densities were highest, during the light period. On average pCO_2 values dropped from their preset concentrations to values of 170±100 ppm, 330±140 ppm, and 1080±190 ppm respectively. Flushing the headspaces every 5 minutes thus did not suffice to maintain constant pCO_2 levels. Both pH (7.53±0.27, 7.47±0.17 and 7.43±0.18 in the treatments with 340, 760 and 1910 ppm atmospheric CO_2, respectively) and total inorganic carbon (TIC) (819±76, 857±94 and 800±175 in the respective treatments) of the culture medium remained constant throughout the experiment with no differences at different lev-

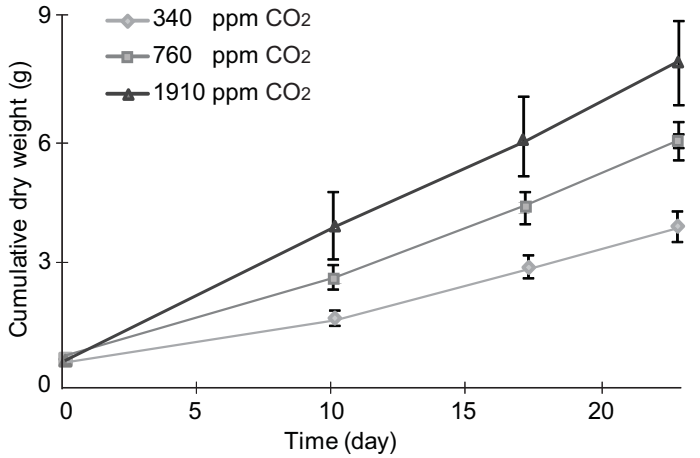

Figure 8.2: Plot of cumulative biomass against time. Cumulative biomass was calculated by using the fresh weight/dry weight ratio of the sub samples that were taken each harvest for dry weight measurements. Using this ratio the total biomass per week was calculated and this was added to the total dry weight of the week before.

els of CO_2 concentrations. Given the low diffusion rate of CO_2 into water (0.21 m/d or 2.4 μm/s) (Zeebe and Wolf-Gladrow 2001) and the observed stability of pH and TIC in the culture medium, the rapid decreasing CO_2 concentrations in headspace can only be attributed to high CO_2 (g) uptake rates of *Azolla*.

Analyses of the chemical composition of the culture medium showed that the supply rate of fresh medium of 0.2 l/h was not high enough to keep the phosphorus concentration at a constant level (P concentrations dropped from 20 μmol/l to 6 μmol/l). The concentrations of the other elements in the culture medium remained constant. The measured nutrient concentrations in *Azolla* all fall within the range of average concentrations of mineral nutrients in plant dry material matter (Marschner 1995). The decreasing nutrient and N concentrations probably reflect diluting effects. Given the preserved linear growth rates during the experiments (Fig. 8.2), this dilution did not adversely influence *Azolla* biomass production.

These experiments indicate that at elevated CO_2 (g) concentrations the carbon dioxide uptake of *Azolla filiculoides* increases and that biomass is produced at higher rates at higher pCO_2 concentrations, suggesting that CO_2 might be a limiting factor for *Azolla* growth. Hence, *Azolla* could potentially grow at significantly higher rates under the elevated Eocene pCO_2 conditions than under present-day circumstances. However, it should be noted that other environmental conditions like salinity (Rai et al., 2001), pH (Moretti and Gigliano, 1988; Cary and Weerts, 1992) or nutrient availability (Sah et al., 1989) also affect *Azolla* biomass production.

8.3.2 Sedimentary signals of the Eocene Arctic *Azolla* bloom

8.3.2.1 Bulk parameters of ACEX sediments

Our high-resolution ACEX TOC profile reveals values ranging between 3.1 and 6.0 wt% (Fig. 8.3). After the *Azolla* phase (above 289.7 mbsf) TOC decreased to lower levels, around 2 wt%. The high-resolution record of *Azolla* spore counts (Fig. 8.3) confirms the cyclic nature of the abundance pattern in the *Azolla* record as previsouly described in Brinkhuis et al. (2006). These cycles have a spacing of just over 1 meter and are positively correlated with the TOC content (Fig. 8.3). Sangiorgi et al. (2008) applied a Blackman-Tuckey power spectral analysis to palynological and siliceous microfossil data for the middle Eocene (~ 46 Ma) core section between ~236 to 241 mcd (meters composite depth) and also found a 1 meter periodicity. The available age model for the ACEX core (Backman et al., 2008), and the derived sedimentation rate of 24.3 meters per Ma during the middle Eocene (~ 46 Ma), suggest that the 1 meter cyclicity is compatible with a Milankovitch-type orbital forcing, representing obliquity. Based on the high latitudinal setting, an obliquity signal is expected to be present. However, since for the *Azolla* phase the age model suggests an overall sedimentation rate of 12.7 m/Ma (Backman et al., 2008), the 1 m cyclicity would correspond to ~ 80.000 year. Yet, given that the onset of *Azolla* is missing due to failure in core recovery (Backman et al., 2006), it could be possible that the observed cyclicity in the *Azolla* record still represents obliquity. If these cycles indeed respond to obliquity the amount of time included in the entire *Azolla* event, represented in the recovered sections of the ACEX core, can be calculated. In this case, the estimated minimum duration would only be 160 kyr, based on the observed four obliquity cycles within the recovered part from the *Azolla* interval in the ACEX core (Fig. 8.3). However, as described before, it is possible that a major part of the *Azolla* phase has not been retrieved in the ACEX core. The recovered *Azolla* interval in the ACEX core thus represents 160 kyr, with a 24.3 m/Ma sedimentation rate. The duration of the entire interval is 1.2 Ma as inferred from dating of the *Azolla* phase in ODP Leg 151 Hole 913B (Eldrett et al., 2004) (with a 12.7 m/Ma sedimentation rate based on the overall age model (Backman et al., 2008)).

Sulphur concentrations are high throughout the interval, varying between 47 and 72 mg/g dry sediment. C/S ratios show an atomic C_{org}/S ratio of 1-2 during and after the *Azolla* interval (Fig. 8.4a). The correlation between Fe and S indicates that most of the S is present in the form of pyrite (Fig. 8.4b). The black dots represent samples from the *Azolla* interval plotting around the pyrite line. Samples falling above the line are indicative of the presence of excess S. This indicates that S must be present as organically bound S as well (Chapter 2). The four points in grey plotting under the pyrite line represent samples from after the *Azolla* interval (above 298.8 mbsf). The accumulation of large quantities of organic matter in an euxinic environment is consistent with the findings of Kurtz et al. (2003) who showed a global minimum in C_{org}/S pyrite (C_{org}/S ratio of 2-4) during the early Eocene. The

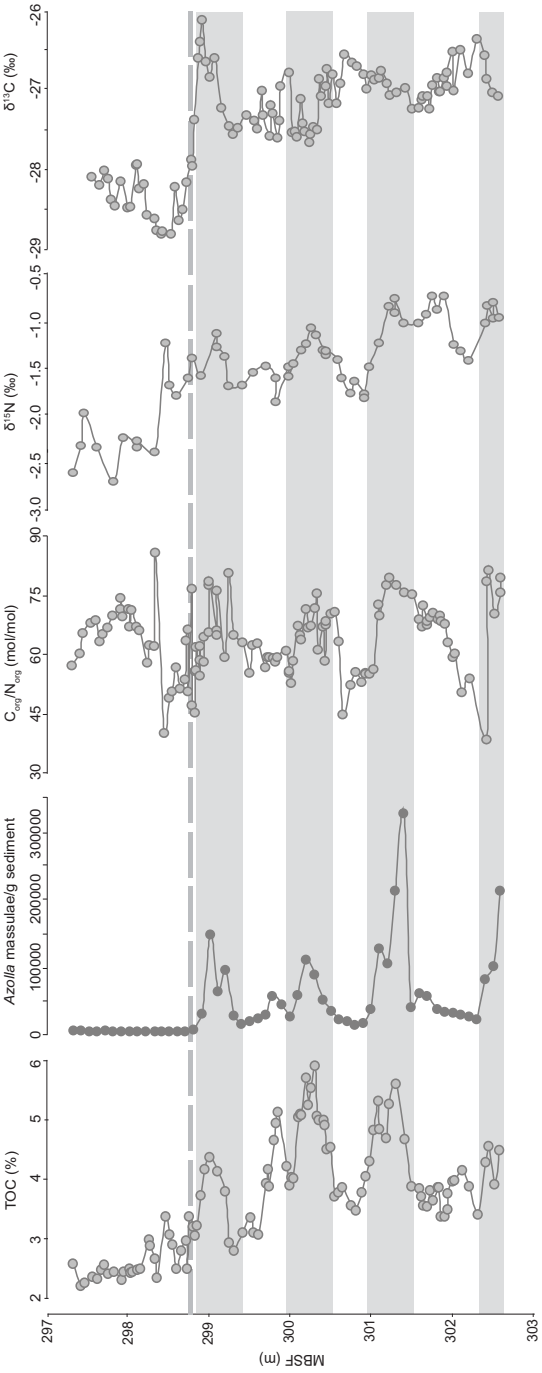

Figure 8.3: Palynological and geochemical data of high resolution analyses of ACEX sediment, including Azolla megaspore counts, TOC (%), δ^{13}CTOC (‰), $\delta^{15}N_{tot}$ (‰) and C_{org}/N_{org} ratio.

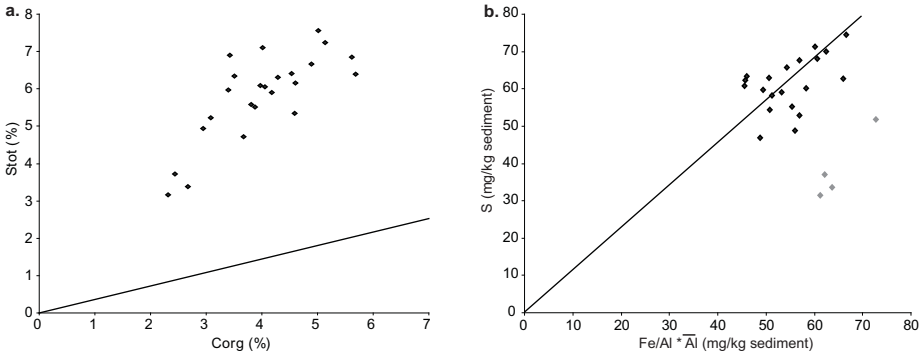

Figure 8.4: (a) Plot of weight percent organic carbon (wt%) versus weight percent total sulphur concentration (wt%). The black line indicates the modern normal marine (non-euxinic) sediments (Berner 1984), (b) Fe normalized over aluminum concentration (mg/kg sediment) versus total sulphur content (mg/kg sediment). The S/Fe weight ratio of pyrite (1.15) is plotted. Black dots represent samples from the Azolla interval, grey dots represent samples from after the interval.

presence of sulphate-rich waters in the deeper parts of the Arctic Basin provides additional evidence for the salinity stratification of the basin (Chapters 6&7).

In view of the co-occurrence of *Azolla* and nitrogen fixating hetrocystous cianobacteria (Chapter 3), fixing of atmospheric nitrogen must have played a major role in nitrogen supply. Bulk sedimentary nitrogen isotope ratios are persistently low, between -0.7 and -2.4‰ throughout the *Azolla* phase (Fig. 8.3) and drop to even lower values (<-2‰) afterwards. Variations in $\delta^{15}N_{tot}$ in surface sediments generally reflect differences in relative nutrient utilization (Schubert and Calvert, 2001) and denitrification or anammox (Altabet and Francois, 1994; Montoya et al., 2004), but can also be influenced by exchange with open-ocean water or runoff. Under oxygen depleted conditions, the reduction of nitrate leads to enrichment of the residual nitrate in ^{15}N relative to the mean value because $^{14}NO_3$ is more readily reduced by bacteria. Under the prevailing anoxic conditions in the Eocene Arctic relatively enriched $^{15}N_{tot}$ values are thus expected as upwelling of nitrate deficit waters generated in the dysoxic deeper parts of the water column by denitrification or anammox bacteria (Cline and Kaplan, 1975; Kuypers et al., 2003) followed by Redfield-type nutrient drawdown should result in nitrate limitation in the photic zone, which would result in a positive $^{15}N_{tot}$ excursion. The small and constant offset (mean 0.9‰) between the $\delta^{15}N_{tot}$ and $\delta^{15}N_{org}$ found earlier by Knies et al. (2008) confirms that there is little net influence of NH_4^+ generation or vertical diffusion on the sedimentary ^{15}N values. Hence we use bulk $\delta^{15}N$ values for reconstruction of the marine nitrogen cycle. The low $\delta^{15}N_{tot}$ values encountered in the Arctic sediments are in line with the presence of N_2-fixing organisms. Also cultured *Azolla filiculoides* biomass had a similarly low average $\delta^{15}N$ of -1.5‰, which is consistent

with ^{15}N values reported for other biomass produced by N_2 fixation (between -1‰ and -2‰) (Minagawa and Wada, 1986; Kuypers et al., 2004). Whereas the oxygen depleted water condition resulted in the large scale loss of biologically available nitrogen, phosphorus might have been regenerated more efficiently under such conditions (Gächter et al., 1988; Van Cappellen and Ingall, 1994, Chapter 7). Organisms with nitrogen fixating symbionts, like *Azolla*, would have had an ecological advantage.

In extant *Azolla* C/N ratios vary between 9 and 15. C_{org}/N_{tot} ratios in the ACEX core were adjusted for the contribution of inorganic nitrogen by subtracting a fixed amount of inorganic nitrogen (47 μmol/g). This amount is based on extrapolation of the linear relation between C_{org} and N_{tot} content. This concentration is similar to the amount used for subtraction as determined by Knies et al. (2008) using $\delta^{15}N$ values. The C_{org}/N_{tot} ratios in the ACEX sediments vary from 27 to 46. The calculated C_{org}/N_{org} ratios vary from 40 to 80 (Fig. 8.3) and are significantly higher than those of extant *Azolla*. These higher C_{org}/ N_{org} ratios point towards extensive selective degradation of nitrogen-rich organic compounds (e.g. amino acids), despite the continuous anoxic bottom waters as evidenced by the presence of laminations in the sediment. After each *Azolla* megaspore abundance peak, a marked decrease in C/N ratio can be observed, which coincides with a drop in $\delta^{15}N_{tot}$ (Fig. 8.3). Changes in C/N ratios, therefore, could be linked to changes in source organisms (*Azolla* vs marine plankton) or changes in N preservation. Compositional changes, on the other hand, are not reflected in the observed bulk ^{13}C values, which vary around -27.7‰ throughout the interval (Fig. 8.3). The decrease in $\delta^{15}N$ probably indicates that after periods of extensive *Azolla* growth, the water column became slightly more oxygenated, decreasing the impact of denitrification/anammox until the next *Azolla* bloom.

8.3.2.2 Compound specific carbon isotope analyses

In addition to the existing palynological data, a recent study provided molecular evidence for the pervasive past presence of *Azolla* in a freshwater Eocene Arctic setting (Chapter 2). It was shown that the total lipid fraction of extant *Azolla* ferns contains a series of mid-chain ω20 alkanols, 1,ω20 diols and ω20 hydroxy fatty acids with carbon chain lengths ranging from $C_{27} – C_{36}$. Selective extraction of extant *Azolla* leaf surface lipids revealed that these compounds most likely originate from *Azolla* leaf waxes. The ACEX sediments from the *Azolla* interval contained most of the described ω20 compounds. Especially relatively high quantities of compounds identified as 1,ω20 $C_{30} – C_{36}$ diols were detected in both extant *Azolla* species and in sediments from the ACEX core. Based on the uniqueness of the ω20 hydroxy compound series and their relative stability, these compounds can be considered to be excellent biomarkers for *Azolla*, can thus be used for compound specific isotope ($\delta^{13}C$) analyses, and therefore serve as paleo-environmental indicators for *Azolla*.

Compound specific $\delta^{13}C$ values can provide insight into Eocene $\delta^{13}CO_2$. As β-sitosterol is the most abundant sterol present in extracts from *Azolla* (Chapter 2), the ^{13}C of β-sitosterol was measured both for extant *Azolla* and ACEX sediments (Table 8.1). Here we compare stable carbon isotopic compositions of TOC, spores and specific biomarkers of extant *Azolla* and ACEX sediments from the *Azolla* phase to gain insight into differences in the present-day and Eocene environmental conditions at which *Azolla* fixed carbon.

Bulk $\delta^{13}C$ values for recent *Azolla* of ~ -30‰ (Table 8.1) are consistent with the findings by Bunn and Boon (1993) for ferns (Pterophyta) in general and in line with their use of the C3 pathway of carbon fixation (Hayes, 2001). The $\delta^{13}C$ of the megaspores of extant *Azolla* is also ~ -30‰, indicating that there is no significant difference in ^{13}C content between *Azolla* biomass and spores. However, the $\delta^{13}C$ ratios of the lipids extracted from *Azolla* are substantially depleted: the 1,ω20 C_{30} – C_{36} diols have $\delta^{13}C$ values of -38.0 to -39.9‰ and the $\delta^{13}C$ values for β-sitosterol is -32.6‰ (Chapter 2). Such differences are generally observed in biomass (Hayes, 2001) and lipids are typically 4 - 8‰ depleted in ^{13}C values relative to total cell material. The TOC and the *Azolla* megaspores contain isotopically heavy sugars and proteins and, therefore, their $\delta^{13}C$ are higher than those of the individual lipids. The difference in $\delta^{13}C$ values between the β-sitosterol and the diols is ca. 6.5‰. Differences in the biosynthetic pathways of isoprenoids (including β-sitosterol) and the compounds with straight chain carbon skeletons (i.e. ω20 diols) will influence the ^{13}C composition of the individual compounds. These differences may, possibly as a result of the alternative pyruvate/glyeraldehyde-3-phosphate pathway, differ by up to 8‰ (Schouten et al., 1998), which is sufficient to explain the observed 6.5‰ difference between the isoprenoid β-sitosterol and the straight chain ω20 diols in extant *Azolla*.

Of all measured parameters (Table 8.1) the $\delta^{13}C$ values of the diols probably give the most reliable insight into differences in the present-day and Eocene environmental conditions at which *Azolla* fixed carbon. The *Azolla*-specific diols in the ACEX sediments show an enrichment of at least 8‰ relative to values observed

Table 8.1: $\delta^{13}C$ compound specific isotopes (‰ vs PDB) for selected compounds and $\delta^{13}C$ for bulk organic matter and manually picked *Azolla* megaspores encountered in extant *Azolla* and ACEX sediment extracts.

Diols extant *Azolla*	$\delta^{13}C$ (‰)	Diols ACEX	$\delta^{13}C$ (‰)	Extant *Azolla*	$\delta^{13}C$ (‰)	ACEX	$\delta^{13}C$ (‰)
1,11 C_{30} diol	-39.1	1,11 C_{30} diol	-	ß-sitosterol	-32.6	ß-sitosterol	-29.1
1,13 C_{32} diol	-38.0	1,13 C_{32} diol	-30.1	$d^{13}CTOC$	-30.3	$d^{13}CTOC$	-27.6
1,15 C_{34} diol	-38.7	1,15 C_{34} diol	-31.3	Megaspores	-30.5	Megaspores	-27.7
1,17 C_{36} diol	-39.9	1,17 C_{36} diol	-29.7				

in extant *Azolla*, between -29.7 to -31.3‰ (Table 8.1). β-sitosterol is also enriched in ^{13}C in the Eocene material but only by ~3‰, a similar enrichment as observed for $\delta^{13}C$TOC and $\delta^{13}C$ of the megaspores (Table 8.1). The difference between the β-sitosterol and the ω20 diols is only ~1‰ in the sediment instead of 6.5‰ in extant *Azolla*. This could be due to a mixed origin for the Eocene β-sitosterol. This sterol is not specific for *Azolla* and is probably also produced by algae growing in the water column in the Eocene Arctic, producing β-sitosterol with a different ^{13}C content. Alternatively, the different offsets could be explained by a difference in biosynthetic pathways between Eocene *Azolla* and extant *Azolla*, resulting in a much smaller difference between isoprenoidal and acetogenic lipids. Based on the similarity of the distribution of the ω20 diols in extant and Eocene *Azolla* this seems unlikely. Sedimentary TOC does not solely contain *Azolla* remains so it also represents mixed contributions. The difference between the $\delta^{13}C$ values of the extant and Eocene *Azolla* megaspores is also only 3‰. This could be caused by diagenesis. Extant *Azolla* megaspores still contain a shell mainly consisting of both sugars and protein components, which are typically substantially enriched in $\delta^{13}C$ (Hayes, 2001). During diagenesis, sugar and protein carbon degrades more easily, leaving the megaspores increasingly isotopically depleted. The $\delta^{13}C$ values of the *Azolla*-specific ω20 diols indicate the largest and probably most accurate difference (8‰) in isotopic composition between the present and the Eocene.

Based on reconstructions of Eocene atmospheric pCO_2 levels, suggesting higher concentrations, and the observation that *Azolla* also takes up atmospheric CO_2, and grows faster at elevated pCO_2 levels, at first sight, lighter rather than heavier $\delta^{13}C$ values (Hayes et al., 1999) for *Azolla* biomarkers in ACEX sediment compared to extant *Azolla* are expected. Additionally, the cultured *Azolla* does not seem to fractionate to the full extent during carbon fixation (i.e. bulk values of ca. -33‰ would be expected). $\delta^{13}C$ of atmospheric CO_2 taken up by *Azolla* was probably different in the Eocene and could thus also influence the $\delta^{13}C$ ratios. In fact, based on $\delta^{13}C$ analyses on foraminifera, the atmospheric CO_2 $\delta^{13}C$ was 3‰ enriched in the Eocene relative to the present-day atmospheric CO_2 $\delta^{13}C$ (Hayes et al., 1999; Pearson et al., 2001; Zachos et al., 2001). A similar enrichment of Eocene *Azolla* biomass and lipids would be expected if they would grow under identical conditions as the extant *Azolla*. This explains part of the 8‰ enrichment. Secondly, elevated CO_2 levels substantially enhance *Azolla* growth rates, as has been shown in the cultivation experiments (see par 8.4.1.1). Increased growth rates decreases isotopic fractionation (Hayes et al., 1999), possibly explaining the higher $\delta^{13}C$ values for the ω20 diols in the ACEX sediments, and counteracting the effect of higher CO2 levels. Based on *Azolla* microspore massulae abundances in the core (~50.000 /g dry sediment), or 5.2 10^6 spores /m^2/yr, high Eocene Arctic production rates are inferred. For comparison, it was estimated that a thick mat of 8 kg/m^2 fresh biomass is needed to produce 380.000 microsporocarps and 85.000 megasporocarps per m^2 (Janes, 1998).

The high ^{13}C values found here are also consistent with the high ^{13}C encountered in fish apatite by Waddell and Moore (2008). These were found to reflect extremely high primary production, which resulted in enhanced growth rates and decreased isotopic fractionation, followed by burial of fish bones with 13C enriched organic matter.

8.3.2.3 Impact of the Arctic Azolla bloom on CO_2 drawdown

Using sedimentary TOC content and sedimentation rates the potential CO_2 drawdown during the *Azolla* interval can be estimated. Combining TOC values of 4 wt% (Fig. 8.3) with a mass accumulation rate (MAR) of 35 g/m^2/yr results in a net carbon burial rate of 1.4 gC/m^2/yr. Recently, Knies et al. (2008) estimated a maximum primary paleoproductivity during the *Azolla* phase of 120 gC/m^2/yr, using sedimentary organic carbon content, correcting for decomposition in the water column, burial efficiency, and dilution by inorganic sediment (Knies and Mann, 2002). Our experiments show average production rates for extant *Azolla* under ambient conditions: 4.5-5 g dry weight per m^2/d or 2 gC/ m^2/d. A production rate of 2 gC/m^2/d would have yielded 120 gC/m^2 within 2 months, a primary production estimate of 120 gC/m^2/yr thus seems reasonable, albeit a bit on the low side given Eocene pCO_2 levels and associated enhanced *Azolla* growth. Also the prolonged photoperiod during the Arctic summer would have stimulated higher *Azolla* production. Estimated primary productivity of 120 gC/m^2/yr in combination with a net carbon burial rate of 1.4 gC/m^2/yr, demonstrates a fairly low burial efficiency of 1.2%. Hence, despite the water column anoxia extensive biodegradation must have occurred either during transport in the water column or at the sediment-water interface, or over time within the sediments.

The preservation of diols is better than that of for instance fatty acids, neutral lipids, sterols, *n*-alkanols, and *n*-alkanes (Sun and Wakeham, 1994), but these compounds are probably more susceptible to degradation than spores. If the preservation of diols reflects the average degree of preservation of *Azolla*-derived organic matter, comparison of the Eocene Arctic diol fluxes with current *Azolla* diol production rates will give a minimum estimate of *Azolla* growth. Diol (ω20 C_{30} - C_{36}) concentrations in the ACEX core sum up to 4.5 μg/g sediment, or 80 μg/g TOC. In cultured extant *Azolla* the total diol concentration for fresh *Azolla* amounts to 480 μg/g (dry weight) *Azolla* or 190 μg/gC in *Azolla*. If all organic constituents in *Azolla* would preserve equally well, this would indicate that about 40% of the Eocene TOC would be derived from *Azolla*. Based on the palynological composition (Brinkhuis et al., 2006), this is an underestimate.

CO_2 fixation by *Azolla* and subsequent burial of *Azolla*–derived organic matter has direct consequences for the carbon inventory of the atmosphere - ocean system. The burial of *Azolla*-derived organic matter is assumed to occur in conjunction with

ongoing cycling of carbon. To quantify the effect of enhanced organic carbon storage in the Eocene Arctic Basin on atmospheric pCO_2 levels and ocean-atmosphere partitioning, equation 1 should be solved.

$$\Delta pCO_2 = \int_{\Sigma C_1}^{\Sigma C_2} \frac{pCO_2}{\left(I_A + \frac{I_O}{R_{global}} \right)} d\Sigma C \quad (1)$$

Where ΔpCO_2 is the change in atmospheric partial CO_2 pressure resulting from a perturbation in the global carbon inventory. $\Delta\Sigma C$ represents the total carbon perturbation: the amount of carbon added to or removed from the inventory. I_A is the carbon inventory of the atmosphere, I_O is the carbon inventory of the ocean and R_{global} is the average Revelle buffer factor (Revelle and Suess, 1957). Goodwin et al. (2007) showed that this equation can be solved analytically. Here we apply and compare two analytical methods to solve equation 1. The first analytical method used follows a linear approximation (e.g. Archer, 2005) described by equation 2:

$$\Delta pCO_2 = \frac{1}{M} \left(1 + \frac{I_O}{R_{global} I_A} \right)^{-1} \Delta\Sigma C \quad (2)$$

Where M represents the molar volume of the atmosphere. I_A, I_O and R_{global} are evaluated at a steady-state carbon partitioning between ocean and atmosphere, assuming a mean annual global SST of 20 °C, with total air-sea carbon levels corresponding to Eocene values (Table 8.2).This relation is found to be valid if either the change in carbon inventory is small or as long as the value of R_{global} increases when charge neutral carbon is extracted from the system.

The second analytical solution has been found to better approximate carbon emissions up till 5000 GtC (corresponding to a pCO_2 level of 1050 ppm, starting from 280 ppm) (Goodwin et al., 2007). This solution makes use of a total air-sea "buffered" carbon inventory, I_B (Goodwin et al., 2007). The buffered amount of carbon represents the CO_2 available for redistribution between the atmosphere and the ocean. I_B is assumed to be constant. This last approximation can also be used for larger emissions as it allows for variation in R_{global} .

Table 8.2: Calculated values for I_A, I_O, R_{global}, and I_B, for two sets of Eocene conditions.

	I_A (gC)	I_O (gC)	I_B (gC)[a]	R_{global}
Eocene ~800 ppm[b]	$1.70\ 10^{18}$	$1.491\ 10^{20}$	$1.26\ 10^{19}$	13.7
Eocene ~2000 ppm[c]	$4.25\ 10^{18}$	$1.901\ 10^{20}$	$1.49\ 10^{19}$	17.8

[a] I_B is calculated as $I_B = I_O / R_{global} + I_A$, using a mean annual SST of 20 °C and salinity of 35 psu
b 800 ppm: sea surface alkalinity of 2800 ìmol eq/kg, after Pearson and Palmer (2000)
c 2000 ppm : sea surface alkalinity of 3400 ìmol eq/kg, after Pearson and Palmer (2000)

$$pCO_2 = P_i e^{\frac{\Delta\Sigma C}{I_B}} \quad (3)$$

P_i is the initial partial pressure of carbon dioxide. Each of the analytical methods is applied to two different sets of Eocene initial pCO_2 conditions. Despite the extensive biodegradation, after a period of 160.000 yr still 224 kg/m^2 organic carbon, based on net carbon flux of 1.4 gC/m^2/yr, accumulated. For the entire Eocene Arctic basin (4.0 10^6 km^2), provided TOC contents are laterally uniform at 4%, this would amount to 9.0 10^{17} gC or 3.3 10^{18} gCO_2. Alternatively the *Azolla* phase also included the unrecovered sections below 11x till 15x, which using an average accumulation rate of 1.27 cm/kyr corresponds to a duration of 1.2 Ma. This maximum extent of the sedimentary sequence corresponds to a carbon storage of 3.5 10^{18} gC or 13 10^{18} gCO_2.

Based on Eocene partial CO_2 pressure, and corresponding Eocene alkalinity (Pearson and Palmer, 2000), the atmospheric I_A, oceanic I_O, and the Revelle buffer factor can be calculated. The total amount of buffered carbon (I_B) is then computed for the Eocene case (Table 8.2). The first Eocene case uses an initial partial CO_2 pressure of 800 ppm, with an alkalinity of 2800 μmol/kg (Pearson and Palmer et al. (2000) estimate for ~49 Ma). The second case assumes a 2000 ppm pCO_2 and corresponding alkalinity of 3400 μmol/kg (Pearson and Palmer estimate for ~53 Ma) (Table 8.2). Both are evaluated for two estimates of organic carbon accumulation in the *Azolla* interval (Table 8.2). In figure 8.5 the two analytical solutions are shown for the two different Eocene scenarios. Differences in I_B lead to differences in decrease in atmospheric pCO_2, following equation 3, which explains why the impact of sequestration of similar amounts of carbon burial results in different effects on pCO_2 levels. For both scenarios, R_{global} initially decreases as charge neutral CO2 is extracted from the air-sea system, making the linear approximation less suitable for the larger perturbations in ΔΣC. Still, the two different analytical approaches (linear and exponential) give very similar results (Table 8.3; Fig. 8.5) for the same Eocene scenarios. In absolute amounts, CO_2 drawdown is higher in the 2000 ppm case than in the 800 ppm. Relatively, however, drawdown falls in the same range: ~7% for 9.0 10^{17} gC and ~25% for storage of 3.5 10^{18} gC. The close match between the two is explained by the fact that for both the 800 and the 2000 ppm cases a similar ocean carbon inventory (I_O/R_{global}) of ~1.1 10^{19} gC was inferred. Based on our calculations sequestration of 9.0 10^{17} gC in the Arctic Basin had the potential to lower the concentration of atmospheric pCO_2 by ca. 55 - 120 ppm. When an estimated total extent of the *Azolla* interval of ~15 m is used, an even higher CO_2 drawdown of 195 - 470 ppm is calculated, based on 3.5 10^{18} gC storage. However, the exact magnitude of atmospheric CO_2 drawdown was also influenced by carbon cycle related feedback mechanisms. For instance, storage of carbon results in an increase in ocean water pH and an increase in CO_3^{2-} concentration. This perturbs the $CaCO_3$ cycle by increasing global burial rates of $CaCO_3$. Such a perturbation in turn acts to buffer

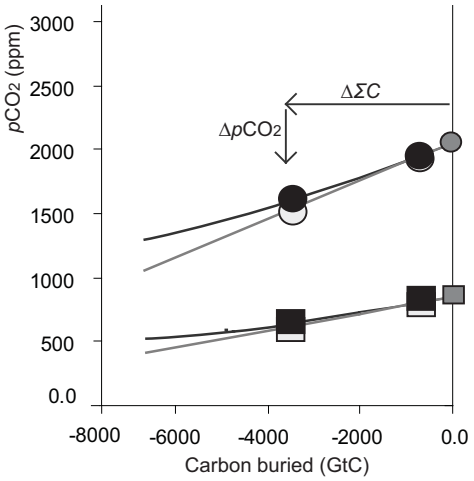

Figure 8.5: Atmospheric pCO_2 against emission/drawdown of -6.000 to + 10.000 GtC. Light grey lines: pCO_2 responds linearly with emissions, as described by equation 2. Dark grey lines: pCO_2 decreases exponentially with carbon drawdown, following equation 3. Calculated $^{p}CO_2$ levels for the different carbon storages (0.9 10^{18} and 3.5 10^{18} gC respectively) are plotted in white for the linear and in black for the exponential solution. For both analytical solutions I_A, I_O, $R_{global,}$ and I_B are evaluated at a steady state at the two chosen Eocene pCO_2 levels of 800 and 2000 ppm. Sea surface salinity is set to 35 psu, global SST to 20 °C, Eocene pCO_2 and alkalinity are obtained from Pearson and Palmer (2000).

changes in oceanic pH and thus reduces amplitude of atmospheric pCO_2 changes. On the other hand, a temperature feedback (i.e. cooling) would increase solubility of CO_2 in the ocean and thus further decrease atmospheric pCO_2 levels. On longer timescales (~100 kyr), reduced silicate weathering would possibly counteract CO_2 storage to some extent.

Forty percent of the calculated 55 - 470 ppm CO_2 drawdown is directly attributable to *Azolla* production, because 40% of TOC consists of *Azolla*–derived carbon. Indirectly, however, nitrogen fixation by organisms associated with *Azolla* could have increased the regional fixed nitrogen availability. The excess fixed nitrogen would have been available for other organisms in the Arctic Basin as well. If trans-

Table 8.3: Response of atmospheric pCO_2 to calculated burial of organic matter during the *Azolla* interval for two different Eocene initial partial pressure estimates.

	1. linear pCO_2 drawdown (burial of 0.9 10^{18} gC)	1. linear pCO_2 drawdown (burial of 3.5 10^{18} gC)	2. exponential pCO2 drawdown (burial of 0.9 10^{18} gC)	2. exponential pCO_2 drawdown (burial of 3.5 10^{18} gC)
Eocene ~800 ppm	57 ppm	220 ppm	55 ppm	195 ppm
Eocene ~2000 ppm	120ppm	470ppm	120 ppm	420 ppm

ported from the basin this excess fixed nitrogen could have increased productivity in an even larger area. In this way, Arctic *Azolla* blooms could also have enhanced carbon drawdown indirectly in a much larger area potentially contributing even more to decreasing CO_2 levels in the Eocene.

8.4 Conclusion

Azolla megaspore counts from sediments recovered during IODP expedition 302 at the Lomonosov Ridge indicate in situ growth. Eocene *Azolla*, by not only profiting from the freshwater input, but also by helping to maintain stratification and thus oxygen depletion, provided its own feedback. Stable isotope analyses ($\delta^{13}C$) of extracted biomarkers for *Azolla* revealed that values in the Eocene differ from the present day by 3‰ (β-sitosterol) and 8‰ (1,ω20 C_{30} – C_{36} diols), respectively. These differences are partly due to the different composition of the Eocene global DIC reservoir but also suggest that *Azolla* primary production rates were much higher in the Eocene than nowadays, leading to less ^{13}C fractionation. Culturing experiments of extant *Azolla* mimicking Eocene pCO_2 conditions show doubling growth rates of *Azolla* filiculoides in the 1910 ppm atmospheric pCO_2 treatment compared to the control of 340 ppm. Under Eocene pCO_2 conditions, *Azolla* could thus reproduce at higher rates than under present-day CO_2 concentrations and could fix carbon at higher rates. Based on bulk sediment analyses, including high organic carbon contents, low C/S ratios, overall, euxinic bottom water conditions are inferred, which is consistent with previous reports (Knies et al., 2008; Chapter 7). Bulk $\delta^{15}N_{tot}$ values are persistently low (<-1‰) and mark the importance of nitrogen fixation as a source of fixed N in the stratified basin. The high C_{org}/N_{org} ratios point toward extensive selective degradation of nitrogen-rich organic compounds, despite the continuous anoxic bottom waters. Given the low reconstructed burial efficiency of 1.2%, considerable biodegradation must indeed have occurred despite the reconstructed euxinic bottom water conditions. A minimum and maximum estimate of carbon storage in the Arctic for the *Azolla* interval has been obtained. Calculations are based on extrapolation of the organic carbon accumulation rates over the entire Eocene Arctic basin, leaving out the Nordic Sea areas. The maximum organic carbon storage of $3.5\ 10^{18}$ gC is calculated based on accumulation rates of 12.7 cm/kyr and a time interval of 1.2 Ma for the *Azolla* interval. The minimum estimate is based on only the recovered ACEX sediments as age control and an associated accumulation rate of 2.43 cm/kyr, in which case still a substantial amount of $9.0\ 10^{17}$ gC stored is computed. Storage of $3.5\ 10^{18}$ g carbon roughly corresponds to a 195 - 470 ppm and $9.0\ 10^{17}$ gC to a 55 - 120 ppm CO_2 drawdown. It has been estimated that the growth of *Azolla* itself contributed at least 40% to this carbon drawdown via net carbon fixation and subsequent sequestration.

Acknowledgements
This research used samples and data provided by the Integrated Ocean Drilling Program (IODP). Funding for this research was provided by the DARWIN centre for Biogeology. Authors would like to thank StatoilHydro for general support and additional samples from exploration wells. We would also like to thank Gijs Nobbe and Rinske Knoop for technical laboratory assistance.

References

Abruzzese, M. J., Waldbauer, J. R., Chamberlain, C. P., 2005. Oxygen and hydrogen isotope ratios in freshwater chert as indicators of ancient climate and hydrologic regime. Geochim. Cosmochim. Acta 69(6), 1377-1390.

Agnini, C., Muttoni, G., Kent, D.V., Rio, D., 2006. Eocene biostratigraphy and magnetic stratigraphy from Possagno, Italy: The calcareous nannofossil response to climate variability. EPSL 241, 815–830.

Akhmetiev, M.A., 2007. Paleocene and Eocene Floras of Russia and Adjacent Regions: Climatic Conditions of Their Development Paleontological Journal 41(11), 1032–1039 ISSN 0031-0301, © Pleiades Publishing, Ltd.

Akhmetiev, M., 2009. Paleocene and Eocene floristic and climatic change in Russia and Northern Kazakhstan. Bulletin of Geosciences 85 (1), 17-34. doi 10.3140/bull.geosci.1145.

Allen, S.G., Idso, S.B., Kimball, B.A., Anderson, M.G., 1988. Interactive effects of CO_2 and environment on photosynthesis of *Azolla*. Agricultural and Forest Meteorology 42, 209-217.

Altabet, M.A., Francois, R., 1994. Sedimentary nitrogen isotopic ratio as a recorder for surface ocean nitrate utilization. Global Biogeochemical Cycles 8, 103–116.

Andreasson, F. P., Schmitz, B., 2000. Temperature seasonality in the early middle Eocene North Atlantic region: evidence from stable isotope profiles of marine gastropod shells. GSA Bull. 112(4), 628-640.

Archer, D., 2005. The fate of fossil fuel in geologic time. Journal of Geophysical Research 110, C09S05.

Arnosti, C., Jørgensen, B.B., 2006. Organic carbon degradation in arctic marine sediments, Svalbard: A comparison of initial and terminal steps. Geomicrobiol. J. 23, 551-563.

Arthur, M.A., Dean,W.E., Pratt, L.M., 1988. Geochemical and climatic effects of increased marine organic-carbon burial at the Cenomanian Turonian boundary. Nature 335, 714–717.

Backman, J., Moran, K., McInroy, D.B., Mayer, L.A., The Expedition 302 Scientists,2006. In: Proceedings of the Integrated Ocean Drilling Program 302. ManagementInternational, Inc., Edinburgh. doi:10.2204/iodp.proc.302.2006.

Backman, J., Jakobsson, M., Frank, M., Sangiorgi, F., Brinkhuis, H., Stickley, C., O'Regan, M., Løvlie, R., Pälike, H., Spofforth, D., Gattacecca, J., Moran, K., King, J., Heil, C., 2008. Age model and core-seismic integration for the Cenozoic Arctic Coring Expedition sediments from the Lomonosov Ridge. Paleoceanography 23, PA1S03.

Barke, J., Abels, H.A., Sangiorgi, F., Greenwood, D.R., Sweet, A.R., Donders, T., Lotter, A.F., Reichart, G.J., Brinkhuis, H. Orbitally-forced *Azolla* blooms and middle Eocene Arctic hydrology; clues from palynology. Geology, under review.

Barron, E. J., Fawcett, P.J., Peterson, W.H., Pollard, D., Thompson, S.L., 1995. A "simulation" of mid-Cretaceous climate. Paleoceanography 10, 953.

Basinger, J. F., 1991. The fossil forests of the Buchanan Lake Formation (Early Tertiary), Axel Heiberg Island, Canadian Arctic Archipelago: preliminary floristics and paleoclimate. Geol. Surv. Can. Bull. 403, 39-65.

Basinger, J. F., Greenwood, D.R., Sweda, T., 1994. Early Tertiary vegetation of Arctic Canada and its relevance to paleoclimatic interpretation, in: Boulter, M. C (Ed.) Arctic plants and climates: 65 million years of change, Berlin, Springer-Verlag.

Bauersachs, T., Hopmans, E.C., Compaoré, J., Stal, L.J., Schouten, S., Sinninghe Damsté, J.S., 2009a. Rapid analysis of long-chain glycolipids in heterocystous cyanobacteria using highperformance liquid chromatography coupled to electrospray ionization tandem mass spectrometry. Rapid Commun. Mass Spectrom. 23, 1387-1394.

Bauersachs, T., Schouten, S., Compaoré, J., Stal, L.J., Sinninghe Damsté, J.S., 2009b. Distribution of heterocyst glycolipids in cyanobacteria. Phytochem. 70, 1370-1376.

Berner, R.A., 1984. Sedimentary pyrite formation: An update. Geochimica and Cosmochimica Acta 48, 605-615.

Bjerrum, C.J., Bendtsen, J., Legarth, J.J.F., 2006. Modeling organic carbon burial during sea level rise with reference to the Cretaceous. Geochemistry, Geophysics, Geosystems 7(5), 1-24.

Bligh, E.G., Dyer, W.J., 1959. A rapid method for total lipid extraction and purification. Can. J. Biochem. Physiol. 37, 911-917.

Bonan, G., 1996. A land surface model (LSM version 1.0) for ecological, hydrological, and atmospheric studies: Technical description and user's guide. TN-417+STR, Natl. Cent. For Atmos. Res., Boulder, Colorado.

Bonan, G.B., Oleson, K.W., Vertenstein, M., Levis, S., Zeng X.B., Dai, Y.J., Dickinson, R.E., and Yang, Z.L., 2002. The land surface climatology of the community land model coupled to the NCAR community climate model. Journal of Climate 15, 3123 – 3149.

Braun-Howland, E.B., Nierzwicki-Bauer, S.A., 1990. *Azolla*-Anabaena azaollae symbiosis: biochemistry, ultrastructure and molecular biology. In: Handbook of symbiotic cyanobacteria (ed. Rai AN), 65-118. Boca Raton, FL, USA.

Brinkhuis H, Schouten, S., Collinson, M.E., Sluijs, A., Sinninghe Damsté, J.S., Dickens, G.R., Huber, M., Cronin, T.M., Onodera, J., Takahashi, K., Bujak, J.P., Stein, R., van der Burgh, J., Eldrett, J.S., Harding, I.C., Lotter, A.F., Sangiorgi, F.,van Konijnenburg-van Cittert, H., de Leeuw, J.W., Mathies-

sen, J., Backman, J., Moran, K., and the Expedition 302 Scientists, 2006. Episodic fresh surface Episodic fresh surface waters in the Eocene Arctic Ocean. Nature 441, 606–609.

Broecker, W.S., Peng, T-H., 1982. Tracers in the sea, Lamont-Doherty Geological Observatory, Palisades, New York, 690 pp.

Bruland, K. Trace elements in sea-water, in: Riley, J.P., Chester, R. (Eds.), Chemical Oceanography (Vol. 8), Academic Press, London, 1983, 157–220.

Brumsack, H.J., 2006. The trace metal content of recent organic carbon-rich sediments: Implications for Cretaceous black shale formation. Palaeogeography, Palaeoclimatology, Palaeoecology 232 (2-4), 344-361. doi:10.1016/j.palaeo.2005.05.011.

Buenning, N.H., and Noone, D., 2010. An evaluation of annual mean and seasonal timing of local and non-local processes controlling the isotopic composition of precipitation from observations and comprehensive models. in prep.

Buenning, N.H., Noone, D.C., Randerson, J., Riley, W.J., Still, C.J. White, J.W.C., 2010a. Correlations between the observed interannual variations in $d^{18}O$ of atmospheric CO_2 and hydrological changes. in prep.

Buenning, N.H., Noone, D.C., Randerson, J., Riley, W.J., Still, C.J., 2010b. Modelling the Response of the Terrestrial Biosphere and $d^{18}O$ of Atmospheric CO_2 to Changes in Atmospheric Conditions. in prep.

Bunn, S.E., Boon, P.I., 1993. What sources of organic carbon drive food webs inbillabongs: a study based on stable isotope analysis? Oecologia 96, 85–94.

Caballero, R., Langen, P.L., 2005. The dynamic range of poleward energy transport in an atmospheric general circulation model. Geophys. Res. Lett. 32, L02705, doi:10.1029/2004GL021581.

Canavan, R.W., Slomp, C.P., Jourabchi, P., Van Cappellen, P., Laverman, A.M., van den Berg, G.A., 2006. Organic matter mineralization in sediment of a coastal freshwater lake and response to salinization. Geochimica Cosmochimica Acta 70, 2836-2855.

Canuel, E.A., Martens, C.S., 1996. Reactivity of recently deposited organic matter:degradation of lipid compounds near the sediment-water interface. Geochimicaet Cosmochimica Acta 20, 1793–1806.

Capone, D.G., Burns, J.A., Montoya, J.P., Subramaniam, A., Mahaffey, C., Gunderson, T., Michaels, A.F., Carpenter, E.J., 2005. Nitrogen fixation by Trichodesmium spp.: An important source of new nitrogen to the tropical and subtropical North Atlantic Ocean. Global Biogeochem. Cy. 19: GB2024, doi:10.1029/2004GB002331.

Carpenter, E.J., Janson, S., 2001. Anabaena gerdii sp nov., a new planktonic filamentous cyanobacterium from the South Pacific Ocean and Arabian Sea. Phycologia 40: 105-110.

Cary, P.R., Weerts, P.G.J., 1992. Growth and nutrient composition of *Azolla pinnata* R. Brown and *Azolla* filiculoides Lamarck as affected by water temperature, nitrogen and phosphorus supply, light intensity and pH. Aquatic Botany 43, 163-180.

Chikaraishi, Y., Naraoka, H., 2003. Compound-specific dD-$d^{13}C$ analyses of n-alkanes extracted from terrestrial and aquatic plants. Phytochemistry 63(3), 361-371.

Chikaraishi, Y., Naraoka, H., Poulson, S.R., 2004. Carbon and hydrogen isotopic fractionation during lipid biosynthesis in a higher plant (Cryptomeria japonica). Phytochemistry 65, 323-330.

Church, M.J., Bjorkman, K.M., Karl, D.M., Saito, M.A., Zehr, J.P., 2008. Regional distributions of nitrogen-fixing bacteria in the Pacific Ocean. Limnol. Oceanogr. 53, 63-77.

Cline, J.D., Kaplan, I.R., 1975. Isotopic fractionation of dissolved nitrate during dentrification in the eastern tropical north pacific Ocean. Marine Chemistry 3, 271-299.

Collier, R.W., 1984. Particulate and dissolved vanadium in the North Pacific Ocean, Nature 309, 441–444.

Collins, W. D., Rasch, P.J., Boville, B.A., Hack, J.J., McCaa, J.R., Williamson, D.L., Briegleb, B., Bitz, C.M., Lin, S.J., Zhang, M.H., 2006. The formulation and atmospheric simulation of the Community Atmosphere Model version 3 (CAM3). J. Climate 19, 2144-2161.

Collinson, M.E., 2002. The Ecology of Cainozoic ferns. Review of Palaeobotany Palynology 119, 51-68.

Collinson, M.E., Barke, J., van der Burgh, J., van Konijnenburg-van Cittert, J.H.A., 2009. A new species of the freshwater fern *Azolla* (*Azolla*ceae) from the Eocene Arctic Ocean. Review of Palaeobotany and Palynology 155, 1–14.

Colodner, D., Edmond, J., Boyle, E. 1996. Rhenium in the Black Sea: comparison with molybdenum and uranium. EPSL 131, 1 – 15.

Craig, H., 1961. Isotopic variations in meteoric waters. Science 133, 1702-1703.

Craig, H., Gordon, L.I., 1965. Deuterium and oxygen 18 variations in the ocean and the marine atmosphere, in Stable Isotopes in Oceanographic Studies and Paleotemperatures, Tongiorgi, E. (Ed.), Lab. di Geol. Nucl., Pisa, Italy, pp. 9–130.

Crowley, T.J., Zachos, J.C., 2000. Comparison of zonal temperature profiles for past warm time periods, in Warm Climates in Earth History, Huber, B.T., MacLeod, K.G., Wing, S.L. (Eds.), Cambridge University Press.

Dansgaard, W., 1964. Stable isotopes in precipitation. Tellus 16, 436-468.

de Leeuw, J.W., Rijpstra, W.I.C., Schenk, P.A., 1981. The occurrence andidentification of C_{30}, C_{31} and C_{32} alkan-1,15-diols and alkan-15-one-1-ols inUnit I and Unit II Black Sea sediments. Geochimica et Cosmochimica Acta 45,2281–2285.

Deutsch, C., Sarmiento, J.L., Sigman, D.M., Gruber, N., Dunne, J.P., 2007. Spatial coupling of nitrogen inputs and losses in the ocean. Nature 445, 163-167.

Dongmann, G., Nürnberg, H. W., Förstel, H., Wagener, K., 1974. On the enrichment of $H_2{}^{18}O$ in the leaves of transpiring plants, Radiat. Environ. Biophys. 11, 41-52.

Eglinton, G., Hamilton, R.J., 1967. Leaf Epicuticular Waxes. Science 156 (3780) 1322 - 1335 doi: 10.1126/science.156.3780.1322.

Eldrett, J.S., Harding, I.C., Firth, J.V., Roberts, A.P., 2004. Magnetostratigraphic calibration of Eocene-Oligocene dinoflagellate cyst biostratigraphy from the Norwegian-Greenland Sea. Marine Geology 204, 91-127.

Eldrett, J.S., Greenwood, D.R., Harding, I.C., Huber, M., 2009. Increased seasonality through the Eocene to Oligocene transition in Northern high latitudes. Nature 459, 969- 974, doi:10.1038.

Elovson, J., 1974. Biosynthesis of chlorosulfolipids in *Ochromonas danica*, origin of primary and secondary hydroxyl groups determined by ^{18}O incorporation in vivo. Biochemistry 13, 2105–2109.

Emanuel, K., 2001. Contribution of tropical cyclones to meridional heat transport by the oceans. Journal of Geophysical research 106 (D14), 14771-147781.

Epstein, S., Yapp, C.J., Hall, J.H., 1976. Determination of the D-H ratio of non-exchangeable hydrogen in cellulose extracted from aquatic and land plants. Earth Planet. Sci. Lett. 30 (2), 241-251.

Federer, B., Brichet, N., and Jouzel, J., 1982. Stable isotopes in hailstones, I, the isotopic cloud model. J. Atmos. Sci. 39, 1323-1336.

Feng, X.H., Epstein, S., 1995. Climatic temperature records in dD data from tree-rings. Geochim. Cosmochim. Acta 59 (14), 3029–3037.

Ferreira, A.M., Miranda, A., Caetano, M., Baas, M., Vale, C., Sinninghe Damsté, J.S.,2001. Formation of mid-chain alkane keto-ols by post-depositional oxidation ofmid-chain diols in Mediterranean sapropels. Organic Geochemistry 32, 271–276.

Flanagan, L. B., Comstock, J.P., Ehleringer, J.R., 1991. Comparison of modeled and observed environmental influences on stable oxygen and hydrogen isotope composition of leaf water in Phaseolus-vulgaris L. Plant Physiol. 96, 439-443.

Franich, R.A., Gowar, A.P., Volkman, J.K., 1979. Secondary diols of Pinus radiataneedle epicuticular wax. Phytochemistry 18, 1563–1564.

Frankenberg, C., Yoshimura, K., Warneke, T., Aben, I., Butz, A., Deutscher, N., Griffith, D., Hase, F., Notholt, J., Schneider, M., Schrijver, H., Röckmann, T., 2009. Dynamic processes governing lower-tropospheric HDO/H_2O ratios as observed from space and ground. Science 325, 1374.

Fricke, H.C., 2003. Investigation of early Eocene water-vapor transport and paleoelevation using oxygen isotope data from geographically widespread mammal remains. Geol. Soc. Am. Bull. 115, 1088 – 1096.

Gächter, R., Meyer, J.S., Mares, A., 1988. Contribution of bacteria to release and fixation of phosphorus in lake sediments. Limnology and Oceanography 33, 1542–1558.

Gambacorta, A., Pagnotta, E., Romano, I., Trincone, A., 1998. Heterocyst glycolipids from nitrogen-fixing cyanobacteria other than Nostocaceae. Phytochemistry 48, 801-805.

Gradstein, 2004. Luterbacher, H.P., Ali, J.R., Brinkhuis, H., Gradstein, F.M., Hooker, J.J., Monechi, S., Ogg, J.G., Powell, J., Röhl, U., Sanfilippo, A., Schmitz, B.. The paleogene period. In: A geologic time scale (eds. Gradstein, F.M., Ogg, J.G., Smith, A.G.). Cambridge University Press, UK, page 396.

Gelin, F., Boogers, I., Noordeloos, A.M.M., Sinninghe Damsté, J.S., Hatcher, P.G., deLeeuw, J.W., 1996. Novel, resistant microalgal polyethers: an important sink oforganic carbon in the marine environment? Geochimica et Cosmochimica Acta60, 1275–1280.

Gelin, F., Volkman, J.K., de Leeuw, J.W., Sinninghe Damsté, J.S., 1997. Mid-chainhydroxy long-chain fatty acids in microalgae from the genus Nannochloropsis.Phytochemistry 45, 641–646.

Gleason, J. D., Thomas, D.J., Moore Jr., T.C., Blum, J.D., Owen, R.M., Haley, B.A., 2009. Early to middle Eocene history of the Arctic Ocean from Nd-Sr isotopes in fossil fish debris, Lomonosov Ridge. Paleoceanography 24, PA2215. doi:10.029/2008PA001685.

Glebovsky, V.Y., Kaminsky, V.D., Minakov, A.N., Merkuriev, S.A., Childers, V.A., Brozena, J.M., 2006. Formation of the Eurasia Basin in the Arctic Ocean as inferred from geohistorical analysis of the anomalous magnetic field. Geotectonics 40 (4), 263–281.

Goossens, H., de Leeuw, J.W., Rijpstra, W.I.C., Meyenburg, G.J., Schenck, P.A., 1986.Lipids and their mode of occurrence in bacteria and sediments-I. Amethodological study of the lipid composition of Acinetobacter calcoaceticusLMD 79-41. Organic Geochemistry 14, 15–25.

Gradstein, F.M., 2004. Luterbacher, H.P., Ali, J.R., Brinkhuis, H., Gradstein, F.M., Hooker, J.J., Monechi, S., Ogg, J.G., Powell, J., Röhl, U., Sanfilippo, A., Schmitz, B. The paleogene period. In: A geologic time scale (eds. Gradstein FM, Ogg, JG, Smith AG). Cambridge University Press, UK, page 396.

Greenwood, D.R., Wing, S.L., 1995. Eocene continental climates and latitudinal temperature gradients. Geology 23, 1044-1048.

Greenwood, D.R., Archibald, S.B., Mathewes, R.W., Moss, P.T., 2005. Fossil biotas from the Okanagan Highlands, southern British Columbia and northeastern Washington State: climates and ecosystems across an Eocene landscape. Can. J. Earth Sci. 42, 167–185. doi: 10.1139/E04-100.

Haq, B.U., Hardenbol, J., Vail, P.R., 1987. Chronology of Fluctuating Sea Levels since the Triassic Science, New Series 235(4793), 1156-1167.

Harvey, H.R., Fallon, R.D., Patton, J.S., 1986. The effect of organic matter and oxygen on the degradation of bacterial membrane lipids in marine sediments. Geochim. Cosmochim. Acta 50, 795-804.

Hayes, J.M., 1993. Factors controlling ^{13}C contents of sedimentary organiccompounds: Principles and evidence. Marine Geology 113, 111-125.

Hayes, J.M., Strauss, H., Kaufman, A.J., 1999. The abundance of ^{13}C in marine organic matter and isotopic fractionation in the global biogeochemical cycle of carbon during the past 800 Ma. Chemical Geology 161, 103-125.

Hayes, J.M., 2001. Fractionation of carbon and hydrogen isotopes in biosynthetic processes. Stable isotope geochemistry 43, 225-277.

Heilmann-Clausen, C., Nielsen, O.B., Gersner, F. 1985. Lithostratigraphy and depositional environments in the Upper Paleocene and Eocene of Denmark. Bulletin of the Geological Society of Denmark 33, 287-323.

Hoffmann, L., 1999. Marine cyanobacteria in tropical regions: diversity and ecology. Eur. J. Phycol. 34, 371-379.

Holloway, P.J., Brown, G.A., 1977. The ketol constituents of Brassica epicuticularwaxes. Chemistry and Physics of Lipids 19, 1–13.

Huber, M., Sloan, L.C., 2000. Climatic responses to tropical sea surface temperature changes on a "greenhouse" earth. Paleoceanography 15 (4), 443-450.

Huber, M., Caballero, R. ,2003. Eocene El Nino: Evidence for robust tropical dynamics in the "hothouse". Science 299, 877 -881.

Huber, M., Sloan, L. Shellito, C.J., 2003. Early Paleogene oceans and climate: a fully coupled modeling approach using the NCAR CCSM. In, Causes and Consequences of Globally Warm Climates in the Early Paleogene, Special Paper-Geological Society of America, Wing, S.L., Gingerich, P.D., Schmitz, B., Thomas, E. (Eds.). Geological Society of America, Boulder, Colorado, pp. 25– 47.

Huber, M., Nof, D., 2006. The ocean circulation in the southern hemisphere and its climatic impacts in the Eocene. Palaeogeogr, palaeoclimatol, palaeoecol 231, 9-28.

IAEA/WMO, 2006. Global Network of Isotopes in Precipitation. The GNIP Database. Accessible at: http://isohis.iaea.org.

Idso, S.B., Allen, S.G., Anderson, M.G., Kimball, B.A., 1989. Atmospheric CO_2 enrichment enhances survival of *Azolla* at high temperatures. Environmental and Experimental Botany 29, 337-341.

Ingraham, N.L., 1998. Isotopic variation in precipitation, in Isotope Tracers in Catchment Hydrology, Kendall, C., McDonnell, J.J. (Eds.). Elsevier, New York, pp. 87– 118.

IPCC, 2007. Climate Change 2007: Synthesis report. Contribution of working groups I, II and III to the fourth Assessment Report of the Intergovernmental Panel on Climate Change. Tech. Rep.

Jacobs, B.F., Herendeen, P.S., 2004. Eocene dry climate and woodland vegetation in tropical Africa reconstructed from fossil leaves in northern Tanzania. Paleogeog., Paleoclim., Paleoecol. 213, 115-123.

Jahren, A.H., Sternberg, L.S.L., 2003. Humidity estimate for the middle Eocene Arctic rain forest. Geology 31 (5), 463– 466.

Jahren A.H., Byrne, M.C.,Graham, H.V., Sternberg, L.S.L., Summons, R.E., 2009. The environmental water of the middle Eocene Arctic: Evidence from δD, $\delta^{18}O$ and $\delta^{13}C$ within specific compounds. Palaeogeogr., Palaeoclimatol., Palaeoecol. 271, 96-103.

Jahren, A.H., Byrne, M.C.,Graham, H.V., Sternberg, L.S.L., Summons, R.E., 2009. The environmental water of the middle Eocene Arctic: Evidence from δD, $\delta^{18}O$ and $\delta^{13}C$ within specific compounds. Palaeogeogr., Palaeoclimatol., Palaeoecol. 271, 96-103.

Jakobsson, M., Backman, J., Rudels, B., Nycander, J., Frank, M., Mayer, M., Jokat, W., Sangiorgi, F., O'Regan, M., Brinkhuis, H., King, J., Moran, K., 2007. The early Miocene onset of a ventilated circulation regime in the Arctic Ocean. Nature 447, 986– 990.

Janes, R., 1998. Growth and survival of *Azolla* filiculoides in Britain, II Sexual reproduction. New Phytologist 138,377-384.

Jetter, R., 2000. Long-chain alkanediols from Myricaria germanica cuticular leafwaxes. Phytochemistry 55, 169–176.

Jetter, R., Riederer, M., 1996. Cuticular waxes from the leaves and fruit capsules ofeight Papaveraceae species. Canadian Journal of Botany 74, 419–430.

Jetter, R., Riederer, M., 1999. Long-chain alkanediols, ketoaldehydes, ketoalcoholsand ketoalkyl esters in the cuticular waxes of Osmunda regalis fronds. Phytochemistry 52, 907–915.

Jetter, R., Riederer, M., Seyer, A., Mioskowski, C., 1996. Homologous long-chainalkane diols from Papaver leaf cuticular waxes. Phytochemistry 42, 1617–1620.

Joussaume, S., Sadourny, R., Jouzel, J., 1984. A general circulation model of water isotope cycles in the atmosphere. Nature 311, 24–29.

Jouzel, J., Koster, R.D., Suozzo, R.J., Russell, G.L., White, J.W.C., Broecker, W.S., 1987. Simulation of the HDO and H2 ^{18}O atmospheric cycles using the NASA GISS general circulation model: The seasonal cycle for present-day conditions. J. Geophys. Res. 92(14), 739–14,760.

Jouzel, J., Barkov, N.I., Barnola, J.M., Bender, M., Chappellaz, J., Genthon, C., Kotlyakov, V.M., Lipenkov, V., Lorius, C., Petit, J.R., Raynaud, D., Raisbeck, G., Ritz, C., Sowers, T., Stievenard, M., Yiou, F., Yiou, P., 1993. Extending the Vostok ice-core record of palaeoclimate to the penultimate glacial period. Nature 364, 407-12.

Jouzel, J., C. Waelbroeck, B. Malaize, M. Bender, J.R. Petit, M. Stievenard, N.I. Barkov, J.M. Barnola, T. King, V.M. Kotlyakov, V. Lipenkov, C. Lorius, D. Raynaud, C. Ritz, and T. Sowers., 1996. Climatic interpretation of the recently extended Vostok ice records. Clim. Dyn. 12, 513-521.

Jouzel, J., Hoffmann, G., Koster, R.D., Masson, V., 2000. Water isotopes in precipitation: data/model comparison for present-day and past climates. Quaternary Science Reviews 19, 363 - 379.

Kaplan, D., Peters, G.A., 1988. Interaction of carbon metabolism in the *Azolla*–Anabaena symbiosis. Symbiosis 6, 53–68.

Kemp, A.E.S., Pearce, R.B., Koizumi, I., Pike, J., Rance, S.J., 1999. The role of mat-forming diatoms in the formation of Mediterranean sapropels. Nature 398, 57-61.

Kingston, H.M., Haswell, S.J., 1997. Microwave Enhanced Chemistry: Fundamentals, sample Preparation and Applications. American Chemical Society, Washington DC, USA.

Knies, J., Mann, U., 2002. Depositional environment and source rock potential of Miocene strata from the central Fram Strait: Introduction of a new computing tool for simulating organic facies variations. Marine Petroleum Geology 19, 811– 828.

Knies, J., Mann, U., Popp, B.N., Stein, R., Brumsack, H.J., 2008. Surface water productivity and paleoceanographic implications in the Cenozoic Arctic ocean. Paleoceanography 23, PA1S16.

Koizumi, H., Kibe, T., Mariko, S., Ohtsuka, T., Nakadai, T., Mo, W., Toda, H., Seiichi, N., Kobayashi, K. 2001. Effects of free-air CO_2 enrichment (FACE) on CO_2 exchange at the flood-water surface in a rice paddy field. New Phytologist 150, 231-239.

Korty, R.L., Emanuel, K.A., Scott, J., 2008. Tropical cyclone-induced upper ocean mixing and climate: application to equable climates. Journal of Climate 21, 638 - .654. doi: 10.1175/2007JCLI1659.1

Kraal, P., Slomp, C.P., Forster, A., Kuypers, M.M.M., Sluijs, A., 2009. Pyrite oxidation during sample storage determines phosphorus fractionation in carbonate-poor anoxic sediments. Geochimica et Cosmochimica Acta 73. 3277 – 3290.

Krylov, A.A., Andreeva, I.A., Vogt, C., Backman, J., Krupskaya, V.V., Grikurov, G.E., Moran, K., Shoji, H., 2008. A shift in heavy and clay mineral provenance indicates a middle Miocene onset of a perennial sea ice cover in the Arctic Ocean. Paleoceanography 23. PA1S06, doi:10.1029/2007PA001497.

Kurtz, A.C., Kump, L.R., Arthur, M.A., Zachos, J.C., Paytan, A., 2003. Early Cenozoic decoupling of the global carbon and sulfur cycles. Paleoceanography 18 (4).

Kuypers, M.M.M., Sliekers, A.O., Lavik, G., Schmid, M., Jorgensen, B.B., Kuenen, J.G., Sinninghe Damsté, J.S., Strous, M., Jetten, M.S.M., 2003. Anaerobic ammonium oxidation by annamox bacteria in the Black Sea. Nature 422, 608-611.

Kuypers, M.M.M., van Breugel, Y., Schouten, S., Erba, E., Sinninghe Damsté, J.S., 2004. N_2-fixing cyanobacteria supplied nutrient N for Cretaceous oceanic anoxic events. Geology 32, 853-856.

Lammers, B., Shiklomanov, A.I., Vørøsmarty, C.J., Fekete, B.M., Peterson, B.J. 2001. Assessment of contemporary Arctic river runoff based on observational discharge records. Journal of Geophysical Research 106 (D4), 3321-3334.

Lawrence, J.R., Gedzelman, S.D., Dexheimer, D., Cho, H.-K., Carrie, G.D., Gasparini, R., Anderson, C.R., Bowman, K.P., Biggerstaff, M.I., 2004. Stable isotopic composition of water vapor in the tropics. J. Geophys. Res. 104, D06115.

Lawrence, J. R., Gedzelman, S.D., 1996. Low stable isotope ratios of tropical cyclone rains, Geophys. Res. Lett., 23, 527– 530.

Leaney, F.W., Osmond, C.B., Allison, G.B., Ziegler, H., 1985. Hydrogen-isotope composition of leaf water in C-3 and C-4 plants – its relationship to the hydrogen isotope composition of dry-matter. Planta 164(2), 215-220.

Lee, J-E, Fung, I., DePaolo, D.J., Henning, C.C., 2007. Analysis of the global distribution of water isotopes using the NCAR atmospheric general circulation model. J. Geophys. Res. 112, D16306, doi:10.1029/2006JD007657.

Lipp, J.S., Morono, Y., Inagaki, F., Hinrichs, K-U., 2008. Significant contribution of Archaea to extant biomass in marine subsurface sediments. Nature 454, 991-994.

Liu W., Yang, H., Liwu, L., 2006. Hydrogen isotopic composition of n-alkanes from terrestrial plants correlate with their ecological life forms. Oceologia. 150, 330-338.

Mangini, A., Eisenhauer, A., Walter, P., 1990. Response of manganese in the ocean to the climatic cycles in the Quaternary. Paleoceanography 5(5), 811-821. doi:10.1029/PA005i005p00811.

Manabe, S., 1997. Early development in the study of greenhouse warming: The emergence of climate models. Ambio 26(1), 47– 51.

Manum, S.B., Boulter, M.C., Gunnarsdottir, H., Rangnes, K., Scholze, A., 1989. Eocene to Miocene palynology of the Norwegian Sea (ODP Leg 104). In: Proceedings of Ocean Drilling Program, Scientific Results 104 (eds: Eldholm O, Thiede J, Taylor E et al.) College Station, TX, 611–662.

Marschner, H., 1995. Mineral Nutrition of Higher Plants (2nd edn.). Academic Press, London.

Markwick, P. J., 1994. "Equability", continentality, and Tertiary "climate": The crocodilian perspective. Geology 22, 613–616.

Martin, J.M., Whitfield, M. The significance of the river input of chemical elements to the ocean, in: Wong, C.S., Boyle, E., Bruland, K.W., Burton, J.D., Goldberg, E.D. (Eds.), Trace Metals in Sea Water, Plenum Press, New York, 1983, pp. 265–296.

Martinez, N.C., Murray, R.W., Dickens, GR., Kölling, M., 2009. Discrimination ofsources of terrigenous sediment deposited in the Central Arctic Ocean during the Cenozoic, Paleoceanography, 24, PA1210, doi:10.1029/2007PA001567.

März, C., Schnetger, B., Brumsack, H.J., 2010. Paleoenvironmental implications of Cenozoic sediments from the Central Arctic Ocean (IODP Expedition 302) using inorganic geochemistry. Paleoceanography, 25, PA3206, doi:10.1029/2009PA001860.

Masson-Delmotte, V., Shugui, H., Ekaykin, A., Jouzel, J., Aristarain, A., Bernardo, R.T., Bromwhich, D., Cattani, O., Delmotte, M., Falourd, S., Frezzotti, M., Galle, H., Genoni, L., Landais, A., Helsen, M., Hoffmann, G., Lopez, J., Morgan, V., Motoyama, H., Noone, D., Oerter, H., Petit, J.R., Royer, A., Ruemura, R., Schmidt, G., Schosser, E., Simaes, J., Steig, E., Stenni, B., Stievenard, M., Vimeux, F., White, J.W.C., 2008. A review of Antarctic surface snow isotopic composition: observations, atmospheric circulation and isotopic modelling. J. Climate 21(13), 3359-3387.

Meeks, J.C., Elhai, J., 2002. Regulation of cellular differentiation in filamentouscyanobacteria in free-living and plant-associated symbiotic growth states. Microbiology and molecular biology reviews 66, 94–121.

Merlivat, L., Jouzel, J., 1979. Global climatic interpretation of the Deuterium-Oxygen 18 relationship for precipitation. Journal Geophysical Research 84, 5029–5033.

Meybeck, M., 1982. Carbon, nitrogen and phosphorus transport by world rivers. Amer. J. Sci. 282, 282-450.

Miller, K.G., Kominz, M.A., Browning, J.V., Wright, J.D., Mountain, G.S., Katz, M.E., Sugarman, P.J., Cramer, B.S., Christie-Blick, N., Pekar, S.F., 2005. The Phanerozoic record of global sea-level change. Science 310, 1293 – 1298.

Minagawa, M., Wada, E., 1986. Nitrogen isotope ratios of red tide organisms in the East China Sea: a characterization of biological nitrogen fixation. Marine Chemistry 19, 245–259.

Montoya, J.P., Holl, C.M., Zehr, J.P., Hansen, A., Villareal, T.A., Capone, D.G., 2004. High rates of N_2 fixation by unicellular diazotrophs in the oligotrophic Pacific Ocean. Nature 430, 1027-1031.

Moore, A.J.W., 1969. *Azolla*: biology and its agronomic significance. BotanicalReview 35, 17–34.

Moran, K., Backman, J., Brinkhuis, H., Clemens, S.C., Cronin, T., Dickens, G.R., Eynaud, F., Gattacceca, J., Jakobsson, M., Jordan, R.W., Kaminski, M., King, J., Koc, N., Krylov, A., Martinez, N., Matthiessen, J., McInroy, D., Moore, T.C., Onodera, J., O'Regan, M., Pälike, H., Rea, B., Rio, D., Sakamoto, T., Smith, D.C., Stein, R., St John, K., Suto, I., Suzuki, N., Takahashi, K., Watanabe, M., Yamamoto, M., Farrell, J., Frank, M., Kubik, P., Jokat, W., Kristoffersen, Y., 2006. The Cenozoic palaeoenvironment of the Arctic Ocean. Nature 441, 601– 605.

Moretti, A., Siniscalco Gigliano, G. 1988. Influence of light and pH on growth and nitrogenase activity on temperate-grown *Azolla*. Biology and Fertility of soils 6, 131-136.

Mulch, A., Graham, S.A., Chamberlain, C.P. 2006. Hydrogen isotopes in Eocene river gravels and Paleoelevation of the Sierra Nevada. Science 313, 87–89.

Mulch, A., Teyssier, C. Cosca, M.A., Chamberlain, C.P., 2007. Stable isotope palaeoaltimetry of Eocene core complexes in the North American Cordillera. Tectonics 26, TC4001.

Nemani, R.R., Keeling, C.D., Hashimoto, H., Jolly, W.M., Piper, S.C., Tucker, C.J., Myneni, R.B., Running, S.W., 2003. Climate-Driven Increases in Global Terrestrial Net Primary Production from 1982 to 1999. Science 300, 1560-1563.

Nijenhuis, I.A., Bosch, H.J., Sinninghe Damsté, J.S., Brumsack, H.J., de Lange, G.J., 1999. Organic matter and trace element rich sapropels and black shales: a geochemical comparison. EPSL 169, 277 – 290.

Noone, D., Simmonds, I., 2002. Associations between delta O-18 of water and climate parameters in a simulation of atmospheric circulation for 1979-95. J. Climate 15, 3150-3169.

Noone, D., Still, C., Riley, W., 2002. A global biophysical model of ^{18}O in terrestrial water and CO_2 fluxes. Research Activities in Atmospheric and Oceanic Modeling, Report No. 32, H. Ritchie, Ed., World Meteorological Organization 4.19-4.20.

Noone, D., 2003. Water isotopes in CCSM for studying water cycles in the climate system. 8th Annual CCSM workshop, Breckenridge, Colorado, June 2003.

Noone, D., Simmonds, I., 2004. The sea ice control on water isotope transport to Antarctica and implications for ice core interpretation. J. Geophys. Res. 109, D07105, doi:10.1029/2003JD004228.

Noone, D., 2006. Isotopic composition of water vapor modeled by constraining global climate simulations with reanalyses. Research Activities in Atmospheric and Oceanic Modelling, J. Cote (Ed.), 35, 2-37 pp.

Noone, D., 2008. The influence of midlatitude and tropical overturning circulation on the isotopic composition of atmospheric water vapor and Antarctic precipitation. J. Geophys. Res. 113, D04102, doi:10.1029/2007JD008892.

Noone, D., 2009. A kink in the thermometer. Nature 462, 295-296.

Noone, D., Sturm, C., 2010. Comprehensive dynamical models of global and regional water isotope distributions. In: West, J., Bowen, G., Dawson, T, Tu, K. (eds.) Isoscapes: Understanding movement, patterns, and process on Earth through isotope mapping. Springer, 477, pp. 195 -219.

Norris, R.D., Jones, L.S., Corfield, R.M., Cartlidge, J.E., 1996. Skiing in the Eocene Uinta mountains? Isotopic evidence in the Green river formation for snow melt and large mountains. Geology 24, 403-406.

Oleson, K.W., Dai, Y., Bonan, G., Bosilovich, M., Dickinson, R., Dirmeyer, P., Hoffman, F., Houser, P., Levis, S., Niu, G.Y., Thornton, P., Vertenstein, M., Yang, Z.L., and Zeng, X, 2004. Technical Description of the Community Land Model (CLM), Technical Note NCAR/TN-461+STR, 186pp, National Center for Atmospheric Research.

Onodera, J., Takahashi, K., Jordan, R.W., 2008. Eocene silicoflagellate and ebridian paleoceanography in the central Arctic Ocean, Paleoceanography, 23, PA1S15, doi:10.1029/2007PA001474.

Pagani, M., Zachos, J.C., Freeman, K.H., Tipple, B., Bohaty, S., 2005. Marked decline in atmospheric carbon dioxide concentrations during the Paleogene. Science 309, 600-603.

Pagani, M., Pedentchouk, N., Huber, M., Sluijs, A., Schouten, S., Brinkhuis, H.,Sinninghe Damsté, J.S., Dickens, G.R.Expedition 302 Scientists, 2006. Arctichydrology during global warming at the Palaeocene/Eocene thermal maximum. Nature 442, 671–675.

Paillard, D., L., L.,Yiou, P., 1996. Macintosh program performs time-series analysis: Eos, Transactions, American Geophysical Union, 77, 379.

Passier, H.F., Böttcher, M.E. and De Lange, G.J., 1998. Sulphur Enrichment in Organic Matter of Eastern Mediterranean Sapropels: A Study of Sulphur Isotope Partitioning, Aquatic Geochemistry, 5, 99-118.

Pearson, P.N., Palmer, M.R., 2000. Atmospheric carbon dioxide concentrations over the past 60 million years. Nature 406, 695-699.

Pearson, P.N., Ditchfield, P.W., Singano, J., Harcourt-Brown, K.G., Nicholas, C.J., Olsson, R.K., Shackleton, N.J., Hall, M.A., 2001. Warm tropical sea surface temperatures in the Late Cretaceous and Eocene epochs. Nature 413, 481-487.

Pearson, P. N., van Dongen, B.E., Nicholas, C.J., Pancost, R.D., Schouten, S., Singano, J.M., Wade, B.S., 2007. Stable warm tropical climate through the Eocene Epoch. Geology 35(3), 211-214.

Pearson, A., 2008. Biogeochemistry - Who lives in the sea floor? Nature 454, 952-953.

Peters, G.A., Toia Jr., R.E., Evans, W.R., Crist, D.K., Mayne, B.C., Poole, R.E., 1980.Characterization and comparisons of five N_2 – fixing *Azolla*–Anabaenaassociations. I. Optimization of growth conditions for biomass increase and Ncontent in a controlled environment. Plant, Cell and Environment 3, 261–269.

Peters, G.A., Meeks, J.C., 1989. The *Azolla*–Anabaena symbiosis: basic biology. AnnualReview of Plant Physiology and Plant Molecular Biology 40, 193–210.

Peters, K.E., Walters, C.C., Moldowan, M., 2005. The biomarker guide: Biomarkers and isotopes in the environment and human history. 2nd ed. Cambridge University Press.

Petit, J.R., J. Jouzel, D. Raynaud, N.I. Barkov, J.-M. Barnola, I. Basile, M. Bender, J. Chappellaz, M. Davis, G. Delayque, M. Delmotte, V.M. Kotlyakov, M. Legrand, V.Y. Lipenkov, C. Lorius, L. Pépin, C. Ritz, E. Saltzman, and M. Stievenard, 1999. Climate and atmospheric history of the past 420,000 years from the Vostok ice core, Antarctica. Nature 399, 429-436.

Ploug, H., 2008. Cyanobacterial surface blooms formed by Aphanizomenon sp and Nodularia spumigena in the Baltic Sea: Small-scale fluxes, pH, and oxygen microenvironments. Limnol. Oceanogr. 53, 914-921.

Powers, L.A., Werne, J.P., Johnson, T.C., Hopmans, E.C., Sinninghe Damsté, J.S., Schouten, S., 2004. Crenarchaeotal membrane lipids in lake sediments: A new Paleotemperature proxy for continental paleoclimate reconstruction? Geology 32, 613–-616.

R Development Core Team, 2010. R: A language and environment for statistical computing. R Foundation for Statistical Computing, Vienna, Austria. ISBN 3-900051-07-0, URL http://www.R-project.org.

Rai, A.N., Söderback, E., Bergman, B., 2000. Tansley review No. 116. Cyanobacterium-plant symbiosis. New Phytologist 147, 449–481.

Rai, V., Tiwari, S.P., Rai, A.K., 2001. Effects of NaCl on nitrogen fixation of unadapted and NaCl adapted *Azolla* pinnata-Anabaena azollae. Aquatic Botany 71, 109-117.

Rampen, S.W., Schouten, S., Wakeham, S.G., Sinninghe Damsté, J.S., 2007. Seasonaland spatial variation in the sources and fluxes of long chain diols and mid-chainhydroxy methyl alkanoates in the Arabian Sea. Organic Geochemistry 38, 165–179.

Rau, G.H., Arthur, M.A., Dean, W.A., 1987. $^{15}N/^{14}N$ variations in Cretaceous Atlantic sedimentary sequences: implications for past changes in marine nitrogen biogeochemistry. Earth Planet. Sci. Lett. 82, 269-279.

Reichart, G.J., den Dulk, M., Visser, H.J., van der Weijden, C.H., Zachariasse, W.J., 1997. A 225 kyr record of dust supply, paleoproductivity and the oxygen minimum zone from the Murray Ridge (northern Arabian Sea). Palaeogeography, Palaeoclimatology, Palaeoecology, 134, 149-169.

Reuveni, J., Gale, J., Zeroni, M. 1997. Differentiating day from night effects of high ambient CO_2 on the gas exchange and growth of Xanthium strumarium L exposed to salinity stress. Annual Botany 9, 191–196.

Revelle, R., Suess, H.E., 1957. Carbon dioxide exchange between atmosphere and ocean and the question of an increase of atmospheric CO_2 during the past decades. Tellus 9, 18-27.

Riederer, M., 1989. The cuticles of conifers: structure, composition and transportproperties. Ecological Studies 77, 157–192.

Riley, W.J., Still, C.J., Torn, M., and Berry, J.A., 2002. A mechanistic model of $H_2{}^{18}O$ and $CO^{18}O$ fluxes between ecosystems and atmosphere: model description and sensitivity analyses. Glob. Biogeochem. Cycles 16, 1095-1108.

Rind, D., 1998. Latitudinal temperature gradients and climate change. Journal of geophysical research 103(D6), 5943-5971.

Rippka, R., Deruelles, J., Waterbury, J.B., Herdman, M., Stanier, R.Y., 1979. Generic assignments, strain histories and properties of pure cultures of cyanobacteria. J. Gen. Microbiol. 111, 1-61.

Risi, C., Bony, S., Vimeux, F., 2008. Influence of convective processes on the isotopic composition ($\delta^{18}O$ and δD) of precipitation and water vapor in the tropics: 2. Physical interpretation of the amount effect. J. Geophys. Res. 113, D19306, doi:10.1029/2008JD009943.

Roberts, C.D., LeGrande, A.N., Tripati, A.K. 2009. Climate sensitivity to Arctic seaway restriction during the early Paleogene. EPSL 286, 576-585.

Rossignol-Strick, M., Nesteroff, W., Olive, P., Vergnaudgrazzini, C., 1982. After the deluge -Mediterranean stagnation and sapropel formation Nature 295, 105-110.

Royer, D.L., Wing, S.L., Beerling, D.J., Jolley, D.W., Koch, P.L., Hickey, L.J., Berner, R.A., 2001. Paleobotanical evidence for near present day levels of atmospheric CO_2 during part of the Tertiary. Science 292, 2310—2313.

Ruttenberg, K.C., 1992. Development of a sequential extraction method for different forms of phosphorus in marine sediments. Limnol. Oceanogr. 37, 1460-1482.

Rütters, H., Sass, H., Cypionka, H., Rullkötter, J., 2002. Phospholipid analysis as a tool to study complex microbial communities in marine sediments. J. Microbiol. Meth. 48, 149-160.

Sachs, J.P., Repeta, D.J., 1999. Oligotrophy and nitrogen fixation during eastern Mediterranean sapropel events. Science 286, 2485-2488.

Sachse, D., Radke, J., Gleixner, G., 2004. Hydrogen isotope ratios of lacustrine sedimentary n-alkanes record modern climate variability. Geochimica and Cosmochimica Acta 68 (23), 4877-4889. doi:10.1016/j.gca.2004.06.004

Sachse, D., Radke, J., Gleixner, G., 2006. dD values of individual n-alkanes from terrestrial plants along a climatic gradient – Implications for the sedimentary biomarker record. Org. Geochem. 37, 469-483.

Sah, R.N., Goyal, S.S., Rains, D.W., 1989. Interactive effects of exogenous combined nitrogen and phosphorus on growth and nitrogen fixation by *Azolla*. Plant and Soil 117, 1-8.

Sangiorgi, F., van Soelen, E.E., Spofforth, D.J.A., Pälike, H., Stickley, C.E., St. John ,K., Koç, N., Schouten, S., Sinninghe Damsté, J.S., Brinkhuis, H. 2008. Cyclicity in the middle Eocene central Arctic Ocean sediment record: Orbital forcing and environmental response. Paleoceanography 23, PA1S08.

Saunders, R.M.K., Fowler, K., 1993. The supraspecific taxonomy and evolution of the fern genus *Azolla* (*Azolla*ceae). Plant Systematics and Evolution 184, 175-193.

Sauer, P.E., Eglington, T.I., Hayes, J.M., Schimmelmann, A., Sessions, A.L., 2001. Compound-specific D/H ratios of lipid biomarkers from sediments as a proxy forenvironmental and climatic conditions. Geochimica et Cosmochimica Acta 65 (2), 213–222.

Schmidt, G.A., Bigg, G.R., Rohling, E.J., 1999. "Global Seawater Oxygen-18 Database". http://data.giss.nasa.gov/o18data/

Schenau, S. J., Reichart, G.J., de Lange, G.J., 2002. Oxygen minimum zone controlled Mn redistribution in Arabian Sea sediments during the late Quaternary. Paleoceanography 17(4), 1058. doi: 10.1029/2000PA000621.

Schmidt, G. A., Hoffmann, G., Shindell, D.T., Hu, Y., 2005. Modeling atmospheric stable water isotopes and the potential for constraining cloud processes and stratosphere-troposphere water exchange. J. Geophys. Res. 110, D21314, doi:10.1029/2005JD005790.

Schouten, S., Klein Breteler, W.C.M., Blokker, P., Schoot, N., Rijpstra, W.I.C., Grice, K.,Baas, M., Sinninghe Damsté, J.S., 1998. Biosynthetic effects on the stable carbonisotopic compositions of algal lipids: implications for deciphering the carbonisotopic biomarker record. Geochimica et Cosmochimica Acta 62, 1397–1406.

Schouten, S., Hopmans, E.C., Schefuß, E., Sinninghe Damsté, J.S., 2002. Distributional variations in marine crenarchaeotal membrane lipids: a new tool for reconstructing ancient sea water temperatures? Earth and Planetary Science Letters 204, 265-274.

Schouten, S., Hopmans, E.C., Forster, A., van Breugel, Y., Kuypers, M.M.M., Sinninghe Dampsté, J.S., 2003. Extremely high sea surface temperatures at low latitudes during the middle Cretaceous as revealed by archaeal membrane lipids. Geology 31, 1069–1072.

Schouten S., Middelburg J., Hopmans E.C., Sinninghe Damsté, J.S., 2010. Fossilization and degradation of intact polar lipids in deep subsurface sediments: A theoretical approach. Geochim. Cosmochim. Acta 74, 3806-3814.

Schubert, C.J., Calvert, S.E., Stein, R., 2001. Tracking nutrient and productivity variations over the last deglaciation in the Arctic Ocean. Paleoceanography 16, 199– 211.

Scotese, C.R., Gahagan, L.M., Larson, R.L., 1988. Plate tectonic reconstructions of the Cetaceous and Cenozoic ocean basins. Tectonophysics 155, 27-48.

Sessions, A.L., Burgoyne, T.W., Schimmelmann, A., Hayes, J.M., 1999. Fractionation of hydrogen isotopes in lipid biosynthesis. Organic Geochemistry 30 (9), 1193–1200.

Sewall, J.O., Sloan, L.C., Huber, M., Wing, S., 2000. Climate sensitivity to changes in land surface characteristics. Global and Planetary Change 26 (4), 445–465.

Shaw, T.J., Gieskes, J.M., Jahnke, R.A., 1990. Early diagenesis in differing depositional environments-the response of transition metals in pore water. Geochimica et Cosmochimica Acta 54, 1233 – 1246.

Shellito, C.J., Sloan, L.C., Huber, M., 2003. Climate model sensitivity to atmospheric CO_2 levels in the Early-Middle Paleogene. Palaeogeogr., Palaeoclim., Palaeoecol. 193 (1), 113–123.

Shiller, A.M., Boyle, E.A., 1987. Dissolved vanadium in rivers and estuaries, Earth Planet. Sci. Lett. 86, 214–224.

Sinninghe Damsté, J.S., Rijpstra, W.I.C., Reichart, G-J., 2002. The influence of oxicdegradation on the sedimentary biomarker record II. Evidence from Arabian Seasediments. Geochimica et Cosmochimica Acta 66, 2737–2754.

Sinninghe Damsté, J.S., Rampen, S., Rijpstra, W.I.C., Abbas, B., Muyzer, G., Schouten,S., 2003. A diatomaceous origin for long-chain diols and mid-chain hydroxylmethyl alkanoates widely occurring in Quaternary marine sediments:indicators for high nutrient conditions. Geochimica et Cosmochimica Acta 67,1339–1348.

Skipski, V.P., Smolowe, A.F., Sullivan, R.C., Barclay, M., 1965. Separation of lipidclasses by thinlayer chromatography. Biochimica et Biophysica Acta 196, 386–396.

Sloan, L.C., Barron, E.J., 1992. A comparison of Eocene climate model results to quantified paleoclimate interpretations. Paleogeogr. Paleoclim. Paleoecol. 93, 183-202.

Sloan, L.C., 1994. Equable climates during the early Eocene— significance of regional paleogeography for North-American climate. Geology 22 (10), 881– 884.

Sloan, L.C., Huber, M., Crowley, T.J., Sewall, J.O., Baum, S., 2001. Effect of sea surfca etemperature configuration on model simulations of "equable" climate in the Early Eocene. Palaeogeogr. Palaeoclim. Palaeoecol. 167, 321-335.

Slomp, C. P., Epping, E. H. G., Helder, W., van Raaphorst, W., 1996. A key role for iron-bound phosphorus in authigenic apatite formation in North Atlantic continental platform sediment, J. Mar. Res., 54, 1179–1205.

Slomp, C.P., van Cappellen, P., 2007. The global marine phosphorus cycle: sensitivity to oceanic Circulation. Biogeosciences 5, 155 – 171.

Sluijs, A., Schouten, S., Pagani, M., Woltering, M., Brinkhuis, H., Sinninghe Damsté, J.S., Dickens, G.R., Huber, M., Reichart, G.J., Stein, R., Matthiessen, J., Lourens, L.J., Pedentchouk, N., Backman, J., Moran, K., & the Expedition 302 Scientists, 2006. Subtropical Arctic Ocean temperatures during the Palaeocene/Eocene thermal maximum. Nature 441, 610– 613.

Sluijs, A., Röhl, U., Schouten, S., Brumsack, H.-J., Sangiorgi, F., Sinninghe Damsté, J.S., Brinkhuis, H., 2008. Arctic late Paleocene–early Eocene paleoenvironments with special emphasis on the Paleocene-Eocene thermal maximum (Lomonosov Ridge, Integrated Ocean Drilling Program Expedition 302). Paleoceanography 23, doi:10.1029/2007PA001495.

Smith, F.A., Freeman, K.H., 2006. Influence of physiology and climate on dD of leaf wax n-alkanes from C3 and C4 grasses. Geochim. Cosmochim. Acta 70, 1172-1187.

Soetaert K. and Herman P.M.J., 2009. A practical guide to ecological modelling: using R as a simulation platform. Springer.

Soetaert, K., Petzoldt, T., Setzer, R.W., 2010. Solving Differential Equations in R: Package deSolve, Journal of Statistical Software 33(9), 1-25.

Speelman, E.N., van Kempen, M.M.L., Barke, J., Brinkhuis, H., Reichart, G.J., Smolders, A.J.P., Roelofs, J.G.M., Sangiorgi, F., de Leeuw, J.W., Lotter, A.F., Sinninghe Damsté, J.S., 2009. The Eocene Arctic *Azolla* bloom: environmental conditions, productivity and carbon drawdown. Geobiology 7, 155-170.

Spofforth, D. J. A., Pälike, H., Green, D., 2008. Paleogene record of elemental concentrations in sediments from the Arctic Ocean obtained by XRF analyses, Paleoceanography, 23, doi:10.1029/2007PA001489.

Stein, R., Boucsein, B., Meyer, H., 2006. Anoxia and high primary production in the Palaeogene central Arctic Ocean: First detailed records from Lomonosov Ridge, Geophys. Res. Lett., 33, L18606, doi:10.1029/ 2006GL026776.

Stickley, C.E., Koc, N., Brumsack, H.J., Jordan, R.W., Suto, I., 2008. A siliceous microfossil view of middle Eocene Arctic paleoenvironments: A window of biosilica production and preservation. Paleoceanography 23, PA1S14, doi:10.1029/2007PA001485.

Stickley, C.E., St John, K., Koç, N., Jordan, R.W., Passchier, S., Pearce, R.B., Kearns, L.E., 2009. Evidence for middle Eocene Arctic sea ice from diatoms and ice-rafted debris. Nature 460, 376 - 379.

Still, C.J., Riley, W.J., Biraud, S.C., Noone, D., Buenning, N.H., Randerson, J.T., Torn, M.S., Welker, J., White, J.W.C., Vachon, R., Farquhar, G.D., Berry, J.A., 2009. The influence of clouds and diffuse radiation on ecosystem-atmosphere CO_2 and $CO^{18}O$ exchanges. J. Geophys. Res. 114, G01018, doi:10.1029/2008JG000675.

Sturt, H.F., Summons, R.E., Smith, K., Elvert, M., Hinrichs, K.U., 2004. Intact polar membrane lipids in prokaryotes and sediments deciphered by high-performance liquid chromatography/electrospray ionization multistage mass spectrometry - new biomarkers for biogeochemistry and microbial ecology. Rapid. Commun. Mass Spectrom. 18, 617-628.

Summons, R.E., Jahnke, L.L., Hope, J.M., Logan, G.A., 1999. 2-Methylhopanoids as biomarkers for cyanobacterial oxygenic photosynthesis. Nature 400, 554-557.

Sun, M-Y., Wakeham, S.G., 1994. Molecular evidence for degradation andpreservation of organic matter in the anoxic Black Sea Basin. Geochimica et Cosmochimica Acta 58, 3395–3406.

Thunell, R.C., Williams, D.F., Belyea, P.R., 1984. Anoxic events in the Mediterranean Sea in relation to the evolution of Late Neogene climates. Mar. Geol. 59, 105-134.

Tomitani, A., Knoll, A.H., Cavanaugh, C.M., Ohno, T., 2006. The evolutionary diversification of cyanobacteria: Molecular phylogenetic and paleontological perspectives. Proc. Nat. Acad. Sci. USA 103, 5442–5447.

Tripati, A., Backman, J., Elderfield, H., Ferretti, P., 2005. Eocene bipolar glaciation associated with global carbon cycle changes. Nature 436, 341-346.

Turekian, K.K., Wedepohl, K.H., 1961. Distribution of elements in some major units of the earth's crust. Geological Society of America Bulletin 72, 175-192.

van Bentum, E.C., Hetzel, A., Brumsack, H.J., Forster, A., Reichart, G.J., Sinninghe Damsté, J.S., 2009. Reconstruction of water column anoxia in the equatorial Atlantic during the Cenomanian–Turonian oceanic anoxic event using biomarker and trace metal proxies. Palaeogeagraphy, Palaeoclimatology, Palaeoecology 280, 489 – 498.

Van Cappellen, P., and Ingall, E.D., 1994. Benthic phosphorus regeneration, net primary production, and ocean anoxia: A model of the coupled marine biogeochemical cycles of carbon and phosphorus. Paleoceanography 9, 677-692.

van der Meer, M.T.J., Baas, M., Rijpstra, W.I.C., Marino, G., Rohling, E.J., Sinninghe Damsté, J.S., Schouten, S., 2007. Hydrogen isotopic compositions of long-chain alkenones record freshwater flooding of the Eastern Mediterranean at the onset of sapropel deposition. Earth. Planet. Sc. Lett. 262, 594-600.

van der Weijden, C.H., 2002. Pitfalls of normalization of marine geochemical data using a common divisor. Marine Geology 184(3-4), 167 – 187.

van Dongen, B.E., Schouten, S., Sinninghe Damsté, J.S., 2002. Carbon isotopevariability in monosaccharides and lipids of aquatic algae and terrestrial plants. Marine Ecology Progress Series 232, 83–92.

van Kempen, M.M.L., Smolders, A.J.P., Bogemann, G.M., Roelofs, J.G.M. Long term effects of salt stress on the growth, nutrient content and amino acid 3 composition of the *Azolla* filiculoides Lam.–Anabaena azollae Stras. Association, Annals of Botany, under review.

Vermeer, C.P., Nastold, P., Jetter, R., 2003. Homologous very long-chain 1,3-alkanediols and 3-hydroxyaldehydes in leaf cuticular waxes of Ricinuscommunis L. Phytochemistry 62, 433–438.

Versteegh, G.J.M., Bosh, H.-J., de Leeuw, J.W., 1997. Potential palaeoenvironmentalinformation of C_{24}–C_{36} mid-chain diols, keto-ols and mid-chain hydroxy fattyacid; a critical review. Organic Geochemistry 27, 1–13.

Villareal, T.A., 1992. in Marine pelagic cyanobacteria: Trichodesmium and other diazotrophs, eds. Carpenter, E. J., Capone, D. G., & Rueter, J. G. (Kluwer Academic, Dordrecht), pp. 163-175.

Volkman, J.K., 1986. A review of sterol markers for marine and terrigenous organicmatter. Organic Geochemistry 9, 83–100.

Volkman, J.K., Barrett, S.M., Dunstan, G.A., Jeffrey, S.W., 1992. C_{30}–C_{32} alkyl diols andunsaturated alcohols in microalgae of the class Eustigmatophyte. OrganicGeochemistry 18, 131–138.

Wada, E., Hattori, A., 1976. Natural abundance of ^{15}N in particulate organic matter in the North Pacific Ocean. Geochim. Cosmochim. Acta 40, 249-251.

Waddell, L.M., and Moore, T.C., 2008. Salinity of the Eocene Arctic Ocean from oxygen isotope analysis of fish bone carbonate. Paleoceanography 23, PA1S12, doi:10.1029/2007PA001451.

Wagner, G.M., 1997. *Azolla*: A review of its biology and utilization. The Botanical Review 63, 1-26.

Walsby, A.E., 2007. Cyanobacterial heterocysts: terminal pores proposed as sites of gas exchange. Trends Microbiol. 15, 340-349.

Wedepohl, K.H., 1971. Environmental influences on the chemical composition of shales and clays. Physics and Chemistry of the Earth 8, 305–333.

Wen, M., Jetter, R., 2007. Very long-chain hydroxyaldehydes from the cuticular waxof Taxus baccata needles. Phytochemistry 68, 2563–2569.

Wen, M., Au, J., Gniwotta, F., Jetter, R., 2006a. Novel very long-chain secondaryalcohols and alkanediols in the leaf cuticular waxes of Pisum sativum. Phytochemistry 67, 2494–2502.

Wen, M., Buschhaus, C., Jetter, R., 2006b. Nanotubules on plant surfaces: chemicalcomposition of epicuticular wax crystals on needles of Taxus baccata L. Phytochemistry 67, 1808–1817.

Wilf, P, Wing, S.L., Greenwood, D.R., Greenwood, C.L., 1998. Using fossil leaves as paleoprecipitation indicators: An Eocene example. Geology 26(3), 203–206.

Wing, S.L., Greenwood, D.R., 1993. Fossils and fossil climate: the case for equable continental interiors in the Eocene. Phil. TransR. Soc. L ond. B. 341, 243-252.

Wolfe, J.A., 1994. Tertiary climatic changes at middle latitudes of western North America. Palaeogeogr. Palaeoclimatol. Palaeoecol. 108, 195-205.

Worden, J., Noone, D., Bowman, K., 2007. Importance of rain evaporation and continental convection in the tropical water cycle. Nature 445, 528-532.

Xu, Y., Simoneit, B.R.T., Jaffé, R., 2007. Occurrence of long-chain n-alkenols, diols,keto-ols and sec-alkanols in a sediment core from a hypereutrophic, freshwaterlake. Organic Geochemistry 38, 870–883.

Yang, H., Huang, Y., 2003. Preservation of lipid hydrogen isotope ratios in Miocene lacustrine sediments and plant fossils at Clarkia, northern Idaho, USA. Org. Geochem. 34, 413-423.

Yang, H., Pagani, M., Briggs, D.E.G., Equiza, M.A., Jagels, R., Leng, Q., LePage, B.A., 2009. Carbon and hydrogen isotope fractionation under continuous light: implications for paleoenvironmental interpretations of the High Arctic during Paleogene warming. Oecologia 160, 461–470. doi 10.1007/s00442-009-1321-1.

Yao, Y-F., Bera, S., Ferguson, D.K., Mosbrugger, V., Paudayal, K.N., Jin, J-H., Li, C-S., 2009. Reconstruction of paleovegetatin and paleoclimate in the Eraly and Middle Eocene, Hainan Island, China. Climatic Change 92, 169-189.

Yapp, C.J., 2004. Fe(CO_3)OH in goethite from a mid-latitude North American Oxisol: Estimate of atmospheric CO_2 concentration in the early Eocene ''climatic optimum,'' Geochimica et Cosmochimica Acta, 68, 935–947.

Yeager, S.G., Shields, C.A., William, G.L., Hack, J., 2006. The Low-Resolution CCSM3. Journal of Climate 19, 2545 - 2566.

Zachos, J. C., Lohmann, K.C, Walker, J.C.G., Wise, S.W., 1993. Abrupt climate change and transient climates in the Paleogene: A marine perspective. J. Geol. 101, 193-215.

Zachos, J.M., Scott, L.D., Lohmann, K.C., 1994. Evolution of early Cenozoic marine temperatures. Paleoceanography 9(2), 353-387.

Zachos, J.C., Pagani, M., Sloan, L.C., Thomas, E., Billups, K., 2001. Trends, rhythms, and aberrations in global climate 65Ma to present. Science 292, 686-693.

Zachos, J.M., Dickens, G.R., Zeebe, R., 2008. An early Cenozoic perspective on greenhouse warming and carbon-cycle dynamics. Nature 451, 279 - 283.

Zeebe, R.E., Wolf-Gladrow, D. (eds), 2001. CO_2 in seawater: equilibrium, kinetics, isotopes. Elsevier Oceanography Series 65.

Summary

Upon the discovery that the Arctic Ocean was covered with enormous quantities of the aquatic floating fern *Azolla* in the Early/Middle Eocene (49 Ma), questions regarding the Eocene conditions facilitating these blooms arose. This dissertation describes the reconstruction of the paleo-environmental conditions that supported the large-scale occurrence of the freshwater fern *Azolla* in a marine environment. Sediment samples of the Eocene *Azolla* interval, including sediments from the Lomonosov Ridge in the central Arctic Ocean obtained during the Arctic Coring Expedition (ACEX; Integrated Ocean Drilling Program Expedition 302), were analysed for their (organic) geochemical properties. Obtained proxy records were extrapolated and interpreted using numerical modelling approaches.

Biomarker analyses

Novel and unique lipids, identified as 1,ω20 long chain mid-chain diols, ω20 hydroxy fatty acids and ω20 *n*-alkanols, were encountered in the Arctic sediments from the Eocene *Azolla* interval. The same compounds were found to be biosynthesized by extant *Azolla filiculoides*. Furthermore, several intact wax esters with a C_{16} fatty acid, including ω20 mono-hydroxy C_{46} to C_{52} wax esters, C_{46} ω20,ω21 and C_{49} ω9,ω10 di-hydroxy wax esters, were present in both *Azolla filiculoides* and the Eocene sediments. In addition, structurally related C_{29} ω20, ω21 diols, C_{29} 1,20,21 triols and C_{29} dihydroxy fatty acids were discovered. The similar chain length and isomer distributions of all encountered ω20 compounds suggest a common origin and biosynthetic production pathway, where it seems most likely that these compounds originate from the epicuticular wax layers of *Azolla*. As most of these compounds were well preserved in the Eocene sediments, these lipids may serve

as palaeo-environmental indicators of the Arctic *Azolla* interval and as markers for the past occurrence of *Azolla* in general.

Analyses of extracts of extant *Azolla filiculoides* also showed the presence of 1-(O-hexose)-3,25-hexacosanediol and its corresponding keto-ol. These heterocyst glycolipids (HGs) are synthesized in the cell envelope covering the heterocyst cell in heterocystous N_2-fixing cyanobacteria of the family of Nostocaceae and are most probably derived from the cyanobacterium *Anabaena azollae* that lives in symbiosis with *Azolla*. The presence of the same heterocyst glycolipids in the Eocene Arctic sediments shows that the symbiosis between *Azolla* and *Anabaena azollae* dates back to at least the Early/Middle Eocene. Furthermore, the finding of these heterocyst glycolipids indicates that this symbiosis played a major role in adding newly fixed nitrogen to the surface waters of the past-stratified Arctic.

Extracts of sediments of the Eocene Arctic and other Early/Middle Eocene sediments from Western Europe also contained long chain *n*-alkanes with a strong odd over even predominance, indicative of the presence of fossil leaf waxes derived from higher plants.

Hydrogen isotopes

Through the application of stable water isotope tracers, the water sources for and the actual salinity of the Eocene Arctic basin could be constrained. The hydrogen isotopic composition (δD) of biomarkers can potentially be used to reconstruct the δD of their source water, provided the fractionation between source water and the biomarkers is known. Through culturing experiments with extant *Azolla*, the hydrogen isotopic fractionation of the *Azolla*-specific 1,ω20 C_{32} diols relative to culture water was determined (ca. -100‰). The δD value of the Early/Middle Eocene Arctic surface waters was thus reconstructed using the calibrated hydrogen isotopic composition of *Azolla* biomarkers and was found to have a value of -116 to -133‰. In turn, the δD of fossil leaf wax derived *n*-alkanes can be used to reconstruct past precipitation δD. Numerical climate modeling (see below) showed that the offset between δ_{precip} and δD values of leaf wax *n*-alkanes ($\varepsilon_{w/a}$) varies in space and that in the Northern mid- to high-latitudes the apparent hydrogen isotope fractionation ($\varepsilon_{w/a}$) is on average 6‰ lower under Eocene environmental conditions. Hence, region and time specific $\varepsilon_{w/a}$ values should be used for the reconstruction of δD_{precip} from measured *n*-alkane δD. δD_{precip} values reconstructed using C_{29} *n*-alkanes encountered in sediments from the *Azolla* interval from Western Europe are significantly enriched relative to today's, which is indicative of the prevalence of enhanced moisture transport from lower latitudes towards the high latitudes. Consistently, Eocene Arctic δD_{precip} values, corrected using the model computed $\varepsilon_{w/a}$ values, are also notably enriched (-105 to -133‰). These values fall in the same range as the reconstructed δD of Early/Middle Eocene Arctic surface waters for

this interval, indicating that only limited mixing (up to 14%) occurred between the deeper saline waters (δD -8‰; salinity 21 - 34) and surface waters (-105 to -133‰; salinity 0). This also provides independent evidence for the existence of a niche for the freshwater fern *Azolla* in the Eocene Arctic Ocean.

Climate Modeling

Using the isotope-enabled version of the National Center for Atmospheric Research (NCAR) atmospheric general circulation model, Community Atmosphere Model v.3 (isoCAM3), moisture pathways and runoff responsible for freshening of Arctic surface waters were quantified. Furthermore, the spatial and temporal distribution of δD values in precipitation are simulated on a global scale for both the present-day and the Early/Middle Eocene. The Eocene simulation with a proxy-inferred imposed reduced equator-to-pole temperature gradient showed that δD_{precip} was more enriched in the Eocene, with values ranging between 0 – 140‰ compared to 0 – 300‰ for the present-day control simulation. Model outcomes were broadly consistent with the terrestrially derived *n*-alkane inferred δD_{precip} and a compilation of δD and $\delta^{18}O$ estimates from a suite of different proxies. This overall good correlation between our model results, using a reduced meridional sea surface temperature gradient, and δD_{precip} proxy records confirms the prevalence of a reduced equator-to-pole temperature gradient during the Eocene *Azolla* interval.

The validated model was subsequently used to quantify moisture pathways and to constrain water sources for and the isotopic composition of precipitation entering the Arctic (and adjacent areas). Results of model simulations with Eocene boundary conditions show increased moisture transport towards the Northern high latitudes, with a net supply of 1.5×10^{13} m^3/yr (the equivalent of ca. 1700 mm/yr) freshwater (sum of runoff and precipitation) entering the Arctic Ocean. Overall, model outcomes and proxy data confirm the freshening (salinity of 0 - 6) of the Eocene Arctic surface waters that allowed the *Azolla* blooms to develop.

Biogeochemistry

During the *Azolla* interval surface waters thus freshened, while the presence of marine diatoms indicate that bottom waters remained saline (21 – 34). This implies that the Eoceen Arctic was highly stratified. This stratification limited ventilation of the deeper waters. This restricted ventilation in concert with ongoing export of organic matter was most likely responsible for the observed development of anoxic conditions in the lower part of the water column and the accumulation of organic-rich sediments. By comparing excess trace metal accumulation in sediments in the Eocene Arctic Ocean with input of trace metals from the different sources (i.e. fluvial, eolian, and via seawater inflow) we constrained water circulation in the Eocene Arctic Ocean. An inflow of Nordic Sea water of at least 1.3 to 20 $\times 10^{12}$ m^3/yr was needed to sustain the elevated molybdenum and vanadium burial

rates. Such a relatively limited exchange of water between the Arctic and adjacent seas implies that a relatively low export productivity of organic matter (e.g. *Azolla*) would have been sufficient to render Arctic bottom waters anoxic.

As *Azolla arctica* lived in symbiosis with nitrogen fixing cyanobacteria, it depended on phosphorus as a limiting nutrient only. Sedimentary phosphorus data, freshwater fluxes -based on climate modeling- and the reconstructed deepwater inflow were combined in a new mass balance box model for the Eocene Arctic to examine the relationships between Arctic oceanic circulation, primary productivity, and sedimentary burial and regeneration of phosphorus. Model outcomes showed that a combination of a sustained riverine influx of phosphorus, enhanced phosphorus regeneration in the surface waters and upwelling of phosphorus-rich deepwater is needed to explain the sustained growth of *Azolla* in the Eocene Arctic Ocean. The sustained growth of *Azolla* during a period of 160.000 to 1.200.000 Myr in the anoxic Arctic oceanic basin may have resulted in burial of 0.9 – 3.5 10^{18} g organic carbon in sediments in the Arctic, corresponding to a 55 to 470 ppm drawdown of atmospheric CO_2. This indicates that the Arctic *Azolla* blooms may have had a significant effect on global atmospheric pCO_2 levels through enhanced burial of organic matter.

In conclusion: (1) The climate modeling results and compound-specific δD measurements confirm the extreme freshening of the Arctic surface waters during the *Azolla* interval. (2) The good correlation between the *Azolla* megaspore counts and heterocyst glycolipid abundance, and the similar distribution of heterocyst glycolipids in the Eocene sediments and extant *Azolla* suggests that the symbiotic relationship between *Azolla* and diazotrophic cyanobacteria of the family of Nostocaceae was already established in the Early/Middle Eocene. Hence, *Azolla arctica* production mainly depended on phosphorus supply. (3) Box modeling shows that a combination of enhanced phosphorus regeneration and upwelling of deep water is needed to ensure sustained *Azolla* growth in the Eocene Arctic. (4) Through increased production and subsequent burial of organic matter *Azolla* growth likely contributed to lowering atmospheric pCO_2 levels in the Early/Middle Eocene.

Samenvatting

De ontdekking dat de Arctische Oceaan in het vroeg/midden Eoceen (49 Ma) bedekt was met enorme hoeveelheden *Azolla* werpt vragen op over de Eocene milieuomstandigheden waaronder deze groei van zoetwater kroosvarens op kon treden. Dit proefschrift beschrijft de reconstructie van de paleo-milieucondities die het mogelijk maakten dat de zoetwatervaren *Azolla* op grote schaal kon voorkomen in het mariene milieu. Sedimentmonsters van het Eocene *Azolla* interval, met inbegrip van sedimenten van de Lomonosov Rug in de centrale Arctische Oceaan, verkregen tijdens de Arctic Coring Expedition (ACEX; Integrated Ocean Drilling Program Expedition 302), zijn geanalyseerd op hun (organisch) geochemische samenstelling. De verkregen proxy gegevens zijn vervolgens geëxtrapoleerd en geınterpreteerd met behulp van numerieke modellen.

Biomarker analyse

Nieuw ontdekte en unieke lipiden, geïdentificeerd als 1,ω20 langketige diolen, ω20 hydroxy vetzuren en ω20 *n*-alkanolen, zijn aangetroffen in Arctische sedimenten uit het Eocene *Azolla* interval. Dezelfde verbindingen bleken ook te worden gebiosynthetiseerd door *Azolla filiculoides,* een *Azolla* soort die vandaag de dag voorkomt. Bovendien waren diverse intacte wasesters die een C_{16} vetzuur bevatten, waaronder ω20 mono-hydroxy C_{46} tot C_{52} wasesters, C_{46} ω20,ω21 en C_{49} ω9,ω10 di-hydroxy wasesters, aanwezig in zowel *Azolla filiculoides* als in de Eocene sedimenten. Daarnaast zijn er structureel verwante C_{29} ω20,ω21 diolen, C_{29} 1,20,21 triolen and C_{29} dihydroxy vetzuren ontdekt. De identieke ketenlengtes en isomeerdistributies van alle aangetroffen ω20 verbindingen duiden op een gemeenschappelijke oorsprong, waarbij het het meest waarschijnlijk lijkt dat deze verbindingen afkomstig zijn van de epicuticulaire waslaag van *Azolla.* Aangezien de meeste van deze verbindingen

goed bewaard zijn gebleven in de Eocene sedimenten, kunnen deze lipiden dienen als paleo-milieu indicatoren voor het Arctische *Azolla* interval en als indicatoren voor het vóórkomen van fossiele *Azolla* in het algemeen.

Analyses van extracten van *Azolla filiculoides* toonden verder de aanwezigheid van 1 - (O-hexose) -3,25-hexacosanediol en de daarmee corresponderende keto-ol. Deze heterocyste glycolipiden (HGs) worden gesynthetiseerd in een omhulsel dat de cel omvat in heterocysten vormende, N_2 fixerende, cyanobacteriën van de familie Nostocaceae. Deze zijn hoogstwaarschijnlijk afkomstig van de met *Azolla* in symbiose levende cyanobacterie *Anabaena azollae*. De aanwezigheid van dezelfde heterocyste glycolipiden in de Arctische Eocene sedimenten toont aan dat de symbiose tussen *Azolla* en *Anabaena azollae* teruggaat tot ten minste het vroeg/midden Eoceen. Het suggereert bovendien dat deze symbiose een belangrijke rol speelde in het toevoegen van stikstof aan de oppervlaktewateren van de toenmalig sterk gestratificeerde Arctische Oceaan door middel van cyanobacteriële N_2 fixatie.

Extracten van de Arctische sedimenten en extracten uit andere vroeg/midden Eocene afzettingen uit West-Europa bevatten ook langketige *n*-alkanen met een sterke oneven over even koolstofnummerverdeling, indicatief voor de aanwezigheid van fossiele, door hogere planten, geproduceerde bladwassen.

Waterstofisotopen

Door de toepassing van methoden voor de bepaling van stabiele waterisotopen (δD, $\delta^{18}O$) konden de oorsprong van het oppervlaktewater en het daadwerkelijke zoutgehalte van het Eocene Arctische bekken worden bepaald. De δD van biomarkers kan in principe worden gebruikt om de δD van het in het organisme opgenomen water te reconstrueren, mits de fractionering tussen dit water en de biomarkers bekend is. Door middel van experimenten met het kweken van bestaande *Azolla* is de waterstof isotopische fractionatie van de *Azolla*-specifieke 1,ω20 C_{32} diolen ten opzichte van het door *Azolla* opgenomen water bepaald (ca. -100‰). De δD waarde van vroeg/midden Eocene Arctische oppervlaktewateren werd aldus bepaald aan de hand van de δD van Eocene 1,ω20 C_{32} diolen en was -116 tot -133‰.

Op haar beurt kan de δD van fossiele *n*-alkanen afkomstig van wassen van hogere planten worden gebruikt om de δD van precipitatie (δD_{precip}) uit het verleden te reconstrueren. Uit numerieke klimaatmodelering (zie hieronder) is gebleken dat het verschil tussen δD_{precip} en δD waarden van de bladwas *n*-alkanen ruimtelijk varieert en dat in de noordelijke midden tot hoge breedtegraden de schijnbare waterstof-isotoopfractionering ($\varepsilon_{w/a}$) gemiddeld 6‰ lager is onder Eocene omstandigheden. Vandaar dat regio- en tijdspecifieke $\varepsilon_{w/a}$ waarden moeten worden gebruikt voor de reconstructie van δD_{precip} uit de gemeten δD van *n*-alkanen. δD_{precip} waarden gereconstrueerd met behulp van C_{29} *n*-alkanen aangetroffen in monsters

uit het *Azolla* interval uit afzettingen in West-Europa zijn sterk verrijkt ten opzichte van de huidige wereld, hetgeen een indicatie is voor het optreden van verhoogd vochttransport van lagere naar hoge breedtegraden. De Eocene Arctische δD_{precip} waarden, gecorrigeerd met behulp van de door het model berekende $\varepsilon_{w/a}$ waarden, zijn ook aanmerkelijk verrijkt (-105 tot -133‰). Deze waarden vallen in dezelfde orde van grootte als de gereconstrueerde δD van vroeg/midden Eoceen Arctische oppervlaktewateren voor dit interval, wat aangeeft dat menging van de diepere zoute wateren (δD -8‰; zoutgehalte 21 tot 34) en oppervlaktewateren (-105 tot -133‰; zoutgehalte 0) zeer beperkt was (tot 14%). Tevens verschaft dit onafhankelijk bewijs voor het bestaan van een niche voor de zoetwatervaren *Azolla* in de Eocene Arctische Oceaan.

Klimaatmodellen

Met behulp van de met een isotopenfunctionaliteit uitgeruste versie van het National Center for Atmospheric Research (NCAR) atmosferische algemene circulatie model, Community Atmosphere Model v.3 (isoCAM3), zijn het atmosferische vochttransport en de rivierafvoeren verantwoordelijk voor de verzoeting van het Arctische oppervlaktewater in het Eocene *Azolla* interval gekwantificeerd. Bovendien is de ruimtelijke en temporele verdeling van de compositie van δD in neerslag gesimuleerd op een wereldwijde schaal, voor zowel de huidige wereld als voor het vroeg/midden Eoceen. De Eocene simulatie, met als randvoorwaarde een proxy-afgeleid gereduceerd evenaar-tot-pool temperatuurgradiënt, liet zien dat de δD_{precip} in het Eoceen meer isotopisch verrijkt was, met waarden variërend tussen 0 tot 140‰ ten opzichte van 0 tot 300‰ voor de simulatie van de hedendaagse situatie. De modeluitkomsten stemden goed overeen met uit terrestrisch *n*-alkaan afgeleide δD_{precip} en een literatuurcompilatie van δD and $\delta^{18}O$ schattingen op basis van een aantal verschillende proxies. Deze over het geheel genomen goede overeenstemming van onze modelresultaten met de δD_{precip} proxy data bevestigt de prevalentie van een verminderd evenaar-tot-pool temperatuurgradiënt tijdens het *Azolla* interval zoals deze eerder met temperatuurproxies was gereconstrueerd.

Het gevalideerde model werd vervolgens gebruikt om vochttransport te kwantificeren en om de oorsprong van precipitatie in en rond de Arctic alsmede de isotopische samenstelling daarvan te bepalen. Resultaten van modelsimulaties met Eocene randvoorwaarden lieten een toename van vochttransport naar de Noordelijke hoge breedtegraden zien. Dit resulteerde in een berekende hoge zoetwatertoevoer (neerslag en waterafvoer van rivieren) naar de Arctische Oceaan van 1.5×10^{13} m^3 per jaar; het equivalent van een neerslag van ca. 1700 mm/jr. Ook deze modelberekeningen bevestigen dus de verzoeting (saliniteit van 0 - 6) van de Eocene Arctische oppervlaktewateren waardoor de enorme bloei van de zoetwatervaren *Azolla* verklaard kan worden.

Biogeochemie

Tijdens het *Azolla* interval verzoette het oppervlaktewater van de Arctische Oceaan dus sterk, terwijl o.a. de aanwezigheid van mariene diatomeeën aangeeft dat bodemwateren zout zijn gebleven (21 - 34). Dit betekent dat de Eocene Arctische Oceaan sterk gestratificeerd moet zijn geweest. Deze stratificatie leidde tot slechte ventilatie van het bodemwater. In combinatie met de continue export van organisch materiaal naar het diepere water, resulteerde dit in de waargenomen ontwikkeling van zuurstofloze omstandigheden in het onderste deel van de waterkolom alsmede de afzetting van organisch-rijke sedimenten.

Door een vergelijking van de extra hoeveelheid zware metalen die accumuleerde in het sediment van de Eocene Arctische Oceaan met de toevoer van zware metalen uit de verschillende bronnen (fluviatiele, eolische, en via zeewater instroom) is getracht de watercirculatie te reconstrueren. Een instroom van water uit de Noordelijke zeeën van 1.3 tot 20 x 10^{12} m^3/yr was nodig om de verhoogde molybdeen en vanadium begravingssnelheden te kunnen handhaven. Een dergelijke relatief beperkte uitwisseling van water tussen de Arctische Oceaan en haar aangrenzende, meer zuurstofrijke, zeeën impliceert dat een relatief lage exportproductiviteit (o.a. *Azolla* groei) van organisch materiaal voldoende moet zijn geweest om de Arctische bodemwateren zuurstofloos te maken.

Aangezien *Azolla arctica* in symbiose leefde met stikstofbindende cyanobacteriën, was het enkel afhankelijk van fosfor als een limiterende nutriënt. De sedimentaire fosfor gegevens, zoetwaterstromen -berekend met klimaatmodellen- en de gereconstrueerde diepwater instroom zijn gecombineerd in een nieuw massabalansmodel voor het Noordpoolgebied. Met behulp van dit model was het mogelijk om de relaties tussen de Arctische oceaancirculatie, primaire productiviteit, en sedimentaire begraving en regeneratie van fosfor te onderzoeken. Modelresultaten toonden aan dat een combinatie van een aanhoudende aanvoer van fosfor door rivieren, versterkte regeneratie van fosfor in het oppervlaktewater en opwelling van fosfor-rijk dieper water nodig zijn om de aanhoudende groei van *Azolla* in de Eocene Arctische Oceaan te kunnen verklaren. De aanhoudende groei van *Azolla* gedurende een periode van 160.000 tot 1.200.000 jaar in het zuurstofloze bekken van de Arctische Oceaan heeft geleid tot het vastleggen van 0.9 - 3.5 10^{18} g organisch koolstof in sedimenten, resulterend in een afname van atmosferische pCO_2 in de orde grootte van 55 tot 470 ppmv. Dit geeft aan dat de Arctische *Azolla* bloei een aanzienlijk effect op het atmosferische CO_2 gehalte moet hebben gehad door verhoogde begraving van organisch materiaal in Eocene sedimenten.

Tot slot, de conclusies van dit proefschrift zijn: (1) De resultaten van klimaatmodelberekeningen en verbinding-specifieke δD metingen bevestigen de extreme verzoeting van het Arctische oppervlaktewater tijdens het *Azolla* interval. (2) De

goede correlatie tussen de *Azolla* megaspoortellingen en de abundantie van heterocyste glycolipiden, en de gelijke verdeling van hetercocyste glycolipiden in de Eocene sedimenten en bestaande *Azolla* suggereert dat de symbiotische relatie tussen *Azolla* en diazotrofe cyanobacteriën in de familie van Nostocaceae al in het vroeg/midden Eoceen bestond. Groei van *Azolla arctica* was dus voornamelijk afhankelijk van toevoer van fosfor. (3) Uit massabalansmodellering blijkt dat een combinatie van verhoogde fosfor regeneratie en opwelling van diep water nodig was om een continue groei van *Azolla* in het Eocene Noordpoolgebied te bewerkstelligen. (4) Door de toename van de productie en de daaropvolgende begraving van organisch materiaal droeg *Azolla* groei zeer waarschijnlijk bij aan een vermindering van atmosferisch CO_2 gehalte in het vroeg/midden Eoceen.

Acknowledgements

Looking back, I realize how lucky I've been the past four years. Numerous opportunities have sprung up, which would not have happened and would not have resulted in as much fun without the support of a large number of people.

First and foremost, I would like to thank my co-promotor and daily supervisor Gert-Jan Reichart. Without you I wouldn't have started in the first place, and I'm glad I did. Based on mutual (?) trust, you gave me a feeling of freedom, both intellectually and socially, which has been invaluable. You supported me to spend time abroad at other universities (probably against better judgment :), attend numerous conferences, and pursue my own aspirations, which is why this dissertation combines my fondness for (organic geo-)chemistry and interest in model applications. Thank you for your continuous encouragement.

Next, I would like to thank my promotor Jaap Sinninghe Damsté, who always found the time to read through my manuscripts and whose constructive criticism and infinite attention to details thus ensured the quality of this dissertation. I would also like to thank Jan de Leeuw, whose continuous enthusiasm for organic geochemistry is contagious and motivational. Then I obviously also have to thank Henk Brinkhuis, the one and only mastermind behind the *Azolla* project. You were always ready to take me along and introduce me to just about everybody else ... and back again, which helped shaping this thesis and made these years more fun, thanks!

Special thanks goes to my roommates in Z214: Jos and Julia, with Aafke and Jordahna as returning visitors. You definitely made the past years enjoyable, with

constant interruptions, never ending supplies of chocolate, coffee and pepernoten, happy bouncing on VW, sphagnum, proxy factories, kip, and this may be the last sunny day…; biertje? More importantly, you helped me snap out of the "oh it's snowing" staring mode, listened when I got overly excited about something or just had to vent off some frustrations. Thanks, I'll miss you.

Then, my project partners, or the *Azolla* girls, as we're so lovingly called: Monique and Judith. Stuck with the same aquatic floating fern till the point you find yourself jumping of your bike just because there is a chance you spotted a floating reddish greenish blob. I'd also like to mention my students (more girls): Rolande en Merel, who extended the project even further the past year.

I would also like to thank Jacob Sewall, David Noone and Mark Pagani for giving me the opportunity to work as part of their scientific teams at Virginia Tech, CU Boulder and Yale, respectively. I'm indebted to David Noone for giving me the isotope code (which saved me from the lab). I was lucky to meet Jake, you always swiftly helped me out whenever I got stuck in the midst of a piece of CAMcode. It's been a great pleasure, thanks so much.

Thanks also to my other co-authors: Thorsten Bauersachs, Stefan Schouten, Ellen Hopmans (also for Bligh & Dyer and LCMS explanation), Irene Rijpstra (also for the TLC), Nik Buenning, Matthew Huber, Anna von der Heydt, Andy Lotter, Jan Roelofs, Fons Smolders, Francesca Sangiorgi, and Caroline Slomp.

Back to Utrecht: special thanks should go to Elisabeth van Bentum and Cornelia Blaga, who were there from the beginning and got the lab going. I fondly remember the 'scientific' discussions, some of the zillion little "facts", and our memorable group outings. Hence, I also want to thank the rest of my colleagues and ex-collegues of our ever expanding organic geochemistry group: Els van Soelen, Adriana Duenas Bohorquez, Laura Buckles, Johan Weijers, Klaas Nierop, Mohamed Elkelani, Juliana Vasiliev, Lennart de Nooijer, Marieke Lammers, and Gijs Nobbe, Jan Kubiak, Anita van Leeuwen, Helen de Waard, and Arnold van Dijk for technical support.

Of course I shouldn't forget to thank the IPPU corner upstairs, for countless diet cokes & the only decent coffee in the building and genuine enthusiasm: my Eocene (conference) partners, Francesca, Sander, Peter, and Appy (koffie?). Someplace else in our building, or on Texel: Thanks to Lucy, Anja, Hemmo, João, Emmy, Karoliina, Tom, Micha, Peter, Iana, Jose, Marie-Louise, Marjolein, Pien, and special thanks to Leonard (cover) and to Shauna for the final days in Aran. I am grateful to Marcel and Michiel for help with the compound specific isotope measurements, Francien, Isla, Darci, Nicole for a little summer camp fun, and everyone else; thanks!

Special mention should go to my paranymphs: Pernille en Nienke, omdat NEP echt is, voor altijd. Thank you for always being there for me.

My parents, Hessel and Hanneke, and my brother Laurens, who clearly somehow managed to transfer a predisposition to fondness for geosciences to me/us. Thanks so much for your love, support and never failing in faith me.

Outside the university: Chiq; Farida, Frederiek, Mirella, Karlijn, Laurien, Rimke, Susanne, and Niké, warm thanks for a good start of the week:). The girls: Louise, Jasna, Roos, Floor, Julika, Julie, for the weekends, Pasta&Punch, a good laugh and our Friday 'updates'. And, amongst others, Raymond, JP, Steven, Dinu, Suzanne, Lianne, Anna, Folkert, Melissa, Annelies, Jacob, and of course my family; thanks!

Finally, it's time to clean out the heaps of papers, remove the laptop from the couch, and thank Reinder. Thanks for your loving attention, for letting me go, solving software and programming issues (even when I reject all help) and formatting this dissertation. Now we'll finally spend our weekends with the two of us ....

Publications

Articles

Speelman E.N., van Kempen M.M.L., Barke J., Brinkhuis H., Reichart G.J., Smolders A.J.P., Roelofs J.G.M., Sangiorgi F., de Leeuw J.W., Lotter A.F., Sinninghe Damsté J.S., 2009. The Eocene Arctic *Azolla* bloom: environmental conditions, productivity and carbon drawdown. Geobiology 7, 155-170.

Speelman E.N., Reichart G.J., de Leew J.M., Rijpstra W.I.C., Sinninghe Damsté J.S., 2009. Biomarker lipids of the freshwater fern *Azolla* and its fossil counterpart from the Eocene Arctic Ocean. Organic Geochemistry 40, 628 - 637.

Bauersachs T., Speelman E.N., Hopmans E.C., Reichart G.J., Schouten S., Sinninghe Damsté J.S., 2010. Fossilized glycolipids reveal past oceanic N_2 fixation by heterocystous cyanobacteria. PNAS, in press.

Speelman E.N., Sewall J.O., Noone D.C., Huber M., von der Heydt A., Sinninghe Damsté J.S., Reichart G.J., 2010. Modeling the influence of a reduced equator-to-pole sea surface temperature gradient on the distribution of water isotopes in the Early/Middle Eocene. EPSL 298, 57 - 65.

Buenning N., Speelman E.N., Reichart G.J., Noone D.C. Climatic controls on the modeled deuterium isotopic composition of leaf wax *n*-alkanes and implications for Eocene climate proxies. under review.

Speelman E.N., Sewall J.O., Noone D.C., van Kempen M.M.L., Sinninghe Damsté J.S., Reichart G.J. Reconstruction of Eocene Arctic hydrology using proxy data and isotope modeling. under review.

Speelman E.N., Slomp C.P., Barke J., Brinkhuis H., Sinninghe Damsté J.S., Reichart G.J. Geochemical constraints on Eocene Arctic Ocean ventilation and phosphorus cycling during the *Azolla* interval. in prep.

Selected presentations

Poster: "Heterocystous glycolipids in extant *Azolla* and ACEX sediments: evidence for N_2 fixation and symbiosis in the Early/Middle Eocene Arctic Ocean", GRC, Holderness 2010.

Poster: "Arctic Ocean circulation during the anoxic Eocene *Azolla* event ", EGU, Vienna 2010.

Oral Presentation: "Modeling the influence of a reduced equator-to-pole sea surface temperature gradient on the distribution of water isotopes in the Eocene", AGU, San Francisco 2009.

Oral Presentation: "Eocene cooling through sustained growth of *Azolla*?", YES Congress, Beijing 2009.

Poster, Award Winning: "Application of innovative isotope modeling in sea surface salinity reconstruction of the Eocene Arctic Basin", NSG, Amsterdam 2009.

Invited Presentation: "De oceanen: een archief van sediment. Reconstructie van het klimaat tijdens het *Azolla* interval in het Eoceen", Pyrus, Wageningen 2009.

Oral Presentation: "Influence of pCO_2 on *Azolla* isotopic composition: implications for Eocene pCO_2 reconstruction", IMOG, Bremen 2009.

Invited Presentation: "Application of isotope modeling in sea surface salinity reconstruction of the Eocene Arctic Basin", SEM, Utrecht 2009.

Oral Presentation: "Sea surface salinity of the Eocene Arctic *Azolla* event using innovative isotope modeling", EGU, Vienna 2009.

Oral Presentation: "Salinity reconstruction for the Eocene Arctic *Azolla* event using innovative isotope modeling", CBEP, Wellington 2009.

Oral Presentation: "Reconstructing Eocene Arctic surface water conditions using proxy and model data", NAC9, Veldhoven 2008.

Invited Presentation: "The *Azolla* project; a combined biogeochemical and modeling approach", Virginia Tech, Blacksburg 2008

Oral Presentation: "Reconstructing Eocene Arctic conditions during the *Azolla* event using proxy and model data", 33rd IGC, Oslo 2008.

Poster: "Reconstructing the Arctic Mid Eocene Environment – a biogeochemical perspective on the Eocene *Azolla* Bloom", DARWIN Days, Veldhoven 2007.

Oral Presentation: "Biomarker constraints on Arctic surface water conditions during the middle Eocene", AGU, San Francisco 2007.

Curriculum Vitae

Eveline Speelman was born on the 23rd of May 1982 in Delft, The Netherlands. She completed her secondary education (gymnasium) at the St Stanislas College in Delft in 2000 (cum laude). After obtaining her Propedeuse in Chemistry in 2001, she continued her BSc at University College Utrecht (UCU), majoring in Chemistry, Earth Sciences and Pharmacology. In 2003 she graduated (high honours) and started her Masters in Hydrology, also at Utrecht University (UU), which she completed in 2006 (cum laude). During her MSc she participated in a hydrological fieldwork project in Costa Rica under auspices of the Vrije Universiteit Amsterdam (VUA), in a research cruise in the Mediterranean Sea, and worked as an intern at the Water Division at UNESCO's headquarters in Paris. Her MSc thesis was based on the development and outcomes of a new model calculating present and predicting future water stress at the Climate and Global Sustainability Department of the Netherlands Environmental Assessment Agency (PBL). In 2006 she started as a PhD Student in the Darwin Center for Biogeosciences at the department of Geochemistry at the faculty of Geosciences at Utrecht University under supervision of Dr. Gert-Jan Reichart and Prof. dr. ir. Jaap Sinninghe Damsté. During her PhD she spent several months as a visiting scientist at Yale (New Haven), Virginia Tech (Blacksburg) and University of Colorado (Boulder) and became the Netherlands Representative for YES (network for Young Earth Scientists for Society) and YES Vision Support Team member. Her dissertation focuses on the (paleo)climate reconstruction of the "*Azolla* interval", integrating organic geochemistry and climate modeling.